

Sequence stratigraphy of the Mesozoic Domeyko basin, northern Chile



Thesis submitted in accordance with the requirements of the University of Liverpool
for the Degree of Doctor of Philosophy by John Ardill.

(March 1996)

**PAGINATED
BLANK PAGES
ARE SCANNED AS
FOUND IN
ORIGINAL
THESIS**

**NO
INFORMATION
MISSING**

Sequence stratigraphy of the Mesozoic Domeyko basin, northern Chile

John Ardill (University of Liverpool)

The Domeyko basin of northern Chile records Late Triassic-Early Cretaceous mixed carbonate and siliciclastic marine deposition along the western margin of Gondwana. The carbonate and siliciclastic ramp environment is characterised by the deposition of siliciclastic-dominated sediments at times of low accommodation space (lowstand and late highstand systems tracts) and carbonate-dominated sediments during periods of high accommodation space (transgressive and early highstand systems tracts). Along strike variations in siliciclastic sediment supply do not overprint the effects of basin-wide changes of relative sea-level. Sequence stratigraphical analysis identifies five second-order sequences resulting from changes in accommodation space and hence, relative sea-level. Within these second-order cycles a higher-frequency cyclicality has also been identified. Each second-order sequence is composed of between 3 and 5 high-frequency sequences which results in a second-order composite sequence, but does not produce the "typical" sequence-sets normally associated with composite sequences.

Comparison of the relative sea-level fluctuations interpreted from the Domeyko basin succession with those documented from other similar age South American marginal basins and northern hemisphere basins allows the distinction of regional from global events, and a methodology for potentially differentiating between eustatic and tectonic driving mechanisms. The choice of these basins permits an objective analysis of relative sea-level change using basins of different tectonic setting, on different continental plates. Relative sea-level fall in the late Early Sinemurian, earliest Pliensbachian, earliest Aalenian, Early Callovian, earliest Valanginian, and rises in the earliest Hettangian, earliest and Late Toarcian, Early and Late Bajocian, Late Bathonian and earliest Oxfordian of the Domeyko basin appear time-equivalent to similar events in other southern and northern hemisphere basins and thus are interpreted to be products of eustatically driven, global sea-level cycles. Relative sea-level falls in the earliest Bathonian, Late Oxfordian, earliest Valanginian and rises in the Late Kimmeridgian are interpreted to be tectonically-driven, continental-scale changes in accommodation space. Although the earliest Valanginian relative sea-level fall can also be seen globally the sequence boundary is interpreted to be tectonically-enhanced by documented regional uplift in Chile and Argentina. The Domeyko basin succession appears to be dominantly controlled by global sea-level fluctuations during the Early-Middle Jurassic, interpreted to have been driven by glacio-eustasy, and by continental-scale fluctuations during the Middle Jurassic to mid-Cretaceous.

Mesozoic back-arc basins of western South America record both eustatic and subduction-related relative sea-level fluctuations. To date, the latter have been assumed to be driven chiefly by Pacific plate spreading. However, five tectonically-driven sequence boundaries in the Domeyko and Neuquén basins which have no time correlative expressions in northern hemisphere basins display a close temporal association with five major Gondwanan fragmentation phases. They are: (A) the earliest Bathonian (170 Ma) sequence boundary was driven by the separation of Laurasia and Gondwana; (B) the Late Oxfordian (157 Ma) salinity crisis was driven by the separation of west from east Gondwana; (C) the termination of the marine Domeyko basin was driven by the fragmentation of east Gondwana; (D) the termination of the marine Neuquén Basin (114 Ma) was driven by the opening of the South Atlantic; and (E) the major basin inversion associated with the Peruvian tectonic event (100 Ma) was driven by the final fragmentation phase within east Gondwana. It is deduced that plate reorganisation associated with the initiation of new oceans during Gondwanan fragmentation resulted in increased coupling along the Andean subduction zone producing regional uplift and thus relative sea-level fall. Responses variously involve: basin barring and Kimmeridgian evaporite production; erosively-based fluvial sandstones directly overlying offshore marine deposits; closure of the Rocas Verdes oceanic marginal basin; sequential termination of marine conditions in the Domeyko and Neuquén back-arc basins; sudden influx of arc-derived alluvial conglomerates resulting from the onset of contractional tectonics; and an incremental jump in the eastward propagation of the Andean volcanic arc. Discrete contractional episodes in the otherwise extensional Andean active margin were thus driven by the incremental spreading phases of the supercontinent. Associated thermal signatures are recorded near the centre of Gondwana by kimberlite emplacement frequency maxima in southern Africa. Plate tectonic theory emphasises the dynamic interaction between adjacent plates, whereby relative rates of motion can be fixed to either the underriding or overriding plate as a reference frame. With reference to the circum-Gondwana subduction zone, I believe that in the past an overemphasis has been placed on the motions of oceanic plates in the Pacific region, while overlooking the role that the thermal evolution of the Pangean supercontinent played in driving circum-Pangean subduction. Thus, careful sequence stratigraphical analysis of active margin sedimentary basins provides a high resolution record, presently under-utilised in detecting, identifying and analysing global tectonic events in time.

Table of contents

Acknowledgements	7
Chapter 1	9
1.1 Objectives of thesis	10
1.2 Layout of thesis	12
Chapter 2	13
2.1 Objectives of chapter	14
2.2 Plate reconstructions of the circum-Pacific region	14
2.3 Regional geology and structural evolution of northern Chile	16
2.4 Palaeoclimate and oceanography of northern Chile	24
Chapter 3	27
3.1 Objectives of chapter	28
3.2 Time-scales	28
3.3 Ammonite zones	29
3.4 Biogeography and global bio-events	34
3.5 Summary	37
Chapter 4	39
4.1 Objectives of Chapter	40
4.2 Introduction	40
4.3 Continental clastic facies description	41
4.4 Shallow-marine siliciclastic ramp facies description	51
4.5 Shallow-marine carbonate ramp facies description	55
4.6 Shallow-marine carbonate rimmed-shelf facies description	62
4.7 Volcanic and Volcaniclastic facies description	64
4.8 Summary	66
Chapter 5	67
5.1 Objectives of chapter	68
5.2 Lithostratigraphy	68
5.3 Sequence stratigraphical concepts	68
5.4 Sequence stratigraphical surfaces in different depositional settings	76
5.5 Second-order sequence stratigraphy	79
5.5 Characterisation of high-frequency third-order sequences	85
5.6 Summary	91
Chapter 6	93
6.1 Objectives of chapter	94
6.2 Comparison of the sequences with other northern and southern hemisphere basins	94
6.3 Fragmentation of Pangea and its sequence stratigraphical record in the Andean back-arc basins	101
6.4 Pangean plate re-organisations and their thermal signature	105
6.5 Importance of supercontinental fragmentation episodes	106
Chapter 7	107
7.1 Conclusions	108
7.2 Future Research	110
References	111
Appendices	135

Acknowledgements

Firstly, I would like to acknowledge Steve Flint for excellent supervision and the teaching of, “science with attitude”. Then, Guillermo Chong who has added so much to the project with many of his own ideas from a lifetime of work on the Jurassic of northern Chile. Hans Wilke has helped greatly with fieldwork and his knowledge of the Jurassic ammonites. Back in Liverpool, thanks must go to Ian Stanistreet who has provided excellent discussion on the fragmentation of Gondwana.

Thank you to John Callomon for reading the Biostratigraphy and Chronostratigraphy chapter and Finn Surlyk, Angela Coe and Duncan Pirrie for reviewing chapters 5 and 6.

Thank you to all the people in the department at Liverpool who have made the last three years great fun, with a special thanks to Big John and Susie for making fieldwork in Chile an unforgettable experience. Thank you to Alasdair and Dave from R.T.Z. (Antofagasta) and Ruben Pardo (Universidad del Norte) for help in the field.

Finally, thank you to my dad, mum and brother for plenty of support over the past three years.

Chapter 1

Introduction

1.1 Objectives of thesis

In recent years the concepts of sequence stratigraphy have been applied at increasingly high levels of resolution, both spatially and temporally, to better understand the architecture of sedimentary successions and to predict systematic changes in stacking patterns in terms of changing accommodation space. Studies have focused on siliciclastic systems mainly in passive margin and foreland basins (eg. Posamentier & Vail, 1988; Van Wagoner *et al.*, 1990; Van Wagoner *et al.*, 1991). Commonly studied depositional systems have been largely shallow-marine but some detailed studies of fluvial and coastal-plain strata have recently been reported (Dam & Surlyk, 1992; Aitken & Flint, 1994). High resolution sequence stratigraphy of carbonate systems has included analysis of reef and platform systems (Sarg, 1988; Loucks & Sarg, 1993) but few in-depth studies of mixed carbonate and siliciclastic environments (Holmes & Christie-Blick, 1993; Southgate *et al.*, 1993) exist and, to date, none are reported from back-arc basin settings.

This thesis attempts to identify and characterise depositional responses to high-frequency, base-level driven changes in accommodation space in such a setting and examines the effects of local and regional tectonic events versus global eustatic cyclicity on the resultant stratigraphy. The Mesozoic Domeyko basin of northern Chile provides an excellent field example of mixed carbonate and siliciclastic ramp deposits which are constrained within a zone-level ammonite biochronology. The study area is concentrated along the Chilean Precordillera, known locally as the Cordillera Domeyko, which exposes the eastern margin of the basin (Figure 1.1). The stratigraphical nomenclature used in this thesis is that summarised by Callomon (1985) (see also Callomon, 1995) and adopted by the Geological Society of London (Whittaker *et al.*, 1991).

The Jurassic succession of northern Chile provides an example of mixed carbonate and siliciclastic ramp deposits but both logistical difficulties and the nature of this study area have influenced the work presented in this thesis. The logistical difficulties associated with working in northern Chile have been the large regional extent of the study area (400 x 150 km) and the location of sections in remote desert terrain. Local knowledge supplied by workers from the Universidad del Norte in Antofagasta and the use of Landsat imagery have helped minimise these logistical difficulties. The nature of the study area resulted in difficulties with poor levels of exposure and the lack of a structural template for the Late Triassic to Early Cretaceous period of deposition.

The Jurassic sections are typically poorly exposed with only one-dimensional and rarely two-dimensional outcrop. This lack of continuous exposure means that it is impossible to walk out surfaces in the field and therefore correlation of sections is heavily reliant on ammonite biostratigraphy. The poor exposure and lack of lateral continuity is primarily due to the complex regional-scale compressional and strike-slip tectonics which generated the Chilean Precordillera but also produced a sporadic and isolated outcrop pattern. The poor exposure is partly due to the nature of present-day freeze-thaw weathering in northern Chile which produces large quantities of scree. Such quantities of scree cannot efficiently be removed by the modern ephemeral fluvial systems operating in this arid climate and hence resulting in poor exposure.

The Domeyko basin is lacking a structural template for the Late Triassic to Early Cretaceous period of deposition. This lack of a structural template is due to complex regional-scale compressional and strike-slip tectonics which have been active since the Cretaceous, making a detailed structural analysis of the Mesozoic basins more difficult. An additional difficulty associated with the regional-scale compressional and strike-slip tectonics is the high degree of structural deformation within many of the Jurassic successions which often makes sedimentary logging difficult and sometimes impossible.

The impact of these factors on the work presented in this thesis has been to make the collection of sedimentary data more difficult and also to necessitate the use of time consuming ammonite biostratigraphy to permit the correlation and comparison of time-equivalent sections.

The principal aims of this project are.

- (1) To apply and test the concepts of sequence stratigraphy in an extensional back-arc basin setting, using the Jurassic-Cretaceous Domeyko basin of northern Chile. To test the utility and merits of sequence boundaries and flooding surfaces to divide and correlate the basin-fill succession.
- (2) To present the chronostratigraphical evolution of the marine Domeyko basin-fill, constrained by biostratigraphy and sequence stratigraphy. Subsequently, to construct a relative sea-level curve for the Domeyko basin based on sequence stratigraphy.
- (3) To compare the relative sea-level fluctuations identified in the Domeyko basin with those documented from other similar aged South American marginal basins and northern hemisphere basins, to distinguish between regional versus global events.
- (4) To isolate the principal controls on sequence development in the Domeyko basin where local and regional events may reflect a tectonic driving mechanism and global events will reflect a eustatic driving mechanism.
- (5) Finally, to identify and present a potential model to account for formation of the tectonically-driven sequence boundaries.

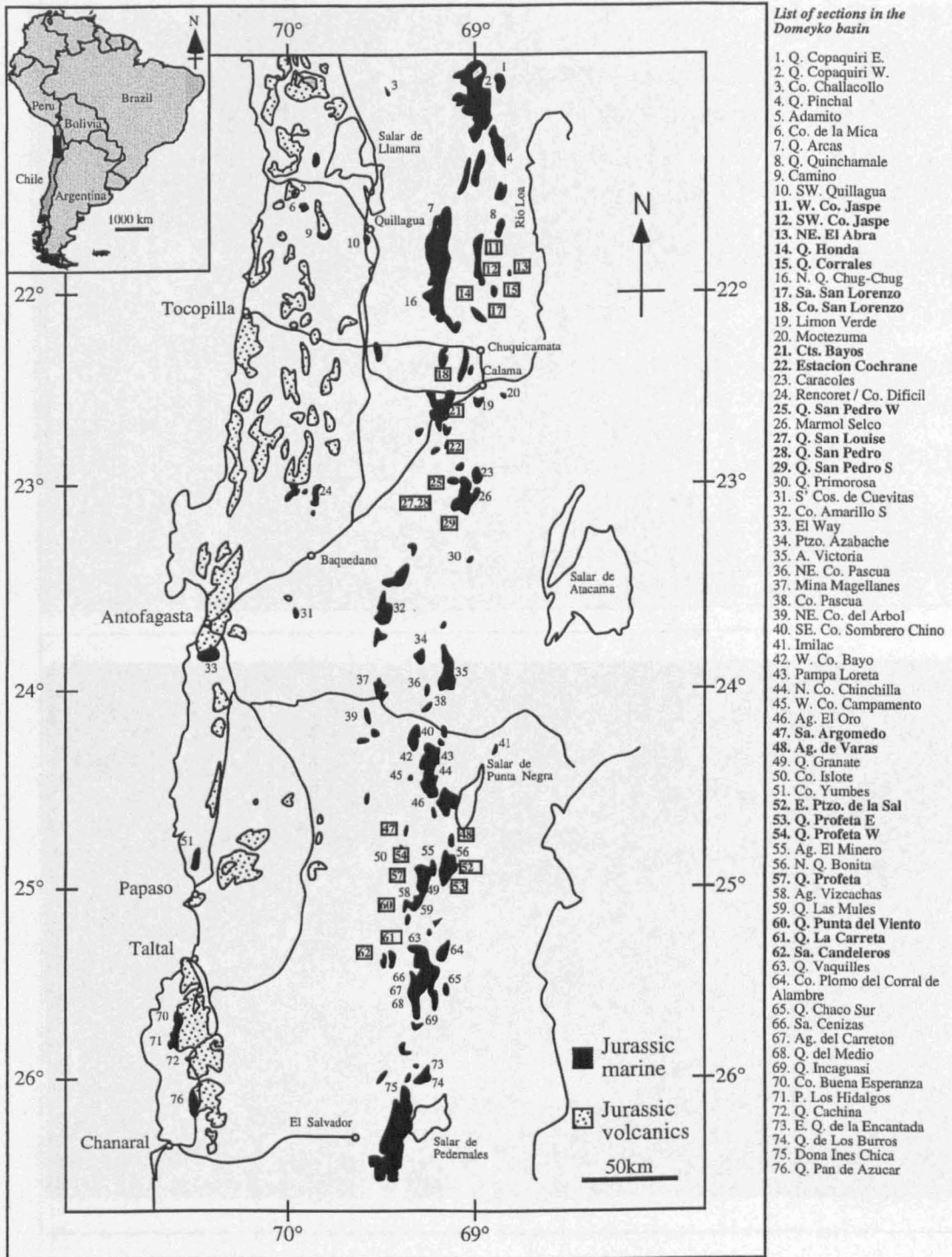


Figure 1.1 Part A Map of Northern Chile showing the Jurassic volcanic arc (La Negra Formation) in stipple outcropping along the Coastal Cordillera and the Jurassic marine rocks in black outcropping predominately along the Chilean Precordillera, (modified from Prinz et al. 1994). The list of Jurassic sections is given with the logged sections highlighted in bold and boxed on the map. **Part B** (overleaf) shows a view looking east at the Domeyko Range at approximately 25°S.



Figure 1.1 *Part B* shows a view looking east at the Domeyko range at approximately 25°S. The core of the Domeyko range is composed of pale brown Palaeozoic volcanic and intrusive basement, flanked by dark purple Triassic syn-rift volcanics and yellow Jurassic post-rift marine rocks. The Jurassic marine rocks in these two photos are from the Quebrada Profeta area (Figure 1A, locality 57) ranging from Bajocian (Middle Jurassic)-Kimmeridgian (Late Jurassic) in age.

1.2 Layout of thesis

Chapter 2 Geological Setting

A detailed literature review of the geological setting of northern Chile from Precambrian to recent times is presented. Firstly, plate tectonic reconstructions of the circum-Pacific region are assessed for the Palaeozoic and subsequent Mesozoic-Cenozoic. The regional geology and structural evolution of northern Chile is integrated to produce a geodynamic evolution for the Palaeozoic Preandean Cycle and Mesozoic-Cenozoic Andean Cycle. Finally, palaeoclimate and oceanography is assessed for the Jurassic Period.

Chapter 3 Biostratigraphy

A review of the Jurassic time-scales is given with the numerical time-scale used in this thesis. Subsequently, the Southern Andes ammonite zones are defined with their correlation back to the Standard European ammonite Zones. Ammonite biogeography is assessed highlighting the key biostratigraphical events of regional and global significance.

Chapter 4 Depositional environments

The Mesozoic sedimentary succession in northern Chile is subdivided into facies on the basis of process sedimentology and characteristic internal structures. The subsequent integration of these facies units into facies associations allows the development of depositional models for each environment.

Chapter 5 Sequence stratigraphy

Firstly, the previously published lithostratigraphical interpretations for the Domeyko basin succession are considered along with the implications of a lithostratigraphical approach to correlation. Sequence stratigraphical analysis of the Domeyko basin succession has identified five second-order unconformity-bounded sequences. The correlation of key chronostratigraphical surfaces, constrained within the ammonite biostratigraphy, has allowed an analysis of both the stratigraphical evolution of the Domeyko basin succession and subsequently second-order changes in relative sea-level. Within these second-order cycles a higher-frequency cyclicity has been identified and is discussed in this chapter.

Chapter 6 Controls on sequence development

The relative sea-level fluctuations interpreted from the Domeyko basin succession are compared with those documented from other similar aged South American marginal basins and northern hemisphere basins to distinguish regional from global events, and differentiate between eustatic and tectonic driving mechanisms. A plate tectonic model is presented to account for the continental-scale tectonic events which affect the marginal basins of western Gondwana.

Chapter 7 Conclusions

A summary of the conclusions to this thesis are presented.

Chapter 2

Geological Setting

2.1 Objectives of chapter

The first objective of this chapter is to review the plate tectonic reconstructions of the circum-Pacific region for the Palaeozoic and Mesozoic-Cenozoic. Secondly, an extensive literature review of the regional geology and structural evolution of northern Chile with the aim of developing a linked geodynamic evolution of the Central Andes. Finally, the palaeoclimate and oceanography of northern Chile have been considered for the Jurassic Period.

2.2 Plate reconstructions of the circum-Pacific region

The plate tectonic reconstructions for the Palaeozoic-Early Mesozoic are entirely based on the distribution and ages of orogenic belts and oceanic sequences, including seamounts and pelagic sediments accreted to the margins of various terranes (Scotese & McKerrow, 1990; Dalziel, 1991; Dalziel *et al.*, 1994). Mesozoic-Cenozoic plate reconstructions are further constrained from sea-floor spreading isochrons as demonstrated by Scotese *et al.* (1988).

2.2.1 Palaeozoic

Bond *et al.* (1984) used tectonic subsidence analysis of ancient passive margin rocks to constrain the break-up of the Late Proterozoic supercontinent, comprising Gondwana, Laurentia, Baltica and Siberia (Piper, 1976; 1983; Ziegler *et al.*, 1981; Morel & Irving, 1978) to between 625 Ma and 555 Ma (Early Cambrian).

Nance *et al.* (1988) built on the Wilson Cycle, by which continents rift to form ocean basins and the ocean basins later close to reassemble the continents. They concluded that the processes of plate tectonics are governed by a regular, cyclic process, noting that the margins of the North Atlantic have undergone a series of Wilson Cycles during the past billion years; the regions bordering the Pacific have apparently undergone none.

Scotese & McKerrow (1990) suggested from palaeobiology and palaeoclimatology that the Upper Proterozoic supercontinent was composed of Laurentia, Baltica and Siberia which disintegrated as Gondwana formed, about 600 Ma. They supported the interpretation of Nance *et al.* (1988), stating that the western margin of South America has always been adjacent to oceanic crust, hence not having undergone a complete Wilson Cycle, as shown in Fig. 2.1.

Dalziel (1991) and Dalziel *et al.* (1994) took a radically different view based on geological and palaeobiological evidence, whereby Laurentia broke from the Upper Proterozoic supercontinent at about 570 Ma (Early Cambrian). Figure 2.2 shows the Appalachian margin of Laurentia colliding with the proto-Andean margin of Gondwana during the Middle Ordovician, before continuing in a clockwise direction and colliding with north-west Africa during the Late Palaeozoic construction of Pangaea. The theory of Dalziel *et al.* (1994) is important as it proposes the proto-Andean margin has; 1. undergone more than one Wilson Cycle, and 2. subduction was stopped between the Middle Ordovician collision and Middle to Late Palaeozoic movement of Laurentia past the Andean margin.

Although the model of Dalziel (1991) and Dalziel *et al.* (1994) is radically different to previous ideas, it may better explain the present day complex structural “grain” of the Central Andes. This degree of structural complexity is unusual for an area which has apparently undergone no Wilson Cycles.

The two opposing models for Early Palaeozoic plate reconstructions both begin and end with similar plate tectonic configurations. Originating with an Upper Proterozoic supercontinent which disintegrates in the Late Precambrian; and culminating in the creation of Pangaea at about 300 Ma (Late Carboniferous), resulting in the formation of the Appalachian, Ural and Mauritande mountain belts (Nance *et al.*, 1988) and a supercontinent stretching from pole to pole (Scotese & McKerrow, 1990).

2.2.2 Mesozoic-Cenozoic

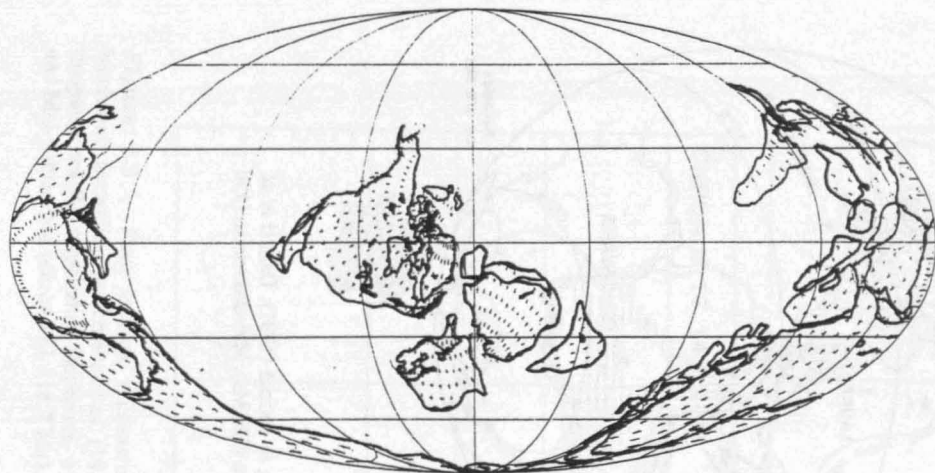
Scotese *et al.* (1988) demonstrated how magnetic sea-floor spreading isochrons can be systematically reconstructed back to the Early Cretaceous. The accuracy of these maps can be evaluated by observing the closure of plates around triple junctions and by noting the predicted relative motion of plates across complex plate circuits (eg. the motion of the Pacific plate relative to North America). Isochrons in the north and central Atlantic, and along the south-west Indian Ridge can be reconstructed with few gaps or overlaps. In the south Atlantic and central Indian Ocean, however, the match between isochrons is not as good, especially for the older reconstructions.

Scotese *et al.* (1988) concluded that the major events seen in the Mesozoic-Cenozoic are:

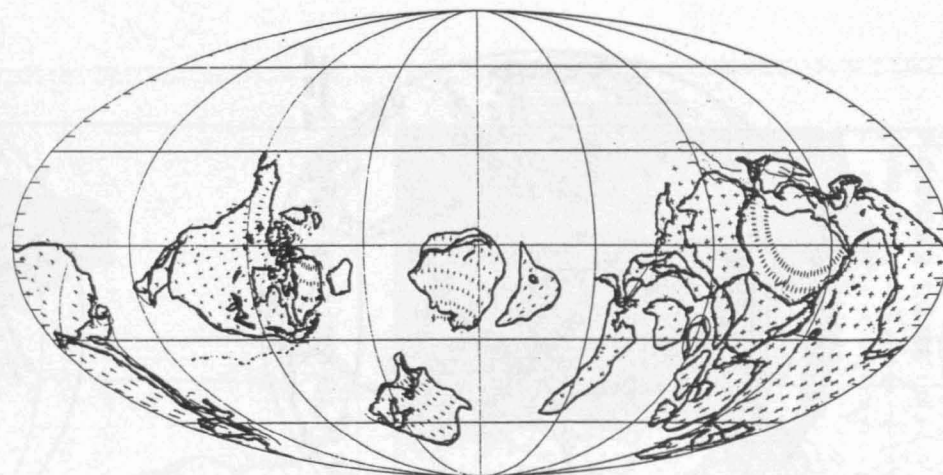
1. *The break-up of Pangaea which began in the Middle Jurassic and continued into the Early Cretaceous*
2. *The break-up of North America and Africa which was preceded by extension and rift related volcanic activity that started in the earliest Jurassic*
3. *Sea-floor spreading in the south Atlantic and between India and the Antarctica which appears to have started in the Early Cretaceous*
4. *The Late Tertiary break-up of the Farallon plate to form the Cocos and Nazca plates.*

The starting point for a discussion of the Mesozoic basin evolution in northern Chile must be an analysis of the break-up and dispersal history of Pangaea. The term “Pangaea”, meaning “all land”, has been used to imply that at some point during the Late Palaeozoic or Early Mesozoic all of the continental crust of the world was amalgamated into a single supercontinent. Subsequently, that supercontinent progressively disintegrated to arrive at the modern, quite widely dispersed continental configuration. Rowley (1992) concludes that a true Pangaea may never have existed, based on the Late Triassic welding of southern Asia to Laurasia and the disintegration of northern Gondwana which, according to Sengör *et al.*, (1988), had begun during the Late Permian and came into being no later than the Middle to Late Triassic.

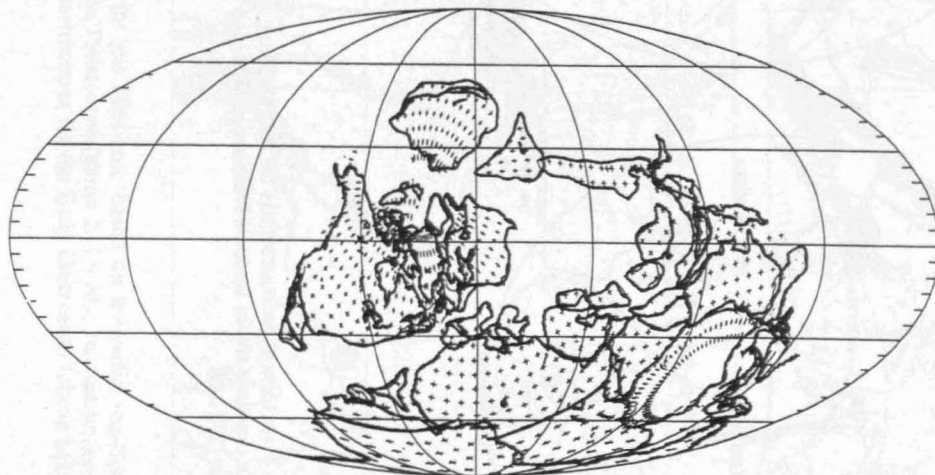
The plate tectonic reconstructions of Scotese *et al.* (1988) highlight the break-up of Pangaea into Laurasia (northern hemisphere) and Gondwana (southern hemisphere), followed by the fragmentation of Gondwana. The timing of Cretaceous continental dispersal can be seen on Fig. 2.3, depicting maps for Early Cretaceous, Chron M17 (143.8 Ma), Mid-Cretaceous, Chron M0 (118.7 Ma) and Late



Latest Precambrian



Cambro-Ordovician (Tremadoc)



Late Early Devonian (Emsian)



Early Permian (Artinskian)

Figure 2.1 Plate tectonic reconstructions for the Palaeozoic according to Scotese & McKerrow (1990). The reconstructions are for the latest Precambrian, Cambro-Ordovician, late Early Devonian and Early Permian.

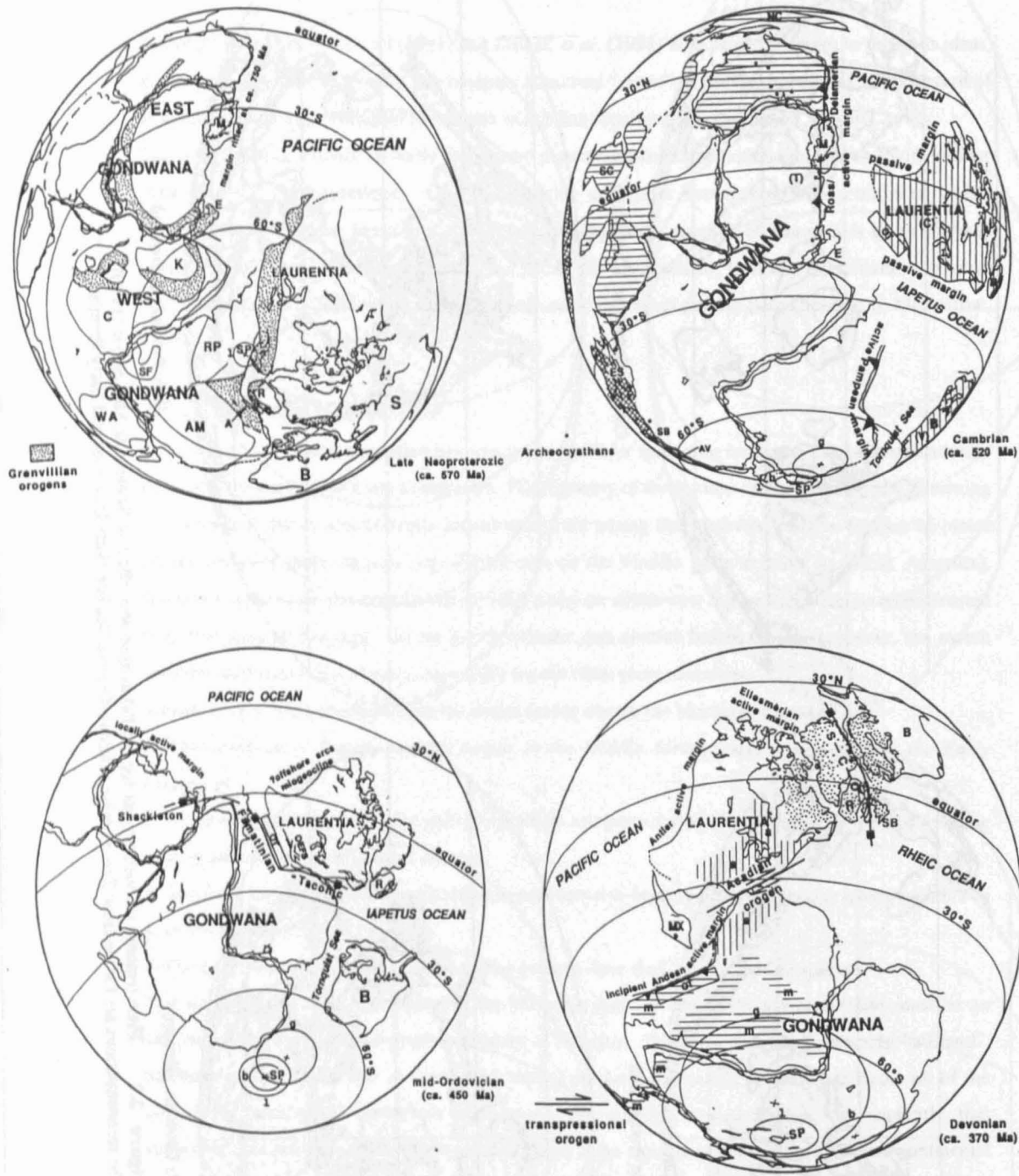


Figure 2.2 Plate tectonic reconstructions for the Palaeozoic according to Dalziel (1991); Dalziel *et al.* (1994). The reconstructions are for the latest Precambrian (570 Ma), Cambrian (520 Ma), Mid-Ordovician (450 Ma) and Devonian (370 Ma).

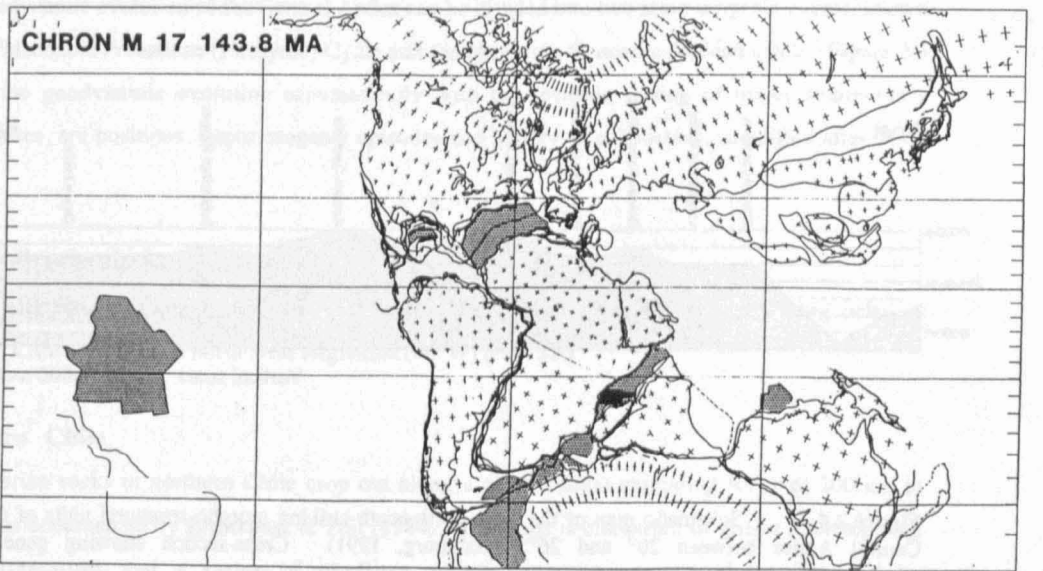
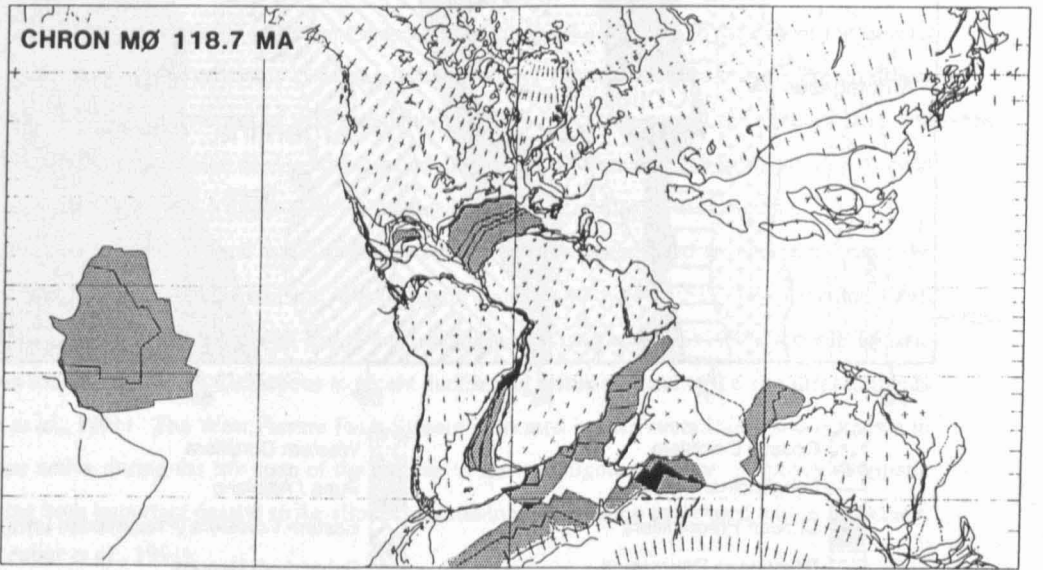
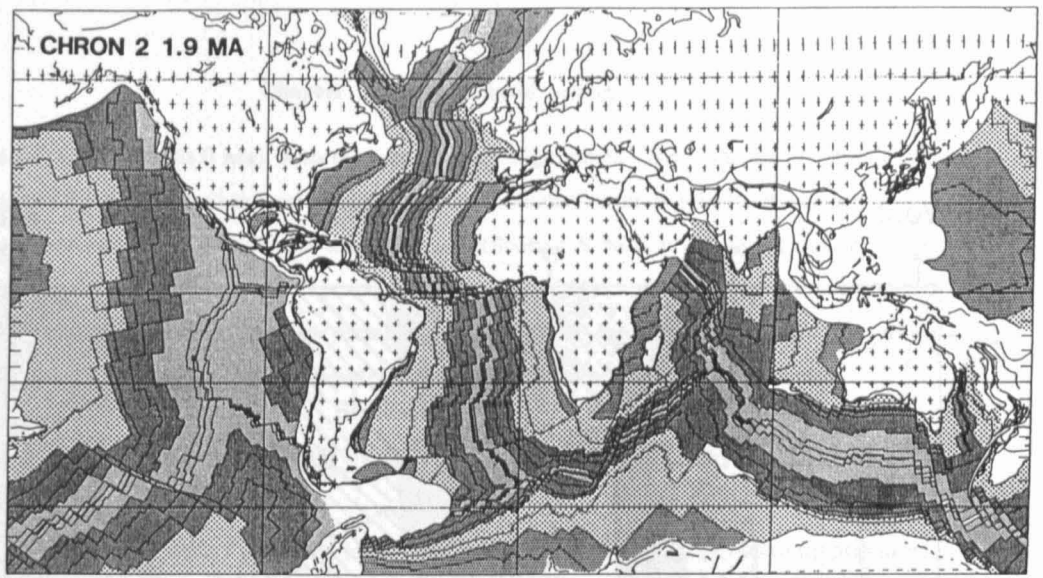


Figure 2.3 Plate tectonic reconstructions for the Mesozoic based on magnetic sea-floor spreading isochrons, according to Scotese *et al.* (1988). The Pleistocene (chron 2, 1.9 Ma) reconstruction displays the magnetic sea-floor spreading isochrons, with reconstructions for the Early Cretaceous (chron M17, 143.8 Ma) and Mid-Cretaceous (chron M0, 118.7 Ma).

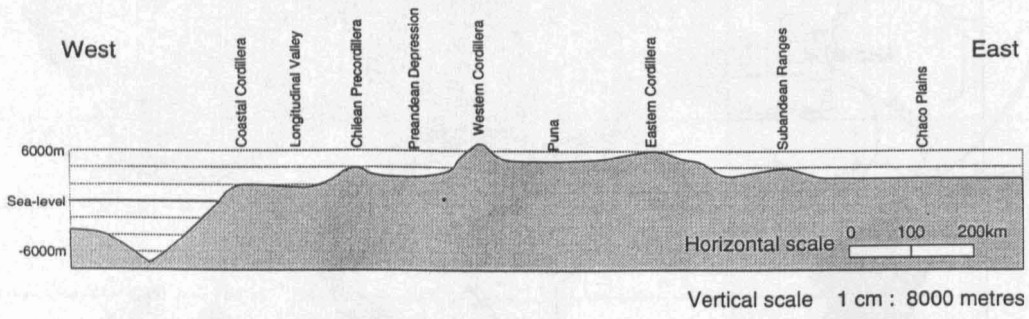
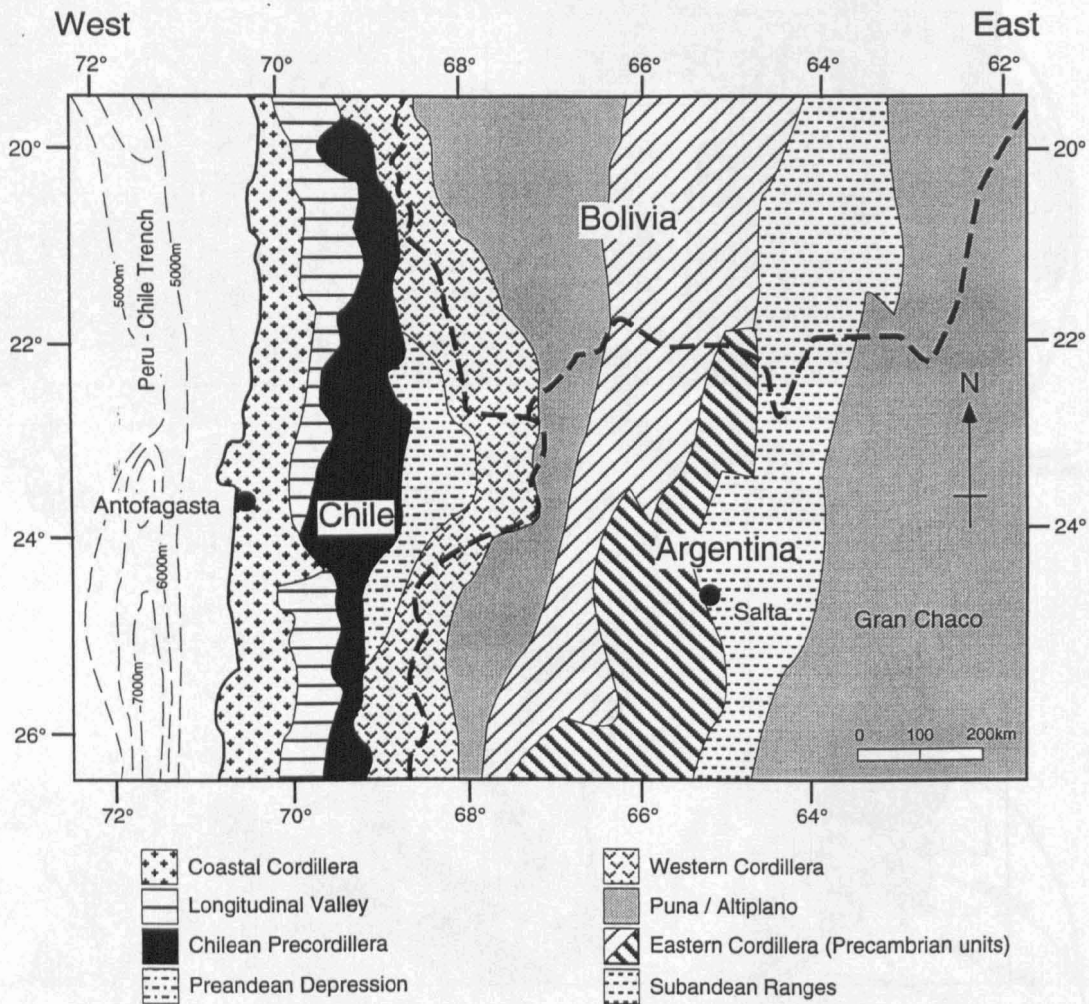


Figure 2.4 Schematic map of the main north-south striking morpho-structural units of the Central Andes between 20° and 26°S (Bahlburg, 1991). Cross-section showing general topographic profile from west to east.

Cretaceous, Chron 34 (84.0 Ma), with the area of study highlighted. Since the Early Jurassic, the west coast of South America has been a convergent plate boundary bordering the Pacific Ocean.

The plate tectonic reconstructions for the Palaeozoic (Scotese & McKerrow, 1990; Dalziel, 1991; Dalziel *et al.*, 1994) and Mesozoic-Cenozoic (Scotese *et al.*, 1988) highlight a complex continental dispersal history. However, the plate tectonic history must be carefully considered if we are to understand the driving mechanism behind Mesozoic basin development in the Central Andes.

2.3 Regional geology and structural evolution of northern Chile

Northern Chile can be broadly divided into five north-south striking morpho-tectonic provinces, shown in Fig. 2.4. The Coastal Cordillera forms a range of mountains with elevations over 2000 m representing the Lower Jurassic to Lower Cretaceous volcanic arc. Directly to the east of the Coastal Cordillera is the wide and relatively flat Longitudinal Valley. Further to the east is the Pre-cordillera range with elevations in excess of 4000 m (Chong, 1977). Lying between the Precordillera and Western Cordillera, the Salar de Atacama and smaller Salar de Punta Negra form the Pre-Andean depression which represents a major offset in the linear Western Cordillera (High Andes).

Two major north-south, crustal scale fault systems have been recognised in northern Chile, the Atacama Fault System (AFS) and the West Fissure Fault System (WFFS). The Atacama Fault System is situated within the Coastal Range and, according to Grocott *et al.*, (1995), records Triassic extension followed by Early Cretaceous to recent ductile and brittle sinistral strike-slip displacements (Brown *et al.*, 1991). The West Fissure Fault System is located in the Precordillera and is known to have been active during the life span of the Eocene to Lower Oligocene copper porphyry magmatic arc, having both important dextral strike-slip and shortening deformation associated with it (Maksaev, 1990; Reutter *et al.*, 1991).

The geodynamic evolution of the Central Andes can be divided into two main orogenic events, known as the Palaeozoic Preandean (Hercynic) Cycle and the Mesozoic-Cenozoic Andean Cycle. Figure 2.5 shows the geodynamic evolution schematically with the tectonic setting of major sedimentary depocentres, arc positions, major orogenic episodes and history of subduction, (modified after Toth, 1995).

2.3.1 Precambrian basement

The Precambrian basement rocks of the Central Andes form two north-south striking belts, in northern Chile (69°W) and north-west Argentina (66°W) (Fig. 2.6).

Northern Chile

Precambrian rocks in northern Chile crop out along a narrow horst extending for over 100 km in length, as documented by Breitzkreuz & Zeil (1984). The horst is composed of gneiss interfingering with migmatites and a series of phyllites which have subsequently been intruded by Ordovician/Silurian granites. Breitzkreuz & Zeil (1984) dated the migmatites using U/Pb to be 1260

\pm 30 Ma. Further Precambrian ages of 1730 Ma have been obtained by Damm *et al.* (1981) from zoned zircons in Upper Palaeozoic anatectic plutons of the Coastal Cordillera. Damm *et al.* (1986) have given widely accepted Early Cambrian dates of 534 \pm 120 Ma for the Mejillones Peninsula, however, according to Breitskreuz & Zeil (1984) part of the peninsula may have been a Precambrian inlier, once representing a southern extension of the Arequipa Massif of Peru.

North-west Argentina

Coira *et al.* (1982) and Allmendinger *et al.* (1983) interpret the Puncoviscana Formation of north-west Argentina as representing the Upper Precambrian-Cambrian passive margin of western Gondwana, cropping out along the Faja Eruptiva de la Puna. Acenolaza & Durand (1986) document metamorphosed greywackes and shales with interbedded ultra-basic volcanics, increasing in metamorphic grade from greenschist facies in the north, to medium- to high-grade facies further south (Coira *et al.*, 1982). The greywackes are interpreted as turbidites (Coira *et al.*, 1982; Acenolaza & Durand, 1984; 1986) indicating a deep marine basin trending from north-east to south-west, bounded by the Arequipa Massif to the west and the Brazilian Shield to the east. Rifting of the South American craton has been proposed by Dalmayrac *et al.* (1980) but as yet, no rift-related volcanics have been identified to support the theory.

Turner (1970) describes granodioritic and granitic intrusions, which, according to Turner & Mon (1979) and Halpern & Latorre (1973) are of Precambrian-Cambrian boundary age, 601 \pm 65 Ma (Turner & Mon, 1979), however these dates are questioned by Breitskreuz (1986b). Breitskreuz & Zeil (1984) pointed out that Precambrian dates from the Chilean basement are compatible with the ages of both the Arequipa Massif (Dalmayrac *et al.*, 1977; Shackleton *et al.*, 1979) and orogenic events within the South American craton (Zeil, 1981).

Ramos (1988) proposed a collisional history for the southern portion of South America based on a complex collage of cratonic blocks which were brought together along the south-western margin of Gondwana in Late Precambrian-Early Palaeozoic times. The model of Ramos (1988) for the docking of cratonic blocks is based on the distribution of mafic and ultra-mafic oceanic rocks, ancient magmatic arcs and the metamorphic and sedimentary sequences of these old orogenic belts. The Late Precambrian-Early Palaeozoic amalgamation of cratonic blocks to form Gondwana (Ramos, 1988) is partly coincident with the Early Palaeozoic Pampean Orogeny, signifying the break-up of the Upper Precambrian supercontinent. Subduction began in the Late Cambrian and the proto-Andean margin of Gondwana changed from a passive to active plate boundary, noted by Willner *et al.* (1987).

The Precambrian basement rocks of the Central Andes have a long and complex history recording the docking of cratonic blocks in the Late Precambrian to Early Palaeozoic (Pampean Orogeny), followed by the break-up of the Upper Precambrian supercontinent and initiation of subduction in Cambrian times (Ramos, 1988).

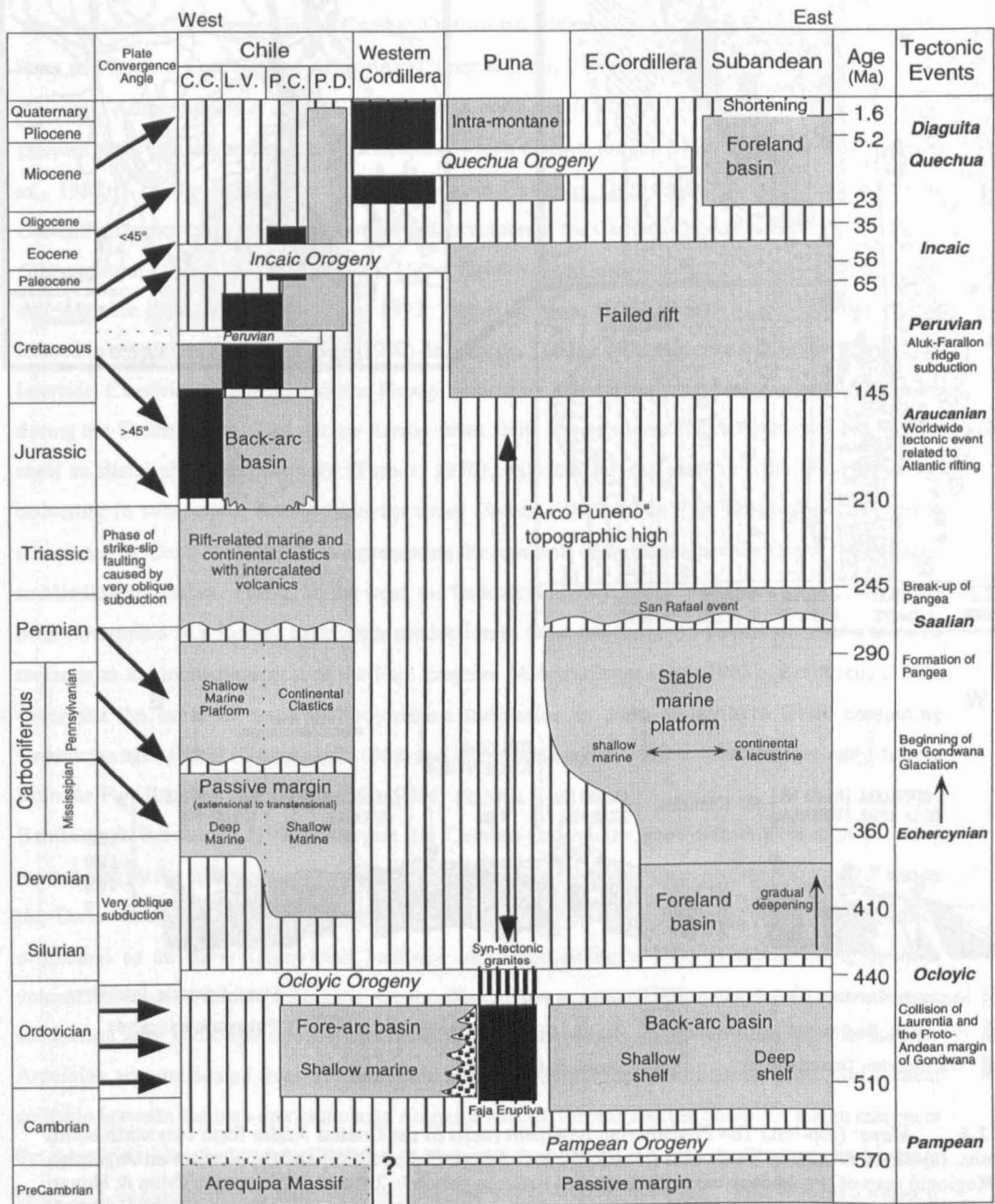


Figure 2.5 Schematic geodynamic evolution of the Central Andes. Showing tectonic setting of major sedimentary depocentres (grey boxes), arc position (black boxes), major orogenic episodes (open boxes) and history of subduction. Modified after Toth (1995). Based on the work of Allmendinger *et al.* (1983); Bahlburg & Breitzkreuz (1991); Bahlburg & Breitzkreuz (1993); Bahlburg (1993); Bahlburg *et al.* (1994); Breitzkreuz (1992); Coira *et al.* (1982); Mpodozis & Kay (1992); Ramos (1994); Scheuber *et al.* (1994); Willner *et al.* (1987).

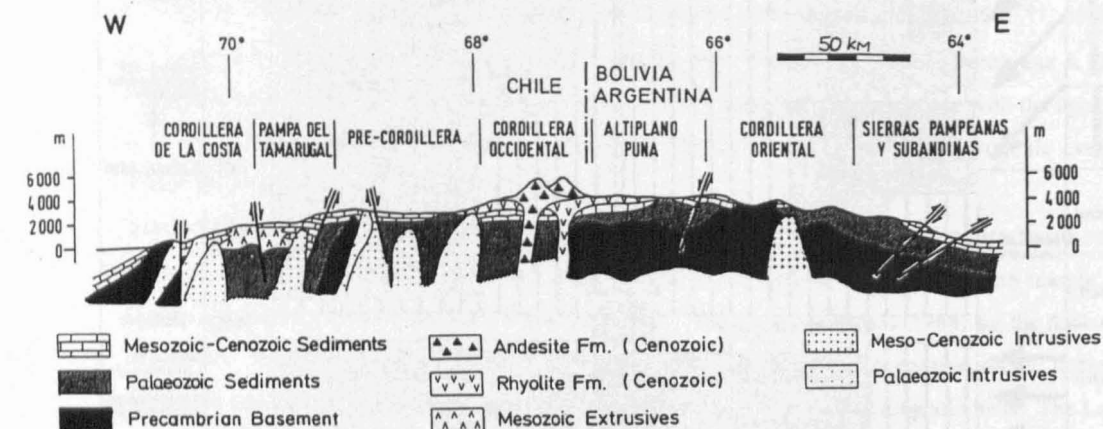
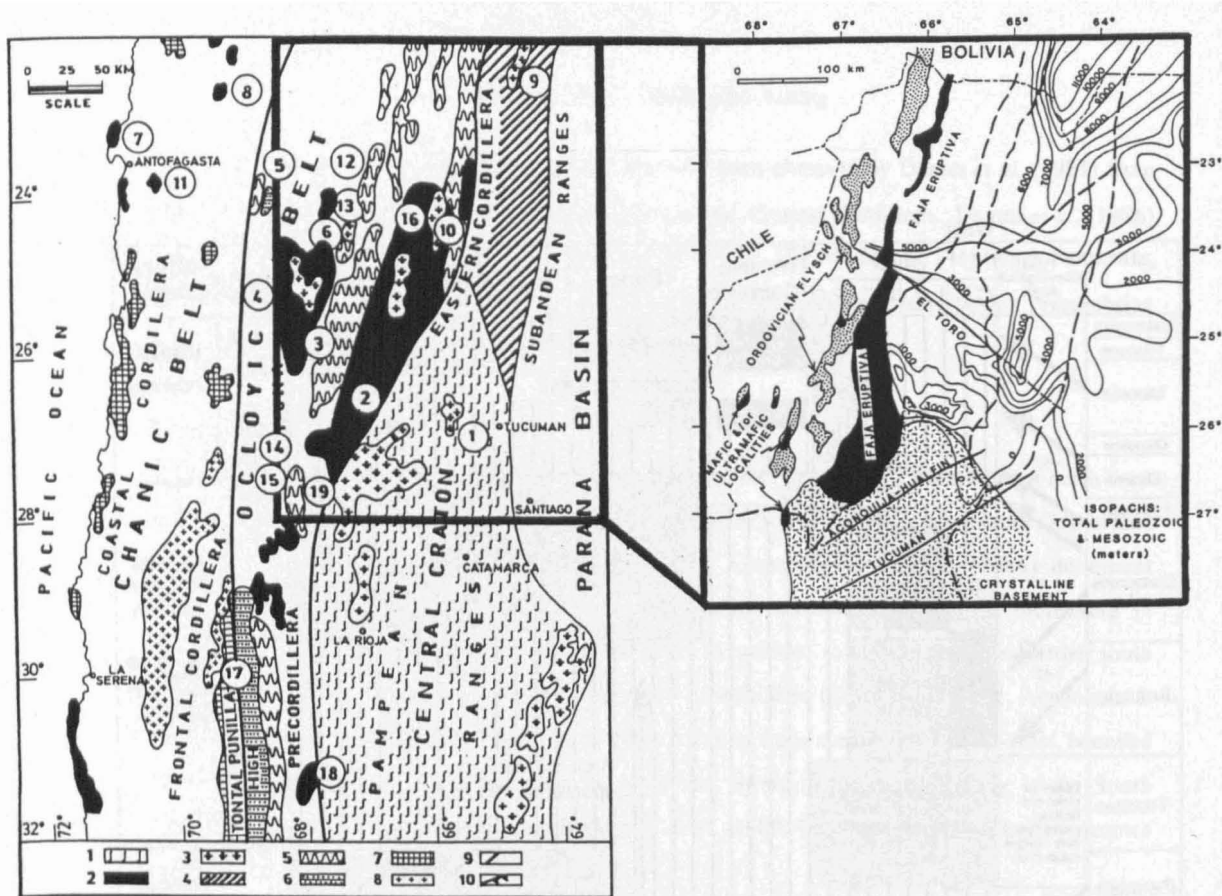


Figure 2.6 *Maps:* (top-left) The Precambrian basement rocks of the Central Andes form two north-south striking belts, (a) Sierra de Limón Verde area (locality 8) in Northern Chile (69°W) and (b) North-west Argentina (66°W). Regional map of the Andean basement outcrops between parallels 22° and 32°S latitude (Mon & Hongn 1991). 1. Crystalline basement of the Central Craton (Pampean Basement); 2. Slabs of crystalline basement included in the oclroyic and chanic belts; 3. Precambrian and Lower Palaeozoic granitoids; 4. Unfolded Cambrian and Ordovician cover of the crystalline basement; 5. Cambrian and Ordovician beds folded by the Oclroyic Orogeny; 6. Unfolded Devonian cover of the oclroyic belt; 7. Devonian beds folded by the Chanic Orogeny; 8. Permian and Triassic granitic bodies. List of localities: 1. Rio Lules; 2. El Peñón; 3. Salar Antofalla; 4. Sierra de la Quebrada Honda; 5. Cerros Lila; 6. Cumbres de Macón; 7. Mejillones; 8. Sierra de Limón Verde; 9. Cañan; 10. Tastil; 11. Salar de Navidad; 12. Aguada de la Perdiz; 13. Salar de Pocitos; 14. Cordillera de San Buenaventura; 15. Chaschuil; 16. San Antonio de los Cobres; 17. Valle de Jáchal; 18. Pie de Palo; 19. Famatina. (top-right) Detailed map of north-west Argentina, showing the major palaeogeographic elements. Heavy dashed lines show outlines of Neogene tectonic provinces. Dashed pattern shows extent of crystalline mechanical basement; note coincidence with the Neogene Sierras Pampeanas. Puncoviscana Formation (black), locally intruded by Late Precambrian granites, everywhere underlies the Palaeozoic and Mesozoic strata north of the crystalline basement (Allmendinger *et al.* 1983). *Cross-section:* Idealised cross-section of the Preandean structure showing the Precambrian basement in black (Mon & Hongn 1991).

2.3.2 Preandean Cycle (Palaeozoic)

Cambro-Ordovician basins

The Preandean Cycle began in the Cambro-Ordovician with a wide marine basin extending over the Puna and Eastern Cordillera of Argentina (Turner & Mon, 1979; Bahlburg & Breitreuz, 1991). To the west, Allmendinger *et al.* (1993) describe a north-south belt of Lower- to Middle-Ordovician granites and volcanics termed the Faja Eruptiva which extends the full 1300 km of the Puna (Coira *et al.*, 1982). To the west of the Faja Eruptiva, in Chile, an Ordovician marine basin is present. Currently, there are two interpretations for the formation of the Cambro-Ordovician basins.

Allmendinger *et al.* (1983) interprets the Upper Cambrian to Devonian coarse- to fine-grained clastic and volcanic shelf deposits (Schwab, 1973; Turner & Mon, 1979; Willner *et al.*, 1987) as having formed in a back-arc setting. Turner (1970) described a 3100 m thick sequence of shallow-marine and intertidal Cambrian sediments (Meson Group) indicating a dominantly shallow-marine environment during the Tremadocian. Ordovician-Arenig times show a west to east facies zonation from shallow shelf to distal shelf, respectively (Turner, 1970), with the largest extent of the Ordovician sea occurring in subsequent Arenig-Llanvirn times (James, 1971). The Faja Eruptiva to the west is interpreted by Coira *et al.* (1982) as representing the remnants of a volcanic arc developed in the Early- to Middle-Ordovician. Further to the west, the Ordovician flysch deposits of Coira *et al.* (1982) have been interpreted as a forearc basin with subduction to the west, based on the presence of a tectonic melange to the immediate west of the Faja Eruptiva (Allmendinger *et al.*, 1983). Breitreuz (1985) described the basin-fill as a shallow-marine succession in parts of northern Chile containing Ordovician aged fossils (Garcia *et al.*, 1962) and interbedded with extensive volcanics, probably derived from the Faja Eruptiva (Bahlburg *et al.*, 1986).

Bahlburg & Breitreuz (1991) interpret the Cambro-Ordovician geodynamic evolution as being represented by the westward progression of orogenic basin formation through time. Figure 2.7 shows the Ordovician basin in north-west Argentina (Bahlburg, 1990; Bahlburg *et al.*, 1990) which originated as an Early Ordovician back-arc basin containing a 3500 m thick, fining-upward, volcanoclastic apron formed during the Arenig. The contemporaneous magmatic arc of an east-dipping subduction zone is thought to have been located in northern Chile. Increased subsidence in the Late Arenigian accommodated thick volcanoclastic turbidites during the Middle-Ordovician. Subsequent collision between the para-autochthonous Arequipa Massif Terrane and the South American margin at the Arenigian-Llanvirnian transition, led to eastward thrusting of the arc complex over its back-arc basin and, consequently, to its transformation into a marine foreland basin. This thrusting event is supported by the contact between the Faja Eruptiva and eastern, Ordovician back-arc basin always being tectonic (Allmendinger *et al.*, 1983). The back-arc basin-fill was then folded during the terminal collision of the Arequipa Massif Terrane in the Ocluyic Orogeny (Ashgillian) with subsequent post-tectonic intrusion of Silurian granitoids along the Faja Eruptiva and formation of the north-south positive relief area of the Arco Puneño. West of the Arco Puneño an Early Devonian marine basin developed with shelfal deposits extending from the Western Cordillera to the Chilean Precordillera and deep marine turbidites to the west, in the region of the Coastal Cordillera. The basin originated as an

extensional structure at the continental margin of Gondwana and is not thought to be related to subduction and hence not a fore-arc basin (Bahlburg & Breitskreuz, 1991), as previously postulated (Allmendinger *et al.*, 1983).

Breitskreuz (1986b) pointed out that no Cambrian igneous activity has been recorded from the Central Andes, with Ordovician calc-alkaline plutonics occurring in two longitudinal belts coincident with Precambrian basement along 69° and 66°W (Huete *et al.*, 1977; Halpern, 1978; Rapela *et al.*, 1982; Breitskreuz, 1986b). The Ordovician plutonics are thought to have been intruded syn-, late- and post-tectonically (Breitskreuz, 1986b). Coira *et al.* (1982) described extensive acid to intermediate volcanism in north-west Argentina and southern Bolivia during the Ordovician. Plutonism and volcanism climaxed at the Ordovician/Silurian boundary associated with the Oclöyic deformation phase.

The Cambro-Ordovician records shallow-marine deposition in a back-arc and fore-arc basin pair, separated by the Ordovician volcanic arc situated along the Faja Eruptiva de la Puna. The Oclöyic Orogeny in the Ashgillian (Late Ordovician) caused compression within the marine basins and thrusting related to syn-tectonic granite emplacement along the Faja Eruptiva de la Puna.

Oclöyic Orogeny

The Oclöyic Orogeny (Ashgillian) is thought to represent the closure of the ocean basin lying between Laurentia and western Gondwana (Dalziel, 1991; Dalziel *et al.*, 1994; Bahlburg, 1993). This collision is marked by a climax in volcanic and plutonic activity, with emplacement of syn-tectonic granites along the Faja Eruptiva and uplift of the Arco Puneño topographic high (Coira *et al.*, 1982). Mon & Hongn (1991) interpreted the Faja Eruptiva as a belt of Precambrian basement thrust over an Ordovician succession, based on the contact always being tectonic (Allmendinger *et al.*, 1983).

Silurian-Early Carboniferous Basins

Silurian-Carboniferous deposition occurred in two depocentres separated by the Arco Puneño topographic high. The eastern depocentre records Mid-Silurian to Mid-Devonian sediments in the region of the Eastern Cordillera and Subandean (Coira *et al.*, 1982), while the western depocentre records a Devonian marine basin which deepened to the west (Bahlburg & Breitskreuz, 1991). There are no Silurian or Devonian sediments in the area of the Puna, indicating that the Arco Puneño was a topographic high.

The eastern depocentre contains greater than 2000 m of shallow-marine shales thought to have been deposited in a foreland basin setting, related to the Oclöyic deformation to the west (Allmendinger *et al.*, 1983). Turner (1970) described the Upper Silurian 30 m thick Mecoyita Formation composed of quartz sandstones and matrix-supported conglomerates, which is unconformably overlain by the 1600 m thick Lipeon Formation of shaly sandstone with oolitic ironstones at the base. This succession is interpreted by Turner (1970) as representing the gradual deepening of a restricted shallow-marine basin. The Upper Silurian succession is conformably overlain by the Lower Devonian (Harrington, 1967) Baritu Formation of Turner (1970), composed of a 2400 m thick unit of shallow-marine sandstone and

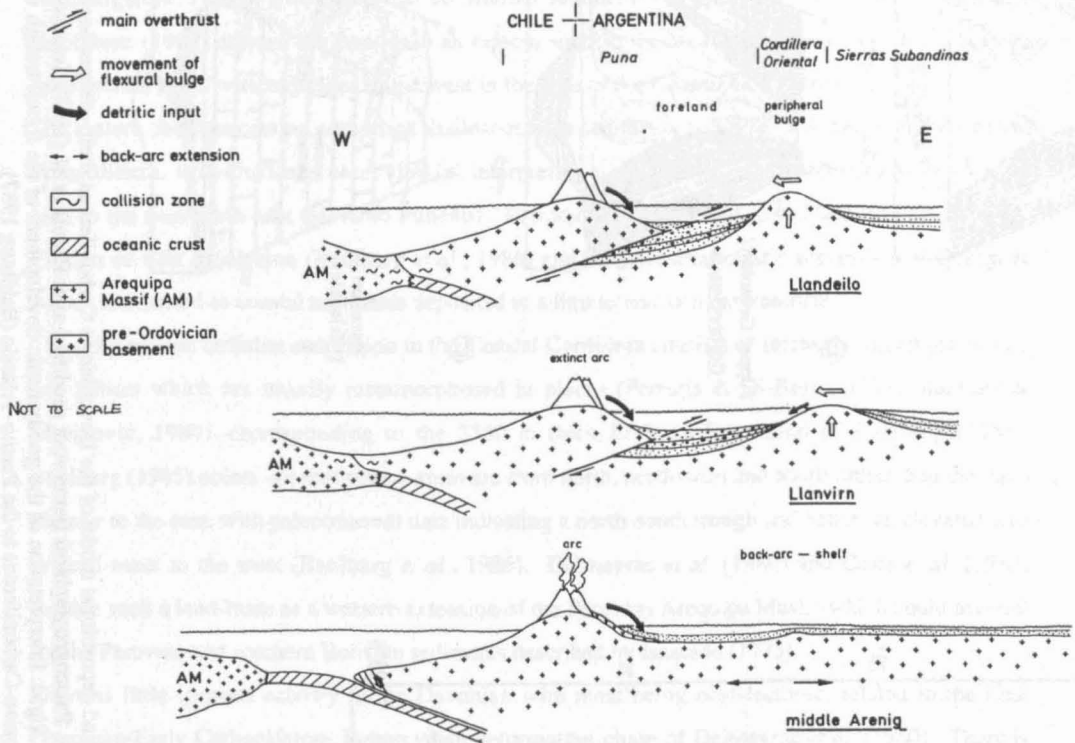
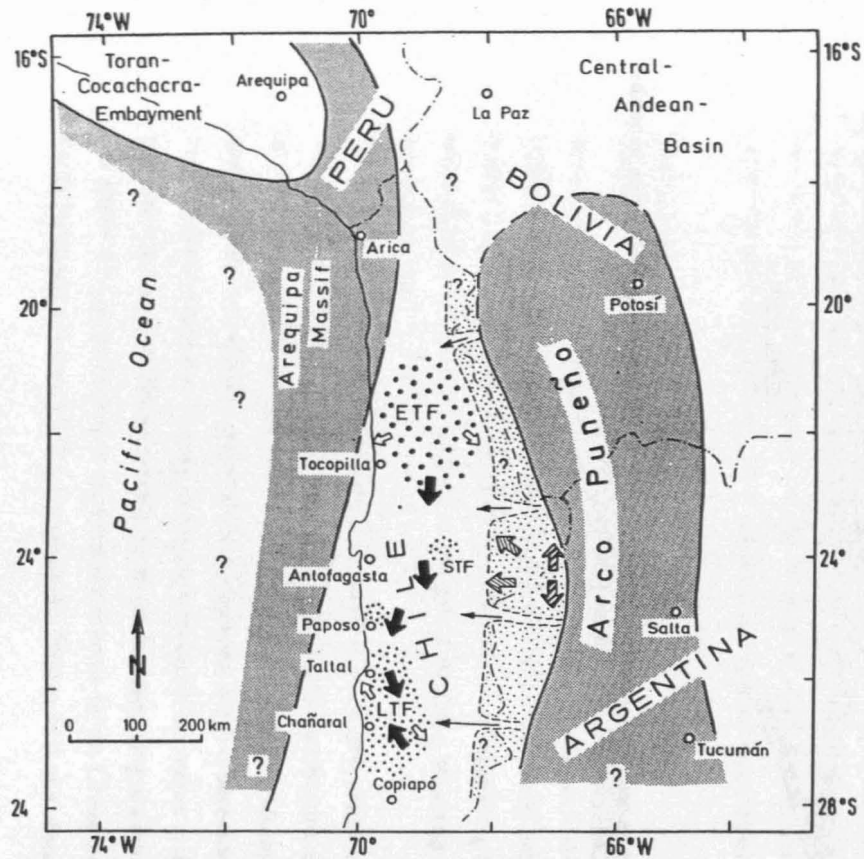


Figure 2.7 Hypothetical cross-sections depicting tectonic evolution of the Gondwanaland margin in north-western Argentina and northern Chile during the Ordovician (Bahlburg 1991).



Palaeocurrents

- ➔ flutes
- ➡ T_c foresets
- ➡ foresets, ebb currents
- ➡ longshore currents
- ➡ inferred bypasses
- proximal sandstone lobes
- lobe fringe to basin plain
- shelf

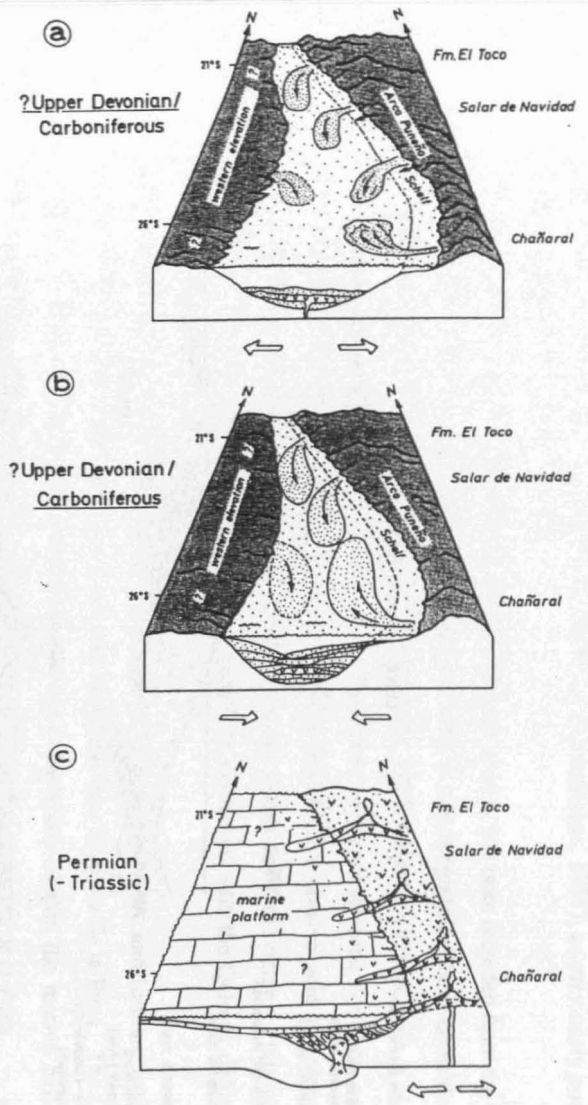


Figure 2.8 *Left:* Palaeogeographical framework and depositional model of the Devonian to Carboniferous shelf - deeper basin system in northern Chile (Bahlburg & Breitkreuz 1993). Palaeogeographical framework modified after Padula *et al.* (1967); Isaacson (1975); Bahlburg (1987); Isaacson & Sablock (1989). *Right:* Interpretation of the geodynamic development of the flysch trough in the north Chilean Coastal Cordillera from the Late Devonian-Carboniferous to the Permo-Triassic (Bahlburg 1987).

shale. The eastern boundary of the basin is unknown (Coira *et al.*, 1982), however similar facies have been found in southern Bolivia and southern Peru (Isaacson, 1975).

The western depocentre is represented by Lower Devonian-Lower Carboniferous deposits (Herve *et al.*, 1981) of an extensional or transtensional passive margin setting (Bahlburg & Breitreuz, 1993). Chong (1977) reported possible Silurian sediments from the Precordillera but this is disputed by Bahlburg *et al.* (1986), who stated that no Silurian sediments occur due to emergence. Bahlburg & Breitreuz (1991) divided the basin into an eastern shelf in the area of the Western Cordillera and a deep marine basin with turbidites to the west in the area of the Coastal Cordillera (Fig. 2.8).

The eastern shelf succession comprises shallow-marine sediments at Sierra de Almeida in the Chilean Precordillera, with Davidson *et al.* (1981a) interpreting a prograding delta succession with a source area to the east/south-east (ie. Arco Puneño). Periodic emergence led to red-bed deposition of the Cordon de Lila succession (Bahlburg *et al.*, 1986) and the terrestrial clastic succession of Quebrada Arcas, interpreted as coastal sediments deposited in a limnic/brackish environment.

The deep marine turbidite succession in the Coastal Cordillera consists of intensely folded psammites and pelites which are heavily metamorphosed in places (Ferraris & Di-Biase, 1978; Maksiyev & Marinovic, 1980), corresponding to the 2300 m thick El Toco Formation of Bahlburg (1985). Bahlburg (1985) points out that source areas are from north, north-west and south rather than the Arco Puneño to the east, with palaeocurrent data indicating a north-south trough and hence, an elevated area or land-mass to the west (Bahlburg *et al.*, 1986). Dalmayrac *et al.* (1980) and Coira *et al.* (1982) include such a land-mass as a western extension of the Peruvian Arequipa Massif which could account for the Peruvian and southern Bolivian sediments described by Isaacson (1975).

There is little igneous activity in the Devonian with most being post-tectonic, related to the Late Devonian-Early Carboniferous Eohercynian deformation phase of Dalmayrac *et al.* (1980). There is abundant Carboniferous acid to intermediate, mainly calc-alkaline volcanism in the Chilean Andes, Argentine Puna and Eastern Cordillera (Huete *et al.*, 1977; Coira *et al.*, 1982; Rogers, 1985), with alkaline and tholeiitic (ultra-) basic volcanics which interfinger with Palaeozoic sediments in the Chanaral area (Bahlburg *et al.*, 1986). Omarini *et al.* (1979) interpret some reactivation of the Faja Eruptiva in the Late Devonian. The Late Devonian-Early Carboniferous Eohercynian tectonic event is associated with folding and plutonism, as well as a major change in Palaeozoic palaeogeography (Coira *et al.*, 1982).

The Silurian-Early Carboniferous records passive margin marine sedimentation in northern Chile and foreland basin deposition in north-west Argentina, separated by the newly uplifted Arco Puneño topographic high. In northern Chile, uplift associated with the Eohercynian deformation phase resulted in shallowing of the marine basin and unconformity formation.

Late Carboniferous-Late Permian basins

Late Carboniferous-Late Permian marks a transition period with the relocation of the locus of igneous activity from the interior (69°W to Puna) to the Jurassic volcanic arc in the Coastal Cordillera. Coira

et al. (1982) noticed two distinct phases of deposition during the Carboniferous-Early Triassic separated by the Mid-Permian Saalian tectonic event (San Rafael event in north-west Argentina).

The Carboniferous-Early Triassic of north-west Argentina is marked by deposition of shallow-marine limestones and sandstones in the Argentine Puna (Acenolaza *et al.*, 1972), which grade eastward into continental and lacustrine sediments in the region of the Eastern Cordillera and Subandean Ranges (Mingramm *et al.*, 1979; Coira *et al.*, 1982). A pronounced unconformity related to the San Rafael deformation event separates folded and faulted Silurian-Lower Permian shallow-marine strata from undeformed Upper Permian Choiyoi volcanic rocks (Mpodozis & Kay, 1992). Similar facies are seen in the Permian of southern Peru (James, 1971), thus indicating the large aerial extent of the Permian sedimentary basin.

In northern Chile, Carboniferous-Lower Permian limestones and siliciclastics of a limnic to brackish sequence termed the "Miembro Medio" (Bahlburg *et al.*, 1986; Breitreuz, 1986a; Breitreuz *et al.*, 1992) formed a shallow-marine/lacustrine platform as a result of uplift associated with the Eohercynian deformation (Fig. 2.9). The base of these Carboniferous-Lower Permian deposits is marked by an unconformity over probable Devonian basement (Davidson *et al.*, 1981b), while the top is marked by an unconformity associated with the Saalian tectonic event (Coira *et al.*, 1982). Marine Lower Permian sediments are followed by Permo-Triassic marine and continental, rift-related sedimentary deposits, associated with basaltic, andesitic and silicic volcanic rocks of the subsequent Andean Cycle (Suarez & Bell, 1992).

Mpodozis & Kay (1992) proposed the Mid-Permian collision of an exotic terrane to explain crustal shortening and thickening, uplift, cessation of block rotation (Rapalini, 1989) and the gradual termination of subduction-related magmatism (Kay *et al.*, 1989). Mpodozis & Kay (1992) also recognised four stages occurring all along the Gondwana margin during the assembly and break-up of Pangaea.

1. *Subduction-related magmatism in the Carboniferous to Early Permian (Elqui complex) occurred during a time of rapid motion of South America (Gondwana) relative to the South Pole (palaeomagnetic data from Valencio et al. (1983); see Kay et al. (1989); Ramos & Kay (1991))*
2. *Collision of the continental blocks completed the assembly of Gondwana (Permian collision of Equis Terrane). During this time, South America was moving less rapidly relative to the South Pole.*
3. *Extensive Late Permian to Early Jurassic crustal melting occurred in Palaeozoic accreted terranes; it was probably aided by an abnormally hot mantle associated with Pangaea. Melting was initiated by post-collisional processes in central Chile (Upper Permian to Triassic Ingaguas complex) and Australia. In other regions, melting was associated with mantle plumes (for example, Chon Aike province) that eventually led to the break-up of Gondwana*
4. *Rifting is associated with the break-up of Gondwana and renewed subduction along much of the margin (Andean period).*

The Late Carboniferous-Early Triassic records continued marine passive margin sedimentation in northern Chile and stable marine platform sedimentation in north-west Argentina, separated by the Arco Puneño topographic high. The Mid-Permian Saalian deformation phase marks the onset of

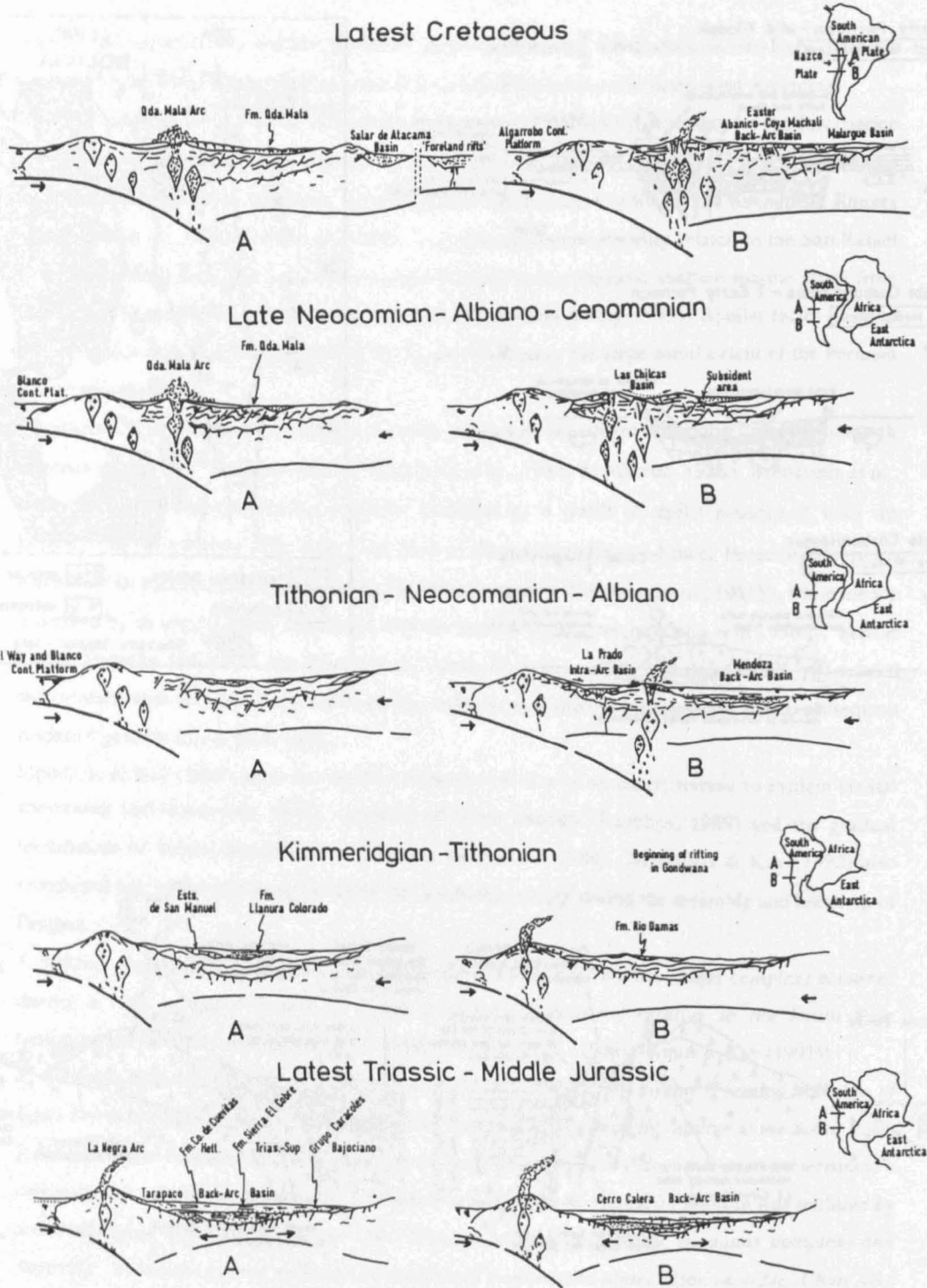


Figure 2.10 Comparative palaeogeographic evolutions for the northern (23°-24°S lat.) and central (34°-35°S lat.) Chilean Andes for the latest Triassic-Middle Jurassic, Kimmeridgian-Tithonian, Tithonian-Neocomian-Albian, late Neocomian-Albian-Cenomanian, and Late Cretaceous (Charrier & Munoz 1994).

rifting in northern Chile and the closure of the marine basin in north-west Argentina. Therefore, for the purposes of the thesis, this unconformity is taken as the start of the Andean Cycle.

2.3.3 Andean Cycle (Mesozoic-Cenozoic)

Permo-Triassic rifting

The Andean Cycle began in the Late Permian with an initial phase of rifting along the western margin of Gondwana which can be traced for the full length of the Andean orogenic chain. This Early Mesozoic, continent-scale rifting event is commonly associated with magmatism and thought to be related to the break-up of Pangaea (Charrier, 1979; Stipanovic, 1983; Suarez *et al.*, 1985; Dalziel, 1986; Dalziel *et al.*, 1987; Uliana & Biddle, 1988; Kokogian & Mancilla, 1989; Ramos & Kay, 1991; Suarez & Bell, 1991a; 1991b; Flint *et al.*, 1993). In northern Chile the Late Permian-Triassic Domeyko basin consists of a series of sub-parallel rift systems exposing a syn-rift succession of up to 2000 m of continental clastic rocks containing thin marine sandstones and limestones with intercalated basic, intermediate and acidic volcanics (Suarez & Bell, 1992). The transtensional rift basin is bounded on the west by the Atacama Fault System (AFS), demonstrated by Grocott *et al.* (1995), and on the east by the West Fissure Fault System (WFFS). Further to the east, a separate rift segment in the area of the Salar de Atacama was subsequently abandoned during the Late Triassic, with a period of non-deposition or erosion resulting in the production of an unconformity spanning Triassic-Late Cretaceous times (Flint *et al.*, 1993). Continued rifting in the area of the Precordillera led to a Norian (Late Triassic) marine transgression (Chong, 1977; Groschke *et al.*, 1988) between 23°30'-26°30'S. Subsequent Jurassic-Early Cretaceous post-rift thermal subsidence records mixed carbonate and siliciclastic marine deposition between the Coastal Cordillera in the west and Precordillera in the east (Chong, 1977; Groschke *et al.*, 1988), although local syn-rift extension continued into the Hettangian and Sinemurian (Early Jurassic) of the Coastal Cordillera between 25°-26°30'S (Pichowiak, 1994). The best exposed Jurassic sections are located along the north-south Chilean Precordillera (69°-69°30'W), delineating the eastern margin of the post-rift marine basin between 21°-27°S (Charrier & Munoz, 1994; Prinz *et al.*, 1994). The initiation of eastward subduction in the Late Sinemurian-Pliensbachian (190 Ma) is marked by arc development in the Coastal Cordillera (190-130 Ma) and the resultant switch of the Domeyko basin to a back-arc setting (Pichowiak, 1994).

Plutonism and volcanism is widespread in the Carboniferous-Early Triassic of the Chilean Andes, Argentine Puna and Western Cordillera (Breitkreuz, 1986b; Coira *et al.*, 1982). An extensive magmatic belt of post-tectonic intermediate to acidic, mainly calc-alkaline intrusions formed along the western margin of northern Chile. This belt of rhyolites, dacites, granites, and granodiorites is associated with continental red-beds and can be traced for 4000 km from northern Chile to southern Argentina. Huge Carboniferous-Triassic age acid batholiths were intruded into the Coastal Cordillera in several phases and are interpreted by Damm & Pichowiak (1981) as the products of crustal anatexis. The relationship of the Chilean intrusive belt to rocks in southern Peru and southern

Bolivia is uncertain but the Peruvian Permo-Triassic batholiths show some rift association (Pitcher, 1984) and may have developed within a back-arc spreading regime (Noble *et al.*, 1978).

The Late Permian-Late Triassic records thick syn-rift marine and continental clastics with intercalated volcanics in northern Chile (Suarez & Bell, 1992), while no preserved evidence of Permo-Triassic deposits are seen in north-west Argentina. Permian rifting in northern Chile is thought to be related to the break-up of Pangaea.

Jurassic arc and back-arc basin

An up to 10 km thick north-south trending volcanic sequence (Garcia, 1967) termed the La Negra Formation developed along the Coastal Cordillera of Chile, overlying Hettangian (Lower Jurassic) marine sediments (Coira *et al.*, 1982), Triassic volcanoclastics (Suarez & Bell, 1992) and Upper Palaeozoic sediments (Omarini *et al.*, 1991). The La Negra Jurassic arc succession is composed of dacites, andesites and basalts, giving rise to tuffs, pillow lavas, breccias and agglomerates (James, 1971) erupted in predominately sub-aerial environments with limited pillow basalts indicating submarine environments (Ferraris & Di-Biase, 1978; Buchelt & Tellez, 1988).

Figure 2.10 shows the post-rift thermal subsidence phase which spanned Norian (Late Triassic)-Early Cretaceous characterised by the deposition of carbonates, marine clastics, evaporites and red-beds with some interbedded volcanics, described by Biese (1961); Harrington (1961); Dingman (1963); Hollingworth & Rutland (1968); Hillebrandt (1973); Moraga *et al.* (1974); Baeza (1976); Chong (1977); and Prinz (1991). The end of the Jurassic-Early Cretaceous is marked by a regional marine regression (Rutland, 1971) and followed by continental red-bed deposition of Early Cretaceous age (Bogdanic, 1990). Further to the east in Chile and north-west Argentina, non-deposition or erosion is marked by a Triassic to Late Cretaceous unconformity surface (Flint *et al.*, 1993). The Late Triassic to Early Cretaceous in northern Chile is represented by an arc/back-arc basin pair, with no preserved evidence of Jurassic deposits in north-west Argentina. Similar extensional basins floored by continental crust developed in Peru (Jaillard *et al.*, 1990) and further south (40°S) in the Southern Andes (eg. Neuquén Basin; Uliana & Biddle, 1988), however, greater rates of extension resulted in back-arc spreading and generation of oceanic crust in the Magellanes Basin in southernmost Chile/Argentina (Dalziel *et al.*, 1974). The Northern and Central Andes of southern Colombia, Ecuador and Peru are characterised by a series of Jurassic extensional basins developed on oceanic crust (Atherton *et al.*, 1983; Dalziel, 1986; Jaillard *et al.*, 1990).

Cretaceous basins

The Lower Cretaceous red-beds record widespread fluvial and alluvial fan deposition with limited lacustrine and aeolian deposits, shown in Fig. 2.11 (Bell, 1991). At the end of the Early Cretaceous the Peruvian compressive tectonic event caused inversion of the Jurassic marine back-arc basin and a major change in the regional palaeogeography of northern Chile, noted by Bogdanic (1990); Bogdanic & Espinoza (1994) and A. Tomlinson, pers. comm. (1994). In association with this Mid-Cretaceous compressive event, the Jurassic volcanic arc of the Chilean Coastal Cordillera and its related back-arc

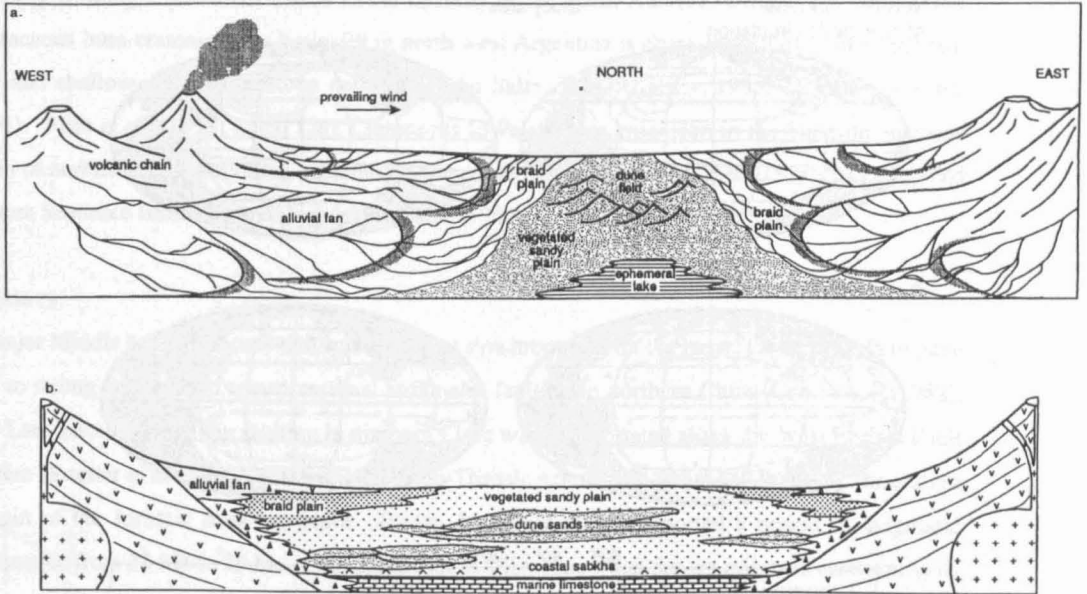


Figure 2.11 (a) Sketch diagram of the depositional environments of the continental red-beds in an extensional intra-arc tectonic setting. The sedimentary basin is approximately 50 km wide. (b) Cross-section showing the vertical and horizontal relationship of facies associations, with braid plains and alluvial fans building out from both sides of the sedimentary basin (Bell & Suarez 1993).

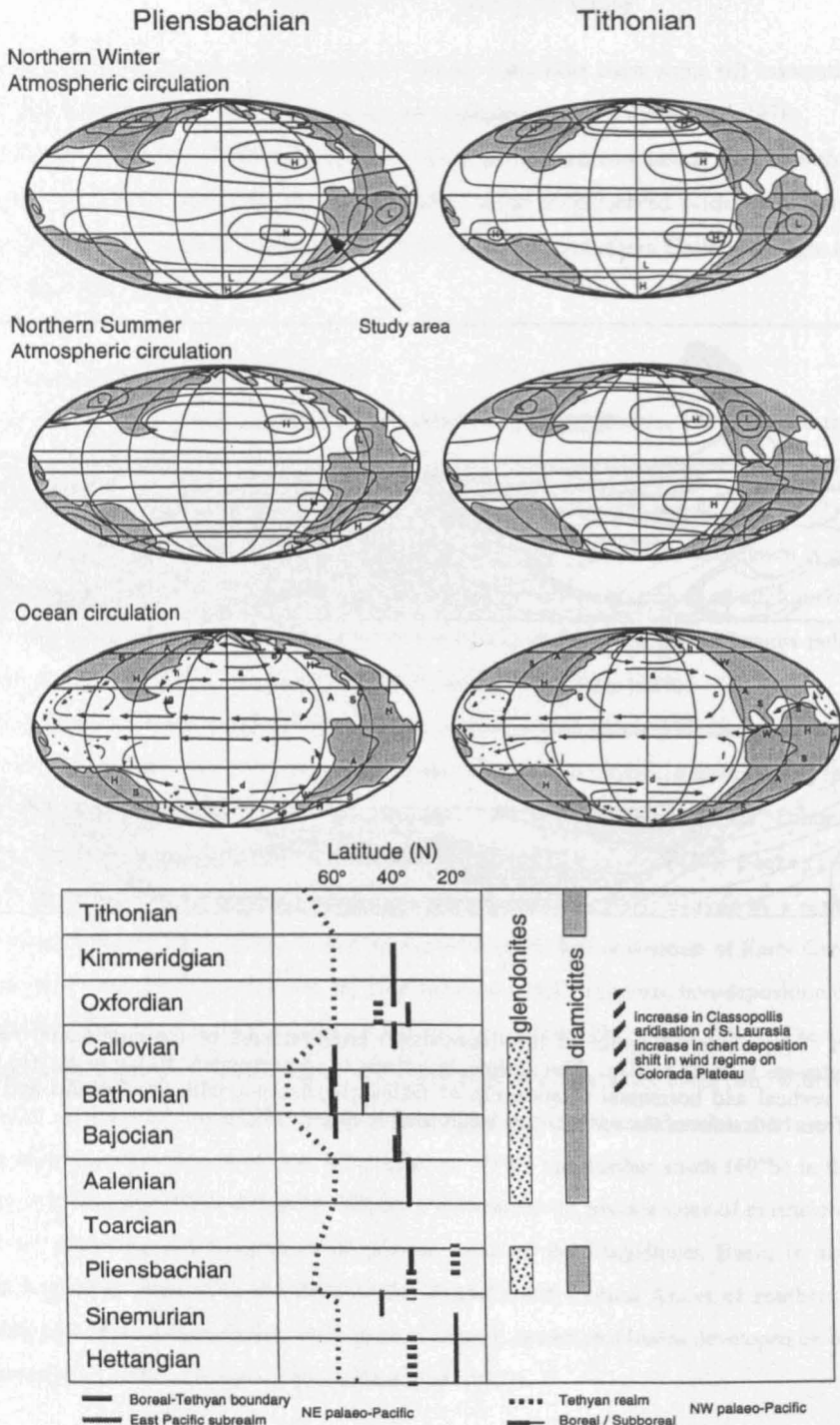


Figure 2.12 Maps: Atmospheric circulation over the circum-Pacific region in the northern winter and northern summer for both the Pliensbachian (Early Jurassic) and Tithonian (Late Jurassic): H, relative high pressure; L, relative low pressure (Parrish et al., 1982). Adapted from Parrish & Curtis, 1982. The plate reconstructions are generalised from the maps of Ziegler et al., 1983. Predicted ocean currents and relative precipitation in the Pliensbachian (Early Jurassic) and Tithonian (Late Jurassic). Oceans: Thin dashed arrows indicate northern summer currents, thin solid arrows indicate northern winter currents; year-round currents are indicated by thick solid arrows. Currents: a, paleo-North Pacific current; b, paleo-Alaska current; c, paleo-California current; d, South Pacific current; e, Antarctic Peninsula current; f, paleo-Peru current; g, paleo-Kuroshio current; h, paleo-Oyoshio current; i, Lord Howe current; j, paleo-East Australia current. Continents: A, arid; S, semi-arid; H, sub-humid; W, humid (Adapted from Parrish et al., 1982). Table: Summary of evidence of biogeographic and climatic change during the Jurassic (Parrish, 1992).

basin were replaced by a single, dominantly eastwardly migrating arc complex (Coira *et al.*, 1982). The diffuse Mid-Cretaceous arc and the latest Cretaceous-Eocene arc were situated in the Longitudinal Valley and Chilean Precordillera, respectively (Reutter *et al.*, 1988).

Further to the east in the Puna, Eastern Cordillera and Subandean, extensive Cretaceous rifting introduced several, partly interconnected, extensional intra-cratonic basins (Coira *et al.*, 1982; Salfity & Marquillas, 1994) which comprised part of a series stretching from the Atlantic coast to Peru, possibly forming a failed rift linked to the opening of the south Atlantic (Grier *et al.*, 1991). The Cretaceous intra-cratonic Salta basin-fill in north-west Argentina is characterised by continental red-bed and shallow-marine limestone deposits of the Salta Group (Salfity, 1985; 1992; Grier *et al.*, 1991). Flint *et al.* (1993) noted Late Cretaceous to Palaeocene extension in the Salar de Atacama basin of northern Chile providing accommodation space for the deposition of the Purilactis Group and Eastern Sequence continental red-beds of Bogdanic (1990).

Tertiary

A major Middle to Late Eocene deformation event synchronous with the Incaic Orogeny in Peru gave rise to strong folding and transpressional strike-slip faulting in northern Chile (Coira *et al.*, 1982). The Late Eocene strike-slip faulting in northern Chile was concentrated along the West Fissure Fault System (Reutter *et al.*, 1988), reactivating Permo-Triassic extensional faults and inverting the eastern margin of the Jurassic back-arc basin. Jordan & Alonso (1987) reported a period of magmatic quiescence from 35 Ma to 25 Ma ending in the latest Oligocene when the arc migrated eastward to its present position along the Western Cordillera (High Andes). The Quechua deformation phase (10 Ma) caused the major uplift associated with the Puna/Altiplano and eastern Cordillera, with extensive thrusting and reverse faulting thought to account for greater than 200 km of shortening (Isaacks, 1988).

2.4 Palaeoclimate and oceanography of northern Chile

Global palaeobiogeographic patterns are principally dependant on climate and continental drift. The Jurassic was a time of climatic transition, with the break-up of Pangaea into Gondwana and Laurasia resulting in changes in continental climates in response to the break-up of the northern Pangaeon monsoonal circulation (Parrish *et al.*, 1982; Parrish & Doyle, 1984). This climatic change may have triggered subsequent changes in ocean circulation.

The present day coastline of northern Chile causes the channelling of winds, where the surface winds associated with the eastern limb of the southern Pacific subtropical high-pressure cell are limited to the coastal region by the Andes. The rain-shadow effect is well expressed in northern Chile and north-west Argentina where the cordillera is perpendicular to the zonal circulation, thus creating the rain shadow associated with the Atacama desert.

A strong monsoonal circulation should have existed for Pangaea because of the great size of the continental area in mid-latitudes, exceeding even the size of Eurasia, and the presence of such land

areas in both hemispheres and their positions opposite one another across Tethys (Fig. 2.12), (Parrish *et al.*, 1979; 1982; Parrish & Curtis, 1982).

At least four different types of climatic patterns are expected to have been consequences of the Pangaeon monsoon.

1. *strong seasonality*
2. *an equatorial region that is dry on the east and possibly humid on the west*
3. *absence of latitude-parallel climatic belts*
4. *alternating oceanic current flow, including upwelling in western Tethys*

Monsoonal conditions in Pangaea would be expected to have reached a maximum sometime during the Triassic (Parrish *et al.*, 1986; Parrish & Peterson, 1988), with the main southern monsoon concentrated over what is now Africa (Fig. 2.12). The combination of the break-up of Pangaea and the flooding of Laurasia meant that the Pangaeon monsoonal circulation would have ceased by the Tithonian. However, the amount of exposed land in Gondwana and its latitudinal position meant that weak monsoonal circulation may have persisted there.

On the eastern side of the palaeo-Pacific, the latitudinal temperature gradient between about 70° north and south would have been low. In the south, the South Pacific Current centred on about 45°S, would have divided into the southward-flowing Antarctic Peninsula Current and the northward-flowing palaeo-Peru Current (Fig. 2.12).

Except in the vicinity of Tethys, the conceptual models of Parrish *et al.* (1982) predict that climate and ocean surface circulation did not change very much during the Jurassic. Parrish & Curtis (1982) regard the subtropical high-pressure cells to be a relatively constant and predictable feature of global circulation in the Jurassic Pacific, hence driving upwelling currents at mid-latitudes on the eastern sides of the ocean basins (Fig. 2.12). Upwelling was probably active off the coast of northern Chile throughout the Jurassic, even though Gondwana had moved 5° further south by the latest Jurassic. The thermal effects of upwelling are to enhance cool-temperature conditions along the west coasts (Philander & Pacanowski, 1980), hence keeping the palaeo-Peru current cool.

Continental climates are predicted by Parrish *et al.* (1982) as having been warm and dry at low latitudes on the eastern side of the palaeo-Pacific and arid inland on the western margin of Gondwana (Fig. 2.12). Climatic changes in the southern hemisphere roughly paralleled those seen in the northern hemisphere. Red-beds, with local occurrences of evaporites and aeolian sandstones were widespread in South America in the Triassic, suggesting seasonally wet climates (Van Houten, 1982), consistent with the predicted monsoonal circulation (Volkheimer, 1967; Rocha-Campos, 1971; Parrish & Peterson, 1988). In the Early Jurassic, abundant fossil floras and widespread peat deposition occurred and humid conditions continued into the Middle Jurassic (Volkheimer, 1967). In the Late Jurassic, arid conditions were established in mid-latitudes, resulting in extensive aeolian sand deposition.

2.5 Conclusions

When considering the Mesozoic basin evolution in northern Chile we must take into account the complicated Palaeozoic history of the basement and its structure. The Palaeozoic structuring of basins and highs represent important controls on basin development during the Mesozoic, while the distribution of basement rocks and their timing of uplift have implications for the provenance of the Mesozoic basin-fill.

The palaeo-climatic conditions in northern Chile during the Mesozoic are typically semi-arid to arid with seasonal precipitation and abundant faunal and floral diversity (Parrish, 1992).

Chapter 3

Biostratigraphy and Chronostratigraphy

3.1 Objectives of chapter

The first objective of this chapter is to review the currently available numerical and magnetic-polarity time-scales used to calibrate the ammonite chronology for the Jurassic Period. Secondly, the chronostratigraphical scheme defined originally by the European ammonite zones and the subsequently calibrated Southern Andes ammonite zones will be considered along with the implications of ammonite biogeography. Finally, an assessment of Jurassic bio-events is considered and, where possible, an interpretation of the driving mechanism.

3.2 Time-scales

Numerical time-scale

The numerical time-scale is a tool used to calibrate the ammonite chronology. However, often such scales are based on a minimal amount of radiometric data (geochronometers). Adequate geochronometers consist of stratigraphically well controlled (within a stage) potassium- or uranium-bearing minerals or rocks. The stratigraphical constraint eliminates most plutonic rocks, leaving only volcanics or glauconitic sediments as possible sources for precise geochronological tie points. Due to the limited number of adequate control points along the succession, it is usually necessary to interpolate between these geochronologically founded tie points in order to suggest numbers for stage boundaries. There are several syntheses which discuss the calibration of the Jurassic time-scale and summarise the large collection of radiometric studies from which it was calibrated (Harland *et al.*, 1990). More recently, an integrated geomagnetic polarity and stratigraphical time-scale used a suite of 324 radiometric dates including high-resolution $^{40}\text{Ar}/^{39}\text{Ar}$ age estimates (Gradstein *et al.*, 1994). This framework involves the observed ties between (1) radiometric dates, biozones and stage boundaries, and (2) between biozones and magnetic reversals on the sea-floor and in sediments (Gradstein *et al.*, 1994). The numerical time-scale of Gradstein *et al.*, (1994) is the most recent and hence has been adopted for use in this thesis. The use of numerical ages for stage boundaries is avoided where possible, with reference to the particular biochron, thus avoiding confusion as the numerical time-scale becomes more refined.

Jurassic magnetic-polarity time-scale

A recent magnetic-polarity time-scale has been compiled from several magnetostratigraphical studies (Ogg, 1992). Correlation of the marine magnetic-anomaly M sequence with Upper Jurassic-Lower Cretaceous sedimentary successions has enabled assignment of precise biostratigraphical ages to the corresponding polarity Chrons M0 through M25 (Ogg, 1994). These ages are markedly different from those proposed by Westermann (1992) and Odin (1992) and are not adopted in this study due to the limited dataset from which they are derived and the fact that they only span the Late Jurassic. Although still in its infancy for the Jurassic Period, the magnetic-polarity time-scale promises advances as a technique for precise correlations (J. G. Ogg pers. comm., 1994) but the limitations on

practical applications lie in being able to identify the chron in which the age of a particular bed lies (Callomon, 1995).

3.3 Ammonite zones

The Jurassic succession of the Domeyko basin has been subdivided using ammonite biochronology based on ammonite successions found in Peru, Chile and Argentina which have allowed the development of a detailed biozonation, partly based on endemic East Pacific ammonites (Hillebrandt, 1987; 1988; 1990; Riccardi *et al.*, 1988). The Southern Andes regional ammonite zonation has been calibrated against the Standard European ammonite zonation, thus giving a joint chronology to at least sub-stage level resolution (Hillebrandt *et al.*, 1992; Westermann, 1992). The Jurassic Domeyko basin succession records 85% of ammonite zones, exceptions being those of the Late Oxfordian-Late Kimmeridgian and Tithonian. Although ammonites provide the primary biochronology for Upper Triassic-Lower Cretaceous rocks (Callomon, 1995) many other faunas including conodonts (McKie, 1994) and bivalves (Aberhan, 1993a; 1993b; Damborenea, pers. comm., 1995), have supplied additional biochronological and palaeobathymetric information (specific references cited in texts).

Late Triassic

The Rhaetian (Late Triassic) has been subdivided into four ammonite zones based on fauna from northern Chile (Hillebrandt, 1990) and supported by recent work from Peru (Hillebrandt, 1994). The *P. ex. gr. roemeri-peruvianum* and *Ch. cf. nobile* Zones define the Early Rhaetian, while the *Ch. cf. crickmayi* and *Ch. cf. marshi* Zones characterise the Late Rhaetian (Fig. 3.2). The Late Triassic conodont *Epigondolella bidentata* (Fig. 3.2) has been reported from shallow-marine limestone facies in northern Chile (McKie, 1994) and ranges from *G. cordilleranus* to half way through the *C. amoenum* North American ammonite Zones (Orchard, 1983). This conodont is assigned a Norian age in the original literature (Orchard, 1983) but is considered Lower Rhaetian (Fig. 3.2), equivalent to the *P. ex. gr. roemeri-peruvianum* and *Ch. cf. nobile* ammonite Zones. A Norian marine transgression in northern Chile is described by several authors (Groschke *et al.*, 1988; Hillebrandt, 1990), an apparent time discrepancy arising from different placings of the Norian-Rhaetian Stage-boundary (Hillebrandt, 1990; 1994).

Hettangian

Hillebrandt (1988; 1990) established five Early-Middle Hettangian zones characterised by endemic species, the *P. tilmanni*, *P. primocostatum*, *P. rectocostatum*, *Curviceras ssp.*, and *D. reissi* Zones (Fig. 3.3). The South American *Psiloceras tilmanni* Zone is coeval, but not exactly comparable with the European *Planorbis* Subzone, while the overlying *Psiloceras primocostatum* Zone (Hillebrandt, 1988) is coeval with the upper part of the *Planorbis* Subzone or the lower part of the *Plicatulum* Subzone in Europe (Hillebrandt *et al.*, 1992). The Andean *Psiloceras rectocostatum* Zone is equivalent to the upper part of the *Plicatulum* Subzone or the lower part of the *Johnstoni* Subzone, while the zone with *Curviceras ssp.* may be correlated with the upper part of the *Johnstoni* Subzone

Period	Stage	Age (Ma)	Duration (Ma)
LATE JURASSIC	TITHONIAN	144.2 Ma	6.5 Ma
	KIMMERIDGIAN	150.7 Ma	3.4 Ma
	OXFORDIAN	154.1 Ma	5.3 Ma
MIDDLE JURASSIC	CALLOVIAN	159.4 Ma	5.0 Ma
	BATHONIAN	164.4 Ma	4.8 Ma
	BAJOCIAN	169.2 Ma	7.3 Ma
	AALENIAN	176.5 Ma	3.6 Ma
EARLY JURASSIC	TOARCIAN	180.1 Ma	9.5 Ma
	PLIENSACHIAN	189.6 Ma	5.7 Ma
	SINEMURIAN	195.3 Ma	6.6 Ma
	HETTANGIAN	201.9 Ma	3.8 Ma
	RHAETIAN	205.7 Ma	3.9 Ma
LATE TRIASSIC	NORIAN	209.6 Ma	11.1 Ma
		220.7 Ma	

Figure 3.1 Numerical time-scale of (Gradstein et. al., 1994).

		Standard European Zones		Northern Calcareous Alps		Southern Andes (Hillebrandt, 1990)	Southern Andes			
		Zones	Subzones	Zones	Subzones	Zones	Peru (Hillebrandt, 1994) Zones	Chile Zones		
HETTANGIAN	LATE	S. angulata	S. depressa	S. marmorea		S. angulata	S. cf. marmorea	S. cf. marmorea		
	MIDDLE		S. complanata				K. megastoma	D. reissi	D. reissi	D. reissi
			S. extranodosa							
EARLY	A. liasicus	S. laqueus	P. calliphylum	C. peruvianum	P. rectocostatum	Curvicerias ssp.				
		C. portlocki								
	P. planorbis	C. johnstoni	P. primocostatum	P. primocostatum	P. primocostatum					
		P. plicatulum								
	P. planorbis	P. tilmanni	P. tilmanni	P. tilmanni						
RHAETIAN	LATE	North America (Tozer 1979)	Ch. marshi	Ch. marshi	Ch. cf. marshi	Ch. cf. marshi	Ch. cf. marshi			
	EARLY	Ch. crickmayi		V. stuerzenbaumi	Ch. cf. crickmayi	Choristoceras ssp.	Ch. cf. crickmayi			
		C. amoenum	Rh. suessi	S. reticulatus	Ch. cf. nobile	Rhabdoceras	Ch. cf. nobile			
		G. cordilleranus	Epigondolella Bidentata	S. quinque- punctatus	P. ex. gr. roemeri- peruvianum	Peripleurites Metasibirites	P. ex. gr. roemeri- peruvianum			

Figure 3.2 Late Triassic ammonite zones of Europe and the Southern Andes (Hillebrandt, 1990; Hillebrandt, 1994). Additional ammonite zones from North America are included in order to calibrate the conodont zone, Epigondolella bidentata (Orchard, 1983).

		Standard European Zones		Southern Andes		
LOWER JURASSIC	TOARCIAN	L	LEVESQUEI — 180.1 Ma	P. fluitans & P. lotharingica	P. tenuicostatum	
			THOUARSENSE	P. copiapense		
		M	VARIABILIS — (9.5 Ma)	P. toroense	C. chili, P. moerckel	P. bolivense
			BIFRONS	P. pacificum	P. largeense	
		E	FALCIFERUM	D. hoelderi		
		TENUICOSTATUM	D. tenuicostatum	D. simplex		
	PLIENSCHACHIAN	L	SPINATUM — 189.6 Ma	F. disciforme		
			MARGARITATUS	F. fannini		
		E	DAVOEI — (5.7 Ma)	F. behrendseni	E. meridianus	
			IBEX	Tropidoceras		
			JAMESONI	Eoderoceras & Apoderoceras		
	SINEMURIAN	L	RARICOSTATUM — 195.3 Ma	E. raricostatum		
			OXYNOTUM	O. oxynotum		
		E	OBTUSUM — (6.6 Ma)	A. obtusum		
			TURNERI	C. turneri		
			SEMICOSTATUM	A. semicostatum		
	HETTANGIAN	L	BUCKLANDI — 201.9 Ma	A. bucklandi		
		M	ANGULATA	S. angulata		
		E	LIASICUS — (3.8 Ma)	D. reissi	Curvicerias ssp.	
		PLANORBIS — 205.7 Ma	P. rectocostatum	P. primocostatum	P. tilmanni	

Figure 3.3 Early Jurassic ammonite zones of Europe and the Southern Andes (Hillebrandt et. al., 1992). Numerical time-scale of (Gradstein et. al., 1994).

or the lowest part of the Liasicus Zone in Europe. The *Discamphiceras reissi* Zone (*Badouxia reissi* Zone of Hillebrandt (1988)) is thought to be coeval with the European Liasicus Zone. The Late Hettangian European Angulata Zone (Fig. 3.3) was divided in Chile and Peru into two subzones using species of the genus *Schlotheimia* (Hillebrandt, 1994). The lower part of the Angulata Zone is dominated by *Schlotheimia cf. montana* (Wähner), and the upper part by species of the *Schlotheimia marmorea* genus (Hillebrandt *et al.*, 1992).

Sinemurian

In northern and central Chile most European zones and some of the subzones (Fig. 3.3) were discovered (Hillebrandt, 1987), a detailed biostratigraphy of the Lower Sinemurian and lower Upper Sinemurian successions being given by Quinzio (1987). The base of the European Sinemurian (Conybeari Subzone) is defined by the appearance of *Metophioceras conybeari* and a similar species is found in northern Chile (Quinzio, 1987); while Andean species of *Coroniceras* are similar to those of the European Rotiforme Subzone (Hillebrandt, 1987; Quinzio, 1987). The cosmopolitan genus *Arnioceras* is often the most frequent and sometimes the only Sinemurian ammonite found; however it is long-ranging, from the late Early Sinemurian to the early Late Sinemurian (Hillebrandt *et al.*, 1992). In South America, the last *Coroniceras s.l.* or related genera are found together with the first *Arnioceras*, making this assemblage coeval with the European Bucklandi or Reynesi Subzones (Fig. 3.3). The different species of *Arnioceras*, in combination with other genera, provide a detailed biozonation (Quinzio, 1987). In northern Chile, the Obtusum Zone can be subdivided into three subzones (Quinzio, 1987) by means of species of *Asteroceras* and *Eparietites*. The last zone of the European Sinemurian is characterised by *Echioceratidae*. *Echioceras* (= *Plesechioceras arcticum*) occurs in South America (Hillebrandt, 1987) and probably is typical for the early Raricostatum Zone (Hillebrandt *et al.*, 1992).

Pliensbachian

Pliensbachian ammonites are known from many regions around the Pacific Ocean but correlation is often difficult because pandemic genera and species are less frequent (Hillebrandt *et al.*, 1992). In the Late Pliensbachian, a clear differentiation of ammonites into bioprovincial realms and subrealms (Boreal, Tethyan and East Pacific) is observed for the first time (Taylor *et al.*, 1984). In North and South America ammonites often are more frequent in the Pliensbachian than in the Late Sinemurian (Hillebrandt *et al.*, 1992). In North America a detailed biozonation has been worked out (Smith *et al.*, 1988), and significantly, the associations include species typical for the East Pacific and the Mediterranean, as well as for north-eastern and north-western Europe. *Eoderoceratidae* and *Acanthopleuroceratinae* are the most important zonal markers for the Early Pliensbachian of North and South America (Fig. 3.3), while the East Pacific genus *Fanninoceras* is important for the Late Pliensbachian (Hillebrandt *et al.*, 1992). The lower stage boundary in the Americas is drawn above the last *Echioceratidae* (Fig. 3.3).

Toarcian

Provincialism is less strongly marked than in Pliensbachian time, some genera and species being widespread (Hillebrandt *et al.*, 1992). In Chile, the most complete provincial secondary standard chronozone of Toarcian ammonites around the Pacific has been established (Hillebrandt & Schmidt-Effing, 1981; Hillebrandt, 1987), comprising ten zones, some with subzones (Fig. 3.3). The base of the Toarcian is marked by different species of *Dactylioceras s. l.*, some of them with a wide geographic distribution (Fischer, 1984). The lowest subzone in South America is characterised by the Mediterranean species *Dactylioceras (Eodactylites) simplex*, which is also found in north-western Europe at the base of the Toarcian (Schlatter, 1982). The South American Hoelderi Zone is coeval with the lower part of the European Falcifer Zone. The Bifrons Zone of north-western Europe is subdivided into three subzones based on *Dactylioceratidae* (Fig. 3.3), a species which also occurs in different Pacific regions (Hillebrandt *et al.*, 1992). In South America and the Mediterranean, *Peronoceras* appears earlier than in north-west Europe. The genus *Peronoceras* (= *Porpoceras*) is important for the biostratigraphy of South America, North America and north-eastern Asia, where it occurs mainly in the middle and late parts of the Middle Toarcian. The South American zone of *Peronoceras pacificum* is coeval with the European zone of *Peronoceras fibulatum*. *Peronoceras spinatum* was also described from the South American *Peronoceras bolitoense* Subzone (Hillebrandt, 1987) and was found together with *Catacoeloceras cf. crassum*, the index for the north-western European Crassum Zone. The beds with *P. spinatum* and *P. polare* are coeval with at least part of the Crassum Zone and perhaps with the early Variabilis Zone. Beds with *Dactylioceratids* of the Bolitoense Subzone in South America are directly overlain by large *Peronoceras* characterising the Moerickei Subzone, both of which contain the Mediterranean genus *Collina* (Chilensis Zone). The endemic hildoceratid genera *Atacamoceras* and *Hildaitoides* were also reported from this zone (Hillebrandt, 1987). *Phymatoceras* is frequent in the Tethyan Realm and is important for the biostratigraphy of the late Middle and early Late Toarcian of South America, with two zones, the *Phymatoceras toroense* Zone and *P. copiapense* Zone (Fig. 3.3), based on endemic species of this genus (Hillebrandt, 1987). The Late Toarcian genera *Grammoceras* and *Pseudogrammoceras* are important in north-western European biostratigraphy (Hillebrandt *et al.*, 1992). *Pseudogrammoceras* characterises the north-western European Dispansum Zone and is coeval with the South American *Pseudogrammoceras tenuicostatum* Zone. *Dumortieria* and *Pleydellia* are restricted to the uppermost part of the European Toarcian and are typical for the uppermost Toarcian of South America where they may range into the lowermost Aalenian (Bogdanic *et al.*, 1985).

Toarcian/Aalenian boundary

In the circum-Pacific the lower boundary of the Aalenian (Early-Middle Jurassic boundary) can be recognised with some precision in north-east Russia and in the Southern Andes. Elsewhere the boundary lies in a faunal hiatus and/or among poorly known faunas (Hillebrandt *et al.*, 1992). In northern Chile, the late Levesquei Zone with *Pleydellia (Walkericeras) spp.*, is overlain by the Manflasensis Zone (Hillebrandt & Westermann, 1985). The Manflasensis Zone contains dominant

Bredya, indicating the Opalinum-Scissum Zones in Europe (Fig. 3.4) but the presence of *Ancolloceras* may indicate the European Scissum-Murchisonae Zones (Hillebrandt *et al.*, 1992), making possible the presence of a hiatus missing the Opalinum Zone.

Aalenian

The best known sections in northern Chile (Hillebrandt & Westermann, 1985) show the Manflasensis Zone overlain by the *Zurcheria groeberi* Zone (Fig. 3.4), indicating the European Murchisonae Zone (Westermann & Riccardi, 1982). There follows the Malarguensis Zone which appears to span late Murchisonae-early Discites Zone ages and was recently divided into two or three subzones (Hillebrandt & Westermann, 1985).

Early Bajocian

The Early Bajocian probably begins with the late part of the Malarguensis Zone (Fig. 3.4), that is, all or part of the *Podagrosiceras maubeugei* biozone with *Euhoploceras amosi* (Westermann & Riccardi, 1972; 1979). The Singularis Zone yields abundant *Sonninia (Fissiloboceras) ssp.*, including rare *S. (F.) ovalis (Qu.)*, as from the European Ovalis Subzone (Hillebrandt *et al.*, 1992). The Giebeli Zone is approximately coincident with the range zones of the genus *Emileia* and subgenus *Sonninia (Papilliceras)*. The *E. submicrostoma* Subzone with late *Pseudotoites*, the *E. multiformis* Subzone of *Emileia (E.) cf. vagabunda* Buck., *E. (E.) aff. brochii* (Sow.), and *Stephanoceras (Skirroceras) spp.*, are dated as European Laeviuscula Zone. The top of the Giebeli Zone is marked by the *Dorsetensia blancoensis* biozone, a species closely resembling *D. hebridica* Morton from Scotland, index of a subzone in the highest Sauzei Zone. The overlying fauna in northern Chile is specifically so close to that of the European Humphriesianum Zone (Fig. 3.4) that no new zonal name is required (Hillebrandt *et al.*, 1992). In the lower part of the zone the Romani Subzone is marked by the index species *Dorsetensia romani*, as well as *D. gr. complanata-TECTA* Buck. and *Stephanoceras (S.) pyritosum (Qu.)* (Westermann & Riccardi, 1972; 1979), while the upper part of the zone is distinguished as the *Duashnoceras chilense* Subzone including *Stephanoceras gr. umbilicum (Qu.)*, *S. (Stemmatoceras) spp.*, and *Teloceras spp.*, indicating the Blagdeni and Humphriesianum Subzones.

Late Bajocian

The Early-Late Bajocian boundary is marked throughout most of the circum-Pacific area by a strong faunistic change with the sudden beginning of extreme provincialism and the appearance of the East Pacific Subrealm (Hillebrandt *et al.*, 1992). Boundary events include the birth of the Boreal *Cardioceratidae* and the East Pacific *Eurycephalitinae*. In northern Chile, only a single fragment of alleged *Strenoceras* has been discovered although faunas of Subfurcatun Zone age are richly developed there and in west-central Argentina (Riccardi *et al.*, 1989). The Rotundum Zone includes large *Spiroceras* and *Teloceras* and below *Lupherites Domeykoceras* marks the *L. dehmi* Subzone (Fig. 3.4). In Neuquén Province, *Teloceras*, *Lepto-sphinctes coronoides* Buck., *Megasphaeroceras magnum spissum* and a single minute *Strenoceras* (or *Parastrenoceras*) occur in the Rotundum Zone.

Megasphaeroceras magnum magnum ranges higher than the other taxa (Fig. 3.4) into the Garantiana Zone (Riccardi *et al.*, 1989; Riccardi & Westermann, 1991). In the absence of *Parkinsoniidae*, the uppermost Bajocian cannot be identified with certainty but the Parkinsoni Zone is suggested by the occurrence of *Lobosphinctes intersertus* Buck..

Bathonian

In the Southern Andes, Early-Middle Bathonian fauna are poorly documented and possibly largely missing (Hillebrandt *et al.*, 1992). The only pre-Late Bathonian ammonites are known from reworked submarine mudflows of the *Cadomites-Tulitidae* mixed assemblage from the Chacay Melehue section of Neuquén Province (Riccardi *et al.*, 1989). Apparently reworked *Tulites* (*Rugiferites*) *cf. davaiacensis* (Liss.), *T. (R.) aff. sofanus* (Boehm), and *Cadomites ex gr. orbignyi-bremeri* clearly indicate Middle Bathonian, whereas *Bullatimorphites* (*Kheraicerus*) *cf. bullatus* (Orb.) in the matrix indicates Late Bathonian. In northern Chile, similar *Cadomites* occur, partly together with *Epistrenoceras*, indicating either (1) that *Epistrenoceras* appears earlier in the Andean Province than in Europe, where the genus is cryptogenic in the late Retrocostatum Zone, or (2) that these *Cadomites* are in fact Late Bathonian, a local occurrence in Europe. The Steinmanni Zone (Riccardi *et al.*, 1989) contains, besides the dominant East Pacific *Eurycephalitinae* and *Neuquenicerus s. str.*, also cosmopolitan *Choffatia* as well as *Hecticoceras* (*Prohecticoceras*) *blanazense* Elmi and *Eohecticoceras sp.*, indicating the early Retrocostatum Zone (Fig. 3.4). In northern Chile the upper part of the zone is marked by the *Choffatia jupiter* biozone, with or just above *Hecticoceras* (*Prohecticoceras*) *retrocostatum*, guide of the late Retrocostatum Zone in Europe. The Steinmanni Zone is therefore dated as Retrocostatum-Discites Zones (Fig. 3.4).

Callovian

The Early Callovian begins with the Vergarensis Zone (Riccardi *et al.*, 1989) which is dominated by East Pacific *Eurycephalitinae* (Riccardi & Westermann, 1991) constrained by its stratigraphical position between the better dated Steinmanni and Bodenbenderi Zones (Fig. 3.4). The overlying Bodenbenderi Zone containing *Neuquenicerus* (*Frickites*) *spp.*, *Choffatia spp.*, and rare *Eurycephalites* is dated as middle Early Callovian (late Herveyi to early Calloviense Zones). The Proximum Zone, with a Tethyan *Hecticoceratid* fauna of *Hecticoceras* (*H.*) *proximum*, *H. boginense* and *H. cf. hecticum*, and *H. (Chanasia) navense* and *H. (C.) ardescicum*, can be dated as late Gracilis-Calloviense Zone, Patina and Enodatum Subzones, respectively. *Rehmannia* (*R.*) *brancoi* and *douvillei* occur in northern Chile (eg. Caracoles) within a few metres of the thick succession, together with *Neuquenicerus* (*Frickites*) or *Jeanneticeras cf. meridionale* Elmi, indicating uppermost Early Callovian (Hillebrandt *et al.*, 1992). The Middle-Late Callovian is characterised by *Rehmannia patagoniensis* and *Oxyceri. oxynotus* which are coeval with the Jason-Lamberti Zones of Europe (Fig. 3.4).

		Standard European Zones		Southern Andes		
MIDDLE JURASSIC	CALLOVIAN	L	LAMBERTI	Rehmannia patagoniensis and <i>Oxyceri. oxynotus</i>		
			ATHLETA			
		M	CORONATUM		(5.0 Ma)	
			JASON			
		E	GRACILIS		CALLOVIENSE	Proximum Zone
			MACROCEPHALUS			Bodendenderi Zone
			164.4 Ma	Vergarensis Zone		
	BATHONIAN	L	DISCUS	Steinmanni Zone		
			RETROC.			
		M	BREMERI	(4.8 Ma)	Cadomites - Tullitidae Association	
			SUBCONTRACTUS			
		PROGRACILIS				
	E	ZIGZAG	169.2 Ma			
	BAJOCIAN	L	PARKINSONI	Lobosphinctes		
			GARANTIANA			
			SUBFURCATUM		Megasph. magnum ss.	
		E	HUMPHRIESIANUM	(7.3 Ma)	Humphr. Zone	
			SAUZEI		Giebeli Zone	
			LAEVIUSCULA			
			DISCITES		Singularis Zone	
AALENIAN	L	CONCAVUM	176.5 Ma	Malarg. Zone		
		MURCHISONAE		(3.6 Ma)	"Zurch." groeberi Zone	
	E	SCISSUM		Manflasensis Zone		
		OPALINUM	180.1 Ma			

Figure 3.4 Middle Jurassic ammonite zones of Europe and the Southern Andes (Hillebrandt *et al.*, 1992). Numerical time-scale of Gradstein *et al.* (1994).

			Standard European Zones	Southern Andes
CRET	EARLY BERIASIAN		OCCITANICA	Spiticeras damesi Zone
			EUXINUS — 144.2 Ma	Argentineras noduliferum Zone Substeueroceras koeneni Z. Corong. altemans Zone
LATE JURASSIC	TITHONIAN	L	Durangites spp.	Windhauseniceras interspinosum Zone
			MICRACANTHUM	
		M	PONTI	Anlacosphinctes proximus Zone
			FALLAUXI (6.5 Ma)	
			SEMIFORME	Pseudolissoceras zitteli Zone Virgatosphinctes mendozanus Zone
		E	DARWINI	
	HYBONOTUM — 150.7 Ma		Torquatisphinctes	
	KIMMERIDGIAN	L	BECKERI	
			EUDOXUS	Orthaspidoceras
			ACANTHICUM	
		E	DIVISUM (3.4 Ma)	EVAPORITES
			HYPSELOCYCLUM	
			PLATYNOTA	
	L	PLANULA		
		BIMAMMATUM — 154.1 Ma		
		BIFURCATUM		
	OXFORDIAN	M	TRANSVERSARIUM (5.3 Ma)	
			PLICATILIS	Perisphinctes-Araucanites Association
E		CORDATUM		
		MARIAE — 159.4 Ma	Peltoceratoides	

Figure 3.5 Late Jurassic standard ammonite zones of Europe and of the Southern Andes (Hillebrandt et. al., 1992), and their presumed correlations. Numerical time-scale of (Gradstein et. al., 1994).

Europe		Chile
Chron	Subchron	
PLANULA	Galar Planula	<i>Idoceras cf. neogaëum</i>
		Onset of evaporite deposition
BIMAMMATUM	Hauffianum Bimammatum Hypselum	<i>Larcheria aff. greidingensis</i>
		<i>Perisphinctes andium</i> <i>Gregoryceras fouquei</i> <i>Mirosphinctes frickensis</i>
BIFURCATUM	Bifurcatum	
TRANSVERSARIUM	Schilli Parandieri	large <i>Gregoryceras transversarium</i> <i>Gregoryceras chongi</i> <i>Gregoryceras raizi</i> <i>Perisphinctes (Antilloceras) prophetae</i>

Figure 3.6 Correlation between the Middle-Late Oxfordian zones of Submediterranean Europe and the ammonite zones of the Southern Andes (Modified from Gygi & Hillebrandt, 1991). The shaded area indicates the onset of evaporite deposition in northern Chile. Planula Zone is now known to occur in the Kimmeridgian (J. H. Callomon pers. comm. 1996).

Oxfordian

In northern Chile there is evidence for Early Oxfordian in the form of *Peltoceras* (*Parawedekindia*), a group restricted in Europe to the *Mariae* and *Cordatum* Zones of the Early Oxfordian (Fig. 3.5). Gygi & Hillebrandt (1991) described the *Gregoryceras* of northern Chile which are coeval with those of Europe. In northern Chile, large *Gregoryceras transversarium*, *Gregoryceras chongi*, *Gregoryceras riazii* and *Perisphinctes* (*Antilloceras*) *prophetae* define the *Transversarium* Zone, while *Perisphinctes andium*, *Gregoryceras fouquei* and *Mirosphinctes frickensis* define the *Bifurcatus* Zone (Hillebrandt *et al.*, 1992). *Larcheria aff. gredingensis* is indicative of the *Bimammatum* Zone while *Idoceras cf. neogaenum* possibly indicates lowest *Planula* Zone (Fig. 3.6). Gygi & Hillebrandt (1991) use many of the successions from northern Chile, all of which date the onset of evaporite deposition within the late *Bimammatum* Zone (Fig. 3.6). It should be noted that the *Planula* Zone is now included in the *Kimmeridgian* (J. H. Callomon pers. comm., 1996). The presence of *Gregoryceras* and *Mirosphinctes* is indicative of faunal exchange between Europe and Chile in the *Transversarium*-*Bifurcatus* Zones (Middle-Late Oxfordian). The absence of *Leiostraca* from the *Precordilleran* basins of northern Chile is most simply explained as being due to the isolation of these basins from oceanic influences (Callomon in, Hillebrandt *et al.*, 1992).

Kimmeridgian-Tithonian

Kimmeridgian-Tithonian ammonites are almost unknown from northern Chile with a *Kimmeridgian* *Orthaspidoceras* (Fig. 3.5) having been reported from sediments above the gypsum in the *Cordillera de Domeyko* (Forster & Hillebrandt, 1984).

Summary

A direct biostratigraphical time correlation between the Southern Andes and Standard European ammonite zones is possible for the *Rhaetian* (Late Triassic)-*Oxfordian* (Late Jurassic), with only an interpolated correlation possible for the *Late Bajocian*-*Bathonian* due to a lack of north-south faunal transfer between the *Tethyan* and *Boreal* ammonite Realms, resulting in high provincialism. This time correlation provides the potential for direct comparison of events seen in the *Domeyko* basin with those seen in the basins of the northern hemisphere.

3.4 Biogeography and global bio-events

Ammonite biogeography has been the subject of several recent reviews (Westermann, 1981; 1993; Callomon, 1984; Taylor *et al.*, 1984), highlighting particular Jurassic biogeographic events (Fig. 3.7). The Middle Jurassic is probably the most interesting part of the Jurassic from the point of view of palaeobiogeography because it provides good examples of biogeographic changes (Fig. 3.7), which can be explained in terms of unifying plate-tectonic theory (Hillebrandt *et al.*, 1992). In the case of ammonoids, epicontinental seaways should filter out deep-water and oceanic taxa (*Leiostracans*), and the degree of endemism in the basins should vary with the seaway constriction. These changes through time are thought to reflect changes in global eustatic sea-level (Westermann in, Hillebrandt *et*

al., 1992), but could equally reflect regional tectonic events. The biogeographic events observed in the circum-Pacific are considered below.

(1) Early Toarcian global eustatic rise in sea-level

Documented ammonite data for the circum-Pacific (Hillebrandt *et al.*, 1992) shows faunal differentiation was strong in the Pliensbachian but in the overlying Early and Middle Toarcian most genera and some species were widely distributed. The marked increase in faunal exchange at the base of the Toarcian has been attributed to a global eustatic rise in sea-level (Hillebrandt *et al.*, 1992).

(2) Base Aalenian hiatus

The lower boundary of the Aalenian (Early-Middle Jurassic boundary) can be placed with some precision only in north-east Russia and in the Southern Andes, elsewhere the boundary lies in a hiatus and/or among poorly known faunas (Hillebrandt *et al.*, 1992).

(3) Aalenian evidence for faunal exchange via the Hispanic Corridor

The Andean Province has an Aalenian Tethyan fauna with strong European-Mediterranean affinities associated with plentiful endemics, indicating that the Hispanic Corridor (Smith, 1983) may have been open at this time allowing two-way faunal exchange (Hillebrandt *et al.*, 1992).

(4) Early Bajocian evidence for the early drift phase between Laurasia (North America) and Gondwana (Africa)

In the Northern Andes, cosmopolitan *Stephanoceras* (*Skirroceras*) and *Emileia* of Early Bajocian age are associated with submarine basaltic lava flows in Venezuela, interpreted by Bartok *et al.* (1985) to represent the early stages of sea-floor spreading between Laurasia (North America) and Gondwana (Africa).

(5) Early Bajocian evidence for faunal exchange via the Hispanic Corridor

The Southern Andes assemblage of the Humphriesianum Zone is close to that of Tethys and north-western Europe, partly down to species level, so that even its subzones can be identified (Fig. 3.4). This degree of faunal exchange indicates that the eastern Pacific was well connected with the Tethys toward the end of the Early Bajocian, possibly through the Hispanic Corridor (Hillebrandt *et al.*, 1992). Whereas *Sphaeroceratids* may have originated in the eastern Pacific and then migrated eastward via the Hispanic Corridor, *Stephanoceratids* probably arrived by westward migration from the Mediterranean-north-western Europe area (Westermann & Riccardi, 1985; Hillebrandt *et al.*, 1992). This dispersal theory has recently been questioned after the discovery of authentic *Neuquéniceras* from the Bathonian of the Himalayas and *Reineckeia* from the Bathonian of Kutch, India (J. H. Callomon pers. comm., 1996).

		Standard European Zones	Southern Andes	A	B	Jurassic Bio-events			
CRET EARLY RYAZ		OCCITANICA	<i>Spicoceras damali</i> Zone						
		EUXINUS	<i>Argenticeras noduliferum</i> Zone						
		Durangites spp. 144.2 Ma	<i>Sichelinoceras koppeni</i> Zone						
	LATE	TITHONIAN	L	<i>Corong alternans</i> Zone	Full marine connection	East Pacific Subrealm			
				<i>Winhuasenceras interspersum</i> Zone					
				<i>Antacosphinctes proximus</i> Zone					
			M	FALLAUXI (6.5 Ma)			<i>Planulosoceras zitteli</i> Zone		
				SEMIFORME			<i>Virgatosphinctes mendocense</i> Zone		
		KIMMERIDGIAN	E	DARWINI					
				HYBNOTUM					
				BECKERI 150.7 Ma			<i>Torquaisphinctes</i>		
			L	EUDOXUS			<i>Orthaspidoceras</i>		(11) Oxfordian-Kimmeridgian long-term global eustatic sea-level rise
				ACANTHICUM (3.4 Ma)					
	MIDDLE	OXFORDIAN	E	HYPSELOCYCLUM	EVAPORITES		(10) Upper Oxfordian-Upper Kimmeridgian evaporite facies in South America		
				PLATYNOTA 154.1 Ma					
			L	BIMAMMATUM					
				BIFURCATUM		<i>Euspid. hypsolum</i>			
			M	TRANSVERSARIUM (5.3 Ma)		<i>Cubaspidoceras</i>			
		CALLOVIAN	E	CORDATUM	<i>Perisphinctes-Araucanites</i> Association				
				MARIAE 159.4 Ma	<i>Pelliceratoides</i>				
			L	LAMBERTI			(9) Middle-Late Callovian opening of the central Atlantic Ocean and breakdown of the East Pacific Subrealm		
			M	CORONATUM (5.0 Ma)	<i>Rehmannia patagoniensis</i> and <i>Oxycer. oxynotus</i>		(8) Late Early Callovian opening of Hispanic Corridor		
				JASON					
	EARLY	BATHONIAN	E	GRACILIS CALLOVIENSE	<i>Prosiman</i> Zone				
				MACROCEPHALUS	<i>Bodendendri</i> Zone				
				DISCUS 164.4 Ma	<i>Verasensis</i> Zone				
			L	RETROC.	<i>Steinmanni</i> Zone				
			M	BREMERI (4.8 Ma)			(7) Bathonian closure of Hispanic Corridor		
		BAJOCIAN	E	SUBCONTRACTUS	<i>Cadomites - Tullidae</i> Association				
				PROGRACILIS					
			L	PARKINSONI 169.2 Ma	<i>Lobosphinctes</i>		(6) Mid-Bajocian closing of Hispanic Corridor		
				GARRANTIANA	<i>Megasph. magnum</i> ss.		(5) Limited faunal exchange along Hispanic Corridor		
M			SUBFURCATUM	<i>Rotundum</i> Zone		(4) Early stages of drift between Laurasia and Gondwana			
ALEENIAN	E	HUMPHRIESIANUM	<i>Humphr. Zone</i>						
		SAUZEI (7.3 Ma)							
	L	LAEVIUSCULA	<i>Giebell</i> Zone						
		OVALIS	<i>Singularis</i> Zone						
	M	DISCITES 176.5 Ma			(3) Limited faunal exchange along Hispanic Corridor				
TOARCIAN	E	CONCAVUM	<i>Malarg. Zone</i>						
		MURCHISONAE (3.6 Ma)	<i>"Zurch." groeberi</i> Zone						
	L	SCISSUM	<i>Manifasensis</i> Zone						
		OPALINUM 180.1 Ma			(2) Base Aalenian hiatus				
	M	LEVESQUEI	<i>P. fullana</i> & <i>P. lobarinica</i>						
		THOUARSENSE	<i>P. tenuicostatum</i>						
	E	VARIABILIS	<i>P. copiapense</i>						
		BIFRONS (9.5 Ma)	<i>P. torosae</i>						
	L	FALCIFERUM	<i>P. (P. mediana)</i>						
		TENUICOSTATUM 189.6 Ma	<i>P. (P. mediana)</i>						
PLIENSCHACHIAN	E	SPINATUM	<i>D. hoelderi</i>		(1) Base Toarcian global eustatic rise				
		MARGARITATUS	<i>D. tenuicostatum</i>						
	L	DAVOEI (5.7 Ma)	<i>D. simplex</i>						
		IBEX	<i>F. disciforme</i>						
	E	JAMESONI	<i>F. fannini</i>						
		RARICOSTATUM 195.3 Ma	<i>F. behrendseni</i>						
	L	OXYNOTUM	<i>E. medianus</i>						
		OBTUSUM (6.6 Ma)	<i>Tropidoceras</i>						
		TURNERI	<i>Eoderoceras</i> & <i>Apoderoceras</i>						
		SEMICOSTATUM	<i>E. raricostatum</i>						
SINEMURIAN	L	BUCKLANDI	<i>O. oxynotum</i>						
		ANGULATA 201.9 Ma	<i>A. obtusum</i>						
	M	LIASICUS (3.8 Ma)	<i>C. turneri</i>						
HETTANGIAN	E	PLANORBIS 205.7 Ma	<i>A. semicostatum</i>						
			<i>A. bucklandi</i>						

Figure 3.7 A summary of ammonite bio-events in the Jurassic. The two columns (A) and (B) represent the degree of faunal transfer via the Hispanic Corridor / central Atlantic Ocean (grey = limited transfer; black = full transfer); and the duration of the East Pacific Subrealm, respectively. Numerical time-scale of (Gradstein et al., 1994).

			Standard European Zones	Southern Andes Zones	Absolute ages
CRET	EARLY	RYAZANIAN	OCCITANICA	Spiticeras lambei Zone	144.2 Ma
			EUXINUS	Argenticeras noduliferum Zone	
JURASSIC	LATE	TITHONIAN	L Durangites spp.	Subuloceras Logani Zone	(6.5 Ma)
			M MICRACANTHUM	Conoc. alternans Zone	
			PONTI	Windhausioceras iserpinosum Zone	
		KIMMERIDGIAN	M FALLAUXI	Aniacosphinctes proximus Zone	150.7 Ma
			E SEMIFORME	Pseudoliasoceras zitteli Zone	
			DARWINI	Virgiosphinctes mendocanus Zone	
		OXFORDIAN	E HYBONOTUM	Torquatisphinctes	154.1 Ma
			L BECKERI		
			L EUDOXUS	Orthaspidoceras	
			E ACANTHICUM		
			DIVISUM	EVAPORITES	
		CALLOVIAN	E HYPSELOCYCLUM		159.4 Ma
			L PLATYNOTA		
			L PLANULA		
			M BIMAMMATUM	Euaspid. hypselum	
	M BIFURCATUM		Cubaspidoceras		
	E TRANSVERSARIUM		Perisphinctes-Araucanites Association		
	BATHONIAN	M PLICATILIS		164.4 Ma	
		E CORDATUM	Peltoceratoides		
		M LAMBERTI	Rehmannia patagoniensis and Oxyceri. oxynotus		
		M ATHLETA			
	BAJOCIAN	E CORONATUM		169.2 Ma	
		M JASON			
		L GRACILIS/CALLOVIENSE	Proximum Zone		
		E MACROCEPHALUS	Bodendeneri Zone		
		L DISCUS	Steinmanni Zone		
	AALENIAN	M RETROC.		176.5 Ma	
		E BREMERI			
		M SUBCONTRACTUS	Cadomites - Tullitidae Association		
		E PROGACILIS			
L ZIGZAG					
L PARKINSONI		Lobosphinctes			
TOARCIAN	L GARANTIANA	Megasp. magnum ss.	180.1 Ma		
	E SUBFURCATUM	Rotundum Zone			
	L HUMPHRIESIANUM	Humphr. Zone			
	E SAUZEI				
	L LAEVIUSCULA	Giebeli Zone			
	E OVALIS	Singularis Zone			
	L DISCITES				
PLIENSBACHIAN	L CONCAVUM	Malarg. Zone	189.6 Ma		
	E MURCHISONAE	"Zurch." grobeli Zone			
	L SCISSUM	Manflasensis Zone			
	E OPALINUM				
SINEMURIAN	L LEVESQUEI	P. finians & P. isbariologica	195.3 Ma		
	M THOUARSENSE	P. tenuicostatum			
	E VARIABILIS	P. copiapense			
	L BIFRONS	P. toroense			
	M FALCIFERUM	C. chil. P. moerckel P. boltoni			
HETTANGIAN	E TENUICOSTATUM	P. gressini	201.9 Ma		
	L SPINATUM	P. hoelderi			
	M MARGARITATUS	D. tenuicostatum			
	E DAVOEI	D. simplex			
HETTANGIAN	L IBOX	F. disciforme	205.7 Ma		
	E JAMESONI	F. fannini			
	L RARICOSTATUM	F. holmpleini			
	M OXYNOTUM	F. meridiana			
	E OBTUSUM	Tropidoceras			
HETTANGIAN	L TURNERI	Eoderoceras & Apoderoceras	195.3 Ma		
	E SEMICOSTATUM	E. raricostatum			
	L BUCKLANDI	O. oxynotum			
HETTANGIAN	M ANGULATA	A. obtusum	(6.6 Ma)		
	E LIASICUS	C. turneri			
		A. semicostatum	201.9 Ma		
		A. bucklandi			
		S. angulata	(3.8 Ma)		
		D. reiss			
			205.7 Ma		

Figure 3.8 A summary of ammonite zones used in the time-correlation of northern Chile and Europe. Numerical time-scale of Gradstein et. al., (1994).

(6) Early-Late Bajocian closing of the Hispanic Corridor

The Early-Late Bajocian boundary is marked throughout most of the circum-Pacific area by a strong faunistic change with the sudden beginning of extreme provincialism and the appearance of the East Pacific Subrealm (Hillebrandt *et al.*, 1992). Boundary events include the birth of the Boreal *Cardioceratidae* and the East Pacific *Eurycephalitinae*. There is strong evidence to suggest that in the Subfurcatum Zone the corridor was still open: a Mexican speciality also occurs very rarely in the western Tethys (J. H. Callomon pers. comm., 1996). This bio-event is interpreted to represent the closing of the Hispanic Corridor which lasted from Late Bajocian-Early Callovian.

(7) Bathonian closure of the Hispanic Corridor

The Sub-boreal Province of Stikinia and cratonic Western Interior or North America overlapped broadly with the East Pacific Subrealm (Tethyan Realm), which extended along most of the eastern Pacific margin and, at least briefly, even to New Zealand and appears at that time not to have communicated with the west Tethys through the Hispanic Corridor (Hillebrandt *et al.*, 1992).

(8) Late Early Callovian opening of the Hispanic Corridor

The Andean *Frickites* association includes East Pacific *Eurycephalitines* and cosmopolitan *Choffatia*, and is directly overlain by the Tethyan *Reineckeiid* genus *Rehmannia*, which appears to have evolved from the subgenus *Neuquenicerias* (*Frickites*). Very similar *Rehmannia* comprise the first cryptogenic representatives of the *Reineckeinae* in the Mediterranean, so that the ancestor appears to have immigrated from the Andean Province (Cariou, 1984; Westermann, 1984a; Westermann & Riccardi, 1985; Dommergue *et al.*, 1989).

(9) Middle-Late Callovian opening of the Central Atlantic Ocean

In the Mixteca Terrane and Sierra Madre Occidental of eastern Mexico the Middle-Late Callovian yields poorly known fauna of the typically "coronate" *Reineckeia* of west Tethys (Hillebrandt *et al.*, 1992). This signals the end of the East Pacific Subrealm by increased faunal exchange with west Tethys, via the new Central Atlantic Ocean and, in part, via the deepening Gulf of Mexico (Jansa, 1986). The opening of the Central Atlantic Ocean (proto-Atlantic) marks the main biogeographic event affecting the Late Jurassic ammonites worldwide (Callomon in, Hillebrandt *et al.*, 1992). Although faunal exchange via the Hispanic Corridor had occurred since the Aalenian, this was sporadic and predominately from west to east. The Oxfordian-Neocomian records clear evidence of two way migration (Callomon in, Hillebrandt *et al.*, 1992) and the connection of the eastern Pacific and west Tethys.

(10) Late Oxfordian-Late Kimmeridgian evaporite facies

The absence of *Leiostraca* from northern Chile is most simply explained as being due to the isolation of these basins from oceanic influences (Callomon in, Hillebrandt *et al.*, 1992). The late Bimammatum-Acanthicum European ammonite Zones are not represented in the Southern Andes of

Chile and Argentina (Gygi & Hillebrandt, 1991; Hillebrandt *et al.*, 1992) due to widespread evaporite facies spanning five ammonite biochrons.

(11) Oxfordian-Kimmeridgian global eustatic sea-level rise

The largely epicontinental shelf seas of the circum-polar northern hemisphere steadily widened in extent and gave rise to the strongly segregated Boreal Realm in the Late Jurassic, interpreted to be a result of rising eustatic sea-level (Callomon in, Hillebrandt *et al.*, 1992).

The major biogeographic change in the Jurassic Pacific Ocean was the establishment and disappearance of the East Pacific Subrealm (E.P.S.) in the latest Middle Jurassic (Westermann, 1981; 1984b). Prior to the appearance of this subrealm, provincialism was low. Although Gondwana and Laurasia had not yet separated, short-term influxes of taxa from Tethys to the eastern Pacific and vice versa took place, probably as a result of sea-level fluctuations that periodically flooded central Pangaea through the Hispanic Corridor (Westermann, 1981; 1984b; Hallam, 1983; Brandt, 1986).

The appearance of the East Pacific Subrealm roughly coincides with a drop in eustatic sea-level on Hallam's curve (Hallam, 1978; 1983). However, the distinctness of the subrealm in the Middle Jurassic, compared with earlier times when the connection between western Tethys and the Pacific was closed, suggests that some additional cause operated in conjunction with the palaeogeographic change. The disappearance of the subrealm may be attributed to the opening of western Tethys, which was accomplished by both a rise in sea-level (Westermann, 1984b) and rifting between Gondwana and Laurasia (Dickinson & Coney, 1980). In the later part of the Late Jurassic, provinciality may have increased again, with no apparent palaeogeographic cause (Westermann, 1984b).

Taylor *et al.* (1984) noted that the Boreal-Tethyan boundary occurred in low latitudes during the Early Jurassic, with the exception of the Late Sinemurian, when there might have been a brief movement northward. During the Middle Jurassic, the boundary moved northward 15° or 20°, depending on how the sub-boreal faunas are treated, and then moved southward again at the very end of the Middle Jurassic. Provinciality was at a maximum during the late Middle Jurassic (Westermann, 1984b).

The most interesting event is the major northward shift of the boundary between the Boreal and Tethyan realms in the Middle Jurassic (Late Bajocian-Bathonian), which occurred on both sides of the ocean (Fig. 2.12). This shift was coeval with the major drop in sea-level that closed the connection between western Tethys and the Pacific and permitted the strongest differentiation of the East Pacific Subrealm (Westermann, 1984b). The poleward shift of low latitude faunas was mirrored in the southern hemisphere (Stevens, 1980). That time also saw the strongest evidence for cold-climate conditions in northern Pangaea, with deposition of glacial-marine sediments, diamictites (pebbly argillites) and glendonites (Brandt, 1986).

3.5 Summary

In addition to a global time correlation the changing distribution of ammonite species through the Jurassic has presented several particularly interesting bio-events (Fig. 3.9). The main signatures are

Chapter 3 Biostratigraphy and chronostratigraphy

produced by the degree of faunal transfer and endemism, with the development of the endemic East Pacific Subrealm indicating a period of apparently no faunal transfer. Previous authors have interpreted the bio-events to be directly linked to changes in global eustatic sea-level, but for the purpose of this thesis the bio-events will be used in comparison with sequence stratigraphy before an interpretation of the driving mechanism is made.

Chapter 4

Depositional Environments

4.1 Objectives of Chapter

The primary objective of this chapter is to provide a detailed description and subsequent interpretation of individual facies on the basis of process sedimentology and characteristic internal structures. Temporally equivalent facies and facies associations are grouped into discrete depositional environments on the basis of bounding surface character and stratigraphical architecture. The subsequent integration of these environments allows the development of depositional models, based on an amalgamation of temporally and spatially distinct facies and facies associations. Therefore, the integration of field data and observations at a variety of scales will allow the construction of generalised depositional models for the Domeyko basin-fill.

4.2 Introduction

In order to facilitate a study of the application of sequence stratigraphical concepts, a detailed understanding of the sedimentology of the area under study is an essential pre-requisite. This chapter provides an account of the facies and facies associations which have been identified in the Mesozoic Domeyko basin-fill.

The Mesozoic sedimentary succession of northern Chile is highly diverse including continental clastic, mixed carbonate/siliciclastic marine and evaporite deposits. Four temporally distinct depositional systems have been identified including continental siliciclastic, shallow-marine siliciclastic ramp, shallow-marine carbonate ramp and carbonate rimmed-shelf on the basis of their component facies associations. The mixed carbonate/siliciclastic marine basin-fill can be divided into siliciclastic-ramp, carbonate ramp and carbonate rimmed-shelf depositional systems. A general description of the facies associations and component facies which compose each depositional system is given, supported by examples from the Domeyko basin succession.

4.3 Continental clastic facies description

The distribution of Mesozoic continental clastic deposits in northern Chile is restricted to the Late Triassic-Middle Jurassic (pre-marine transgression) and the Early-Late Cretaceous (post-marine regression). There is no evidence of upper Middle-Upper Jurassic continental clastic deposits in northern Chile. These two major periods of continental red-bed sedimentation gave rise to similar depositional facies, but with quite distinct compositional (provenance) and diagenetic differences making the two units easily distinguishable in the field. The process sedimentology and facies descriptions are similar for both units and therefore considered together in this chapter. The compositional and diagenetic differences and their reasons are also discussed.

One marginal-marine and three non-marine depositional environments are interpreted to represent the continental clastic depositional system which encompasses all the Mesozoic continental facies identified in the basin (Fig. 4.1). Each depositional environment is identified on the basis of facies, facies distribution, bounding surface character and internal architectural elements. The floodplain environment comprises four temporally and spatially related facies associations (Fig. 4.1). Six facies associations have been defined for the continental clastic deposits of the Domeyko basin, including conglomeratic alluvial fan, fan-delta, sand-rich braided fluvial, overbank and lacustrine siltstone facies associations (Fig. 4.1).

4.3.1 Conglomeratic alluvial fan facies association

Description

Moderately well-sorted, clast-supported conglomerate facies and more rare matrix-supported conglomerate facies compose the majority of the conglomeratic alluvial fan facies association (Table 4.1). Both conglomerates are dark red in colour with bed thicknesses ranging from 0.2-10 m, defining sharp- to erosively-based, normally-graded units from cobble-grade conglomerate to coarse-grained sand or gravel grain-size. Internally, many of the conglomerates are structureless or crudely stratified, with a preferred clast orientation indicated by pebble imbrication where the long axes are aligned transversely to the flow direction. Within the conglomerates are intercalated lenses and sheets of erosively-based, coarse-grained sandstone facies and well stratified gravel facies, with 0.2-0.5 m scale trough and planar-tabular cross-bedding (Table 4.1). Two examples of conglomeratic alluvial fan facies (Sierra San Lorenzo and Quebrada La Carreta) are described, both of which display different scales of bedding and dominant sedimentary structures.

Sierra San Lorenzo example

Figure 4.2 shows the Lower Cretaceous matrix- and clast-supported conglomerates at Sierra San Lorenzo (Fig. 1.1, Locality 17) where clast-size is predominately pebble- and cobble-grade, ranging from 0.05-0.15 m in diameter with rare boulders reaching 0.25-0.30 m in diameter, marking the maximum clast-size. The grain-size is almost entirely gravel-grade or coarser, with sand-grade material making up less than 5% of the bulk rock (Fig. 4.2). The conglomerates are poorly bedded

Figure 4.1 Schematic representation of the Domeyko basin continental clastic facies and facies associations in northern Chile based on lithology and grain-size, sedimentary structures, body and trace fossils and bounding surface character.

Lithology	Graphic log	Facies	Facies association	Depositional environments	Description	Body and trace fossils	Bounding surfaces & architectural elements	Schematic representation of architectural elements
		Clast- & matrix-supported conglomerates, stratified gravel & coarse-grained sst., medium-grained pedogenic sst.	Conglomeratic alluvial fan	Alluvial fan	clast- and matrix-supported, bedding (1-10 m), normal grading, internal erosion surfaces, trough & planar-tabular cross bedding (0.2-1 m), lenses and sheets of coarse-grained sand to gravel, clast imbrication	plant debris (tree trunks, leaf impressions), reworked concretions containing ammonites	Multi-storey, multi-lateral, erosionally-based channelised clast- & matrix-supported conglomerate bodies	
		Very coarse- to medium-grained sandstone channel-fill No silt-grade material	Sand-rich braided fluvial	Multistorey braided fluvial	erosionally-based, multi-storey, multi-lateral channel sandstones, trough & planar-tabular cross bedding (0.2-0.5 m), gravel to fine pebble lags, normal grading, parallel lamination, current ripples	rare vertebrate and invertebrate remains as well as plant debris (tree trunks, leaf impressions)	Multi-storey, multi-lateral, erosionally-based channel sandstone bodies with no silt-grade material	
		Very coarse- to medium-grained sandstone channel-fill Medium-grained siltstone	Sand/silt fluvial	Floodplain	erosionally-based, single-storey channel sandstones, trough & planar-tabular cross bedding (0.2-0.5 m), gravel to small pebble lags, normal grading, massive siltstone, rare parallel lamination	rare vertebrate and invertebrate remains as well as plant debris (tree trunks, leaf impressions)	Single-storey, erosionally-based channel sandstones in medium-grained, homogeneous siltstone	
		Fine- to medium-grained sheet-geometry sst.	Sandy crevasse splay		sharp- to erosively-based, climbing ripple cross lamination, normal grading, parallel lamination	rare vertebrate and invertebrate remains as well as plant debris (tree trunks, leaf impressions)	Medium-grained homogeneous siltstone with thin, erosionally-based, sheet-geometry sandstone bodies	
		Medium-grained siltstone	Floodplain siltstone		parallel lamination, rare small adhesion ripples			
		Fine- to medium-grained siltstone Rare thin sheet-geometry sandstones	Lacustrine siltstone		massive or fine parallel lamination	rare freshwater bivalves	Fine-grained homogeneous siltstone with rare, thin sheet-geometry sandstone bodies	
		Clast- & matrix-supported conglomerates, bioturbated & wave-rippled sst., algal-laminated & framework-coral limestones	Fan-delta	Fan-delta	clast- and matrix-supported, bedding (1-10 m), normal grading, internal erosion surfaces, trough & planar-tabular cross bedding (0.2-1 m), thin (0.1-0.5 m) sheet-geometry algal & marine limestones & rippled sst.	rare vertebrate & invertebrate remains, plant debris, corals, algal mats, stromatolites, bivalves, brachiopods, belemnites, <i>Skolithos</i>	Multi-storey, erosionally-based channelised conglomerates with thin, laterally extensive sheet-geometry limestones & sandstones	

Alluvial Fan Conglomerates at Sa. San Lorenzo

Large scale packaging
(1 cm : 8 m)

Sedimentary structures
(1 cm : 1 m)

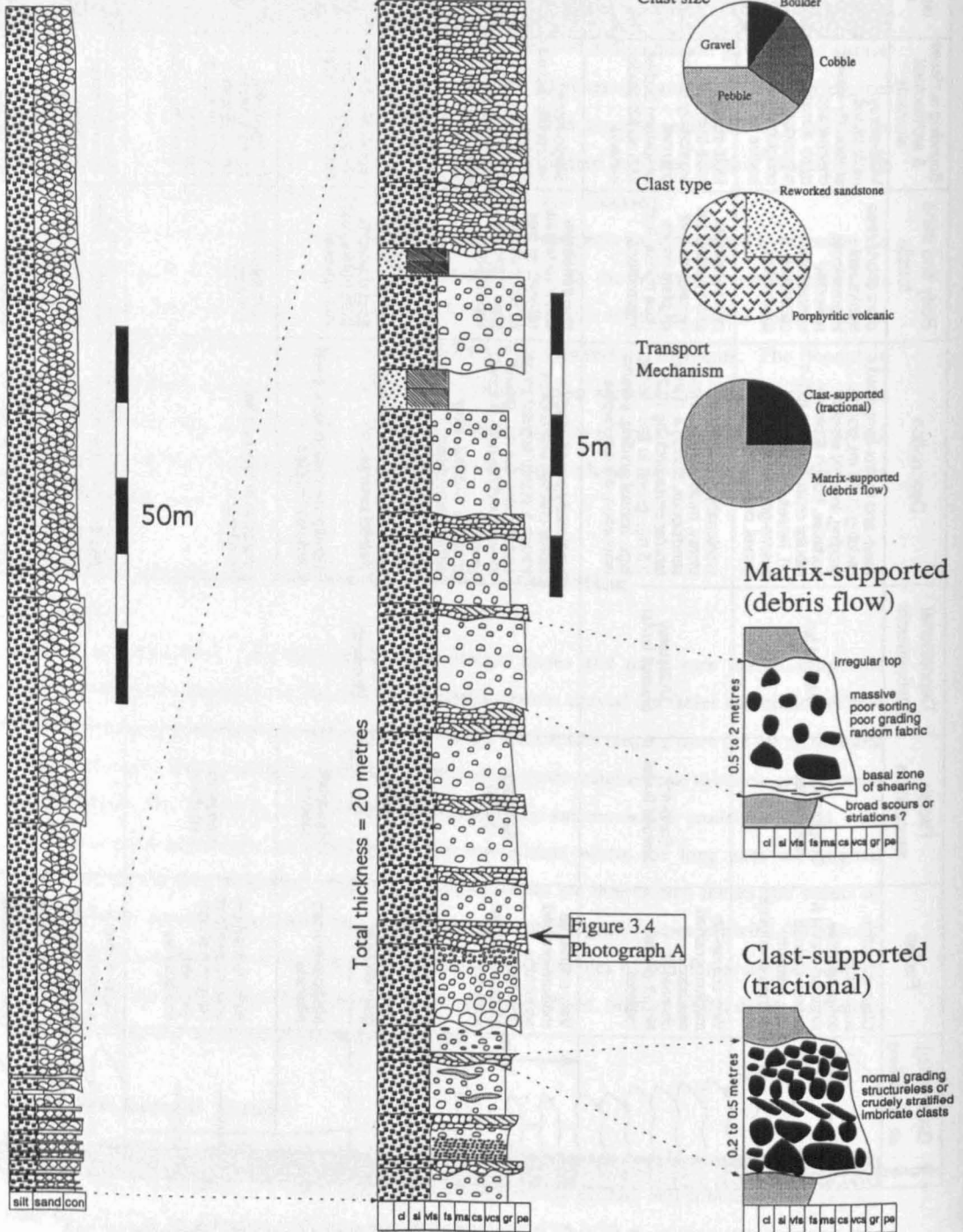


Figure 4.2 Sedimentary log of the Lower Cretaceous conglomerates at Sierra San Lorenzo (Figure 1, locality 17). The log shows the two principle conglomerate facies, matrix-supported and clast-supported, which have been interpreted as debris-flow and tractional deposits, respectively. The evidence for tractional conglomerates rather than non-cohesive debris flow conglomerates is clast imbrication and normal grading. Position of Figure 4.3 (Photograph A) indicated.

with bed thicknesses of 0.2-2 m. Two types of pebble- to cobble-grade conglomerate facies are seen, erosively-based clast-supported conglomerates, which are structureless or crudely-stratified with normal-grading and imbricate clasts, and typically sharp, non-erosively based matrix-supported, conglomerates with a sandy matrix and sheet geometry (Fig. 4.3, *Photograph A*). Internally, the matrix-supported conglomerates are massive with poor sorting and grading giving a random fabric, in contrast to the normally-graded clast-supported conglomerates with trough cross-bedding and imbricate clasts (Fig. 4.3, *Photograph A*). Matrix-supported conglomerates make up 70% of the rock with thinner intercalated clast-supported conglomerates constituting only 30% (Fig. 4.2). The clast-supported conglomerates and in particular the finer-grained gravel horizons both display planar-tabular cross-bedding. The planar-tabular cross-beds develop a foreset height of 0.25-0.5 m and indicate a palaeocurrent direction of 079°N (Bogdanic, 1990), while pebble imbrication indicates palaeocurrent directions of 067° and 069°N. Landsat imagery has allowed a cross-sectional view of the alluvial conglomerates which display a lateral thinning from 700 m to zero in less than 10 km (Fig. 4.4). The structure at Sierra San Lorenzo is based around a large anticline plunging to the south-east and cored by Oxfordian-Kimmeridgian (Upper Jurassic) limestones and evaporites (Fig. 4.4).

Quebrada La Carreta example

Clast-supported, pebble- to cobble-grade conglomerate facies (Table 4.1), coarse-grained sandstone facies and well stratified gravel facies compose the Lower Cretaceous deposits of Quebrada La Carreta (Fig. 1.1, Locality 61). The clast-supported, pebble- to cobble-grade conglomerate facies range from 1-10 m in thickness, displaying normal-grading, planar-tabular and trough cross-bedding (Fig. 4.3, *Photograph B*). The cross-bedding occurs on a scale of 0.5-1 m, decreasing-upwards to 0.2 m at the top of the bed. The thicker units of 5-10 m are organised into 1.5 m thick, normally-graded units, within the general fining-up trend. The conglomeratic clasts are moderately to well sorted and rounded with 90% of clasts having volcanic compositions and only 10% being composed of reworked lithic sandstone (Fig. 4.3, *Photograph B*). Interbedded channels or sheets of erosively-based, coarse-grained sandstone facies and well stratified gravel facies display normal-grading, 0.2-0.5 m planar-tabular and trough cross-bedding, as well as parallel lamination. Internal erosion surfaces are commonly associated with 0.05-0.1 m thick fine pebble lags. A coarse-grained grey/green sandstone facies occurs in 0.5-3 m thick beds containing floating, angular, pebble-grade volcanic fragments, 0.2-0.3 m scale planar-tabular and trough cross-bedding and rare normal-grading. Similar Lower Cretaceous deposits occur at N.E. El Abra (Fig. 1.1, Locality 13) and Quebrada Honda (Fig. 1.1, Locality 14) with Triassic continental conglomerates at Quebradas Punta del Viento and Vaquilles (Fig. 1.1, Locality 60 and 63).

The clast types making up the Triassic conglomerates are almost entirely volcanic or intrusive, 90%, derived predominantly from Palaeozoic (Permo-Triassic) acid volcanic and plutonic rocks with rare reworked volcanoclastics making up less than 10% of clasts. There is little preserved evidence of body or trace fossils, only occasional freshwater bivalves and plant debris in the form of tree trunks and leaf impressions, noted by Chong & Hillebrandt (1985). In rare cases leaf impressions and plant debris

have been diagenetically replaced by the copper silicate, Chrysocolla ($\text{CuSiO}_3 \cdot 2\text{H}_2\text{O}$), giving a bright blue/green colour. This phenomenon is clearly seen in the Triassic sandstones and conglomerates of the Rio San Salvador area (Fig. 1.1, Locality 18) to the west of Calama (G. Chong, pers. comm., 1994).

Bogdanic (1990) describes the Cretaceous conglomerate facies between 21° - 23°S which are composed predominantly, 75%, of reworked igneous clasts of rhyolitic to dacitic composition, with the remaining 25% made up by sandstone and limestone clasts, including reworked concretions (Fig. 4.2). In the Sierra San Lorenzo area (Fig. 1.1, Locality 17) these reworked concretions are found to contain the Oxfordian ammonite *Perisphinctes*. The matrix consists of coarse-grained sub-litharenite (Pettijohn, 1975; Folk *et al.*, 1970) and gravel with a calcite cement. The type of cement provides one of the identification criteria for distinguishing between the Triassic and Cretaceous conglomerates. The Triassic conglomerates have a well developed silica cement making them highly indurated and resistant to erosion, while the Cretaceous conglomerates have a more poorly developed calcite cement. In rare cases such as N.E. El Abra (Fig. 1.1, Locality 13), the characteristic red colour of the Lower Cretaceous conglomerates has been replaced by the pale green colour of epidote as a result of low-grade hydrothermal metamorphism.

Interpretation

The conglomerates and sandstones are predominantly red in colour caused by the breakdown of biotite and hornblende to give clays, immature iron oxides and hydroxides, as discussed by Turner (1980). These oxides are then washed to lower levels in the weathering profile where they coat grains and with time, mature to haematite. These changes will be aided by elevated temperatures but their main prerequisite is water provided by ephemeral rainfall and run-off. Rates of reddening vary with lithology, clay rich sediments altering more slowly due to lower permeabilities. Present day, warm, seasonally humid source areas supply detritus which is mainly grey or brown, with iron present as hydrated oxides (Van Houten, 1982; Turner, 1980). If these are deposited in settings which are then subjected to an oxidising ground-water regime, probably favoured by a lowered water table, then the amorphous hydroxides and oxides may mature in situ to give eventually a red deposit (eg. Pajmans *et al.*, 1971). In the Mesozoic of northern Chile a warm, seasonally humid climate is interpreted, supported by hermatypic coral reef development (Prinz, 1991) and the palaeoclimate discussion presented in Chapter 2 (2.4 Palaeoclimate and oceanography of northern Chile).

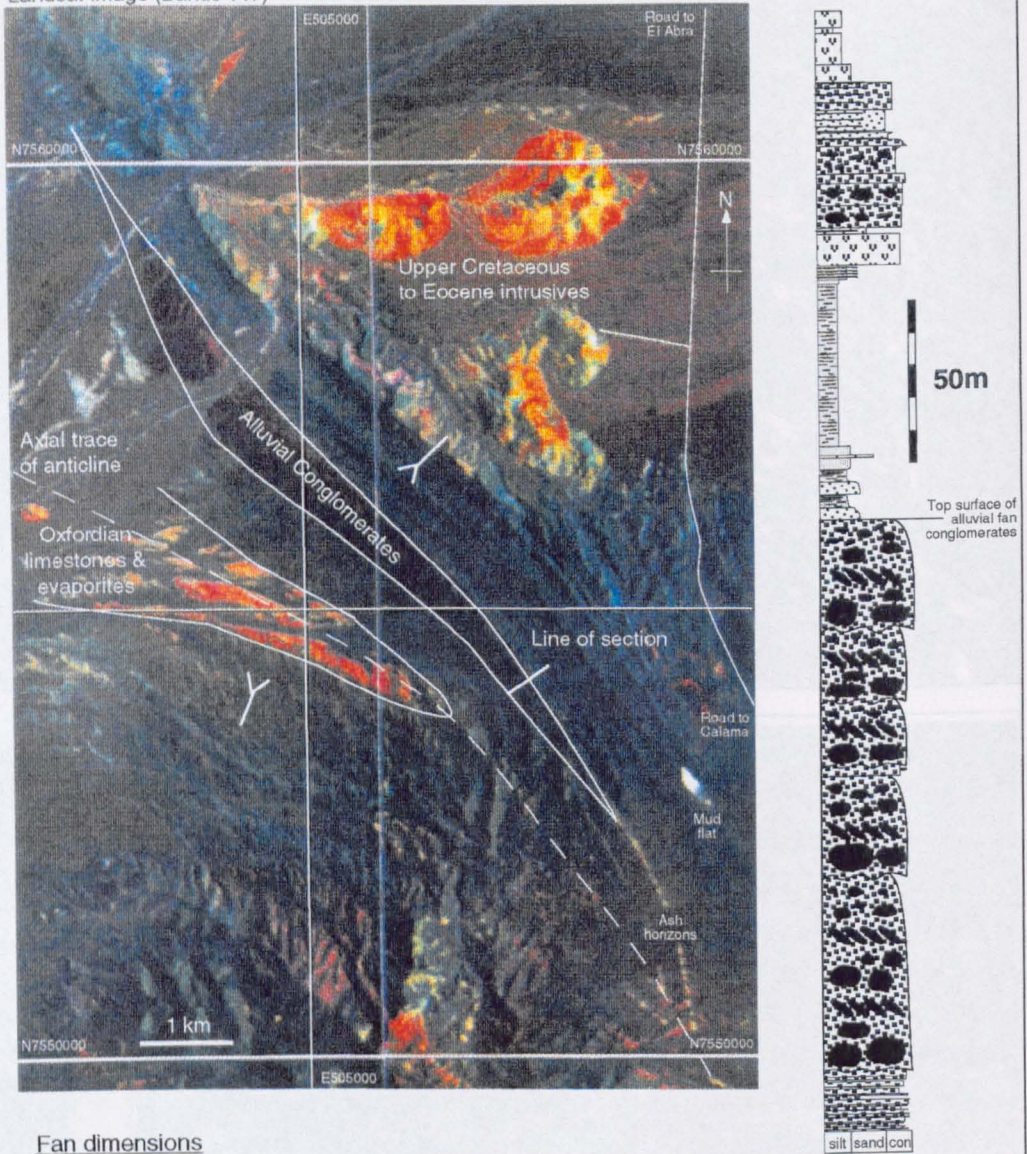
Abundant matrix-supported conglomerate facies make up 70% of the deposits at Sierra San Lorenzo and are interpreted to represent deposition by cohesive debris flow, with the remaining 30% being clast-supported conglomerates interpreted to represent tractional sheet- and stream-flow deposits (Fig. 4.5). Cohesive debris flows are typical of ephemeral alluvial fan deposits laid down during periods of flooding (Fig. 4.5). An alluvial fan interpretation is supported by the Landsat data which demonstrate a fan-type geometry with a lateral thinning from 700 m to zero in less than 10 kilometres (Fig. 4.4). The palaeocurrent data indicates a principle south-west to north-east direction (Bogdanic, 1990), implying a perpendicular section through the alluvial fan (Fig. 4.4). These dimensions are indicative



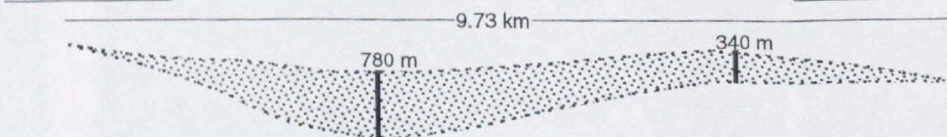
Figure 4.3 *Photograph A:* Lower Cretaceous alluvial conglomerates from Sierra San Lorenzo showing a typical exposure of the interbedded matrix- and clast-supported conglomerate facies with a 1 m thick matrix-supported debris flow conglomerate bed and 0.5 m thick clast-supported tractional conglomerate bed (Figure 4.2). Younging direction is from bottom-left to top-right with a hammer for scale. *Photograph B:* Lower Cretaceous alluvial conglomerates from Quebrada La Carreta which are predominately clast-supported tractional conglomerate facies. Hammer for scale.

Alluvial fan geometry at Sierra San Lorenzo

Landsat Image (Bands 147)



Fan dimensions



Palaeocurrent data (Bogdanic 1990)

Pebble imbrication of conglomerates



Foresets of tabular cross-bedding

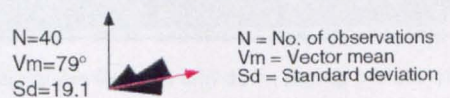


Figure 4.4 An interpreted Landsat image (Bands 147) of the Sierra San Lorenzo area displaying a large anticline plunging to the south-east and cored by Oxfordian-Kimmeridgian (Upper Jurassic) limestones and evaporites. The fold structure is defined by two ash horizons, one below the conglomerate unit and one above. The image presents a cross-sectional view of the alluvial conglomerate facies which show a lateral thinning from 700 m to zero in less than 10 km.

of the classic, “semi-conical” or steep dry-type (cohesive debris flow) fan of Holmes (1965); Schumm (1977); see also review by Rachoeki (1981), which are ideally related to tectonic escarpments, as opposed to the wet-type (stream-dominated) alluvial fan of Nemec & Steel (1988a), which are generally much lower gradient and larger in size.

The time-equivalent Lower Cretaceous erosively-based conglomerates at Quebrada La Carreta in the south are primarily, normally-graded, clast-supported deposits with good evidence of pebble imbrication, planar-tabular and trough cross-bedding (Fig. 4.3, *Photograph B*). These deposits are interpreted as tractional and stream-flow conglomerates laid down in a high-energy, proximal braided fluvial system (Fig. 4.5).

The clast compositions indicate two different source areas for the Triassic conglomerate facies and the Lower Cretaceous conglomerate facies. The Triassic conglomerates are immature, volcanoclastics derived predominantly from Permo-Triassic acid volcanic and plutonic rocks. In contrast, the Lower Cretaceous conglomerate facies are more mature sub-litharenites (Folk *et al.*, 1970; Pettijohn, 1975), thought to have been derived from a recycled orogen, described by Bogdanic (1990). The Lower Cretaceous conglomerate facies also contain evidence for reworking of the Upper Jurassic marine limestones, implying Early Cretaceous uplift of the Jurassic basin.

4.3.2 Fan-delta facies association

Description

The fan-delta facies association consists of clast- and matrix-supported conglomerates and gravels, some of which are similar to those of the previously described conglomeratic alluvial fan facies association (Table 4.1). In addition to the conglomerate and gravel facies, there are also intercalated algal laminated limestone, reef-building coral, wave-rippled sandstone and bioturbated sandstone facies (Table 4.1).

Quebrada Vaquilles and Punta del Viento examples

The Upper Triassic deposits at Quebradas Vaquilles and Punta del Viento (Fig. 1.1, Localities 60 and 63) consist of 1-10 m thick, dark red and pale grey to brown, matrix- and clast-supported conglomerate facies with intercalated 0.1-0.5 m thick, algal laminated limestone, reef-building coral, wave-rippled sandstone and bioturbated sandstone facies (Table 4.1, Figs 4.6 and 4.7). The algal laminated limestone facies shows a distinctive millimetre-scale parallel and convex-upwards lamination with 0.1-0.5 m bed thickness and sheet geometry, which can be traced laterally for greater than 100 m (Fig. 4.6). Reef building coral facies are found in similar 0.1-0.5 m thick sheet geometry beds with convex-upwards coral domes up to 0.1 m in diameter, indicating life position. Medium- to very coarse-grained sandstone facies with abundant symmetrical ripples are found in beds of 0.4-2 m bed thickness (Table 4.1, Fig. 4.7). Similar, 0.4-2 m thick fine- to medium-grained sandstones are found which contain abundant vertical bioturbation of *Skolithos*, as well as bivalves, brachiopods and shell debris (Table 4.1, Fig. 4.7).

Cerro Jaspe example

Dark red and pale grey to brown, clast- and matrix-supported, gravel and pebble-grade conglomerate facies compose the majority of the Lower Jurassic deposits of the Cerro Jaspe area (Table 4.1, Fig. 4.8). The clast-supported conglomerates are normally-graded with sharp to erosive bases incising up to 0.2 m into the underlying unit, while the matrix-supported conglomerates are sharp-based and commonly reverse-graded (Figs 4.8 and 4.9). The conglomerate beds are 0.5-5 m thick and laterally extensive for greater than 100 m defining a characteristic sheet geometry. In addition, there are distinctive matrix- and clast-supported gravel conglomerates ranging in thickness from 0.4-1 m, composed of gravel-grade quartz grains held within a microsparite to sparry calcite matrix (Fig. 4.10). The well rounded and sorted grains are of quartz, porphyritic volcanic and fine-grained red sandstone compositions with abundant broken belemnite and coral fragments but no other evidence of body or trace fossils (Fig. 4.9, *Photograph B*). The gravel facies commonly develop 0.2-0.4 m scale planar-tabular cross-bedding with rare floating fine- to medium-sized pebble clasts (Fig. 4.10). Two pale green to grey, medium- to very coarse-grained sandstone facies occur in the Cerro Jaspe area, a facies characterised by symmetrical ripples of wavelength 0.05-0.1 m and amplitude 0.01-0.015 m, and a heavily bioturbated sandstone with abundant small vertical *Skolithos* burrows (Table 4.1). Both sandstone facies contain bivalve and brachiopod fauna as well as small quantities of shell debris. Reef building coral facies range in bed thickness from 0.15-1.1 m with a microsparite composition and abundant framework coral, as well as bivalve, brachiopod and belemnite fossils (Table 4.1). The framework corals in the Southwest Cerro Jaspe example are generally convex-upwards domes in life position with diameters up to 0.5 m (Fig. 4.12). The limestone beds have a well developed sheet geometry which can be traced laterally for distances greater than 100 m.

Quebrada Honda example

On a markedly smaller scale the Oxfordian/Kimmeridgian of Quebrada Honda records the relatively rapid transition from yellow, algal laminated limestone facies to dark red, coarse-grained sandstone and conglomerate facies (Table 4.1, Fig. 4.11). The transition occurs over several tens of metres with the intercalation of 0.1-0.5 m thick, sharp to slightly erosively based, red and green sandstone beds within the algal laminated limestone facies (Figs 4.11 and 4.13). The intercalated sandstones are structureless with rare, floating, fine to medium pebble-grade clasts (Fig. 4.11). Further through the transition zone intercalations of 0.1-0.3 m thick algal laminated yellow limestone facies occur within the dark red, coarse-grained sandstone and conglomerate facies (Figs 4.11 and 4.13).

Interpretation

The characteristic dark red colour seen in some of the conglomerate facies is caused by haematite staining of grains or fine-grained detrital material, as previously discussed for alluvial fan conglomerates (4.3.1). The dark red conglomerates are both matrix- and clast-supported indicating debris and stream-flow mechanisms, respectively, with high percentages of silt matrix and diverse clast populations reflecting their low maturity (Fig. 4.5). Where the conglomerates are pale to

Sediment Transport Mechanisms

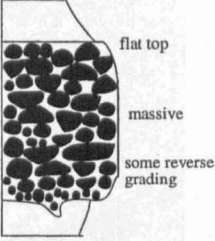
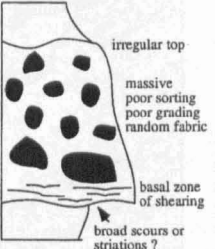
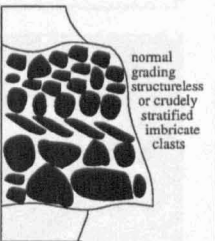
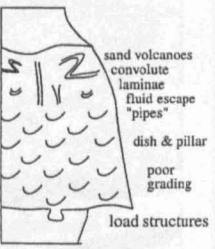
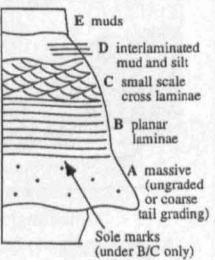
Flow mechanism and facies	Transport mechanism	Sediment texture	Bed thickness and bounding surfaces	Sketch logs (after Middleton & Hampton, 1973)
Grain flow (cohesionless to slightly cohesive debris flow)	Laminar or turbulent, high concentration, slightly cohesive or non-cohesive Clast support from <u>dispersive pressure</u> and dense fine sediment-water fluid (enhanced buoyancy). (Lowe, 1976; Bagnold, 1954)	Clast-supported, pebble and cobble gravels with silt-clay matrix or almost no matrix; beds show reverse-grading in lower part (Bagnold, 1954; Middleton, 1970)	0.4-2 m beds; bounding surfaces poorly defined, non-erosive	
Debris flow (cohesive debris flow)	Turbulent, high concentration, instant "freezing" of flow, clasts supported by the high shear-strength of matrix (clay and silt) and enhanced buoyancy. (Johnson, 1970)	Pebble and cobble gravels dispersed in a clay - silt matrix Possibility of large-scale "eddy" structures caused by high turbulence (Rutgers 1962)	0.5-2 m beds; with sharp, non-erosive boundaries and sheet-like geometry	
Sheet & stream flow (tractional processes)	Tractional processes (subaerial)	Clast-supported, pebble and cobble gravels; normally graded, structureless to crudely stratified; imbricate clasts	0.3-1 m beds with erosional basal surfaces and distinct upper contacts	
Liquefied flow	Laminar, high concentration, cohesionless, additional lift provided by <u>dispersive pressure</u> (Bagnold, 1954)	Dominated by water-escape structures such as convolute laminations, fluid-escape pipes, dish & pillar structures and sand volcanoes	0.2-1 m beds with well-defined boundaries. Flat bases and sheet-like geometry	
Turbidity flow (Bouma sequence)	Both non-cohesive and cohesive (low strength), turbulent low-concentration flow. Entrained / enhanced turbulent suspension at the top.	Clast-supported pebble gravels. Well sorted with little or no matrix. Normal grading in upper part	0.2-2 m beds with well-defined boundaries. Flat bases and sheet-like geometry	

Figure 4.5 Criteria for the description and process interpretation of conglomerate deposits (modified from Flint & Turner 1988)



Figure 4.6 Upper Triassic conglomerate facies at Quebrada Vaquilles (Figure 1, locality 63). *Photograph A* shows Upper Triassic conglomerate facies with 0.2-0.5 m thick sheet-geometry black algal limestone striking from top-left to bottom-right (north-south). People for scale. *Photograph B* shows detail of the 0.2-0.5 m thick sheet-geometry black algal limestone showing convex-upwards lamination, interpreted to be a stromatolite. Notebook for scale.

Punta del Viento section

Marine limestone facies

Fine-grained offshore mudstones containing ammonites (Early Hettangian)

Abrupt flooding event causing drowning of the reef and the deposition of fine-grained offshore mudstone. The flooding event marks the base of the Hettangian (Early Jurassic).

Thecosmilia-dominated reef with bivalves and the conodont *Epigondolella bidentata*, indicating a Late Triassic age (Figure 4.34, Photograph A)

Figure 4.34
Photograph A

50m

10m

Marine sandstone facies

Clast-supported

Medium-grained sandstones with carbonate cement and abundant symmetrical ripples, interpreted to be wave ripples

Mainly clast-supported with rare matrix-supported

Clasts are distinctly more rounded than before

Medium-grained sandstone with trough cross bedding and parallel lamination
Clast- and matrix-supported conglomerate

10m

Figure 4.7 Upper Triassic fan-delta sandstones and conglomerates from Punta del Viento (Figure 1.1, Locality 60) capped by a Rhaetian limestone reef (Figure 4.34, Photograph A).

Fan-delta facies from South-west Cerro Jaspe

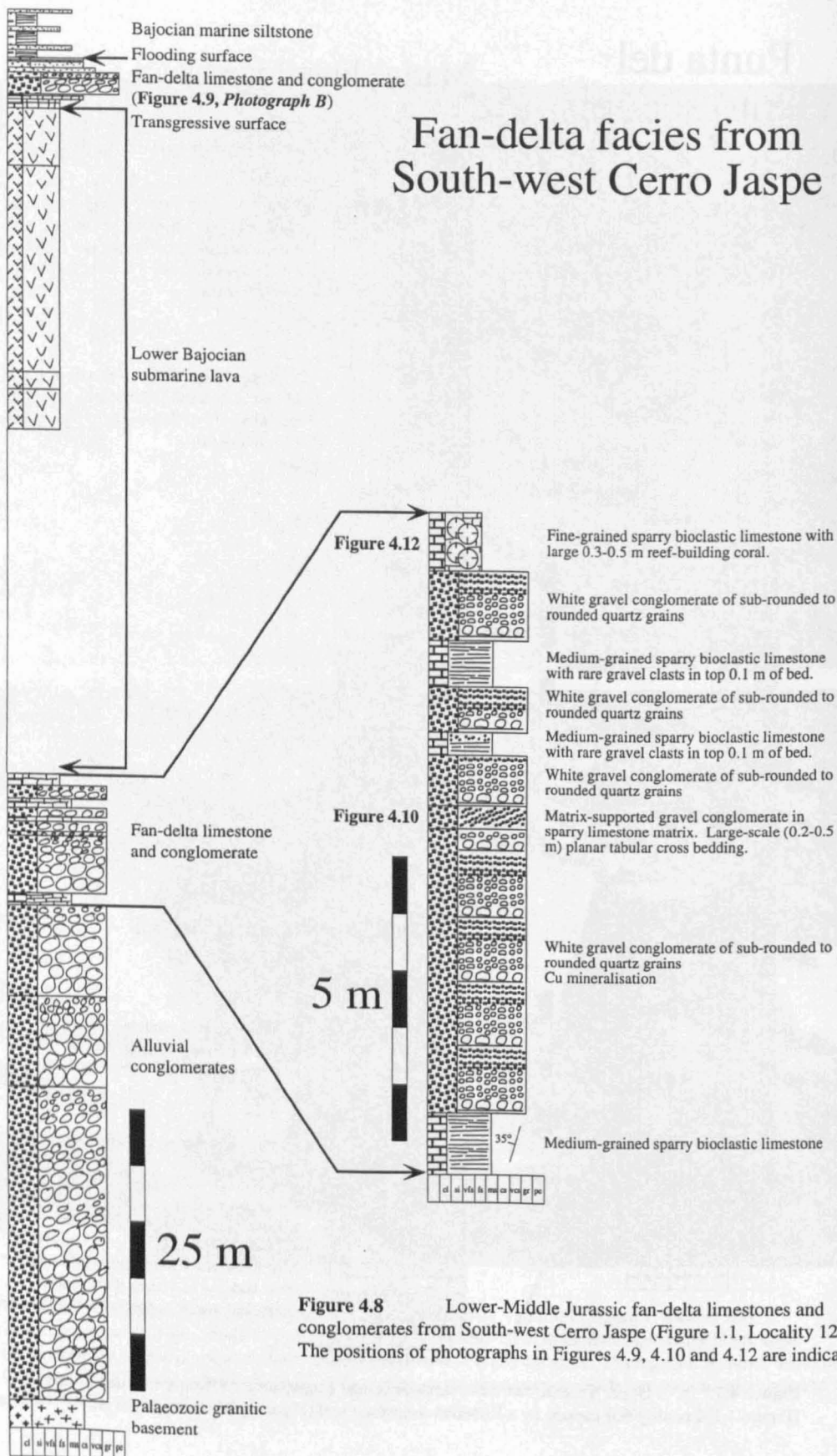


Figure 4.8 Lower-Middle Jurassic fan-delta limestones and conglomerates from South-west Cerro Jaspe (Figure 1.1, Locality 12). The positions of photographs in Figures 4.9, 4.10 and 4.12 are indicated.

medium grey in colour with well developed rounding and sorting of clasts, a higher maturity is interpreted, with the haematite producing iron oxides and fine-grained detrital material having been removed by shallow-marine wave processes (Fig. 4.9). The high percentage of quartz pebbles, abundant broken belemnite fragments and coral debris also support a degree of shallow-marine reworking (Fig. 4.9, *Photograph B*). The matrix- and clast-supported gravel facies contain well developed planar-tabular cross-bedding and a silt-free recrystallised microsparite matrix as well as abundant broken belemnite fragments and coral debris, interpreted to indicate shallow-marine reworking (Fig. 4.10). The medium- to very coarse-grained sandstone facies dominated by symmetrical ripples is interpreted as a shallow-marine wave-dominated deposit occurring above fairweather wave base, supported by the occurrence of marine bivalve and brachiopod fossils with stringer horizons of shell debris (Table 4.1). Fine- to medium-grained sandstone facies with abundant *Skolithos* bioturbation and body fossils is interpreted to represent a shallow-marine deposit (Table 4.1).

The reef building coral facies containing large framework corals in life position is an excellent indicator of shallow-marine conditions (< 10 m water depth) and reduced terrigenous clastic input (Fig. 4.12). These periods of clastic starvation, during which the limestone facies form, are well defined and can be traced laterally up to 100 m, representing local time lines within the section and highlighting the marked variation in rates of sedimentation between the conglomerate and limestone facies (Figs 4.9 and 4.12). This facies association of matrix- and clast-supported conglomerates with thin intercalated marine sandstones and limestones is interpreted to represent the high-concentration, sub-aqueous zone of a fan-delta (Nemec & Steel, 1988b). In the case of Quebradas Vaquilles and Honda where the matrix- and clast-supported conglomerate facies contain thin intercalated laminated limestone facies (Table 4.1, Fig. 4.13). The limestones are interpreted as algal deposits possibly indicating the presence of a fan-delta prograding into a restricted lagoonal setting.

4.3.3 Sand-rich braided fluvial facies association

Description

Individual sandstone beds display a channel geometry and normal-grading from coarse- or very coarse-grained sandstone to fine-grained sandstone facies (Table 4.1). Each bed is 1-4 m in vertical thickness, thinning laterally to zero within 30 m. Basal boundaries are characteristically sharp to erosive with incision up to 0.2 m into the underlying sandstone. At the base of each bed a 0.1-0.3 m thick gravel- to fine pebble-grade lag is commonly developed with reworked fine-grained sandstone intraclasts (Table 4.1). Large, 0.3-0.4 m scale trough and planar-tabular cross-bedding is developed in the coarse-grained lower half of the bed, while climbing ripple lamination, asymmetric ripples, small 0.02-0.1 m scale trough cross-bedding and parallel lamination develop in the fine- to medium-grained upper half of the bed (Table 4.1). The asymmetric ripples have wavelengths ranging from 0.05-0.1 m and amplitudes of 0.01-0.015 m. There are rare continental vertebrate and invertebrate fossils as well as plant debris which are particularly well exposed in the section at Quebrada La Carreta (Fig. 1.1, Locality 61), described by Chong (1973); G. Chong, pers. comm. (1994).

The sandstone channels contain little or no silt-grade material and are amalgamated into multistorey, multilateral sandstone bodies ranging in thickness from 5-35 m (Table 4.1). The lower and upper bounding surfaces are erosive and sharp, respectively, with abrupt facies changes below and above each multistorey sandstone body.

Interpretation

The individual sandstone beds are interpreted as channel fills on the basis of their 1-4 m vertical thickness, sharp to erosive base, normal-grading, internal sedimentary structures and channel geometry. The characteristic internal sedimentary structures include a basal lag deposit, trough and planar-tabular cross-bedding, climbing ripple lamination and asymmetric ripples (Table 4.1). The asymmetric ripples are interpreted as unidirectional current ripples. The deposits are thought to be continental in origin, based on their dark red colour, vertebrate and invertebrate fossils and plant debris, supported by the lack of symmetric ripples or marine body and trace fossils. The amalgamated sandstone beds are interpreted to represent multistorey, multilateral, sand-rich fluvial systems.

4.3.4 Minor fluvial channel facies association

Description

The minor fluvial channel facies association is composed of single-storey channelised sandstone beds within medium-grained red siltstone facies (Table 4.1, Figs 4.14 and 4.15). Individual sandstone beds have a channel geometry and normal-grading from coarse-grained sandstone to very fine-grained sandstone facies (Fig. 4.14). Each bed is 0.5-2 m in vertical thickness, thinning laterally to zero within 50-100 m (Fig. 4.15). Bed boundaries are characteristically sharp to erosive with incision up to 0.2 m into the underlying siltstone (Figs 4.14 and 4.15). At the base of each bed a 0.1-0.2 m thick gravel to fine pebble lag is commonly developed with reworked siltstone rip-up intraclasts (Fig. 4.14). The coarse-grained lower half of the bed contains large, 0.3-0.4 m scale trough cross-bedding or is structureless and massive, while climbing ripple lamination, asymmetric ripples, small 0.02-0.1 m scale trough cross-bedding and parallel lamination characterise the fine- to medium-grained upper half of the bed (Fig. 4.14). The asymmetric ripples have wavelengths of 0.05 m and amplitudes of 0.01 m. The 0.5-5 m thick, medium-grained siltstone facies is commonly red in colour and internally homogeneous with rare parallel lamination and continental vertebrate and invertebrate fossils as well as plant debris (Chong, 1973; G. Chong, pers. comm., 1994) (Table 4.1, Fig. 4.15).

Quebrada La Carreta example

The Lower Cretaceous deposits at Quebrada La Carreta (Fig. 1.1, Locality 61) are composed of erosively-based, channelised sandstone facies within medium-grained siltstone facies, as previously described (Table 4.1). In addition, there are 0.1-0.5 m thick intercalations of yellow to pale brown, fine-grained algal limestone facies containing fine wavy or parallel lamination and small bivalve fossils (Table 4.1). A distinctive 0.2-0.5 m thick, red to brown, fine- to medium-grained mottled sandstone facies contains abundant, greater than 50%, carbonate and sideritic nodules and evidence of



Figure 4.9 Clast- and matrix-supported conglomerate facies from the Cerro Jaspe area. *Photograph A* shows pale grey matrix-supported conglomerate facies showing poor sorting and reverse grading (Table 4.1). Lens cap for scale (5.6 cm in diameter). *Photograph B* shows gravel-grade conglomerate facies containing broken belemnite fragments. Lens cap for scale (5.6 cm in diameter).



Figure 4.10 Clast- and matrix-supported carbonate-cemented gravel facies from the Cerro Jaspe area (Table 4.1). *Photograph A* shows large-scale 0.3-0.5 m planar-tabular cross-bedding within clast-supported carbonate-cemented gravel facies. Hammer for scale. *Photograph B* shows matrix-supported carbonate-cemented gravel facies with gravel-grade grains held within a microsparite to sparry calcite matrix. Lens cap for scale (5.6 cm in diameter).



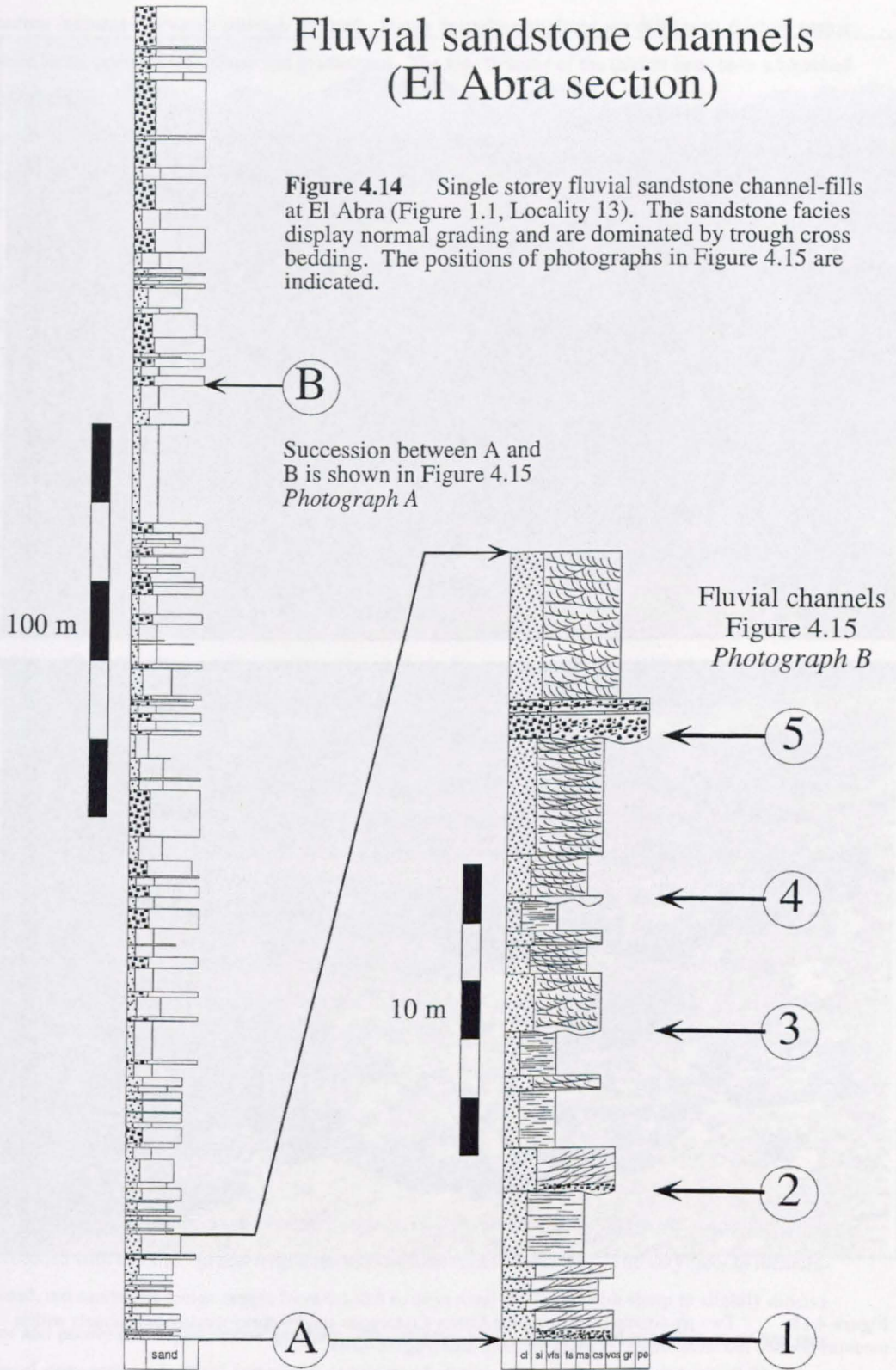
Figure 4.12 A bed of framework corals of 0.3-0.5 m diameter from the Cerro Jaspe area. The beds of reef building coral facies have a sheet geometry and can be traced laterally for greater than 100 m. Lens cap and hammer for scale.



Figure 4.13 The Late Jurassic-Early Cretaceous transition between yellow algal laminated limestone facies and dark red coarse-grained sandstone and conglomerate facies (Figure 4.11). The younging direction is from left to right and the scale-bar is 1 m. Intercalation of the two facies is clearly seen over a transition of tens of metres (Figure 4.11).

Fluvial sandstone channels (El Abra section)

Figure 4.14 Single storey fluvial sandstone channel-fills at El Abra (Figure 1.1, Locality 13). The sandstone facies display normal grading and are dominated by trough cross bedding. The positions of photographs in Figure 4.15 are indicated.



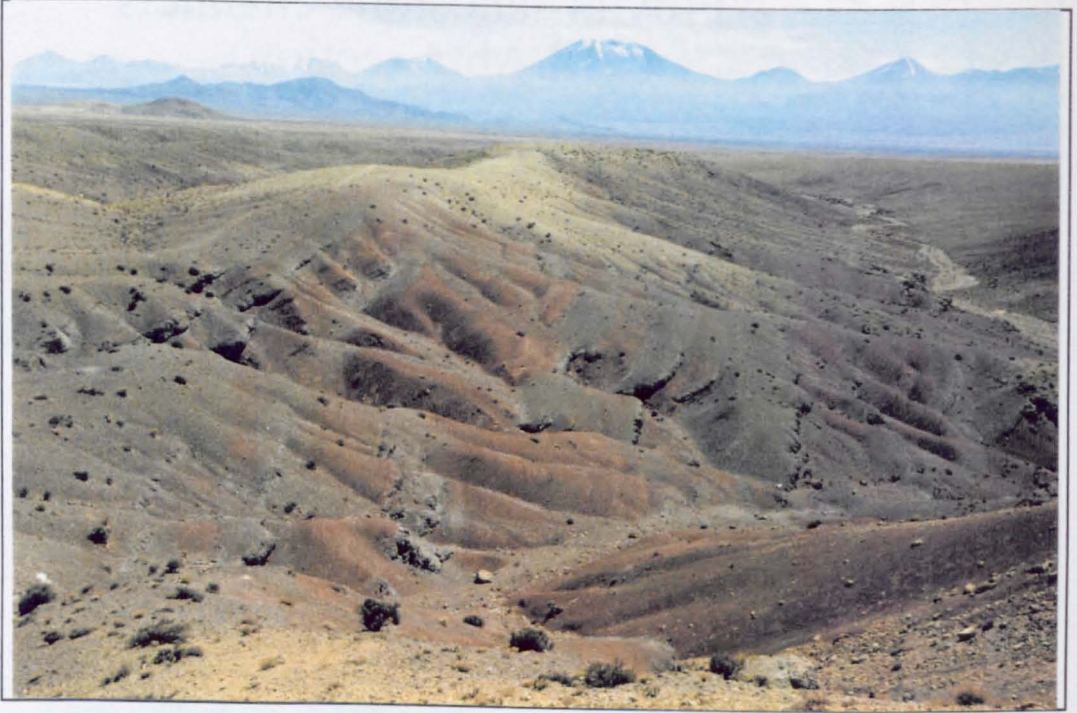


Figure 4.15 Two photographs showing the Lower Cretaceous single-storey sandstone channels within medium-grained red siltstone facies in the El Abra area (Figure 4.14).

small rootlets (Table 4.1). The beds have a sheet geometry and the abundance of both concretions and rooting increases upwards through the bed. Upper bounding surfaces are diffuse to slightly planar while lower contacts are diffuse and gradational. The tops to some of the thicker beds have a bleached appearance.

Recently, new continental vertebrate and invertebrate fossils as well as plant debris have been found in the Lower Cretaceous succession at N.E. El Abra (Fig. 4.15), observed by G. Chong, pers. comm. (1994).

Interpretation

The individual sandstone beds are interpreted as channel fills on the basis of their 0.5-2 m vertical thickness, sharp to erosive base, normal-grading, internal structures and channel geometry (Figs 4.14 and 4.15). The characteristic internal structures include a basal lag deposit, trough cross-bedding, climbing ripple lamination and asymmetric ripples (Fig. 4.14). The asymmetric ripples are interpreted as unidirectional current ripples. The medium-grained siltstone facies is interpreted as overbank siltstones (Table 4.1). The sandstone and siltstone facies are thought to be continental in origin, based on their dark red colour, vertebrate and invertebrate fossils and plant debris. The thin limestone facies at Quebrada La Carreta are interpreted as marginal marine limestones based on their fine algal texture and bivalve fossils (Table 4.1). The distinctive dark red and pale grey mottled sandstone facies is interpreted as an immature paleosol or protosol (Table 4.1), using the scheme of Mack *et al.* (1993). Retallack (1988) describes how waterlogged soils form mottles due to the reduction of iron into its ferrous state (Fe^{2+}) and the presence of rootlets in the upper part of the profile conform to his "O" horizon. Soils of this nature form in conditions of at least seasonally waterlogged strata with prolonged periods of high water-table, in a possibly sub-tropical environment. It is interpreted that this soil type represents a relatively immature paleosol (protosol) due to the lack of any significant peaty material or coal development (histosol), (Retallack, 1988). The variable development of soils may reflect variations in coastal-plain sedimentation with the protosol facies representing lower coastal-plain, low lying, waterlogged areas of floodplain lake, marsh and bay.

The sandstone beds are discrete, single-storey, channelised sandstone bodies within silt-grade rock (Fig. 4.15). These sandstones are interpreted as single-storey fluvial channels within floodplain siltstones deposited in a coastal-plain setting (Fig. 4.14).

4.3.5 Overbank facies association

Description

The overbank facies association comprises thin very fine- to medium-grained red sandstone facies interbedded with medium- to coarse-grained red siltstone facies (Table 4.1). The very fine- to medium-grained, red sandstone facies ranges from 0.1-0.5 m in vertical thickness with sharp to slightly erosive bases and poorly developed normal grading. The sandstone beds are single-storey with sheet and rare channel geometries. Internal structures comprise of climbing ripple cross-lamination, 0.02-0.2 m scale trough and tabular cross-lamination, asymmetric ripple lamination (wavelength 0.05-0.1 m;

amplitude 0.01-0.015 m) and parallel lamination. Fine pebble-grade rip-up clast horizons are composed of fine-grained red siltstone intraclasts. There is also evidence of small pieces of wood and plant debris. The upper 0.05-0.1 m of individual sandstone beds may contain soft sediment deformation in the form of disrupted and contorted laminae. The thin sandstone beds are separated by 0.3-2 m thick beds of medium- to coarse-grained red siltstone facies. The medium- to coarse-grained red siltstone facies display weakly developed parallel lamination and rarely, small ripples (Fig. 4.16). The siltstones are particularly well developed in the Lower Cretaceous deposits of N.E. El Abra (Fig. 1.1, Locality 13), Estacion Cochrane (Fig. 1.1, Locality 22) and Quebrada La Carreta (Fig. 1.1, Locality 61) where they contain rare vertebrate and invertebrate remains as well as plant debris (Chong, 1973; Chong & Gasparini, 1975). The specific fauna and flora are considered in Chapter 5 (Sequence Stratigraphy) where their particular chronostratigraphical significance is discussed.

Interpretation

The sharp base and normal-grading indicate an abrupt introduction of sand-grade material and waning flow conditions. The parallel lamination is interpreted as upper phase plane bedding, while the climbing ripple cross-lamination is known to indicate high rates of sedimentation. Singh (1972) and Klimek (1974) have demonstrated climbing ripple cross-lamination to be a characteristic feature of waning flow crevasse splay sandstones. It is rare however, to see all the structures preserved in a single sandstone bed but this combination of features supports the interpretation of single event flows. The presence of disrupted and contorted laminae at the top of the bed is interpreted to represent water escape structures, supporting rapid rates of sand deposition. The interbedding of these sandstones with red siltstones is thought to represent floodplain deposition, leading to the interpretation of the sandstones as crevasse splay deposits. The crevasse splay sand bodies are distinguished from fluvial channel-fills on the basis of their much thinner, 0.1-0.15 m vertical thickness and distinctive sheet geometry (Fig. 4.15). The crevasse splay deposits are interpreted to represent the area of interfluvial floodplain proximal to a breached levee, with the crevasse splay sandstones indicating periods of floodplain inundation. The sedimentation rates are markedly different, with the sandstones representing single, short duration flood-events, while the siltstones represent longer periods of background sedimentation from suspension. The medium- to coarse-grained red siltstone facies represents the periods of background floodplain sedimentation deposited between crevasse splay flood events (Table 4.1). There is good evidence for shallow-water to subaerial conditions in the form of small ripples and faunal content. This observation is supported by the red coloration which in most cases is indicative of subaerial oxidising conditions, as discussed by Besley & Turner (1983) (Fig. 4.16). Most floodplain sedimentation is from suspension, with a tendency for deposits to fine away from coeval channels (Hughes & Lewin, 1982) which is supported by the absence of levee or crevasse splay sandstones within some of the siltstone facies, indicating a distal floodplain setting with no direct channel influence (Fig. 4.16).

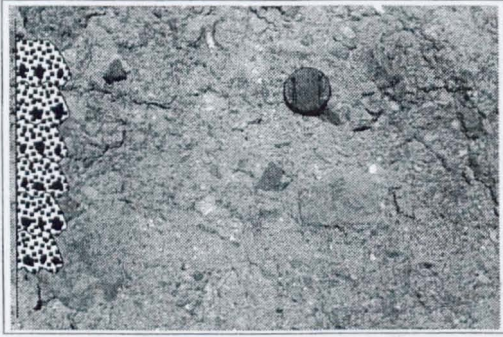


Figure 4.16 Medium-grained red siltstone facies from the Rio San Salvador valley to the south-west of Calama. These red siltstones are interpreted as floodplain deposits. The siltstones are cross-cut by several igneous dykes and unconformably overlain by Tertiary sediments.

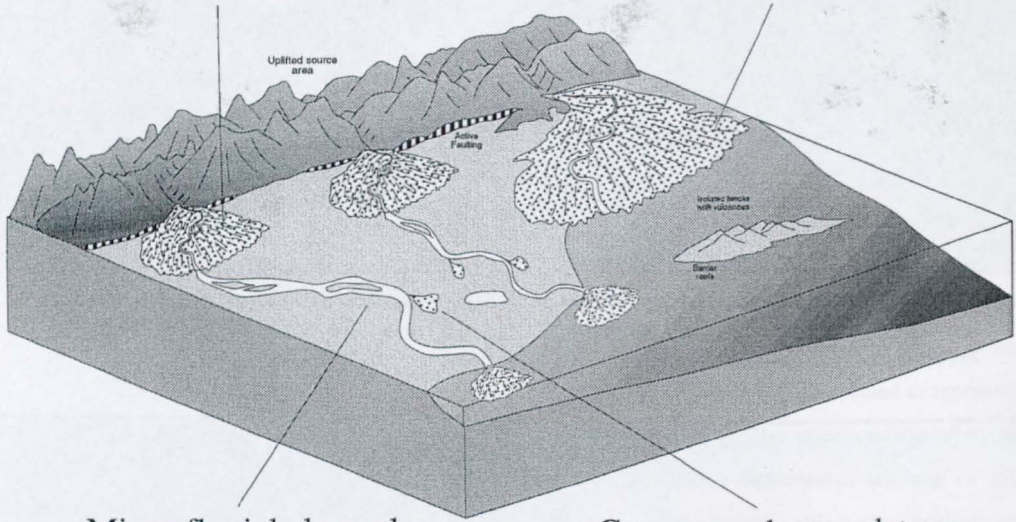
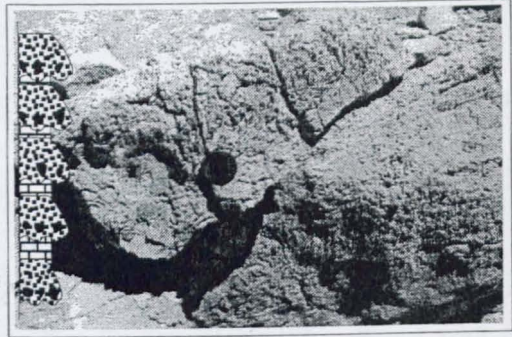


Figure 4.17 Fine-grained red and green siltstones from the Estacion Cochrane section south of Calama (Figure 1.1, Locality 22). These red and green siltstones are interpreted as shallow-water lacustrine deposits.

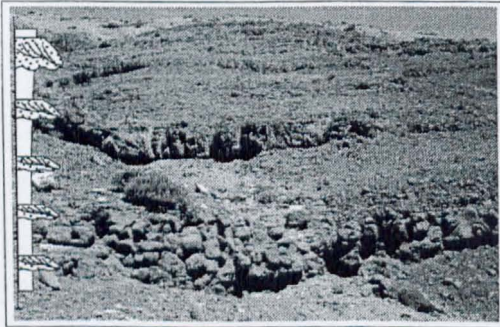
Conglomeratic alluvial fans



Fan-delta



Minor fluvial channels



Crevasse splay sandstones

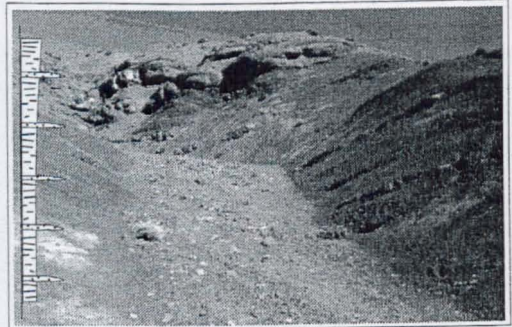


Figure 4.18 The continental clastic facies model is constructed from an analysis of temporally and spatially distinct facies associations which have been integrated to represent the linkage of contemporaneous depositional environments.

Table 4.1 Summary facies table describing all the continental clastic lithofacies found in northern Chile in terms of lithology and grain-size, sedimentary structures and bounding surfaces, thickness and geometry, and body and trace fossils, followed by a process interpretation.

Continental clastic facies description					
Facies and Facies Association	Lithology and Grain Size	Structures and Bounding Surfaces	Thickness and Geometry	Body and Trace Fossils	Process Interpretation
<i>Conglomeratic alluvial fan facies association</i>					
Dark red, clast-supported conglomerate facies (Conglomeratic alluvial fan facies association)	Pebble- to cobble-grade conglomerates with coarse-grained sandstone to gravel-grade matrix Dark red / brown in colour Clast compositions are porphyritic volcanic, plutonic, lithic sandstones and limestones	Clast-supported Normal grading Moderate sorting Moderate rounding Crudely stratified with poorly developed 0.2-1 m scale planar-tabular and trough cross-bedding Clast imbrication Internal erosion surfaces Erosive base and sharp top to bed	When interbedded with dark red, matrix-supported conglomerate facies bed thickness ranges from 0.2-1 m In multi-storey clast-supported complexes individual bed thickness ranges from 1-10 m Sheet and channel geometries	Triassic conglomerates Occasional freshwater bivalves and plant debris (tree trunks and leaf impressions) (Chong & Hillebrandt 1985) Cretaceous conglomerates Rare reworked concretions which contain Oxfordian ammonites (<i>Perisphinctes</i>)	Sheet- and stream-flow deposits laid down by tractional processes
Dark red, matrix-supported conglomerate facies (Conglomeratic alluvial fan facies association)	Pebble- to cobble-grade conglomerates (rare floating 0.25-0.3 m diameter boulder-grade clasts) with fine- to coarse-grained sandstone matrix Dark red / brown in colour Clast compositions are porphyritic volcanic, plutonic, lithic sandstones and limestones	Matrix-supported Poor grading Poor sorting Poor rounding Massive, structureless Basal zone of shearing with broad scours and striations Sharp, non-erosive base and sharp irregular top to bed	0.5-2 m bed thickness Sheet geometry	Rare reworked concretions which contain Oxfordian ammonites (<i>Perisphinctes</i>)	Cohesive debris-flow deposit laid down during a turbulent, high concentration single event flood
Well stratified gravel facies (Conglomeratic alluvial fan facies association)	Very coarse-grained sandstone to gravel-grade grain-size Dark red / brown in colour	Trough and planar-tabular cross-bedding (0.2-0.5 m) Normal grading Internal erosion surfaces associated with thin (0.05-0.1 m) pebble lags Erosive base and sharp top to bed	0.2-0.5 m bed thickness Channel or sheet geometry	None present	Minor channel fills or longitudinal barforms
Erosively-based coarse-grained sandstone facies (Conglomeratic alluvial fan facies association)	Coarse- to very coarse-grained sandstone Dark red / brown in colour	Trough and planar-tabular cross-bedding (0.2-0.5 m) Parallel lamination Normal grading Internal erosion surfaces associated with thin (0.05-0.1 m) pebble lags Erosive base and sharp top to bed	0.2-0.5 m bed thickness Channel or sheet geometry	Triassic sandstones contain occasional freshwater bivalves and plant debris (tree trunks and leaf impressions)	Minor channel fills, dunes or longitudinal barforms Parallel lamination represents upper phase plane bedding
Coarse-grained grey / green sandstone facies (Conglomeratic alluvial fan facies association)	Coarse-grained sandstone Grey / green in colour	Floating, angular, small pebble-grade volcanic clasts Trough and planar-tabular cross-bedding (0.2-0.3 m) Rare normal grading Erosive base and sharp top to bed	0.5-3 m bed thickness Sheet geometry	None present	Volcanogenic sandstone deposited by tractional processes

<i>Fan-delta facies association</i>					
Dark red, clast-supported conglomerate facies (Fan-delta facies association)	Pebble- to cobble-grade conglomerates with coarse-grained sandstone to gravel-grade matrix Dark red / brown in colour Clast composition is predominately plutonic (Cerro Jaspe Palaeozoic plutonics) or porphyritic volcanic (Permo-Triassic), quartz and fine-grained red sandstone	Clast-supported Normal grading Moderate sorting Moderate rounding Crudely stratified with poorly developed 0.2-1 m scale planar-tabular and trough cross-bedding Clast imbrication Internal erosion surfaces Erosive base and sharp top to bed	When interbedded with dark red, matrix-supported conglomerate facies bed thickness ranges from 0.2-1 m In multi-storey clast-supported complexes individual bed thickness ranges from 1-10 m Sheet and channel geometries	Triassic conglomerates Occasional freshwater bivalves and plant debris (tree trunks and leaf impressions) (Chong & Hillebrandt 1985)	Sheet- and stream-flow deposits laid down by tractional processes No evidence of marine reworking
Dark red, matrix-supported conglomerate facies (Fan-delta facies association)	Pebble- to cobble-grade conglomerates (rare floating 0.25-0.3 m diameter boulder-grade clasts) with fine- to coarse-grained sandstone matrix Dark red / brown in colour Clast composition is predominately plutonic (Cerro Jaspe Palaeozoic plutonics) or porphyritic volcanic (Permo-Triassic), quartz and fine-grained red sandstone	Matrix-supported Poor grading Poor sorting Poor rounding Massive, structureless Basal zone of shearing with broad scours and striations Sharp, non-erosive base and sharp irregular top to bed	0.5-2 m bed thickness Sheet geometry	Triassic conglomerates Occasional freshwater bivalves and plant debris (tree trunks and leaf impressions) (Chong & Hillebrandt 1985)	Cohesive debris-flow deposit laid down during a turbulent, high concentration single event flood No evidence of marine reworking
Pale grey, clast-supported conglomerate facies (Fan-delta facies association)	Pebble- to cobble-grade conglomerates with coarse-grained sandstone to gravel-grade matrix Pale grey in colour Clast composition is predominately plutonic (Cerro Jaspe Palaeozoic plutonics) or porphyritic volcanic (Permo-Triassic), quartz and fine-grained red sandstone	Clast-supported Normal grading Clean (silt-free) Well sorted Well rounded Crudely stratified with poorly developed 0.2-1 m scale planar-tabular and trough cross-bedding Clast imbrication Erosive base (incision up to 0.2 m) and sharp top	0.3-1 m bed thickness In multi-storey complex individual bed thicknesses range from 1-10 m Sheet geometry	Abundant broken belemnite, coral, bivalve and brachiopod debris but all has been reworked	Sheet- and stream-flow deposits laid down by tractional processes which have subsequently been reworked by shallow-marine wave processes
Pale grey, matrix-supported conglomerate facies (Fan-delta facies association)	Pebble- to cobble-grade conglomerates (rare boulder-grade clasts) with medium- to coarse-grained sandstone matrix Pale grey / brown in colour Clast composition is predominately plutonic (Cerro Jaspe Palaeozoic plutonics) or porphyritic volcanic (Permo-Triassic), quartz and fine-grained red sandstone	Matrix-supported Massive Clean (silt-free) Poor reverse grading Moderate rounding Moderate sorting Basal zone of shearing with broad scours and striations Sharp, non-erosive base and sharp irregular top	0.5-2 m bed thickness Sheet geometry	Broken belemnite, coral, bivalve and brachiopod debris but all has been reworked	Cohesive debris-flow deposit which has been partly reworked by shallow-marine wave processes
Clast-supported, carbonate-cemented gravel facies (Fan-delta facies association)	Very coarse-grained sandstone to gravel-grade Pale grey / brown in colour Clast composition is predominately plutonic (Cerro Jaspe Palaeozoic plutonics) or porphyritic volcanic (Permo-Triassic), quartz and fine-grained red sandstone	Trough and planar-tabular cross-bedding (0.2-0.4 m) Normal grading Good sorting Angular grains Clean (silt-free) Internal erosion surfaces associated with thin (0.05-0.1 m) pebble lags Rare floating small- to medium-sized pebbles Erosive base and sharp top to bed	0.4-1 m bed thickness Sheet geometry	Abundant broken belemnite, coral, bivalve and brachiopod debris but all has been reworked	High-energy, shallow-marine reworking of gravel-grade area of fan-delta

Matrix-supported, carbonate-cemented gravel facies (Fan-delta facies association)	Gravel-grade grains held in fully carbonate matrix of micro-sparite Pale grey / brown in colour Clast composition is predominately plutonic (Cerro Jaspe Palaeozoic plutonics) or porphyritic volcanic (Permo-Triassic), quartz and fine-grained red sandstone	Angular grains Rare floating small- to medium-sized pebbles Clean (silt-free) Erosive base and sharp top to bed	0.4-1 m bed thickness Sheet geometry	Abundant broken belemnite, coral, bivalve and brachiopod debris but all has been reworked	High-energy, shallow-marine reworking of gravel-grade area of fan-delta Matrix-support is due to limited clastic input
Algal laminated limestone facies (Fan-delta facies association)	Fine-grained micritic limestone Yellow to pale brown in colour	Millimetre-scale parallel (mat) and convex-upwards (stromatolitic) laminations Sharp base and top to bed	0.1-0.5 m bed thickness Sheet geometry (>200 m lateral continuity)	Stromatolites and algal mat limestones No evidence of fully marine body or trace fossils	Thin periods of clastic starvation in very shallow marginal marine or lagoonal environments
Reef-building coral facies (Fan-delta facies association)	Medium-grained microsparite limestone	No primary sedimentary structures Sharp base and top to bed	0.15-1.1 m bed thickness Sheet geometry (>100 m lateral continuity)	Framework coral, bivalve and brachiopod fossils Corals are convex-upwards domes (diameter up to 0.5 m) indicating life position	Shallow-marine (<10 m water depth), clear-water limestone indicating very low clastic input
Medium- to very coarse-grained wave rippled sandstone facies (Fan-delta facies association)	Medium- to very coarse-grained sandstone Pale green to grey in colour	Abundant symmetrical (wave) ripples (wavelength 0.05-0.1 m, amplitude 0.01-0.015 m) Sharp to erosive base and sharp top to bed	0.4-2 m bed thickness Sheet geometry	Bivalve and brachiopods and shell debris Rare vertical bioturbation (<i>Skolithos</i>)	Shallow-marine sandstone recording wave processes
Fine- to medium-grained bioturbated sandstone facies (Fan-delta facies association)	Medium- to very coarse-grained sandstone Pale green to grey in colour	Primary sedimentary structures destroyed by bioturbation Sharp to erosive base and sharp top to bed	0.4-2 m bed thickness Sheet geometry	Abundant vertical bioturbation (<i>Skolithos</i>) Bivalve and brachiopods and shell debris	Shallow-marine sandstone which has undergone heavy bioturbation
Sand-rich braided fluvial facies association					
Gravel- to small pebble-grade lag facies (Sand-rich braided fluvial facies association)	Gravel- to small pebble-grade conglomerate Dark red / brown in colour Clast compositions are intrabasinal fine- to medium-grained sandstone facies	Clast-supported Normal grading Moderate sorting Moderate rounding Erosive base with incision up to 0.2 m into the underlying sandstone and sharp or gradational top to facies	0.1-0.3 m bed thickness making up the base of the channel sandstone unit Channel geometry	No evidence of body or trace fossils	Erosive lag facies deposited at base of fluvial channel (not always present)
Very coarse- to medium-grained channel sandstone facies (Sand-rich braided fluvial facies association)	Very coarse- to medium-grained sandstone Dark red / brown in colour	Trough and planar-tabular cross-bedding (scale 0.2-0.5 m) Normal grading Moderate sorting Moderate rounding Erosive or sharp base and gradational top to overlying sandstone facies	1-3 m bed thickness Channel geometry (thins laterally to zero within 30 m)	Rare continental vertebrate and invertebrate fossils as well as plant debris (Chong 1973b; Chong 1973a)	Fluvial sandstone channel-fill
Fine- to medium-grained channel sandstone facies (Sand-rich braided fluvial facies association)	Fine- to medium-grained sandstone Dark red / brown in colour	Trough and planar-tabular cross-bedding (scale 0.02-0.2 m) Climbing ripple lamination Normal grading Moderate sorting Moderate rounding Asymmetric ripples (wavelength 0.05-0.1 m, amplitude 0.01-0.015 m) Parallel lamination Gradational base over underlying facies and sharp top	0.3-1 m bed thickness making up the top of the channel sandstone unit Channel geometry	Rare continental vertebrate and invertebrate fossils as well as plant debris (Chong 1973b; Chong 1973a)	Fluvial sandstone channel-fill

Minor fluvial channel facies association					
Gravel- to small pebble-grade lag facies (Sand / silt fluvial facies association)	Gravel- to small pebble-grade conglomerate Dark red / brown in colour Clast compositions are intrabasinal medium-grained siltstone facies	Clast-supported Normal grading Moderate sorting Moderate rounding Erosive base with incision up to 0.2 m into the underlying siltstone and sharp or gradational top to facies	0.05-0.15 m bed thickness making up the base of the channel sandstone unit Channel geometry	No evidence of body or trace fossils	Erosive lag facies deposited at base of fluvial channel (not always present) Clasts are intrabasinal rip-up clasts of underlying siltstone
Coarse- to medium-grained channel sandstone facies (Sand / silt fluvial facies association)	Coarse- to medium-grained sandstone Dark red / brown in colour	Trough and planar-tabular cross-bedding (scale 0.2-0.5 m) Normal grading Moderate sorting Moderate rounding	1-2 m bed thickness Channel geometry (thins laterally to zero within 50-100 m)	Rare continental vertebrate and invertebrate fossils as well as plant debris (Chong 1973b; Chong 1973a)	Sandstone channel-fill
Fine- to very fine-grained channel sandstone facies (Sand / silt fluvial facies association)	Fine- to very fine-grained sandstone Dark red / brown in colour	Trough and planar-tabular cross-bedding (scale 0.02-0.2 m) Climbing ripple lamination Normal grading Moderate sorting Moderate rounding Asymmetric ripples (wavelength 0.05-0.1 m, amplitude 0.01-0.015 m) Parallel lamination Gradational base over underlying facies and sharp top	0.2-0.5 m bed thickness making up the top of the channel sandstone unit Channel geometry	Rare continental vertebrate and invertebrate fossils as well as plant debris (Chong 1973b; Chong 1973a)	Sandstone channel-fill
Medium-grained red siltstone facies (Sand / silt fluvial facies association)	Medium-grained siltstone Dark red / brown in colour	Massive Rare parallel lamination Gradational base and incised top due to overlying sandstone channel	1-10 m bed thickness Sheet geometry	Rare continental vertebrate and invertebrate fossils as well as plant debris (Chong 1973b; Chong 1973a)	Background interfluvial floodplain siltstone deposition
Fine- to medium-grained mottled sandstone facies (Sand / silt fluvial facies association)	Fine- to medium-grained sandstone Brown to red in colour with characteristic mottling due to calcareous concretions Tops of thicker beds have bleached appearance	Load structures in lower half of bed Abundant calcareous (carbonate and siderite) nodules concentrated in upper half (>50%) Organic woody material and rootlets concentrated at top Diffuse and gradational lower contacts and diffuse to slightly planar upper contacts	0.3-1 m bed thickness Sheet geometry	None present	Slow sedimentation rates with relative clastic starvation and prolonged high water-table allowing immature palaeosol development (Mack <i>et al.</i> 1993)
Overbank facies association					
Very fine- to medium-grained, red sandstone facies (Sandy crevasse splay facies association)	Very fine- to medium-grained sandstone Dark red / brown in colour	Trough and planar-tabular cross-bedding (scale 0.02-0.2 m) Climbing ripple cross lamination Normal grading Moderate sorting Moderate rounding Asymmetric ripples (wavelength 0.05-0.1 m, amplitude 0.01-0.015 m) Parallel lamination Sharp to slightly erosive base over underlying facies and sharp top	0.1-0.5 m bed thickness Single-storey Sheet and rare channel geometry	Small pieces of wood and plant debris	Deposition by waning flow from an overbank crevasse splay

Medium- to coarse-grained, red siltstone facies (Sandy crevasse splay facies association)	Medium- to coarse-grained siltstone Dark red / brown in colour	Massive Rare parallel or wavy lamination Gradational base and top	0.3-2 m bed thickness Sheet geometry	Rare continental vertebrate and invertebrate fossils as well as plant debris (Chong 1973b; Chong 1973a)	Last stages of crevasse splay and standing water floodplain deposition between crevasse splays
Medium-grained, red siltstone facies (Floodplain siltstone facies association)	Medium-grained siltstone Dark red / brown in colour	Massive Rare parallel lamination Rare small adhesion ripples (wavelength 0.05-0.1 m, amplitude 0.01-0.015 m) Gradational base and top	1-10 m bed thickness Sheet geometry	Rare continental vertebrate and invertebrate fossils as well as plant debris (Chong 1973b; Chong 1973a)	Floodplain siltstone deposition some distance from the fluvial channel area
<i>Lacustrine siltstone facies association</i>					
Fine- to medium-grained red siltstone facies (Lacustrine facies association)	Medium-grained siltstone Dark red / brown in colour	Massive Parallel lamination Rare wavy lamination Gradational base and top	1-10 m bed thickness Sheet geometry	Freshwater molluscs as well as plant debris (Chong 1973b; Chong 1973a)	Subaqueous deposition in an area of floodplain ponding
Fine- to medium-grained green siltstone facies (Lacustrine facies association)	Medium-grained siltstone Pale to dark green in colour	Massive Parallel lamination Rare wavy lamination Gradational base and top	1-10 m bed thickness Sheet geometry	Freshwater molluscs as well as plant debris (Chong 1973b; Chong 1973a)	Subaqueous deposition in an area of floodplain ponding where reducing conditions indicate a lack of any subaerial influence

4.3.6 Lacustrine siltstone facies association

Description

This association consists of alternating fine- to medium-grained, red and green siltstone facies which are massive or finely laminated (Table 4.1). The distinctive green siltstone facies are markedly finer-grained and different in appearance to any of the red floodplain siltstone facies (Fig. 4.17). They are dominated by a fine parallel lamination with rare wavy lamination. Chong (1973) has noted freshwater molluscs from certain horizons. The fine-grained red siltstone facies are similar in appearance to the green siltstone facies with fine parallel lamination and rare wavy lamination (Fig. 4.17).

Interpretation

Although there is no evidence for thick accumulations of well developed lacustrine deposits, there are criteria allowing the distinction of localised floodplain ponding. The fine- to medium-grained, red and green siltstone facies are finer-grained and differ in colour from the floodplain siltstone facies (Fig. 4.17). Besley & Turner (1983) discuss how green coloured siltstones may indicate reducing conditions, relative to the surrounding red, subaerial floodplain, which is a highly oxidising environment. The presence of freshwater molluscs indicates prolonged periods of shallow subaqueous ponding. The red/green siltstones are thought to represent sub-aqueous, freshwater siltstones deposited in an area of shallow water floodplain ponding.

4.3.7 Continental clastic Facies Model

The continental clastic deposits of northern Chile have been shown to include a wide variety of different facies associations from fan-deltas through two distinct fluvial environments to alluvial fans. The continental setting from Late Triassic-Early Cretaceous times appears to have been typically warm to sub-tropical with moderate vegetation cover and faunal diversity (Chapter 2). The rainfall was seasonal with deposits more typical of ephemeral flood events rather than continuous sedimentation. This observation is supported by the apparent lack of lateral accretion structures. The distinct lack of coal deposits and mature paleosols may be due to the high aridity and oxidising nature of the environment. The continental clastic depositional model is based on the integration of temporally and spatially distinct facies and facies associations and does not represent active deposition in all the environments at a particular time (Figs 4.1 and 4.18). The depositional model is modified through time by changing accommodation space and sediment supply, discussed in Chapter 5.

4.4 Shallow-marine siliciclastic ramp facies description

A succession of offshore siltstone, shoreface sandstone and foreshore facies associations have been interpreted to represent a genetically-linked shallowing-upward profile and hence, siliciclastic-ramp parasequence (Figs 4.19 and 4.20). Sheet-geometry sandstones form a typical succession of depositional facies (Table 4.2), sedimentary structures (storm- and wave-dominated), ichnofacies (*Skolithos* and *Cruziana*) and body fossils (Aberhan, 1993a; 1993b) characterising a shallow-marine depositional environment (Fig. 4.19). Overlying erosionally-based, fining-upward sandstone channel-fills are interpreted as marginal-marine deltaic/estuarine deposits displaying both a fluvial and shallow-marine character (Fig. 4.19). The deltaic/estuarine deposits of different depositional architecture and hence interpreted to be genetically-unrelated to the underlying sheet-geometry shoreface deposits (Figs 4.19 and 4.20).

4.4.1 Estuarine facies association

Description

The 1.5-3 m thick sandstone beds are erosively-based with a channel geometry which thins laterally to zero within 50-100 m. Each bed is normally-graded from coarse- or very coarse-grained sandstone facies to fine- to medium-grained sandstone facies, often with a gravel to fine pebble lag at the base (Table 4.2). Each unit displays a characteristic series of internal structures, with the lower, coarse-grained sandstones containing large, 0.2-0.3 m scale trough cross-bedding, followed by climbing ripple cross-lamination and asymmetric ripple structures, with the fine-grained top of the series displaying symmetric ripples, rare parallel lamination and vertical bioturbation (Figs 4.21 and 4.22). The small, 1 cm, vertical burrows are *Skolithos* (Fig. 4.22). The upper fine- to medium-grained sandstone facies commonly have mud and silt drapes on the symmetric ripples and trough cross bedding with isolated sandy wave trains and flaser bedding within muddy siltstone (Fig. 4.22). Yellow to pale brown, fine-grained algal limestone facies range in bed thickness from 0.1-0.5 m with wavy or parallel lamination and small bivalve fossils (Table 4.2). A distinctive 0.2-0.5 m thick, red to brown, fine- to medium-grained mottled sandstone facies contains abundant, greater than 50%, carbonate and sideritic nodules and evidence of small rootlets (Table 4.2). The beds have a sheet geometry and the abundance of both concretions and rooting increases upwards through the bed. Upper bounding surfaces are diffuse to slightly planar while lower contacts are diffuse and gradational. The tops to some of the thicker beds have a bleached appearance.

Interpretation

The normally-graded sandstone beds are interpreted as discrete channel fills with trough cross bedding, climbing ripple cross-lamination and asymmetric ripples, indicating unidirectional current processes. The fine- to medium-grained sandstone facies of the channel tops is dominated by symmetric ripples and *Skolithos* bioturbation, interpreted to represent shallow-marine reworking (Table 4.2, Fig. 4.22).

Lithology	Graphic log	Facies	Facies association	Depositional environments	Description	Body and trace fossils	Bounding surfaces & architectural elements	Schematic representation of architectural elements
		Erosionally-based, normally graded sandstones with fluvial character at base and wave reworked tops	Estuarine	Fluvial / Estuarine	Trough and tabular cross-stratification, draped foresets, wave and current ripples, wavy planar lamination, pebble lags, normal grading	Rootlets and rare small (1-2.5 cm) <i>Skolithos</i> burrows	Fining-upwards, erosionally-based channel-forms.	
		Massive or laminated clean sandstone	MHW Foreshore	Siliciclastic-ramp parasequence	Parallel laminated, planar stratified	Abundant small (1-2.5 cm) <i>Skolithos</i> burrows	Basinward inclined amalgamated sand bodies	
		Trough- and planar-tabular cross-bedded sandstone	MLW Upper Shoreface		Trough and tabular cross-stratification, Localized wavy planar lamination and swales Shell lags	Bivalves, gastropods, brachiopods, belemnites <i>Skolithos</i> , <i>Ophiomorpha</i> , <i>Diplocraterion</i> , <i>Thalassinoides</i> , <i>Arenicolites</i>	Large amalgamated sand bodies	
		Heavily bioturbated and planar-stratified sandstone	Middle Shoreface		Planar-lamination, low angle cross-lamination, swaley-cross-stratification, interbedded at decimeter scale with heavily bioturbated intervals Shell lags	Bivalves, gastropods, brachiopods, belemnites <i>Ophiomorpha</i> , <i>Diplocraterion</i> , <i>Thalassinoides</i> , <i>Arenicolites</i> , <i>Palaeophycus</i>	Amalgamated sheet geometry sandstones	
		Amalgamated, sheet-geometry sandstones derived from fair-weather and storm wave activity	Lower Shoreface MFWWB (15-20m)		Hummocky-cross-stratification, swaley-cross-stratification, parallel lamination, wave and current rippled, abundant disarticulated shell debris, variably bioturbated sandstones and siltstones.	Bivalves, gastropods, brachiopods, belemnites, <i>Rhizocoelium</i> , <i>Teichichnus</i> , <i>Cruziana</i> , <i>Thalassinoides</i> , <i>Palaeophycus</i> , <i>Planolites</i> , <i>Chondrites</i>	Amalgamated sheet geometry sandstones	
		Fine-grained siltstones (fair weather wave activity) with interbedded sheet geometry sandstones (storm wave activity) which thicken and become more frequent upwards.	Offshore Transition MSWB (40-50m)		Hummocky-cross-stratification, swaley-cross-stratification, wave ripples, bioturbated, erosively-based, abundant disarticulated shell debris. Laminated or massive, heavily bioturbated siltstones & silty mudstones	Ammonites, bivalves, gastropods, solitary corals, brachiopods, belemnites, <i>Rhizocoelium</i> , <i>Teichichnus</i> , <i>Cruziana</i> , <i>Thalassinoides</i> , <i>Palaeophycus</i> , <i>Planolites</i> , <i>Chondrites</i>	Fine-grained siltstones interbedded with sheet geometry sandstones which thicken and become more common upwards.	
		Fine-grained siltstones and mudstones with rare intercalated thin sheet-geometry sandstones	Offshore		Fine-grained yellow siltstone or organic-rich black mudstone; Rare thin (2-10 cm), parallel-laminated, fine-grained sandstone	Ammonites; Bivalves; No traces	Fine-grained siltstones and mudstones with rare intercalated thin sheet geometry sandstones	

Figure 4.19 Schematic representation of the Domeyko basin shallow-marine, siliciclastic facies and facies associations in northern Chile based on lithology and grain-size, sedimentary structures, body and trace fossils and bounding surface character. Abbreviations used in are Mean High Water (MHW), Mean Low Water (MLW), Mean Fair Weather Wave Base (MFWWB) and Mean Storm Wave Base (MSWB).

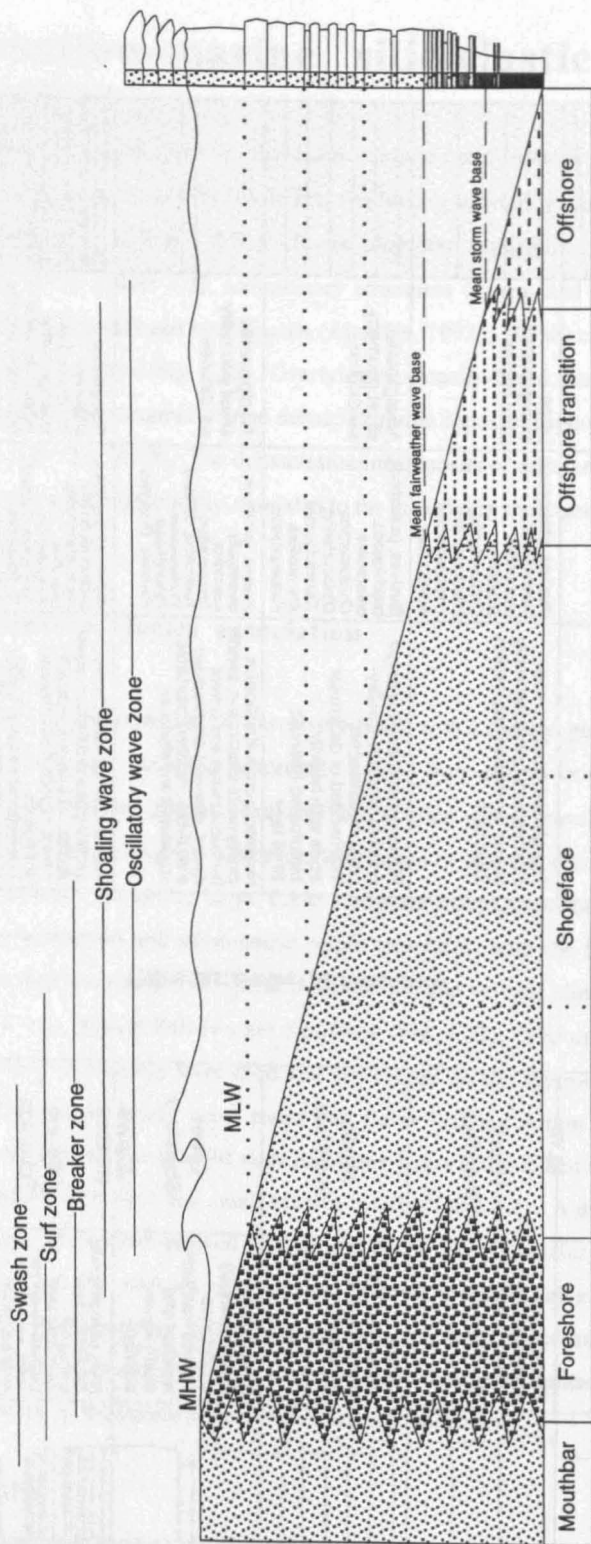


Figure 4.20 The bathymetric profile for a siliciclastic ramp setting with the associated facies association belts (Reading 1986).

Estuarine facies from Quebrada Carreta

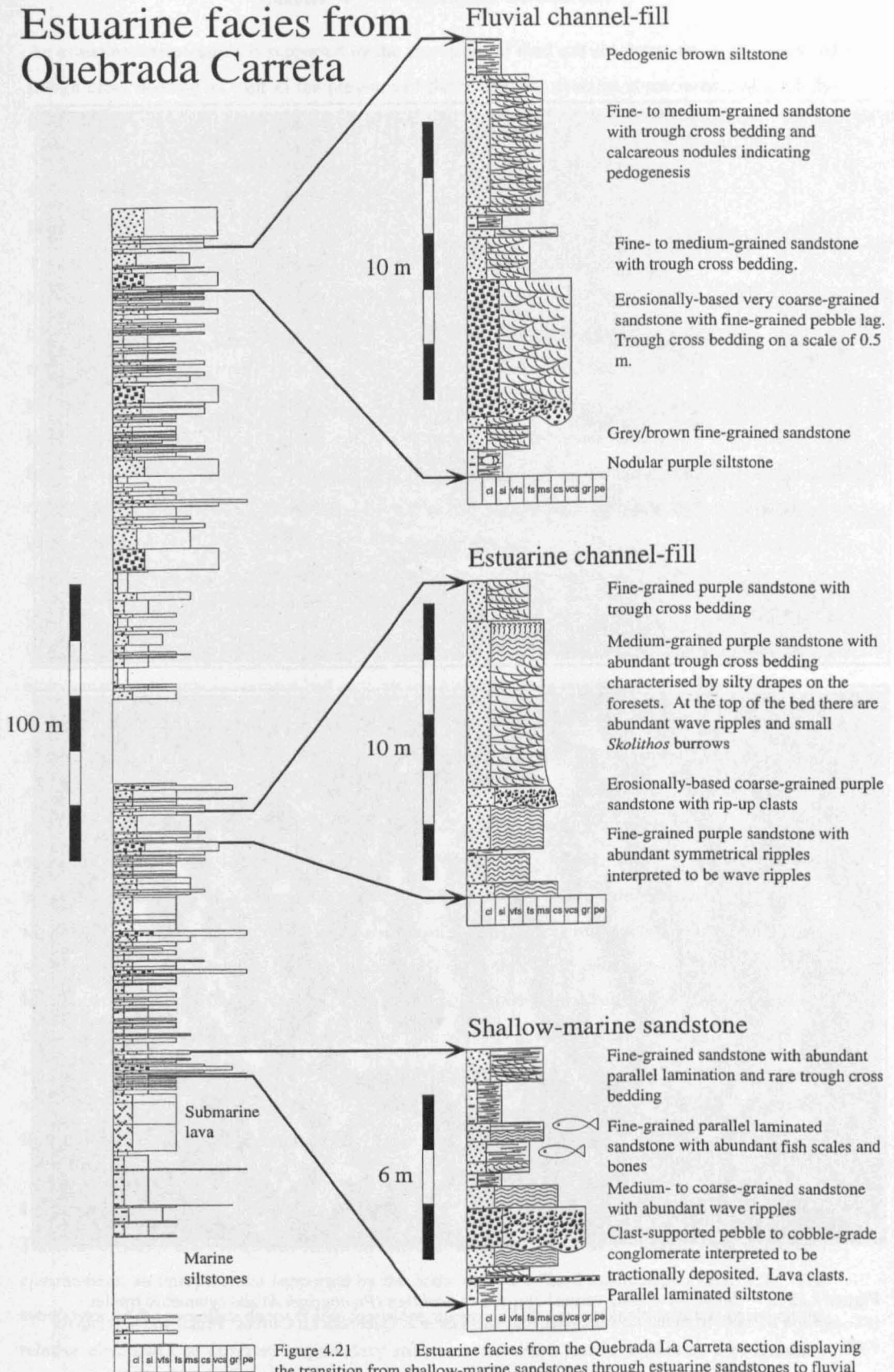


Figure 4.21 Estuarine facies from the Quebrada La Carreta section displaying the transition from shallow-marine sandstones through estuarine sandstones to fluvial sandstones.

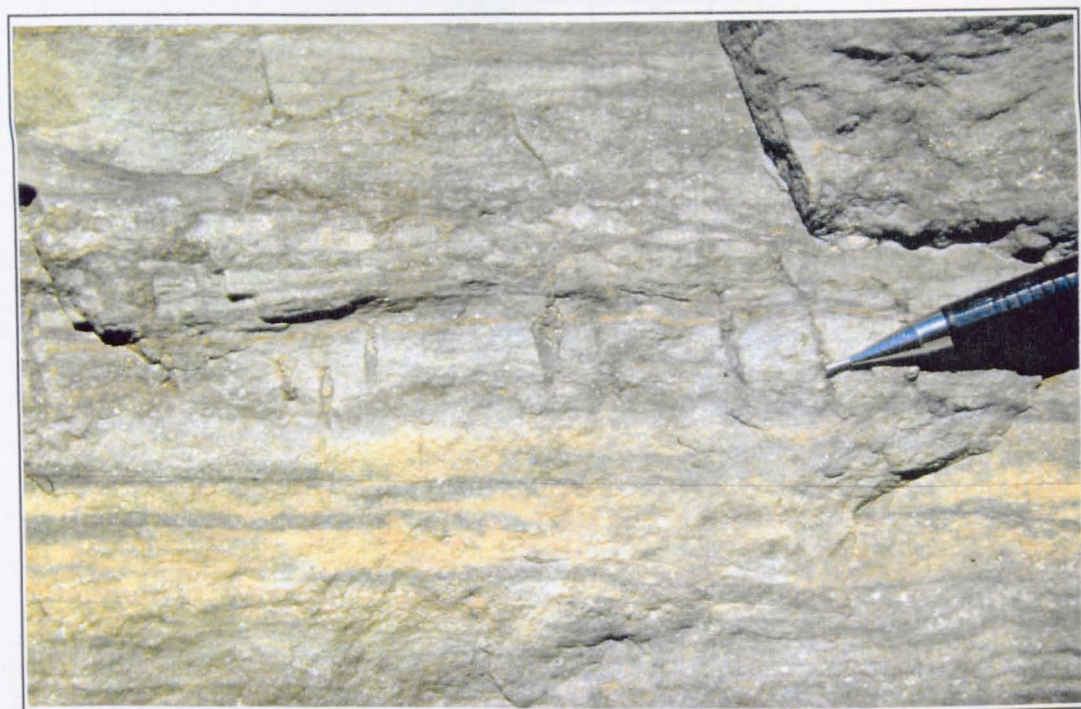


Figure 4.22 Small 1 cm scale vertical burrows of *Skolithos* (Photograph A) and symmetric ripples (Photograph B), both from the Lower Cretaceous succession at Quebrada La Carreta. Pencil and lens cap for scale.

An estuarine interpretation is supported by the abundance of mud and silt drapes on wave ripples and trough cross bedding as well as the presence of flaser bedding, features characteristic of a tidally-influenced estuarine environment (Fig. 4.22).

4.4.2 Shoreface facies association

Description

The sharp to erosively-based, medium- to very coarse-grained sandstone facies ranges from 0.2-1 m in bed thickness, with a well developed sheet geometry (Table 4.2). Internally, the sandstones display trough cross-bedding, symmetrical ripples, wavy and planar lamination, swaley cross-stratification and rare hummocky cross-stratification (Figs 4.23 and 4.24). The sandstones are clean, being composed predominantly of quartz with some feldspar grains. There are abundant examples of 0.01-0.05 m thick shell lags developed both, at the base and within beds. The sandstones have a well developed trace fossil assemblage (Fig. 4.24), including *Skolithos*, *Planolites Palaeophycus*, *Thalassinoides* and *Ophiomorpha*, described by Fernandez-Lopez *et al.* (*in press*). The marine body fossil assemblage includes bivalves (*Gryphaea*, *Exogyra*, *Myophorella*, *Pholadomya*, *Trigonia*, *Astarte*, *Vaugonia*), gastropods (*Pseudomelania*, *Trachynerita*), solitary corals (*Montlivaltia*), colonial corals (*Microphyllia*, *Isastrea*, *Dendrastrea*, *Actinastrea*), brachiopods, belemnites and echinoids, seen in both life position and death assemblage (Fernandez-Lopez *et al.* *in press*). The sandstone beds are amalgamated with sharp to erosive bed contacts and little silt-grade material present (Fig. 4.24).

Closely associated with the amalgamated sandstones are interbedded units of 0.2-0.5 m thick fine- to very coarse-grained hummocky-cross-stratified sandstone facies and 0.2-0.4 m thick medium-grained calcareous siltstone facies (Figs 4.25 and 4.26). The sandstone beds are erosively-based with a sheet geometry and flat or undulose top surfaces (Fig. 4.25). The sandstone bodies have a large lateral extent of greater than 100 m, indicative of a predominately tabular nature. However, lateral termination of beds is also observed, where sandstone beds thin rapidly over 2 m and pinch out into siltstones (Fig. 4.26). Internally, the sandstones display hummocky-cross-stratification, swaley-cross-stratification and symmetrical ripples, with a high content of shell debris in the form of bivalve, brachiopod and oyster fragments (Fig. 4.26). The shell debris is distributed throughout the bed and commonly concentrated into a shelly lag at the base of the bed. Some of the sandstone beds contain small vertical burrows of *Skolithos*. The medium-grained siltstone facies are calcareous in nature with rare parallel lamination and *Scolicia* bioturbation in the form of well developed horizontal feeding burrows formed by gastropods (Fig. 4.26).

Interpretation

The array of sedimentary structures described above are all typical of a shallow-marine wave-dominated environment, an interpretation supported by the body and trace fossil assemblage (Table 4.2). The subdivision of the shoreface deposits into foreshore, upper, middle and lower shoreface is based on the relative abundance of different sedimentary structures and trace fossils, reflecting a progressive

lowering of wave energy (Figs 4.19 and 4.25). These deposits are predominately wave-dominated and hence are interpreted to have been deposited above the fair weather wave base (Fig. 4.19).

The sandstone facies containing well preserved hummocky- and swaley-cross-stratification are interpreted as storm-dominated deposits occurring between the fairweather and storm wave bases (Figs 4.19 and 4.26). The sandstone facies are characterised by a tabular nature, lateral termination of beds, undulatory basal and top surfaces, all features indicative of an oscillatory flow-regime and storm deposited sandstones (Fig. 4.26). While the hummocky-cross-stratified sandstone facies are interpreted to represent individual storm events, the interbedded siltstone facies are interpreted to represent the fine-grained nature of the fairweather sedimentation (Fig. 4.25).

4.4.3 Offshore siltstone facies association

Description

The 1-10 m thick fine- to medium-grained calcareous siltstone facies is either massive or parallel laminated and pale grey to yellow in colour (Table 4.2). Rare intercalated beds of 0.1-0.5 m thick fine-grained calcareous sandstone facies have sharp to slightly erosive bases and sharp tops, displaying poorly developed wavy and parallel lamination (Table 4.2). The sandstones and siltstones contain abundant ammonites, with some bivalve and brachiopod fossils. The jet black, very fine- to fine-grained siltstone facies is usually massive with rare parallel lamination (Table 4.2). The silts are commonly poorly cemented or unconsolidated with abundant ammonite and rare bivalve and brachiopod fossils. When freshly broken, the black siltstones give off a strong sulphurous smell.

Interpretation

On the basis of their fine-grained nature and faunal content, the siltstone and intercalated fine-grained sandstone facies are interpreted to indicate low siliciclastic sediment input with the thin sandstones representing rare, large storm-events or low concentration turbidity currents deposited in an offshore setting. The presence of ammonite, bivalve and brachiopod fauna support the interpretation of an offshore marine environment. The very fine-grained nature of the siltstone facies, black colour and sulphurous smell indicate a high organic carbon content, interpreted to represent low siliciclastic sediment input and dysoxic to anoxic conditions during deposition (Fig. 4.27). Absolute depths of black shale formation remain poorly understood (Wignall & Maynard, 1993), with estimates varying by an order of magnitude from a few tens to hundreds of metres (Hallam, 1967a; 1967b; Wignall, 1991). Thick black shales may form all or part of a sequence in distal marine settings where the water is deep as a result of rapid sea-level rise and/or high subsidence rates (Wignall & Maynard, 1993). These occurrences are adequately explained by the puddle model (Hallam & Bradshaw, 1979; Wignall, 1991). Thin black shales which extend from basinal into marginal settings fall into two categories, basal transgressive black shales and maximum flooding surface black shales (Wignall & Maynard, 1993). The Lower Toarcian Jet Rock of northern England provides an example of early transgressive black shales, while the Late Carboniferous (Pennsylvanian) of northern England contains black shales associated with both early transgression (as in the Jet Rock example) and also maximum flooding



Figure 4.23 The Lower Bajocian marine transgression at West Cerro Jaspe is marked by siliciclastic shoreface deposits overlying Lower-Middle Jurassic fan-delta deposits. *Photograph A* is a strike view of the section younging from left to right (east to west) with sheet geometry Lower Bajocian siliciclastic shoreface deposits overlying Lower-Middle Jurassic fan-delta deposits. The shoreface deposits are overlain by a 40 m thick dark green submarine lava. *Photograph B* displays the four shoreface parasequences underlying the lava (Figure 4.24).

Siliciclastic shoreface at West Cerro Jaspe

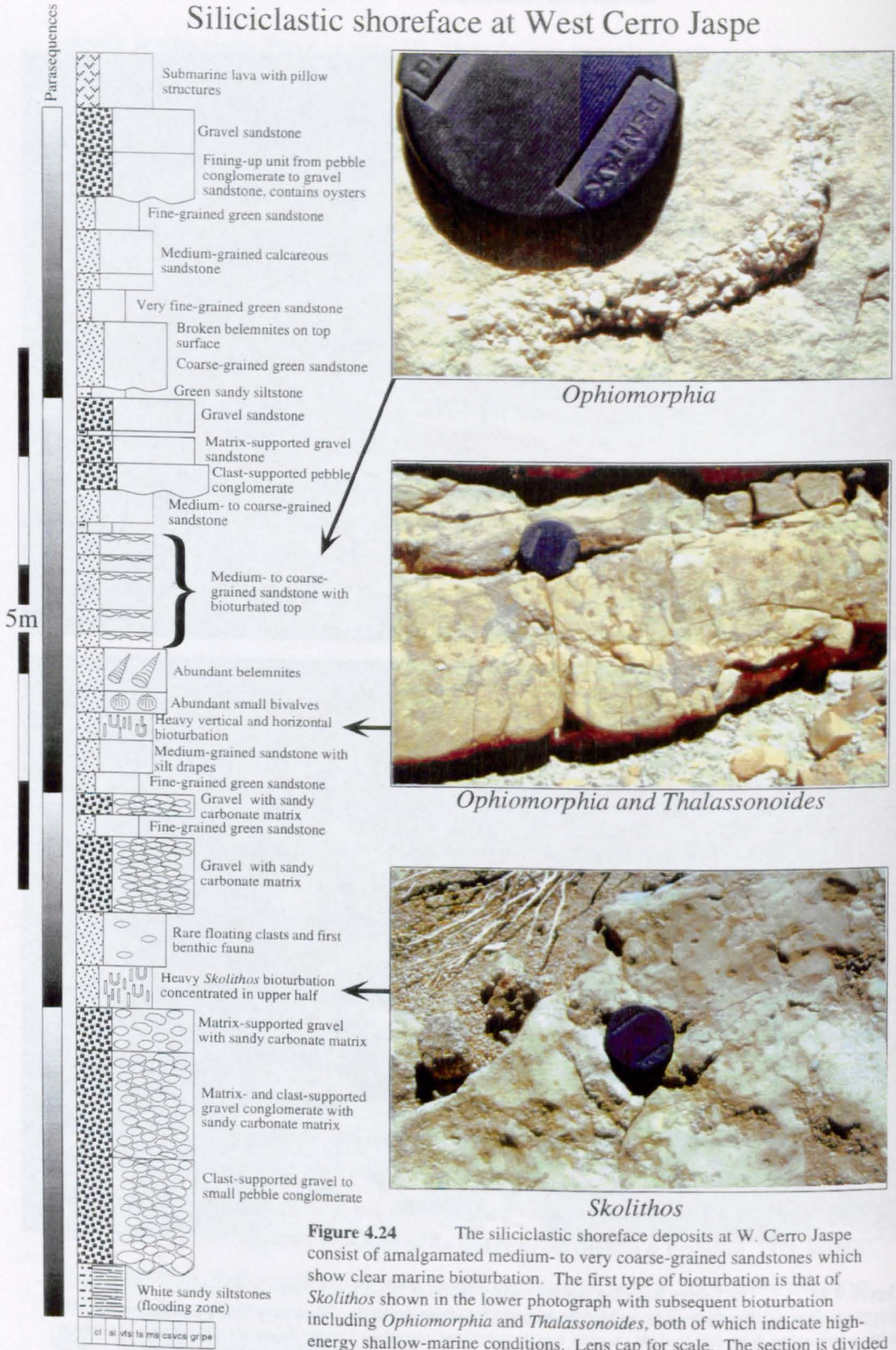


Figure 4.24 The siliciclastic shoreface deposits at W. Cerro Jaspe consist of amalgamated medium- to very coarse-grained sandstones which show clear marine bioturbation. The first type of bioturbation is that of *Skolithos* shown in the lower photograph with subsequent bioturbation including *Ophiomorpha* and *Thalassonoides*, both of which indicate high-energy shallow-marine conditions. Lens cap for scale. The section is divided into four parasequences (Figure 4.23).

Shallow-marine deposits from Quebrada San Pedro

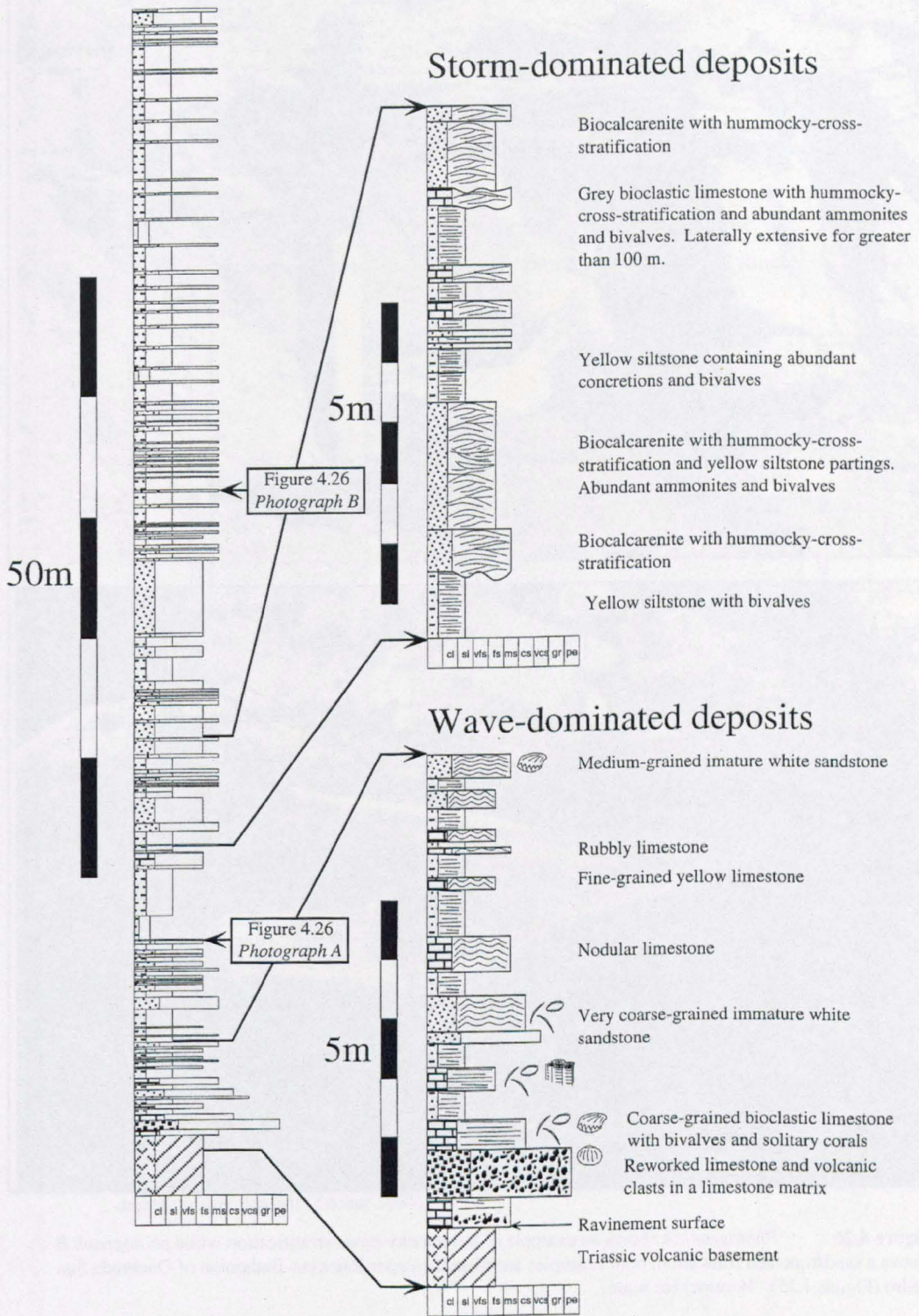


Figure 4.25 Upper Bajocian to Bathonian succession at Quebrada San Pedro displaying a transgressive wave-dominated upper shoreface and subsequent storm-dominated lower shoreface. Positions of photographs in Figure 4.26 are shown.



Figure 4.26 *Photograph A* shows an example of hummocky-cross-stratification while *photograph B* shows a sandstone bed truncation, both examples are from the upper Bajocian-Bathonian of Quebrada San Pedro (Figure 4.25). Hammer for scale.

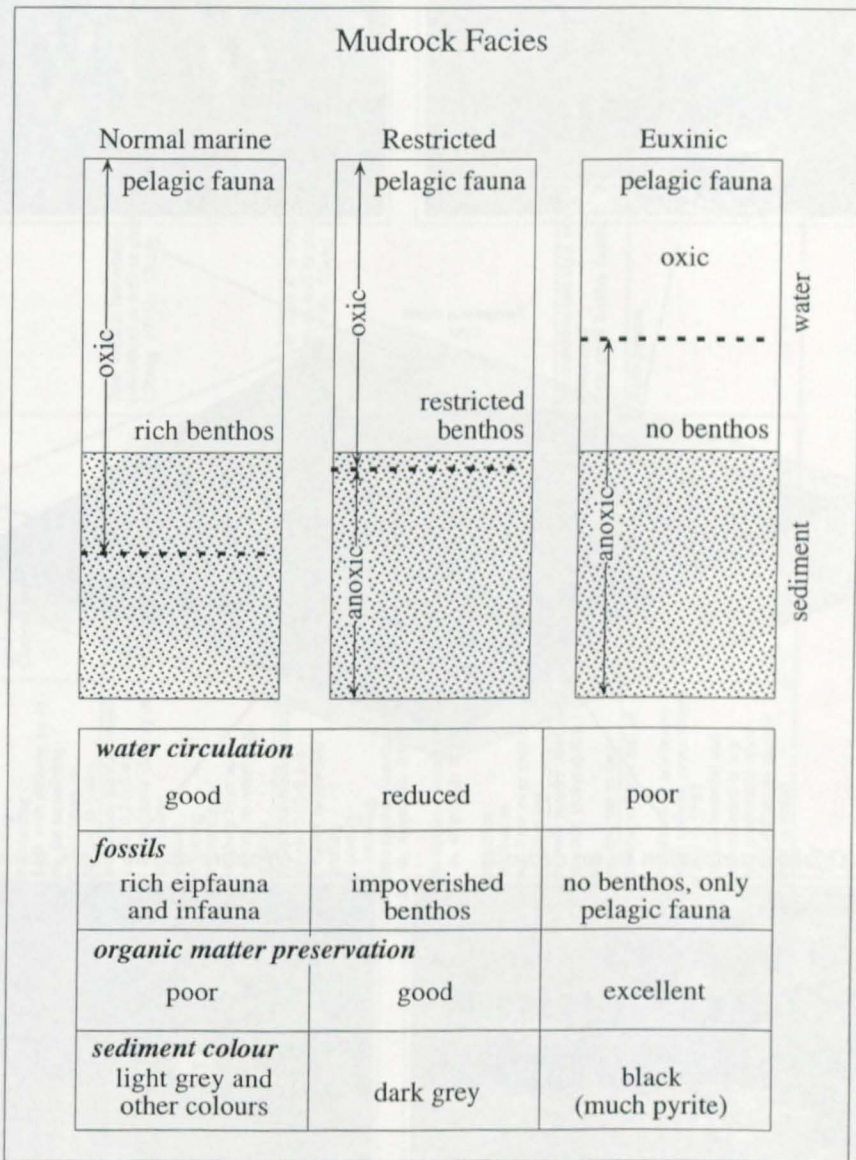
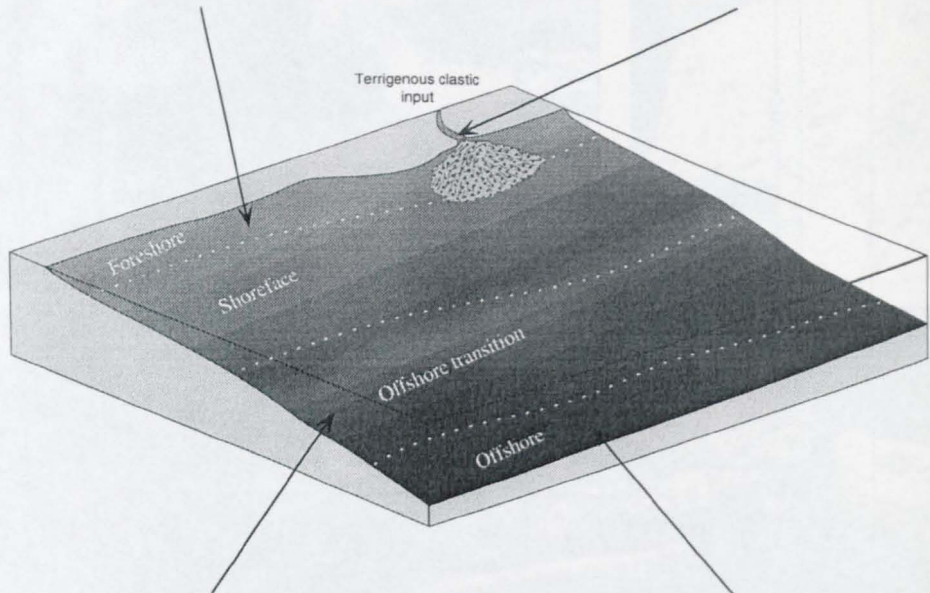
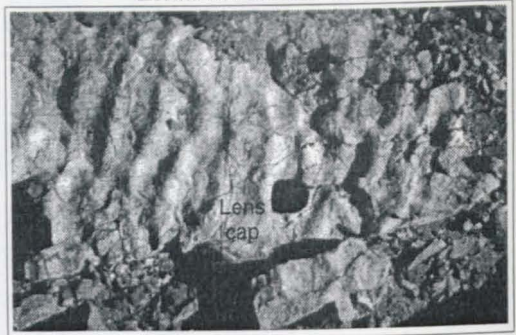


Figure 4.27 The relationship between mudrock facies and oxicity-anoxicity, faunal and organic matter content (Tucker 1991).

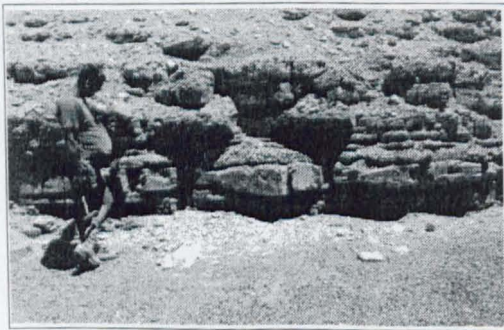
Foreshore and shoreface sandstones



Estuarine sandstones



Offshore transition storm deposits



Offshore anoxic black shales



Figure 4.28 The shallow-marine siliciclastic ramp facies model is constructed from an analysis of temporally and spatially distinct facies associations which have been integrated to represent the linkage of contemporaneous depositional environments.

Table 4.2 Summary facies table describing all the shallow-marine siliciclastic ramp-margin lithofacies found in northern Chile in terms of lithology and grain-size, sedimentary structures and bounding surfaces, thickness and geometry, and body and trace fossils, followed by a process interpretation.

Shallow-marine siliciclastic facies description

Facies and Facies Association	Lithology and Grain Size	Structures and Bounding Surfaces	Thickness and Geometry	Body and Trace Fossils	Process Interpretation
<i>Estuarine facies association</i>					
Gravel- to small pebble-grade lag facies (Estuarine facies association)	Gravel- to small pebble-grade conglomerate Dark red / brown in colour Clast compositions are intrabasinal fine- to medium-grained sandstone facies	Clast-supported Normal grading Moderate sorting Moderate rounding Erosive base with incision up to 0.2 m into the underlying sandstone and sharp or gradational top to facies	0.1-0.3 m bed thickness making up the base of the channel sandstone unit Channel geometry	No evidence of body or trace fossils	Erosive lag facies deposited at base of fluvial channel (not always present)
Very coarse- to medium-grained channel sandstone facies (Estuarine facies association)	Very coarse- to medium-grained sandstone Dark red / brown in colour	Trough and planar-tabular cross-bedding (scale 0.2-0.5 m) Siltstone or mudstone draping of foresets is common Normal grading Moderate sorting Moderate rounding Erosive or sharp base and gradational top to overlying sandstone facies	1-3 m bed thickness Channel geometry (thins laterally to zero within 50-100 m)	Rare vertical bioturbation (<i>skolithos</i>) as well as plant debris (Chong 1973b; Chong 1973a)	Fluvial sandstone channel-fill
Medium- to fine-grained channel sandstone facies (Estuarine facies association)	Fine- to medium-grained sandstone Dark red / brown in colour	Trough and planar-tabular cross-bedding (scale 0.02-0.2 m) Climbing ripple lamination Normal grading Moderate sorting Moderate rounding Asymmetric ripples (wavelength 0.05-0.1 m, amplitude 0.01-0.015 m) Symmetric ripples (wavelength 0.05-0.1 m, amplitude 0.01-0.015 m) Wavy lamination Parallel lamination Gradational base over underlying facies and sharp top	0.3-1 m bed thickness making up the top of the channel sandstone unit Channel geometry	Abundant vertical bioturbation (<i>skolithos</i>) as well as plant debris (Chong 1973b; Chong 1973a)	Fluvial sandstone channel-fill which has undergone wave-reworking
Algal laminated limestone facies (Estuarine facies association)	Fine-grained micritic limestone Yellow to pale brown in colour	Millimetre-scale parallel (mat) and convex-upwards (stromatolitic) laminations Sharp base and top to bed	0.1-0.5 m bed thickness Sheet geometry (>200 m lateral continuity)	Stromatolites and algal mat limestones Rare small bivalve fossils	Thin periods of clastic starvation (base-level rise) with encroachment of very shallow marginal marine or lagoonal environments
Fine- to medium-grained mottled sandstone facies (Estuarine facies association)	Fine- to medium-grained sandstone Brown to red in colour with characteristic mottling due to calcareous concretions Tops of thicker beds have bleached appearance	Load structures in lower half of bed Abundant calcareous (carbonate and siderite) nodules concentrated in upper half (>50%) Organic woody material and rootlets concentrated at top Diffuse and gradational lower contacts and diffuse to slightly planar upper contacts	0.3-1 m bed thickness Sheet geometry	None present	Slow sedimentation rates with relative clastic starvation and prolonged high water-table allowing immature palaeosol development (Mack <i>et al.</i> 1993)

Shoreface facies association					
Bioturbated, medium- to very coarse-grained sandstone facies (Shoreface facies association)	Medium- to very coarse-grained sandstone Pale grey in colour	Normal grading Well sorted and rounded Clean (silt-free) Trough and planar-tabular cross-bedding (scale 0.1-0.3 m) Symmetric ripples (wavelength 0.05-0.1 m, amplitude 0.01-0.015 m) Wavy lamination Parallel lamination Rare hummocky- and swaley-cross-stratification Bounding surfaces are sharp to erosive	Sandstone beds range from 0.2-1 m with a distinctive sheet geometry	Body fossils Bivalves, gastropods, brachiopods, belemnites, ammonites Trace fossils <i>Skolithos, ophiomorpha, diplocraterion, thalassinoides, arenicolites, palaeophycus, rhizocorallium, teichichnus, cruziana, planolites, chondrites</i>	High energy shallow-marine sandstones deposited predominately by wave processes with rare storm beds
Fine- to very coarse-grained sandstone facies (Shoreface facies association)	Fine- to very coarse-grained sandstone Pale grey in colour	Normal grading Well sorted Well rounded Clean (silt-free) Hummocky- and swaley-cross-stratification Symmetric ripples (wavelength 0.05-0.1 m, amplitude 0.01-0.015 m) Wavy lamination Parallel lamination Bounding surfaces are sharp to erosive	Sandstone beds range from 0.1-0.8 m with a distinctive sheet geometry The lower bounding surface has a distinctive wavy form while the upper bounding surface is flat or wavy	Body fossils Ammonites, bivalves, gastropods, brachiopods, belemnites Trace fossils <i>Skolithos, ophiomorpha, diplocraterion, thalassinoides, arenicolites, palaeophycus, rhizocorallium, teichichnus, cruziana, planolites, chondrites</i>	High-energy sandstone deposited during a single storm event
Medium-grained calcareous siltstone facies (Shoreface facies association)	Medium-grained calcareous siltstone Pale grey /yellow in colour	Massive Rare parallel lamination Gradational base and top	Sandstone beds range from 0.1-0.8 m with a distinctive sheet geometry	Body fossils Ammonites, bivalves, gastropods, brachiopods, belemnites Trace fossils Heavy bioturbation similar to that seen in the interbedded Fine- to very coarse-grained sandstone facies but the preservation potential is markedly less	Low-energy siltstone deposited during fairweather periods between storm events
Offshore calcareous siltstone facies association					
Fine-grained calcareous sandstone facies (Offshore calcareous siltstone facies association)	Fine- to medium-grained calcareous sandstone Pale grey /yellow in colour	Massive Rare parallel or wavy lamination Sharp base and top	Sandstone beds range from 0.1-0.5 m thick with a distinctive sheet geometry	Body fossils Ammonites, bivalves	Sandstone deposited during major storm or by distal turbidity current
Fine- to medium-grained calcareous siltstone facies (Offshore calcareous siltstone facies association)	Fine- to medium-grained calcareous siltstone Pale grey /yellow in colour	Massive Rare parallel lamination Gradational base and top	Siltstone beds range from 1-10 m with a distinctive sheet geometry	Body fossils Ammonites, bivalves Trace fossils Rare bioturbation but difficult to identify due to weathering	Low-energy siltstone deposition in a fully marine oxygenated environment
Very fine- to fine-grained black siltstone facies (Offshore calcareous siltstone facies association)	Very fine- to fine-grained calcareous siltstone Black in colour	Massive Rare parallel lamination Gradational base and top	Siltstone beds range from 1-10 m with a distinctive sheet geometry	Body fossils Ammonites, bivalves Trace fossils None noted	Low-energy siltstone deposition in a fully marine anoxic environment

(Wignall & Maynard, 1993). Both these areas provide analogues to the Lower Toarcian and Lower-Middle Oxfordian of northern Chile where the black shale facies are interpreted to represent early transgressive black shales and maximum flooding surface black shales.

4.4.4 Shallow-marine siliciclastic ramp facies model

The shallow-marine siliciclastic ramp deposits of northern Chile have been shown to include a wide variety of different facies associations from offshore black shale through offshore transition and shoreface to estuarine deposits (Fig. 4.19). The marine siliciclastic depositional model is based on the integration of temporally and spatially distinct facies and facies associations and does not represent active deposition in all the environments at a particular time (Fig. 4.28). The depositional model is modified through time by changing accommodation space and sediment supply, discussed in Chapter 5. Although the fairweather and storm processes are well defined and produce distinct facies associations, it is difficult to quantify the depth ranges and widths of particular facies belts (Figs 4.20 and 4.25). These values are heavily dependant on the wave energy and coastal bathymetry of the basin. On the basis of a typical siliciclastic ramp parasequence from the Book Cliffs in North America the depths for fairweather and storm wave bases have been estimated on the assumption that the parasequence records progradation with no aggradation (Figs 4.29) (J. Howell pers. comm., 1996). The mean depths for fairweather and storm wave-base are 21.5 m and 35.5 m, respectively. This method cannot be applied to the parasequences seen in the Domeyko basin because a single complete shallowing-upward succession from offshore to non-marine facies is not preserved. The depth of the marine siltstone and anoxic black shale facies are also difficult to quantify due to their lack of structures and benthic fauna, possibly occurring at shallow depths if the mixed layer is at shallow levels (P. Turner pers. comm., 1994). Their close association with thin wave-rippled sandstones and bioclastic limestones supports the interpretation of relatively shallow depths of deposition associated with early transgressive black shales and maximum flooding surface black shales.

4.5 Shallow-marine carbonate ramp facies description

A succession of offshore lime mudstone/wackestone and shoreface limestone facies associations have been interpreted to represent a genetically-linked shallowing-upward profile and hence, carbonate ramp parasequence (Figs 4.30 and 4.31). Overlying marginal-marine lagoonal limestones and sabkha evaporitic facies are separated from the fully marine limestones by regionally extensive surfaces, and hence, are interpreted to be genetically-unrelated (Fig. 4.30). Internal sedimentary structures observed in the shoreface limestone deposits are analogous to those of the shoreface sandstone deposits indicating that similar wave- and storm-processes controlled carbonate sediment accumulation, with the principle difference being availability of siliciclastic or carbonate sediment (Table 4.3). During periods of restricted siliciclastic sediment input it is interpreted that the siliciclastic-ramp was replaced by a carbonate ramp setting (Fig. 4.31).

The carbonate ramp facies description includes evaporite deposits where precipitation takes place in a range of shallow- to deep-water environments during periods of increasing aridity (Tucker, 1991a; Kendall, 1992). The majority of the world's thickest and most extensive evaporite successions were precipitated in intracratonic basins, which were separated from the world ocean by some barrier (Tucker, 1991b). Examples include the Zechstein, Williston-Elk Point, Michigan, Paradox, Delaware, Moscow and Siberian basins. Once relative sea-level has dropped below the height of the barrier (as a result of global sea-level fall or tectonic uplift of the barrier) to cut off the basin totally, then the basin may drawdown very quickly through evaporation (Tucker, 1991b). Global sea-level may only need to rise several metres to overtop the barrier and replenish the brines. In terms of sequence stratigraphical models for carbonate-evaporite basins, two principle types can be distinguished depending on the degree of drawdown (Tucker, 1991b): *model 1*, incomplete drawdown, giving marginal gypsum wedges and basinal laminated gypsum, and *model 2*, complete drawdown, giving halite basin-fills. The Jurassic evaporite facies of the Domeyko basin, and other South American basins, are interpreted to form by a similar silling process where the barrier is the subaerial Jurassic volcanic arc to the west.

4.5.1 Sabkha evaporite facies association

Description

The evaporites are composed of fine- to medium-grained gypsum with rare anhydrite and significant amounts of carbonate and terrigenous clastic impurities on the basis of petrographic analysis. In hand specimen the impurities give the evaporites a dirty red/brown colour as opposed to the clean white colour associated with pure gypsum and anhydrite. The impurities are concentrated along a network of veins, resulting in the formation of the classic chicken-wire texture. In some cases, tepee structures and small desiccation cracks (0.05-0.1 m in diameter) can be observed on the surfaces of individual bedding planes. Towards the base of the evaporite units there are rare 0.01-0.1 m intraclasts of the underlying limestones.

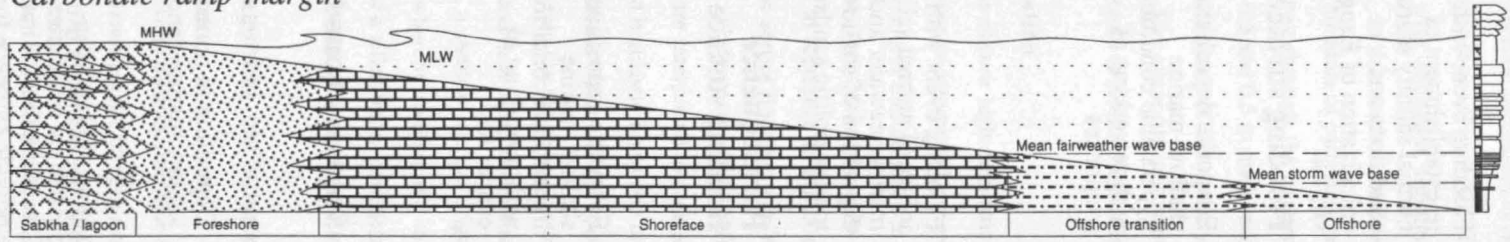
Lithology	Graphic Log Grain Size mud s vf f m	Facies	Lithofacies Association	Genetic Elements	Palaeocurrents	Ichnofossils	Bio Index	Comments	Observed Thickness (m) Mean:Max:Min (Mean:Max:Min after Balsley 1980)	
	C	Tidal Inlet/ Foreshore	Shoreface parasequence		Laminae are seaward dipping	Rootlets, rare vertical burrows	<1	Forms classic "whitecaps" due the disaggregation of detrital dolomites and leaching by organic acids	2.5 : 3.8 : 1 (1.8 : 2.7 : 1.2)	
	S.Px					Broadly shore parallel (NNE-SSW) with principal vector to the SE. Local flood dominant flow to the WNW within tidal inlets. Minor component of offshore flow.	Simple vertical burrows; Skolithos, Cylidrichnus; Ophiomorpha sp., Ophiomorpha nodosa	1	Very clean sandstone, cross beds in extremely well ordered sets	6 : 12 : 3 (4.3 : 5.5 : 2.4)
	S.Bi, S.Px, S.Sc	Middle Shoreface					Ophiomorpha nodosa, Ophiomorpha sp., Thalassinoides. Palaeophycus, Terebellina.	5	Planar lamination, low angle cross lamination, interbedded at decimeter scale with very bioturbated intervals	4 (mean)
	S.Sc, very rare Si.Wx, Si,Cb	Lower Shoreface				Rare wave ripples have shore parallel and oblique crests	Ophiomorpha nodosa, Ophiomorpha sp., Thalassinoides, Chondrites, Palaeophycus, Planolites and Terebellina.	2-3	Hummocky cross stratified, parallel laminated, wave and current rippled, variably bioturbated sandstones and siltstones.	9 : 24 : 5 (13 : 23 : 5)
	S.Hc, S.Wx, S.Sc, Si.Wx, Si.Cb, Si.Bi	Offshore Transition Zone				Ripple lamination approximately shore parallel or sub-parallel directed to the south or southeast and more rarely to the north or northeast. Prod and tool marks (sole structures) also directed oblique offshore to the SE.	Intense bioturbation; Terebellina	4-5	Hummocky cross stratified sandstone, interbedded with laminated or massive, heavily bioturbated silty mudstones/ mudstones.	14 : 22 : 2
	M, M.Bi, Si.Bi, Si.Wx	Offshore					Intense bioturbation; Species identification uncertain	5-6	Grey to light grey, organic rich, bioturbated mudstone Mancos Shale	25 : 80 : 6

Figure 4.29 A typical siliciclastic ramp parasequence from the Book Cliffs in North America displays a complete shallowing-upward succession from offshore to non-marine facies allowing the depths for fairweather and storm wave bases to be estimated on the assumption that the parasequence records progradation with no aggradation (J. Howell pers. comm. 1996). This method cannot be applied to the parasequences seen in the Domeyko basin because a single complete shallowing-upward succession from offshore to non-marine facies is not preserved.

Figure 4.30 Schematic representation of the Domeyko basin carbonate ramp facies and facies associations in northern Chile based on lithology and grain-size, sedimentary structures, body and trace fossils and bounding surface character.

Lithology	Graphic log		Facies	Facies association	Depositional environment	Description	Body and trace fossils	Bounding surfaces & architectural elements	Schematic representation of architectural elements
	micritic	sparry							
			(a) Nodular anhydrite and dolomite on salt flats (b) Laminated evaporites in desiccated ponds Terrigenous interbeds	Platform (sabkha) evaporites	Tidal flat	Irregularly laminated dolomite and anhydrite locally may grade into redbeds Red, yellow, brown in colour Anhydrite after gypsum nodular rosettes, "chicken wire" and blades, irregular lamination, caliche	Stromatolitic algae almost the only indigenous biota	Amalgamated sheet geometry evaporites & clastics	
			(a) Bioclastic wackestone; lagoons (b) Litho-bioclastic sand in tidal channels (c) Lime mud on tidal flats (d) Fine-grained terrigenous clastic interbeds	MHW Restricted lagoonal limestones	Lagoon	Often dolomite and dolomitic limestone, light coloured Clotted pelleted mudstone and grainstone; laminated mudstone; coarser wackestones in channels Birdseye, stromatolites, fine laminations, dolomite crusts Cross-bedded sand in channels	Limited fauna Mostly grazing gastropods, algae and ostracods	Amalgamated sheet geometry limestones	
			Planar-stratified boundstone & grainstone	MLW Upper Shoreface	Carbonate ramp parasequence	Localized wavy planar lamination Shell lags	Bivalves, gastropods, solitary & colonial corals, brachiopods, belemnites	Large amalgamated limestones	
			Planar-stratified boundstone & grainstone	Middle Shoreface		Planar-lamination, low angle cross-lamination, swaley-cross-stratification, Shell lags	Bivalves, gastropods, solitary & colonial corals, brachiopods, belemnites	Amalgamated sheet geometry limestones	
			Amalgamated, sheet-geometry grainstones derived from fair-weather and storm wave activity	Lower Shoreface		Hummocky-cross-stratification, swaley-cross-stratification, parallel lamination, wave and current rippled, abundant disarticulated shell debris	Bivalves, gastropods, solitary corals, brachiopods, belemnites, <i>Skolithos</i> , <i>Thalassinoides</i>	Amalgamated sheet geometry limestones	
			Fine-grained mudstones, wackestones & packstones (fair weather wave activity) with interbedded grainstones (storm wave activity) which thicken and become more common upwards.	MFWWB (15-20m) Offshore Transition		Hummocky-cross-stratification, swaley-cross-stratification, wave ripples, abundant disarticulated shell debris. Laminated or massive, heavily bioturbated mudstones & wackestones	Ammonites, bivalves, gastropods, solitary corals, brachiopods, belemnites, <i>Thalassinoides</i>	Fine-grained mudstones, wackestones & packstones with interbedded grainstones which thicken and become more frequent upwards.	
			Fine-grained mudstones & wackestones with rare intercalated thin sheet-geometry packstones Evaporites	MSWB (40-50m) Offshore (oxic, anoxic, evaporitic)		Fine-grained yellow mudstones & wackestones or organic-rich black mudstone; Rare thin (2-10 cm), parallel-laminated, fine-grained packstones White anhydrite and gypsum with few impurities	Ammonites; Bivalves; No traces No fauna in evaporites	Fine-grained mudstones & wackestones with rare intercalated thin sheet geometry packstones Thick clean sheet geometry evaporites	

Carbonate ramp-margin



Carbonate reef-margin

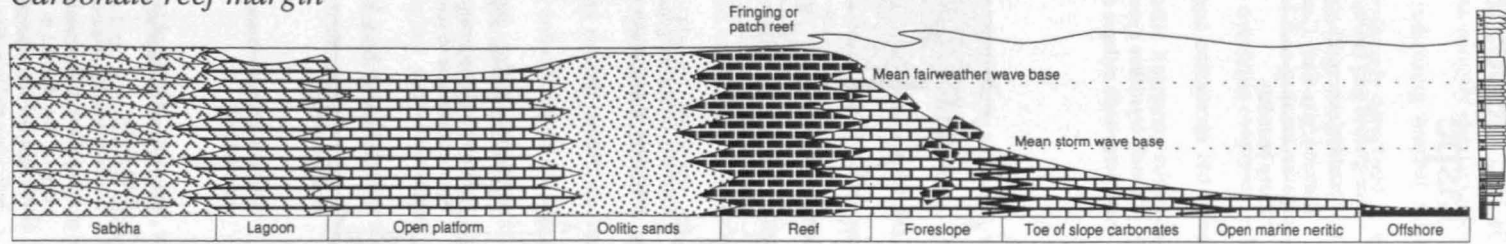
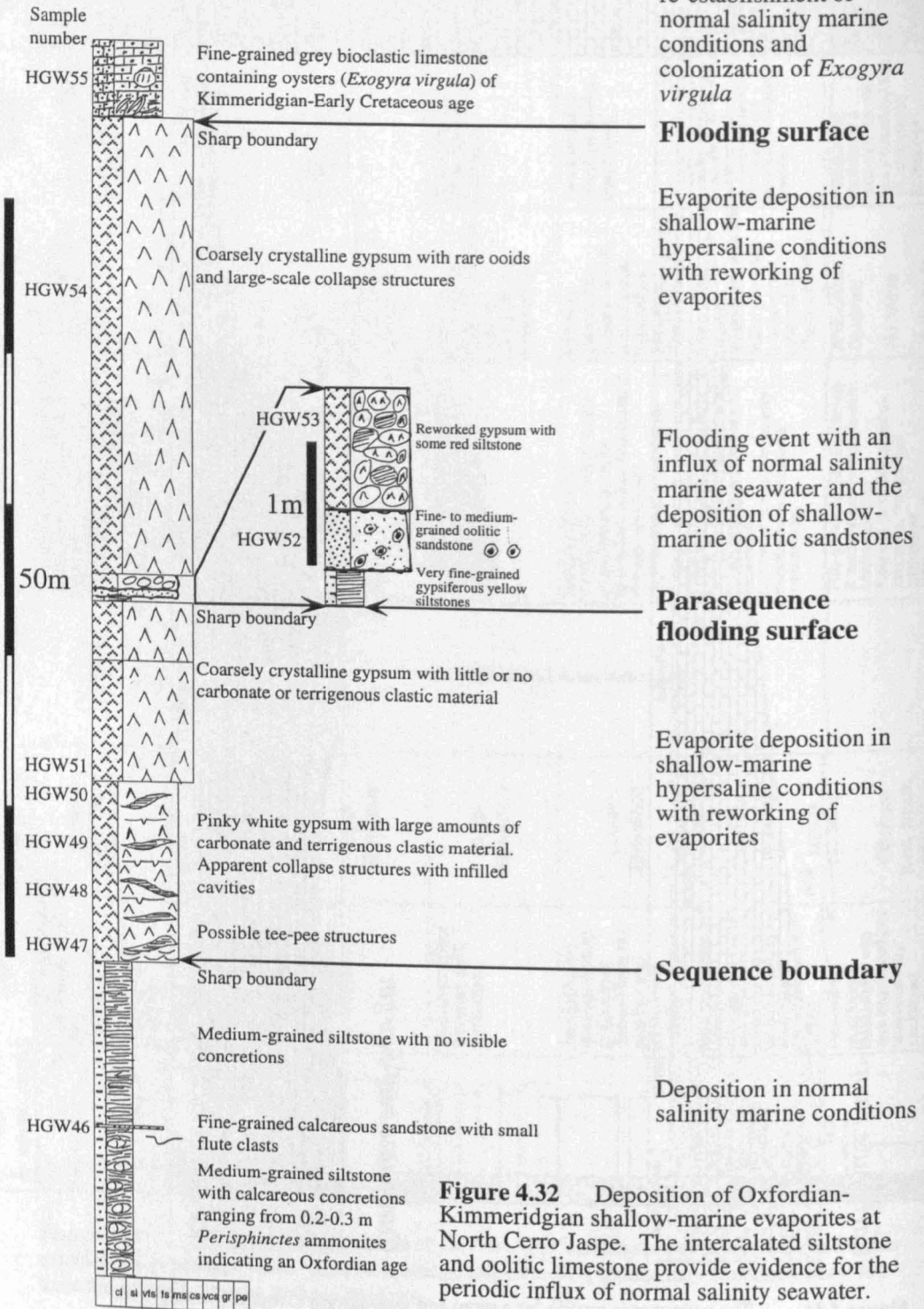


Figure 4.31 The bathymetric profile for a ramp and reef-margin carbonate setting with associated facies belts (Handford & Loucks, 1993).

Evaporite deposition at North Cerro Jaspe



Flooding event with the re-establishment of normal salinity marine conditions and colonization of *Exogyra virgula*

Flooding surface

Evaporite deposition in shallow-marine hypersaline conditions with reworking of evaporites

Flooding event with an influx of normal salinity marine seawater and the deposition of shallow-marine oolitic sandstones

Parasequence flooding surface

Evaporite deposition in shallow-marine hypersaline conditions with reworking of evaporites

Sequence boundary

Deposition in normal salinity marine conditions

Figure 4.32 Deposition of Oxfordian-Kimmeridgian shallow-marine evaporites at North Cerro Jaspe. The intercalated siltstone and oolitic limestone provide evidence for the periodic influx of normal salinity seawater.

North Cerro Jaspe example

The Upper Jurassic succession at North Cerro Jaspe provides an example of Oxfordian-Kimmeridgian aged evaporite facies (Fig. 4.32). The sharp-based evaporite facies abruptly overlie Oxfordian marine siltstones with abundant ammonite fauna (*Perisphinctes*), indicating normal salinity marine conditions. In thin section, the lower evaporite facies are predominately composed of gypsum with significant amounts of carbonate and terrigenous clastic impurities (Fig. 4. , HGW47, 48, 49, 50 and 51). Midway through the evaporite unit are two thin beds of fine-grained siltstone and oolitic sandstone, 0.3 and 0.5 m thick respectively. In thin section, the overlying evaporite unit is found to contain small clasts of the underlying oolitic sandstone, ooids and calcareous red algae (Fig. 4.32, HGW54). The evaporite unit is overlain by fine-grained bioclastic limestone containing abundant *Exogyra virgula* of Kimmeridgian-Early Cretaceous age.

Interpretation

On the basis of their high carbonate and terrigenous clastic content resulting in a chicken-wire texture, the evaporites are interpreted to represent an inter- to supra-tidal marine sabkha setting. The presence of tepee structures and desiccation cracks indicates evaporation to sub-aerial conditions, commonly found in the inter-tidal zone. The two thin beds of fine-grained siltstone and oolitic sandstone are interpreted to represent an influx of normal salinity marine water. This flooding surface is sharp implying an abrupt flooding with the introduction of ooids, interpreted to represent shallow-marine conditions. The presence of reworked oolitic sandstone, ooids and calcareous red algae in the upper evaporites are interpreted to indicate the influx of marine water (Fig. 4. , HGW54). The overlying fine-grained bioclastic limestone containing abundant *Exogyra virgula* is interpreted to represent the influx of marine water and the re-establishment of normal salinity marine conditions, recorded as a flooding event. On the basis of reworked oolitic sandstone, ooids and calcareous red algae within the evaporites and their close association with adjacent marine siltstones, oolitic sandstones and bioclastic limestones, a shallow-marine origin is interpreted. Therefore, an incomplete drawdown model is proposed, whereby sabkha and reworked evaporites form marginal gypsum wedges around the periphery of a silled basin, periodically replenished by an influx of normal salinity seawater. An arid climate implies that there will be little dilution of the brines from freshwater river discharge.

4.5.2 Lagoonal carbonate facies association

Description

There are several distinct limestone facies developed including algal laminated limestone, algal oncoid limestone, monospecific bivalve-rich limestone and crinoid debris limestone facies (Table 4.3). The algal laminated limestones are fine-grained and micritic in nature, ranging from grey to yellow and pink in colour (Table 4.3, Fig. 4.33). They display a distinctive fine millimetre-scale lamination which is commonly flat (mat) and only rarely mounded (stromatolitic) (Fig. 4.33). Hardy & Ginsburg (1977) noted that a fine millimetre-scale lamination is common of intertidal zones and

associated with a fenestral fabric (Fig. 4.33). The algal lamination is commonly highlighted by colour alternation and picked out on the weathered surface, as seen at Quebrada Honda (Fig. 4.33). The 0.1-0.5 m thick algal oncoid limestone facies is composed of abundant 0.001-0.01 m algal oncoids which are cigar-shaped or rarely round (Table 4.3, Fig. 4.33). The beds can be traced laterally for greater than 400 m indicating a sheet geometry (Fig. 4.11). An abundant stunted monospecific bivalve assemblage characterises the monospecific bivalve-rich limestone facies which is grey in colour with sheet geometries (Table 4.3). The 0.05-0.1 m thick crinoid debris limestone facies is composed of yellow to pale brown parallel and wavy laminated limestone facies with abundant broken crinoid debris (Table 4.3).

Interpretation

The algal laminated limestone facies is interpreted to represent low-energy deposition in a shallow marginal marine or muddy lagoonal setting on the basis of the fine algal mat and stromatolite laminations (Fig. 4.33). The algal oncoliths are indicative of an intertidal zone where the coated grains are rolled around causing their continued growth by the snowballing mechanism, first noted by Gebelein (1976) and later described by Jones & Goodbody (1985) (Fig. 4.33). Golubic & Fischer (1975) describe how the asymmetric geometry of the oncoids indicates that they are formed in a relatively low-energy environment such as a lagoon, as opposed to the higher energy shoreface. In the case of the monospecific bivalve-rich limestone facies, an abundant stunted monospecific bivalve assemblage is characteristic of a marginal marine to lagoonal environment where hypersaline conditions control faunal development. The crinoid debris limestone facies is rare, characterised by a coarser grain size, sharp to slightly erosive base and shell or crinoid debris, interpreted to result from storm-related floods into the lagoon. However, the flood breaches are rare, indicating that the deposits occur in an intertidal to supratidal setting and limestone aggradation rates were relatively rapid. The lagoonal carbonate deposits of northern Chile are temporally and spatially restricted to the Late Jurassic-lowest Cretaceous, post Oxfordian/Kimmeridgian evaporites, marking the marine regression between 21°-24°S.

4.5.3 Limestone shoreface facies association

Description

The 0.2-2 m thick, dark grey bioclastic limestone facies has a brown weathering colour and is micro-sparry to sparry in nature with abundant bioclastic material (Table 4.3, Figs 4.25 and 4.34). The bioclastic material includes shell fragments of bivalves, brachiopods, gastropods, belemnites and oysters, along with solitary corals and rare ammonite fragments (Fig. 4.34). All the constituent bioclastic material shows clear evidence of reworking (Fig. 4.34). In several cases, the lowest few limestone beds contain abundant intraclasts of the underlying porphyritic volcanic rock (Table 4.3). The oolitic limestone facies is composed of well developed spherical oolites from 1-3 mm in diameter with a sparry calcite pore filling matrix no evidence of lime mudstone (Table 4.3). There are no apparent internal structures preserved and the limestone has a brown weathered appearance. The oolitic

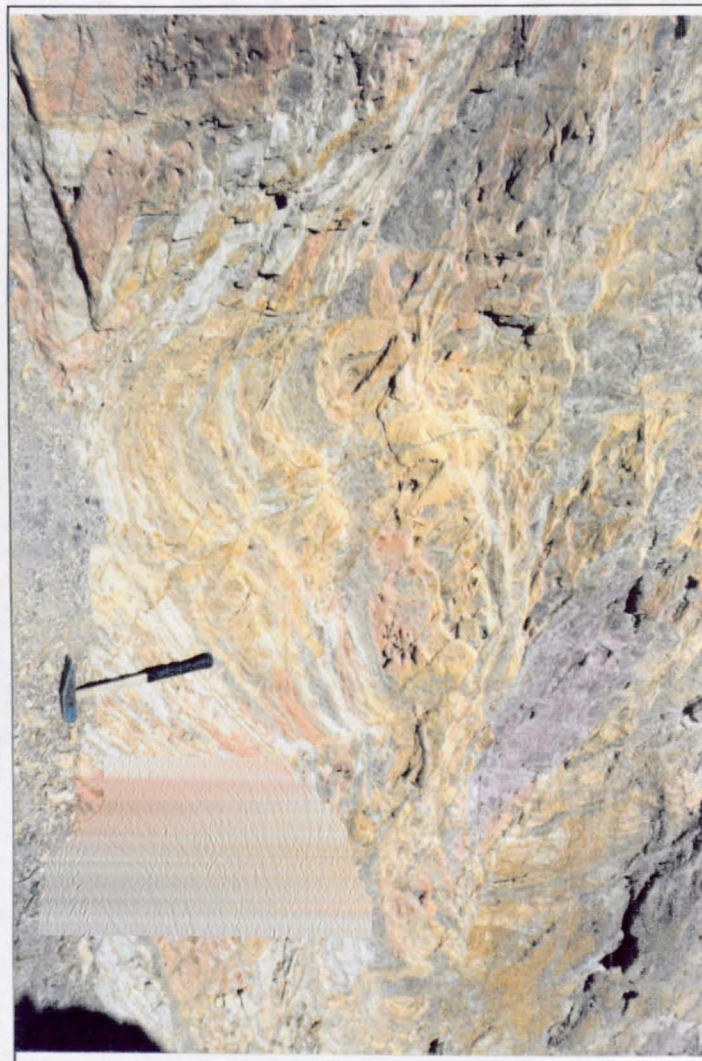
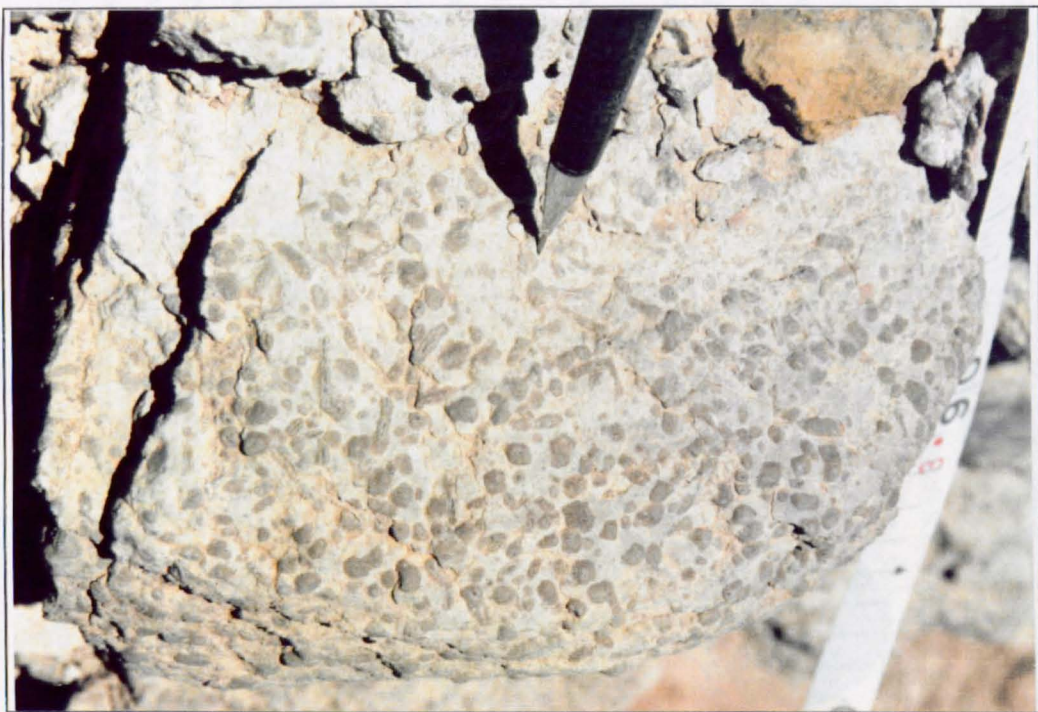


Figure 4.33 *Photograph A:* Algal laminated limestone facies from the Kimmeridgian of Quebrada Honda (Figure 4.11). The limestones range from yellow and grey to pink in colour with a distinctive millimetre-scale parallel lamination. Pencil for scale. *Photograph B:* Algal oncoid limestone facies from the Kimmeridgian of Quebrada San Pedro showing abundant cigar-shaped algal oncoids. Pencil for scale.



Figure 4.34 The Late Bajocian marine transgression at Quebrada San Pedro is recorded by shoreface limestone facies directly overlying Permo-Triassic volcanics. The shoreface limestone facies contains abundant bioclastic shell debris including bivalves, brachiopods, gastropods, belemnites and oysters, with solitary corals and rare ammonite fragments.

limestone unit itself ranges from 0.4-2 m in thickness and is laterally extensive over 1000 m at outcrop (Cerritos Bayos). The coarse-grained calcareous sandstone facies is grey in colour and occurs in 0.5-2 m thick beds with a sheet geometry, displaying 0.1-0.3 m trough and planar-tabular cross bedding, symmetric ripples and both wavy and parallel lamination (Table 4.3). The brown limestone facies is composed of 1-2 m thick beds of pale grey medium-grained grainstone with both wavy and parallel lamination (Table 4.3). The limestone beds have sharp, undulatory bases and a characteristic sheet geometry, with abundant bivalve and brachiopod fossils. The grey limestone facies is composed of 1-2 m thick beds of dark grey fine-grained packstone and wackestone with both wavy and parallel lamination (Table 4.3). The limestone beds have sharp bases and a characteristic sheet geometry with abundant bivalve and brachiopod fossils. In all cases the sheet geometry limestone beds are amalgamated with little or no silt-grade material present.

Closely associated are interbedded units of 0.2-0.5 m thick fine- to very coarse-grained hummocky-cross-stratified grainstone facies and 0.2-0.4 m thick medium-grained mudstone facies (Table 4.3). The grainstone beds are erosively-based with a sheet geometry, flat or undulose top surfaces and a lateral extent of greater than 100 m, indicative of a predominately tabular nature. However, lateral termination of beds is also observed, where grainstone beds thin rapidly over 2 m and pinch out into mudstones. Internally, the grainstones display hummocky-cross-stratification, swaley-cross-stratification and symmetrical ripples, with a high content of shell debris in the form of bivalve, brachiopod and oyster fragments. The shell debris is distributed throughout the bed and commonly concentrated into a shelly lag at the base of the bed. Some of the grainstone beds contain small vertical burrows of *Skolithos*. The medium-grained mudstone facies is calcareous in nature with rare parallel lamination and *Scolicia* bioturbation in the form of well developed horizontal feeding burrows formed by gastropods. The mudstone units contain abundant calcareous concretions which are spherical or ellipsoidal in shape and range in diameter from 0.05-0.5 m, often concentrated along particular horizons.

Interpretation

The bioclastic limestone facies contains a high percentage of reworked shell debris with a sparry (micrite-free) composition and commonly reworking of underlying porphyritic volcanic rock, leading to the interpretation of a high-energy, shallow-marine foreshore deposit (Fig. 4.34). A transgressive interpretation is supported by the relatively thin (several metres) nature of these deposits which are only preserved during periods of marine transgression (Figs 4.25 and 4.34). The oolitic limestone facies is interpreted as a high-energy shallow-marine shoreface limestone on the basis of a micrite-free matrix with the apparent lack of coral growth indicating an unsuitable substrate. The coarse-grained calcareous sandstone facies is interpreted as a high-energy shallow-marine sandstone based on the presence of trough and planar-tabular cross bedding as well as abundant symmetric ripples, indicating shallow-marine wave activity (Table 4.3). The brown limestone facies is predominately of grainstone composition with abundant shallow-marine fauna, indicative of high-energy shoreface deposition (Table 4.3). The grey limestone facies is composed of fine-grained packstone and wackestone

limestones with a more muddy micritic matrix indicating a lower-energy depositional setting but still characteristic of the amalgamated limestone shoreface.

The grainstone facies containing well preserved hummocky- and swaley-cross-stratification are interpreted as storm-dominated deposits occurring between the fairweather and storm wave bases (Table 4.3, Fig. 4.31). The grainstone facies are characterised by a tabular nature, lateral termination of beds, undulatory basal and top surfaces, all features indicative of an oscillatory flow-regime and storm deposited deposits. While the hummocky-cross-stratified grainstone facies are interpreted to represent individual storm events, the interbedded mudstone facies are interpreted to represent the fine-grained nature of the fairweather sedimentation (Fig. 4.31). The interbedded grainstone and mudstone facies occur between the fairweather and storm wave bases and are interpreted as offshore transition storm deposits in a carbonate ramp setting. The concretions are thought to have formed by early diagenetic processes during periods of reduced sedimentation where anaerobic conditions developed at, or slightly below, the sediment surface. The abundance of concretions may be controlled by the length of time that sedimentation was suppressed and the magnitude of carbonate supersaturation in the anaerobic zone (Raiswell, 1987). Such conditions are consistent with parasequence flooding surfaces, and therefore several of the concretionary horizons may reflect parasequence flooding surfaces.

4.5.4 Offshore carbonate mudstone facies association

Description

The 1-10 m thick medium-grained carbonate mudstone facies is either massive or parallel laminated and pale grey to yellow in colour with abundant calcareous concretions which are spherical or ellipsoidal in shape and range in diameter from 0.05-0.5 m (Table 4.3). Rare intercalated beds of 0.1-0.5 m thick fine-grained packstone facies are calcareous in nature, with sharp to slightly erosive bases and sharp tops. Internally, the packstones have poorly developed wavy and parallel lamination. The packstones and mudstones contain abundant ammonite fauna, with some bivalve fauna. Interbedded 0.3-1 m thick jet black mudstone and 0.1-0.5 m thick grey/black, micritic limestone facies are usually massive with rare parallel lamination and abundant ammonite and bivalve fossils (Table 4.3). When freshly broken, the shales give off a strong sulphurous smell. The micritic limestone facies is unique to this facies association, being dark grey to black in colour with a very fine-grained micritic texture (Table 4.3). The grey weathered surface of the limestone picks out poorly developed wavy and parallel lamination. The limestone beds themselves have undulatory bases and flat or undulatory tops with a sheet geometry. The limestones and shales contain abundant ammonite and both articulated and disarticulated bivalve fossils as well as small shell fragments.

Interpretation

The mudstones and intercalated fine-grained packstones are interpreted to have formed in an offshore setting where siliciclastic sediment input was low, with the thin packstones representing carbonate input in the form of rare, large storm-events or low concentration turbidity currents. The presence of ammonite and bivalve fauna support the interpretation of an offshore marine environment. Abundant

calcareous concretions indicate slow rates of deposition, as discussed above in Section 4.5.3. The very fine-grained nature of the mudstone and micritic limestone facies, black colour and sulphurous smell indicate a high organic carbon content, interpreted to represent negligible siliciclastic sediment input and dysoxic to anoxic conditions during deposition (Fig. 4.27). Absolute depths of black shale formation remain poorly understood (Wignall & Maynard, 1993), with estimates varying by an order of magnitude from a few tens to hundreds of metres (Hallam, 1967a; 1967b; Wignall, 1991). The black mudstone facies extend from basinal into marginal settings and are interpreted as basal transgressive black shales and maximum flooding surface black shales, similar to those described for the offshore siltstone facies association (4.3.3) (Wignall & Maynard, 1993).

4.5.5 Subaqueous evaporite facies association

Description

The subaqueous evaporite facies is almost entirely composed of gypsum with only a small proportion of anhydrite and negligible carbonate and terrigenous clastic impurities. In hand specimen, this gives a distinctive clean white appearance to the evaporites, characteristic of pure gypsum, distinguishing them from the previously described dirty red/brown colour of the sabkha evaporite facies (4.5.1). The evaporites are poorly bedded on the scale of 0.5-2 m reaching a total thicknesses of 30-150 m, with sharp lower and upper bounding surfaces. The gypsum has a micro-crystalline amorphous texture, termed alabaster, which weathers to give a sharp jagged appearance at outcrop. The evaporites appear to lack a coherent internal structure making the detection of post-depositional deformation and thus, the measurement of accurate stratigraphical thickness more difficult.

Quebrada San Pedro example

The Upper Jurassic succession at Quebrada San Pedro provides another example of Oxfordian-Kimmeridgian aged evaporite facies. The sharp-based evaporite facies abruptly overlie Oxfordian marine siltstones with abundant ammonite fauna, indicating normal salinity marine conditions (Gygi & Hillebrandt, 1991). In thin section, the lower evaporite facies are predominately composed of gypsum with small amounts of carbonate and terrigenous clastic impurities while the upper evaporite facies contain negligible impurities. The evaporite unit is overlain by fine-grained lagoonal limestone facies (4.5.1) containing abundant oncoids and monospecific bivalve assemblages of Kimmeridgian age. The overlying lagoonal limestones contain no evidence for subaerial exposure similar to those noted for the sabkha evaporite facies (4.5.1).

Interpretation

The absence of carbonate and terrigenous clastic impurities within the gypsum gives a clean white appearance, quite different to the chicken-wire texture of the sabkha evaporite facies. This clean white appearance is interpreted to indicate the subaqueous accumulation of evaporites from hypersaline brines, supported by a lack of tepee structures or desiccation cracks. The evaporites at Quebrada San Pedro are overlain by lagoonal limestone facies and do not record complete drawdown and desiccation

of the basin, thus an incomplete drawdown model is proposed similar to that for the sabkha evaporites (Tucker, 1991b). The incomplete drawdown model suggests sub-aqueous marine evaporites are precipitated from concentrated brines within a silled basin, periodically replenished by an influx of normal salinity seawater. An arid climate implies that there will be little dilution of the brines from freshwater river discharge.

4.5.6 Shallow-marine carbonate ramp facies model

The shallow-marine carbonate ramp deposits of northern Chile have been shown to include a wide variety of different facies associations from offshore black shale through offshore transition and shoreface to lagoonal deposits (Fig. 4.30). On the basis of the above temporally and spatially distinct facies associations it is possible to develop a homoclinal carbonate ramp depositional model. The carbonate ramp model is similar to that of a siliciclastic ramp (Fig. 4.28) except for the substitution of carbonate facies (Fig. 4.30). The depositional model is modified through time by changing accommodation space and sediment supply, discussed in Chapter 5. Although the fairweather and storm processes are well defined and produce distinct facies associations, it is difficult to quantify the depth ranges and widths of particular facies belts, as for the siliciclastic ramp deposits.

Upper Jurassic evaporite deposits in northern Chile mark a short duration, but integral event in the evolution of this basin. The two evaporitic depositional settings are difficult to link genetically, but must be closely related due to their time equivalence and close vertical stacking relationships. The incomplete drawdown model is based around a silled basin setting, where high evaporation rates predominated, causing the formation of concentrated saline brines. These brines must be periodically replenished with sea-water in order to accumulate evaporite units up to 150 m in thickness. Sabkha evaporites formed at the basin margin while subaqueous basinal evaporites precipitated in the basin centre. The incomplete drawdown model of Tucker (1991b) is similar to that proposed for the Messinian evaporites of the Mediterranean, which may provide a realistic analogue (Hsü *et al.*, 1977; Vai & Lucchi, 1977; Butler *et al.*, 1995).

Table 4.3 Summary facies table describing all the shallow-marine carbonate ramp-margin lithofacies found in northern Chile in terms of lithology and grain-size, sedimentary structures and bounding surfaces, thickness and geometry, and body and trace fossils, followed by a process interpretation.

Shallow-marine carbonate ramp environment

Facies and Facies Association	Lithology and Grain Size	Structures and Bounding Surfaces	Thickness and Geometry	Body and Trace Fossils	Process Interpretation
Sabkha evaporite facies association					
Sabkha evaporite facies (Sabkha evaporite facies association)	Fine- to medium grained gypsum and anhydrite with significant amounts of carbonate and terrigenous clastic impurities Red / brown in colour	Desiccation cracks (0.05-0.1 m in diameter) Tepee structures Chickenwire texture At base of unit there are rare intra-clasts of underlying limestone Both the basal and upper bounding surfaces are sharp	Evaporite beds range from 1-10 m with a sheet geometry	None	Inter- to supra-tidal marine evaporites deposited in a sabkha environment
Oolitic limestone facies (Sabkha evaporite facies association)	Sparry limestone Pale grey in colour	Wavy lamination Parallel lamination Sharp bounding surfaces	0.5 m bed thickness Sheet geometry	Body fossils Abundant oolites, calcareous red algae	High-energy shallow-marine limestone
Lagoonal limestone facies association					
Algal laminated limestone facies (Lagoonal limestone facies association)	Fine-grained micritic limestone Yellow, pink and pale brown in colour	Millimetre-scale parallel (mat) and convex-upwards (stromatolitic) laminations Sharp base and top to bed	0.1-0.5 m bed thickness Sheet geometry (>200 m lateral continuity)	Stromatolites and algal mat limestones	Thick accumulations of low-energy, very shallow marginal marine or lagoonal deposits
Algal oncoid limestone facies (Lagoonal limestone facies association)	Fine-grained micritic limestone Grey in colour	Abundant 0.001-0.01 m algal oncoids which are lens-shaped or rarely round Sharp base and top to bed	0.1-0.5 m bed thickness Sheet geometry (>200 m lateral continuity)	Algal oncoids	Low-energy lagoonal deposits (Lens shape is indicative of low-energy conditions)
Monospecific bivalve-rich limestone facies (Lagoonal limestone facies association)	Fine-grained micritic limestone Grey in colour	No evidence of sedimentary structures Sharp base and top to bed	0.1-0.5 m bed thickness Sheet geometry (>200 m lateral continuity)	Very abundant, stunted, monospecific bivalve assemblage	Low-energy, very shallow marginal marine or lagoonal deposits (Monospecific, stunted assemblage is indicative of marginal marine-hypersaline conditions)
Crinoid debris limestone facies (Lagoonal limestone facies association)	Fine-grained micritic limestone Yellow and pale brown in colour	Parallel and wavy laminations Sharp to slightly erosive base and sharp top to bed	0.05-0.1 m bed thickness Sheet geometry	Abundant broken crinoid debris	High-energy wash-over of crinoid debris into lagoonal
Shoreface limestone facies association					
Bioclastic limestone with volcanic clasts facies (Shoreface limestone facies association)	Sparry limestone with small pebble- to boulder-grade (0.05-0.5 m diameter) clasts of porphyritic lava Pale grey in colour	Massive limestone with clast- and matrix-supported clasts of porphyritic lava Sharp to erosive base and sharp top	0.2-2 m bed thickness Sheet geometry	Body fossils bivalves, brachiopods, gastropods, belemnites, oysters, solitary corals and rare ammonite fragments	High-energy shallow-marine limestone reworking underlying lava
Bioclastic limestone facies (Shoreface limestone facies association)	Sparry limestone Pale grey in colour	Massive Sharp to erosive base and sharp top	0.2-2 m bed thickness Sheet geometry	Body fossils bivalves, brachiopods, gastropods, belemnites, oysters, solitary corals and rare ammonite fragments	High-energy shallow-marine limestone
Oolitic limestone facies (Shoreface limestone facies association)	Sparry limestone Pale grey in colour	Trough and planar-tabular cross-bedding (scale 0.1-0.3 m) Symmetric ripples (wavelength 0.05-0.1 m, amplitude 0.01-0.015 m) Wavy lamination Parallel lamination Sharp bounding surfaces	0.2-2 m bed thickness Sheet geometry	Body fossils Abundant oolites, bivalves, gastropods, brachiopods, belemnites	High-energy shallow-marine limestone

Coarse-grained calcareous sandstone facies (Shoreface limestone facies association)	Coarse-grained calcareous sandstone Grey in colour	Trough and planar-tabular cross-bedding (scale 0.1-0.3 m) Symmetric ripples (wavelength 0.05-0.1 m, amplitude 0.01-0.015 m) Wavy lamination Parallel lamination Sharp bounding surfaces	0.5-2 m bed thickness Sheet geometry	No evidence of body or trace fossils	High-energy sandy platform sandstone with very low mudstone content
Brown limestone (Shoreface limestone facies association)	Medium-grained grainstone limestone Brown in colour when weathered and pale grey on a fresh surface	Wavy lamination Parallel lamination Sharp bounding surfaces	1-2 m bed thickness Sheet geometry	Body fossils Abundant bivalves and brachiopods	High-energy sandy platform limestone with very low mudstone content
Grey limestone (Shoreface limestone facies association)	Fine-grained packstone to wackestone limestone Grey in colour when weathered and dark grey on a fresh surface	Wavy lamination Parallel lamination Sharp bounding surfaces	1-2 m bed thickness Sheet geometry	Body fossils Abundant bivalves and brachiopods	Low-energy platform limestone with mudstone content
Grainstone limestone facies (Shoreface limestone facies association)	Fine- to coarse-grained grainstone limestone Pale grey / yellow in colour	Normal grading Well sorted Well rounded Clean (mud-free) Hummocky- and swaley-cross-stratification Symmetric ripples (wavelength 0.05-0.1 m, amplitude 0.01-0.015 m) Wavy lamination Parallel lamination Bounding surfaces are sharp to erosive	Limestone beds range from 0.1-0.8 m with a distinctive sheet geometry The lower bounding surface has a distinctive wavy form while the upper bounding surface is flat or wavy	Body fossils Ammonites, bivalves, gastropods, brachiopods, belemnites Trace fossils Skolithos, ophiomorpha, diplocraterion, thalassinoides, arenicolites, palaeophycus, rhizocorallium, teichichnus, cruziana, planolites, chondrites	High-energy grainstone deposited during a single storm event
Wackestone limestone facies (Shoreface limestone facies association)	Medium-grained wackestone limestone Pale grey /yellow in colour	Massive Rare parallel lamination Gradational base and top	Wackestone beds range from 0.1-0.8 m with a distinctive sheet geometry	Body fossils Ammonites, bivalves, gastropods, brachiopods, belemnites Trace fossils Heavy bioturbation similar to that seen in the interbedded grainstone limestone facies but the preservation potential is markedly less	Low-energy wackestone deposited during fairweather periods between storm events
Offshore carbonate mudstone facies association					
Fine-grained packstone facies (Offshore carbonate mudstone facies association)	Fine- to medium-grained packstone Pale grey /yellow in colour	Massive Rare parallel or wavy lamination Sharp base and top	Packstone beds range from 0.1-0.5 m thick with a distinctive sheet geometry	Body fossils Ammonites, bivalves	Packstone deposited during major storm or by distal turbidity current
Calcareous mudstone facies (Offshore carbonate mudstone facies association)	Medium-grained calcareous mudstone Pale grey /yellow in colour	Massive Rare parallel lamination Gradational base and top	Mudstone beds range from 1-10 m thick with a distinctive sheet geometry	Body fossils Ammonites, bivalves Trace fossils Rare bioturbation but difficult to identify due to weathering	Low-energy mudstone deposition in a fully marine oxygenated environment
Calcareous concretion facies (Offshore carbonate mudstone facies association)	Medium-grained calcareous mudstone with abundant calcareous concretions Mudstone is pale grey /yellow in colour with grey concretions	Massive Rare parallel lamination Internally the concretions are massive or with a poor spherical lamination Gradational base and top	Concretion beds range from 0.1-1 m with a distinctive sheet geometry Concretions range from 0.01-1 m in diameter	Body fossils Abundant ammonites and bivalves preserved within the concretions Trace fossils No preserved evidence of trace fossils	Low-energy mudstone deposition in a fully marine oxygenated environment The concretions may indicate periods of reduced rates of sedimentation

Anoxic black shale (Offshore carbonate mudstone facies association)	Very fine- to fine-grained calcareous mudstone Black in colour	Massive Rare parallel lamination Gradational base and top	Mudstone beds range from 1-10 m with a distinctive sheet geometry	<u>Body fossils</u> Ammonites, bivalves <u>Trace fossils</u> None noted	Low-energy siltstone deposition in a fully marine anoxic environment
Black micritic limestone facies (Offshore carbonate mudstone facies association)	Very fine- to fine-grained micritic limestone Black in colour	Massive Rare parallel lamination Gradational base and top	Limestone beds range from 1-10 m with a distinctive sheet geometry	<u>Body fossils</u> Ammonites, bivalves <u>Trace fossils</u> None noted	Low-energy limestone deposition in a fully marine anoxic environment
<i>Subaqueous evaporite facies association</i>					
Massive evaporite facies (Subaqueous evaporite facies association)	Fine- to medium grained gypsum and anhydrite White in colour	Massive	Evaporite beds range from 1-10 m with a sheet geometry	None	Subaqueous marine evaporites deposited in a hypersaline environment

4.6 Shallow-marine carbonate rimmed-shelf facies description

In the Norian/Rhaetian (Late Triassic) and Bajocian (Middle Jurassic) thin coral reefs developed in the Domeyko basin (Prinz, 1991). The Norian/Rhaetian coral reefs are restricted to the initial marine transgression between 23.5°-25°S where they are closely associated with, and overlie fan-delta deposits (Fig. 4.7). Subsequent Bajocian coral reefs are widespread in the Domeyko basin and are particularly well developed during the Early Bajocian marine transgression in the Cerro Jaspe area (21.5°-22°S), where they are again closely associated with fan-delta deposits (Fig. 4.8). Thin coral reef facies are intercalated with the fan-delta conglomerates and have been previously described as one of the facies composing the fan-delta facies association (Table 4.1). However, the thicker reefs and in particular those capping the fan-delta conglomerates are deposited under fully marine conditions, and hence are considered separately.

4.6.1 Carbonate reef facies association

Description

The pale grey framework coral reef facies is composed of abundant reef-building corals, mainly *Thecosmilia*, with associated solitary corals, bivalve, brachiopod and rare ammonite fossils, described by Chong (1973) (Table 4.4). Without exception, these corals are hermatypic forms, commonly preserved in-situ, life position and constitute a framework reefal carbonate, displaying both patch and fringing geometries (Prinz, 1991) (Fig. 4.36). The reefs range from 1-30 m in thickness with sharp lower and upper bounding surfaces (Fig. 4.36). The fringing reefs seen at Quebrada Corallas occur in a unique depositional setting which has not been previously described from northern Chile (G. Chong pers. comm., 1994). These 0.5-3 m thick framework coral limestones are intercalated with 3-30 m thick units of sub-aqueously deposited volcanic ash facies (Section 4.7.2). The limestones are light to medium grey in colour and fine- to medium-grained, composed almost exclusively of massive, interlocking framework corals in life position. The limestones rest on a relatively flat substrate of fine- to very fine-grained volcanic ash, while the top of the limestone is flat marking an abrupt transition back to fine-grained volcanic ash. The top surface of the limestone shows the draping of the overlying ash onto and between individual corals. The bioclastic limestone facies is principally composed of bivalves and brachiopods with gastropods, belemnites and conodonts forming distinctive mounded geometries, seen at East Portezuelo de la Sal (Table 4.4, Fig. 4.36). The bioclastic mounds are 10-30 m in diameter and have been heavily dolomitized making detailed study more difficult (Chong, 1973) (Fig. 4.36). Between the bioclastic mounds are draped intra-mound heterolithic sediments of thinly interbedded micritic limestone and calcareous mudstone facies (Table 4.4). Beds of the pale grey to yellow micritic limestone facies are 0.05-0.2 m in thickness with a sheet geometry and wavy or parallel lamination, while the interbedded medium-grained calcareous mudstone facies display parallel lamination.

Interpretation

The framework coral reef facies is predominately composed of large reef-building corals in life position and hence is interpreted to represent a shallow-marine carbonate reef displaying both patch and fringing geometries (Fig. 4.36). The corals are exclusively hermatypic forms, whose appearance is not only dependant on a warm climate and the possibility of a supply of larvae, but also from the palaeogeographical features of the Mesozoic Domeyko basin, as discussed by Prinz (1991). Such reef facies are indicative of negligible siliciclastic sediment input and shallow-water conditions of less than 10 m water-depth. The upper surface of the coral reef facies is commonly draped with fine-grained offshore siltstone facies or in the case of Quebrada Corralas, volcanic ash facies, indicating that the drowning of the reef was a rapid event. The bioclastic limestone facies is interpreted as a shallow-marine shell mound on the basis of the abundant bivalve and brachiopod fauna, lack of mud-grade material and characteristic mounded geometry (Fig. 4.36). The interbedded micritic limestone and calcareous mudstone facies are interpreted as lower-energy shallow-marine deposits which occur between and are temporally equivalent to the bioclastic limestone facies, at least at East Portezuelo de la Sal (Fig. 1.1, Locality 52).

4.6.2 Shallow-marine carbonate rimmed-shelf facies model

The coral reef facies association is restricted within the Domeyko basin and does not provide enough information to develop an integrated rimmed-shelf facies model. Instead, a depositional environment is presented for the coral reefs taking into account their close association with fan-delta facies (Fig. 4.37). The prominent depositional setting in the Domeyko basin was a carbonate ramp margin as previously described (Aberhan, 1993a; 1993b), with only limited occurrences of coral reefs (Prinz, 1991). Further more specialised fringing reefs are seen at Quebrada Corralas where they are interbedded with subaqueous volcanic ash and are included in the volcanic facies model (Fig. 4.38).

Figure 4.35 Schematic representation of the Domeyko basin carbonate reef-margin facies and facies associations in northern Chile based on lithology and grain-size, sedimentary structures, body and trace fossils and bounding surface character. Based on the standard facies belts proposed by Wilson (1974).

Lithology	Graphic log	Facies & terrigenous clastic component	Facies association	Depositional environment	Lithology, colour & grain type	Sedimentary structures	Body and trace fossils	Bounding surfaces & architectural elements	Schematic representation of architectural elements
		(a) Nodular anhydrite and dolomite on salt flats (b) Laminated evaporites in desiccated ponds Terrigenous interbeds	Platform (sabkha) evaporites	Tidal flat	Irregularly laminated dolomite and anhydrite locally may grade into redbeds Red, yellow, brown in colour	Anhydrite after gypsum nodular rosettes, "chicken wire" and blades, irregular lamination, caliche	Stromatolitic algae almost the only indigenous biota	Amalgamated sheet geometry evaporites & clastics	
		(a) Bioclastic wackestone; lagoons (b) Litho-bioclastic sand in tidal channels (c) Lime mud on tidal flats (d) Fine-grained terrigenous clastic interbeds	Restricted lagoonal limestones	Lagoon	Often dolomite and dolomitic limestone, light coloured Clotted pelleted mudstone and grainstone; laminated mudstone; coarser wackestones in channels	Birdseye, stromatolites, fine laminations, dolomite crusts Cross-bedded sand in channels	Limited fauna Mostly grazing gastropods, algae and ostracods	Amalgamated sheet geometry limestones	
		(a) Lime sand bodies (b) Wackestone-mudstone areas, bioherms (c) Areas of terrigenous clastics Terrigenous and calcareous beds, well segregated	Open platform	Reef-margin parasequence	Variable carbonates and terrigenous clastics Dark to light in colour Variable textures in grainstone and mudstone Bioturbation	Intense bioturbation	Bivalves, gastropods sponges, less tolerant groups restricted (eg. cephalopods, brachiopods and echinoderms)	Amalgamated sheet geometry limestones	
		(a) Shoal lime sands Local quartz sand	Oolitic sands		Calcarenite - oolitic lime sand or dolomite Light coloured Grainstones, well sorted, rounded	Medium to large scale cross-bedding	Few indigenous organisms, specialised community, shell debris from other platform environments	Landward or basinward inclined (shallow dip) sandstones & limestones	
		(a) Boundstone (b) Encrusting masses (c) Bafflestone No terrigenous clastic component	Reef		Massive limestone dolomite Light coloured Boundstones and pockets of grainstone, packstones	Massive organic structure or open framework with roofed cavities Injection dykes Sometimes stromatolites	Major frame building colonies and communities associated with them	Mounded reef	
		(a) Bedded fine-grained sediments with slumps (b) Foreset debris and lime sands (c) Lime mud masses Some shales and silts	Foreslope		Variable depending upon water turbulence upslope. Sedimentary breccias and lime sands Dark to light in colour Limesilt and bioclastic wackestone, packstone, lithoclasts	Slumps, foreset bedding, slope build-ups, exotic blocks	Colonies of whole fossil organisms and bioclastic debris	Basinward dipping talus deposits	
		Some shales, silt and fine-grained sandstone	Toe of slope carbonates		Fine-grained limestone, locally cherty. Dark to light in colour Dominately lime mudstone with some calcisiltites	Minor lamination. Often massive beds, lenses of graded sediment. Lithoclasts and exotic blocks	Bioclastic debris derived mostly from upslope	Shallowly inclined, basinward dipping sheet geometry limestones	
		(a) Carbonates (b) Shale Quartz silt and shale in well segregated beds	Open marine neritic		Very fossiliferous limestone with marl interbeds Grey, green, red, brown Bioclastic and whole fossil wackestones, some calcisiltites	Bioturbated, thin to medium bedded with nodule layers	Diverse. Shelly fauna and trace fossils represent both infauna and epifauna	Fine-grained marls interbedded with sheet geometry limestones which thicken and become more frequent upwards	
		(a) Fine clastics (b) Carbonates (c) Evaporites Quartz silt and shale, fine-grained siltstone, often cherty	Basin (anoxic or evaporitic)		Dark shale or silt, thin limestones (starved basin). Evaporites fill basin if desiccation occurs. Dark brown, black and red. Lime mudstones, fine calcisiltites	Very even lamination on mm scale. Rhythmic bedding; occasional ripple cross-lamination	Planktonic and nektonic only. Occasional mass-mortality deposits	Black shales with intercalated rare, thin, sheet geometry limestones	

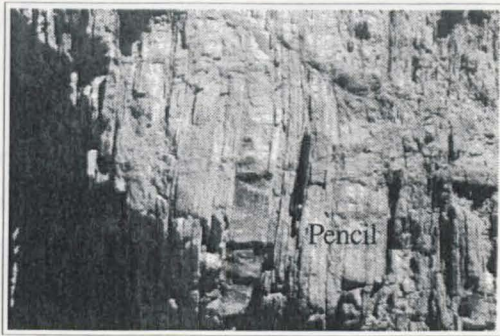


Figure 4.36 *Photograph A* shows a 30 m thick Rhaetian (Upper Triassic) fringing reef overlying fan-delta conglomerates at Punta del Viento (Figure 4.7). The reef at the top of photograph is predominately composed of the reef-building coral *Thecosmilia*. *Photograph B* shows an along strike view of the Upper Triassic mounded shelly limestone facies at East Portezuelo de la Sal (Figure 1.1, Locality 52).

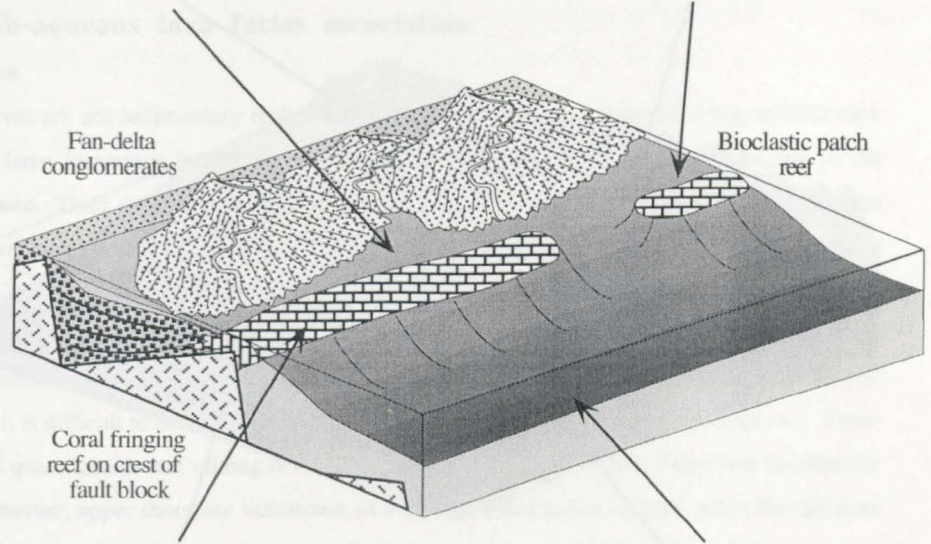
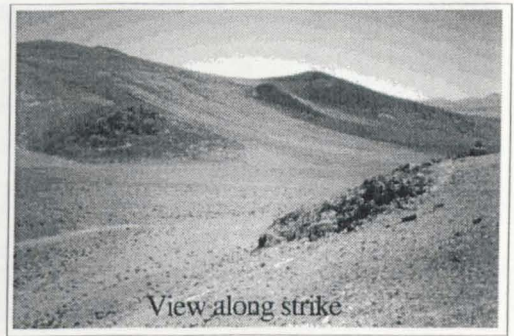
4.7 Volcanic and Volcaniclastic facies description

The shallow-marine carbonate reef-margin facies model is constructed from an analysis of temporally and spatially distinct reef facies which have been integrated to display the different reef geometries seen in the Domeyko basin succession.

Lagoonal limestones



Shelly mounds



Fringing Reef

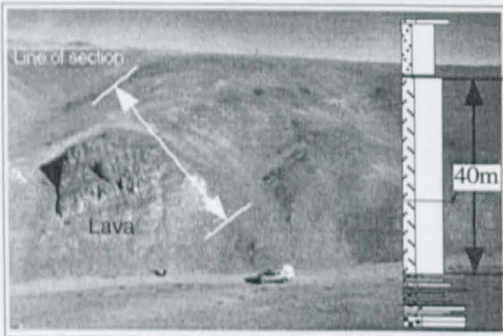


Calcareous siltstones

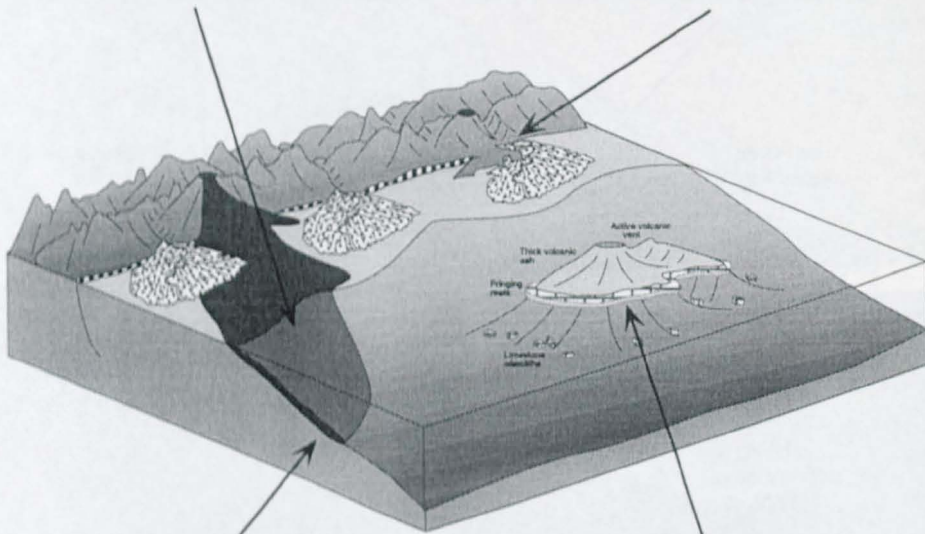
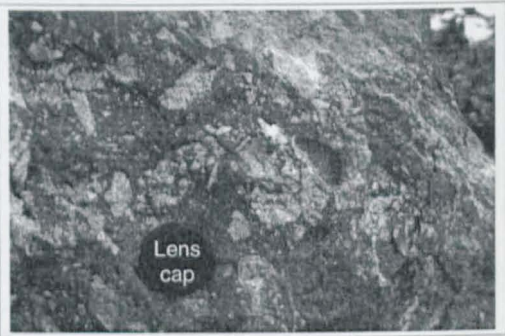


Figure 4.37 The shallow-marine carbonate reef-margin facies model is constructed from an analysis of temporally and spatially distinct reef facies which have been integrated to display the different reef geometries seen in the Domeyko basin succession.

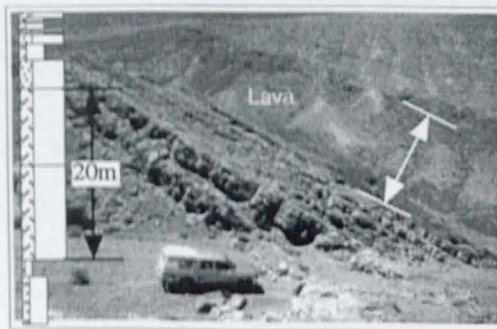
Submarine lava



Volcaniclastic breccia



Sub-marine lava



Fringing reef



Figure 4.38

Volcanic and volcaniclastic deposits and their depositional setting.

4.7 Volcanic and Volcaniclastic facies description

The Mesozoic volcanic-related deposits of northern Chile are widespread, but their origin is poorly understood. The majority of the Permo-Triassic syn-rift volcanics are rhyolitic and andesitic in origin, while the Coastal Cordillera preserves a large proportion of the andesitic Jurassic volcanic arc. This section only considers the volcanic rocks which have a direct influence on the Mesozoic marine basin-fill. Although the volcanic deposits are markedly different to the dominant mixed carbonate/clastic component, they are critical when considering depositional environments and basin evolution. The example from Quebrada Corallas (Fig. 1.1, Locality 15) presents a unique depositional environment where framework carbonate reef facies are interbedded with subaqueous volcanic ash facies, only observed at this locality in northern Chile (G. Chong pers. comm., 1994).

4.7.1 Sub-aqueous lava facies association

Description

Although lavas are not sedimentary rocks, they represent part of the preserved stratigraphical rock record and have important implications for the surrounding depositional environments in the Domeyko basin. Thick units of lava, ranging from 10-50 m, are found in the Lower Bajocian marine rocks of Cerro Jaspe (Fernandez-Lopez *et al. in press*) and Lower Cretaceous marine rocks of Quebrada La Carreta. The lavas are typically very fine-grained to glassy and dark green to grey in colour, with plagioclase phenocrysts. They are always heavily weathered at the surface and have commonly undergone partial alteration and replacement of the feldspar component. Due to the heavy degree of degradation it is difficult to positively identify any internal cooling structures, such as pillows. There are abundant quartz geoids and veining in the Cerro Jaspe example. The Cerro Jaspe lava lies directly on shallow-marine, upper shoreface sandstones (4.4.2) with a thin baked contact, while the unbaked top surface has a small degree of topography (0.1-0.2 m) and is overlain by similar shallow-marine sandstones (Fig. 4.23). The age of the lava is Early Bajocian, based on ammonites from the underlying and overlying marine strata (Fernandez-Lopez *et al. in press*). This particular lava unit ranges from 30-50 m in thickness and can be traced laterally for 25 kilometres (Fig. 4.23). The lava at Quebrada La Carreta is Early Cretaceous in age and lies within offshore marine siltstone facies. The lava has a marked topography of several metres on the top surface and lateral variations in thickness.

Interpretation

The presence of poorly preserved pillow structures, a glassy texture, bedding concordance, and transgressive nature and reworking into the overlying marine rocks implies that the volcanic units are subaqueous lavas, as opposed to intrusive volcanic rocks. The lava at Cerro Jaspe appears to have been erupted into a much shallower marine environment on the basis of the surrounding shoreface

sandstones as opposed to offshore siltstones, supported by a high degree of shallow-marine erosion and reworking of the lava top (Fig. 4.23).

4.7.2 Sub-aqueous volcanic ash facies association

Description

The Quebrada Corallas section consists of 0.5-3 m thick framework coral limestones facies intercalated with 3-30 m thick units of volcanic ash. The poorly consolidated, very fine- to medium-grained ash is white in colour and internally homogeneous. There are rare ammonites preserved within the ash and these tend to be more frequent in the first few metres overlying a framework coral limestone. Although there are few internal structures the overall bedding is defined by 0.05-0.2 m thick horizons of well cemented ash. Within several of the ash horizons there are large blocks and rafts of framework coral limestone, ranging in size from 0.5-3 m in diameter. These olistoliths are randomly orientated relative to the growth direction of the constituent corals.

Interpretation

The volcanic ashes are interpreted as fully marine, sub-aqueous suspension deposits on the basis of their close association with framework coral limestones and the presence of ammonite fauna. A shallow-marine origin is indicated by the coral assemblage and fringing geometry of the reefs (4.6.1). The accretion geometry of the reefs is progradational and the presence of olistostromes is interpreted to indicate a relatively steep margin. These criteria, along with the thickness of the ash units points to the close proximity of an active volcanic vent.

4.7.3 Volcaniclastic breccia facies association

Description

The volcaniclastic breccia facies association is restricted to the area of Sierra Candeleros (Fig. 1.1, Locality 62). This section is composed of interbedded limestone and calcareous siltstone facies and framework coral limestone facies of Early Cretaceous age, which are overlain by a thick unit of volcaniclastic breccia. The breccia is both matrix- and clast-supported, with angular to very angular clasts ranging in size from 0.01-1 m in diameter. The clasts are almost exclusively porphyritic volcanic (95%) in origin, with rare reworked clasts of the underlying limestone (<5%). The matrix is composed of an immature medium- to coarse-grained sandstone with no internal structures. There is no apparent preferred clast imbrication or orientation within the breccia.

Interpretation

The breccia is interpreted as being very proximal, from the highly angular clasts and immature sandstone matrix. The process of deposition is by debris flow, indicated by the matrix-supported horizons and large range in clast sizes (Fig. 4.5). This is supported by the lack of clast imbrication or orientation, also indicative of a debris flow mechanism (Fig. 4.5). The deposit is not a primary

pyroclastic flow based on the absence of any welding within the matrix and the large amount of immature matrix sandstone interpreted to be a debris flow mechanism.

4.7.4 Volcanic and volcanoclastic facies model

The volcanic and volcanoclastic deposits of northern Chile do not represent a genetically-linked series of depositional environments (Fig. 4.38). Instead, they highlight localised occurrences within the mixed carbonate/clastic marine system. Although the separate volcanic and volcanoclastic facies associations cannot be linked at this level, we can consider their individual interaction and effects on the surrounding depositional environments (Fig. 4.38).

4.8 Summary

The Upper Triassic to Lower Cretaceous Domeyko basin-fill comprises a highly diverse sedimentary succession including continental clastic, mixed carbonate and siliciclastic marine and evaporite deposits. The subsequent integration of these facies units has allowed the development of depositional models for each environment, based on an amalgamation of temporally and spatially distinct facies and facies associations. The majority of the mixed carbonate and siliciclastic marine basin-fill is interpreted to have been deposited in a ramp-type setting. Stratal architecture appears to be predominantly controlled by siliciclastic sediment input, basin-margin morphology and rate of relative sea-level change. The distal offshore facies of the mixed carbonate and siliciclastic ramp are dominated by carbonate mudstones, while further up-dip siliciclastic sediment input resulted in sandy shoreface facies. Reef-building coral facies are both temporally and spatially restricted in the Domeyko basin as a result of cool water conditions and a lack of suitable substrate. The marine deposits record an almost complete ammonite biochronology indicating open marine connection, with only a minor input of volcanic material from the Jurassic volcanic arc to the west.

Table 4.4 Summary facies table describing all the shallow-marine carbonate rimmed-shelf and volcanigenic lithofacies found in northern Chile in terms of lithology and grain-size, sedimentary structures and bounding surfaces, thickness and geometry, and body and trace fossils, followed by a process interpretation.

Shallow-marine carbonate rimmed-shelf environment

Facies and Facies Association	Lithology and Grain Size	Structures and Bounding Surfaces	Thickness and Geometry	Body and Trace Fossils	Process Interpretation
Framework coral reef facies (Carbonate reef facies association)	Sparry limestone Pale grey in colour	No evidence of sedimentary structures Sharp bounding surfaces	1-30 m bed thickness Sheet (fringing) and lens (patch) geometries	Body fossils Major frame building corals (colonial and solitary), bivalves, gastropods, brachiopods, belemnites, conodonts	Major shallow-marine reefal limestones deposited during periods of low clastic input
Bioclastic limestone facies (Carbonate reef facies association)	Sparry limestone Pale grey in colour	No evidence of sedimentary structures Sharp bounding surfaces	1-30 m bed thickness Mounded geometry	Body fossils Abundant bivalves and brachiopods with gastropods, belemnites and conodonts	Major shallow-marine bioclastic limestone mounds deposited during periods of low clastic input
Thinly bedded micritic limestone facies (Carbonate reef facies association)	Micritic limestone Pale grey to yellow in colour	Wavy or parallel lamination Sharp bounding surfaces	0.05-0.2 m bed thickness Sheet geometry	Body fossils solitary corals, bivalves, gastropods, brachiopods, belemnites	Shallow-marine carbonate deposition in inter-reef areas
Medium-grained calcareous mudstone facies (Carbonate reef facies association)	Medium-grained calcareous mudstone Pale grey to yellow in colour	Parallel lamination Sharp bounding surfaces	0.05-0.2 m bed thickness Sheet geometry	Body fossils solitary corals, bivalves, gastropods, brachiopods, belemnites	Shallow-marine carbonate deposition in inter-reef areas

Volcanic environment

Facies and Facies Association	Lithology and Grain Size	Structures and Bounding Surfaces	Thickness and Geometry	Body and Trace Fossils	Process Interpretation
<i>Sub-aqueous lava facies association</i>					
Lava facies (Sub-aqueous lava facies association)	Very fine-grained to glassy vesicular lava Dark green / grey in colour	Plagioclase phenocrysts Vesicles and quartz filled amygdalae Quartz geoids and veining Possible pillow structures Sharp bounding surfaces	10-50 m in thickness Sheet geometry	None	Shallow-marine subaqueous lava
<i>Sub-aqueous volcanic ash facies association</i>					
Fine-grained volcanic ash facies (Sub-aqueous volcanic ash facies association)	Fine-grained volcanic ash White in colour	Massive In the thin ash units there are 0.5-1 m limestone olistoliths Sharp lower bounding surface with sharp or gradational upper bounding surface	1-40 m in thickness Sheet geometry	Rare ammonites	Shallow-marine volcanic ash
<i>Volcaniclastic breccia facies association</i>					
Volcaniclastic breccia facies (Volcaniclastic breccia facies association)	Volcaniclastic breccia Dark green / grey in colour	Matrix- and clast-supported Clast-size ranges from 0.01-1 m Very poor grading Very poor sorting Highly angular clasts	1-10 m in thickness Sheet geometry	None	High-energy volcanic breccia deposit deposited by a cohesive debris flow mechanism

Chapter 5

Sequence Stratigraphy

5.1 Objectives of chapter

The principal objective of this chapter is to use sedimentary logging and detailed facies analysis to define sequence stratigraphical surfaces and stratal packages, thus allowing the interpretation and prediction of sedimentary facies development through time. Such changes in sedimentary facies through time are interpreted to be driven by changes in accommodation space and hence relative sea-level, thus permitting an analysis of Jurassic relative sea-level change for the Domeyko basin.

Firstly, the published lithostratigraphical subdivision for the Domeyko basin has been reviewed. Subsequently, the methodology and application of sequence stratigraphical concepts is presented, followed by the characterisation of significant surfaces (sequence boundaries and flooding surfaces). These concepts are then applied to the Domeyko basin succession and the principal second-order sequences are discussed. Finally, several examples of higher frequency sequences are presented and characterised on the basis of their position within the lower-frequency, longer-duration second-order cycles.

5.2 Lithostratigraphy

The lithostratigraphical units for the Mesozoic deposits of northern Chile are summarised in Fig. 5.1 (Ramirez & Gardeweg, 1982; Marinovic & Lahsen, 1984; Naranjo & Puig, 1984). Several authors have described particular Jurassic sections (Harrington, 1961; Perez & Levi, 1961; Garcia, 1967; Chong, 1973; Moraga *et al.*, 1974; Montano, 1976; Chong, 1977; Ramirez & Gardeweg, 1982; Marinovic & Lahsen, 1984; Bogdanic, 1990) and the Jurassic stratigraphy was subsequently summarised by Ramirez & Gardeweg (1982); Marinovic & Lahsen (1984) and Naranjo & Puig (1984) during production of the regional geological maps of northern Chile.

Lithostratigraphical approaches to correlation and basin analysis inherently suffer from the problem of diachroneity of facies and hence the formations lack chronostratigraphical significance. The Domeyko basin succession is characterised by the widespread occurrence of time-transgressive facies units, some of which range from Late Triassic to the Late Bajocian. However, the Millonaria Formation constitutes a regionally mappable lithostratigraphical unit (evaporite facies) which probably also has chronostratigraphical significance; where dated it is always developed between the Bimammatum-Acanthicum Zones of the Oxfordian-Kimmeridgian (Marinovic & Lahsen, 1984) (Fig. 5.1). A sequence stratigraphical approach has been adopted in order to allow a chronostratigraphical analysis of the Domeyko basin succession.

5.3 Sequence stratigraphical concepts

5.3.1 Introduction and historical development of sequence stratigraphy

In addition to sedimentary logging and detailed facies analysis (Chapter 4), the methods and concepts of sequence stratigraphy were critically tested in this back-arc basin setting. Sequence stratigraphy is a multidisciplinary tool for the interpretation and prediction of sedimentary facies through time, thus allowing an analysis of depositional history. The technique is based around the identification and

correlation of key surfaces of chronostratigraphical significance and the characterisation of the intervening stratal packages. Traditionally, sequence stratigraphical studies have been concentrated in passive margin or foreland basin settings (eg. Posamentier & Vail, 1988; Van Wagoner *et al.*, 1990; 1991). This study applies sequence stratigraphical concepts to a back-arc basin. The Mesozoic deposits of northern Chile comprise of siliciclastic, carbonate, evaporite, fluvial and volcanoclastic facies, thus allowing the testing of current sequence stratigraphical models in a variety of depositional environments.

In 1948 Sloss correlated unconformity bounded sequences of several million years duration across the North American craton (Sloss *et al.*, 1949; Sloss, 1950; 1963). Subsequently, a series of papers by Exxon staff, published in A.A.P.G. Memoir 26 (Payton, 1977), refined the approach of correlating unconformity bounded sequences using seismic data from passive margin settings, thus introducing the term "seismic stratigraphy". Seismic stratigraphy uses seismic reflections which are thought to represent time stratigraphical surfaces, as opposed to lithostratigraphical surfaces. Thus, a reflector may pass laterally from a sand into a shale. The characterisation of reflector terminations on the basis of onlap, downlap and truncation allows the delineation of large-scale depositional sequences, bounded by regional unconformities or sequence boundaries (Vail *et al.*, 1977b). Seismic stratigraphy allowed the recognition of typically third-order sequences (0.5-5 Ma), from which systems tracts, the primary building blocks of the sequence were defined. Seismic stratigraphy divides seismic data into genetic units, while seismic facies analysis describes those units. Sangree & Widmier (1977) introduced the procedure termed seismic facies analysis, allowing the interpretation of depositional facies from seismic reflection data. Seismic facies analysis involves the delineation and interpretation of reflection geometry, continuity, amplitude, frequency and interval velocity, as well as the external form and three-dimensional associations of groups of reflections.

Coastal onlap is generally inferred from seismic data as the landward onlap of topset reflections, where these are assumed or demonstrated to represent littoral, paralic or coastal non-marine deposits (Mitchum, 1977). Usage by the Exxon school extends the term to onlap of reflections landward of the offlap break. These topset deposits are assumed to have accumulated close to sea-level and patterns of coastal onlap with respect to the onlapped surface, indicate changes in relative sea-level. Relative sea-level was defined by Mitchum (1977) as, "an apparent rise or fall of sea-level with respect to the land surface as a result of changes in eustatic sea-level and movements (uplift or subsidence) of a pre-existing datum horizon in the underlying sediment pile, whereby a relative change may be operative on a local, regional or global scale" (Fig. 5.2). Coastal encroachment, for example, results from rising relative sea-level, while a basinward shift in coastal onlap results from a fall in relative sea-level. Changes in relative sea-level are measured on seismic data from shifting patterns of coastal onlap (Mitchum, 1977) and, in the rock record, from trace displacement (Bertram & Milton, 1990). A rise in relative sea-level causes coastal encroachment, which may or may not be accompanied by transgression, while a fall in relative sea-level at the basin margin causes a sequence boundary, usually with truncation of reflectors. At this time, the Exxon school made the assumption that sequences were developed due to sea-level changes, linked to a globally synchronous, glacially-moderated eustatic

Group	Formation	Description	Age Range
Chacarilla Group	Chacarilla Formation (Western Sequence of Bogdanic, 1990)	Red alluvial conglomerates & fluvial sandstones, all of continental origin	Early Cretaceous
	Sierra San Lorenzo Beds (1125m) (Marinovic & Lahsen, 1984)	Red conglomerates & coarse-grained sandstones, probably of continental origin	Kimmeridgian-Tithonian
Caracoles Group	Santa Ana Formation (Naranjo & Puig, 1984)	Marine & continental sediments with intercalated andesitic lavas	Early-Late Cretaceous
	Honda Formation (170m) (Ramirez & Gardeweg, 1982)	Calcarenites (pellets, pisoliths & extraclasts) Interpreted as lagoonal limestones	Oxfordian-Kimmeridgian
	Millonaria Formation (30m) (Marinovic & Lahsen, 1984)	Gypsum (Garcia, 1967)	Early Kimmeridgian
	Doralisa Formation (260m) (Marinovic & Lahsen, 1984)	Grey / yellow siltstones with intercalated grey limestones (Garcia, 1967; Montano, 1976)	Oxfordian-Early Kimmeridgian
	Caracoles Formation (150m) (Marinovic & Lahsen, 1984)	Grey calcarenites & calcareous siltstones containing calcareous concretions (Ramirez & Gardeweg, 1982)	Callovian
	Torcasas Formation (210m) (Ramirez & Gardeweg, 1982)	Grey basal conglomerate of volcanic clasts with sandy matrix & sparry cement; grey calcareous sandstones	Middle-Late Bajocian
	Candeleros Formation (Naranjo & Puig, 1984)	<u>Member 1</u> (lower) Andesitic lavas with intercalations of tuffs & limestones <u>Member 2</u> (middle) Fossiliferous limestones with intercalations of andesitic lavas <u>Member 3</u> (upper) Andesitic lavas with fossiliferous calcareous interbeds, locally interfingering with Member 2	Bajocian-Kimmeridgian
	Moctezuma Formation (Marinovic & Lahsen, 1984)	Grey basal conglomerate of volcanic & plutonic clasts with sandy matrix & calcareous cement; grey calcareous sandstones; grey limestone (Perez & Levi, 1961)	Middle Sinemurian-Early Toarcian
	La Negra Formation (Garcia, 1967)	Andesitic volcanics with intercalated marine sediments	Early-Late Jurassic
	Posada de los Hidalgo Formation (Garcia, 1967)	Fossiliferous marine sediments & lavas	Early Sinemurian
	Pan de Azucar Formation (Naranjo, 1978)	Pyroclastic & sedimentary, fossiliferous marine rocks	Hettangian-Early Sinemurian
Profeta Formation (Chong, 1973a)	Marine carbonate rocks with tuffaceous intercalations in the upper part	Hettangian-Kimmeridgian	

Figure 5.1 The pre-existing lithostratigraphy for the Mesozoic deposits of northern Chile (Ramirez & Gardeweg 1982; Marinovic & Lahsen 1984 and Naranjo & Puig 1984). Several authors defined particular parts of the Jurassic stratigraphy (Perez & Levi 1961; Garcia 1967; Chong 1973; Moraga *et al.* 1974; Montano 1976; Ramirez & Gardeweg 1982; Marinovic & Lahsen 1984; Bogdanic 1990) which were subsequently amalgamated by Ramirez & Gardeweg (1982); Marinovic & Lahsen (1984) and Naranjo & Puig (1984) during their production of the regional geological maps of Northern Chile. The interval studied in this thesis is highlighted in grey.

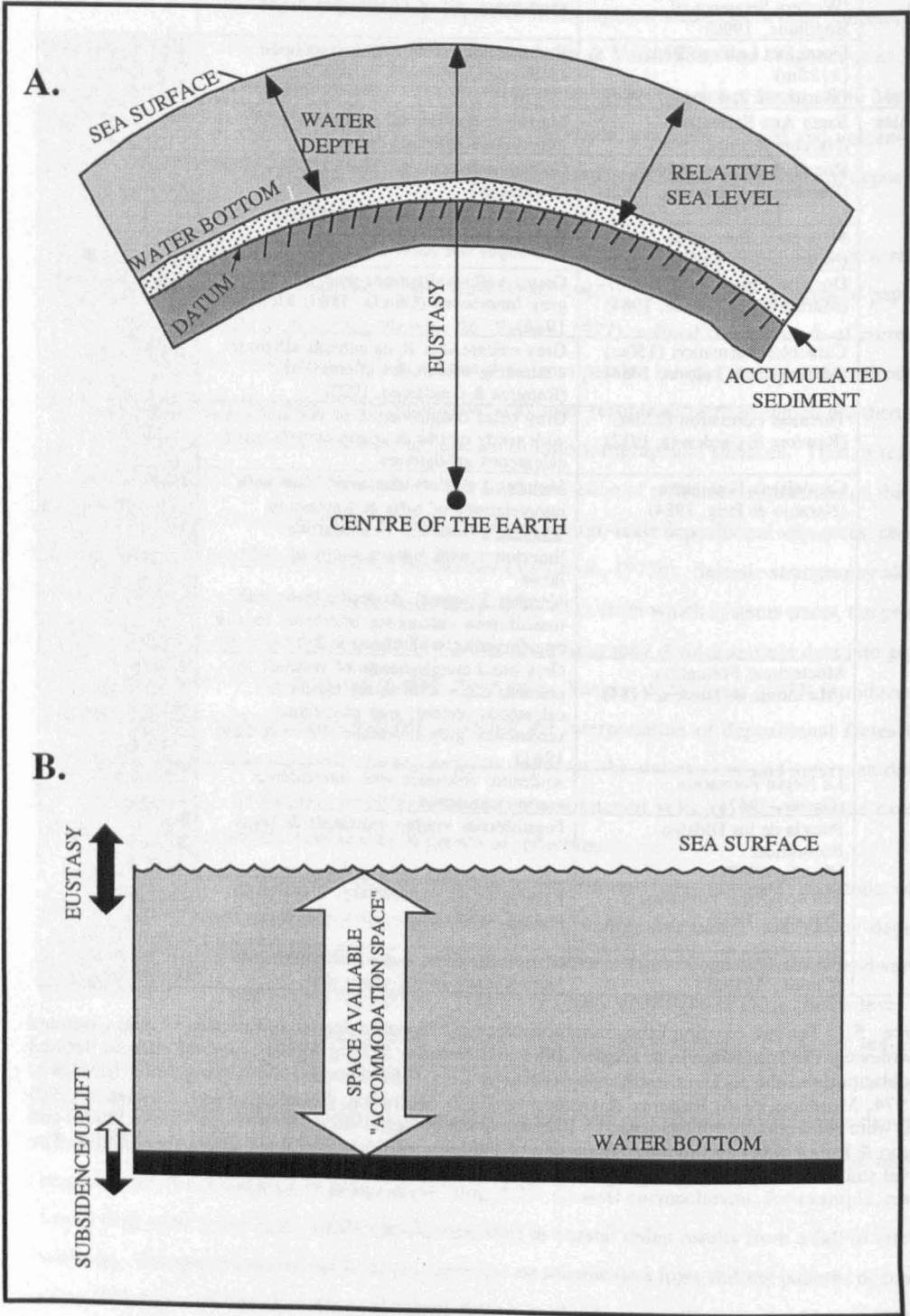


Figure 5.2 The principles of eustasy, relative sea-level and water-depth (Part A) with respect to accommodation space (Part B) (Posamentier et. al., 1988).

sea-level curve (Fig. 5.3). An assumption which led to the publication of the Vail *et al.* (1977b) and Haq *et al.* (1988) "global eustatic cycle charts" (Fig. 5.3). Subsequently, two opposing schools of thought emerged, the Exxon and Galloway methods of sequence stratigraphical analysis, based on the relative importance of key stratigraphical surfaces.

Exxon method of sequence stratigraphical analysis

The original definitions and concepts of sequence stratigraphy (summarised above) were developed within the Exxon Production Research Company and published by Vail *et al.* (1977b); Jervey (1988); Posamentier *et al.* (1988;1992); Van Wagoner *et al.* (1988; 1990); and Mitchum & Van Wagoner (1991). The fundamental unit of the Exxon model is the sequence, defined by Mitchum (1977) as, "a relatively conformable succession of genetically related strata bounded at its top and base by unconformities or their correlative conformities" (Figs 5.4 and 5.5). Exxon sequences are defined by sequence boundaries and composed of systems tracts, which in turn are made up of parasequences (Figs 5.4 and 5.5). Exxon depositional sequences and systems tracts were initially tied to the eustatic sea-level curve (Fig. 5.3). However, Jervey (1988) proposed the principle of accommodation space as, "the space (volume) made available for potential sediment accumulation as a function of both sea-level fluctuation and subsidence", where relative sea-level change controls the creation or destruction of accommodation space, with the rate of change through time being a key factor in the resulting stratigraphical architecture (Fig. 5.2).

The Exxon methodology is one of scale independence, whereby sequences, systems tracts and parasequences occur on a hierarchy of scales, but all have the following properties (Posamentier *et al.*, 1992).

1. Each stratal unit is a genetically related succession of strata bounded by chronostratigraphically significant surfaces.
2. Each surface is a single, physical boundary that everywhere separates all of the strata above from all of the strata below over the extent of that surface.

Few events are synchronous across a basin; faults nucleate and grow, the change from uplift to subsidence is progressive, erosional unconformities propagate outwards from the basin margin. The only events that theoretically could be synchronous across an entire basin are those recording the maximum rates of rise (maximum flooding surface) and fall (sequence boundary) of relative sea-level, when controlled by processes on a greater scale than the basin (ie. plate-wide or eustatic). Exxon sequence stratigraphy provides "a detailed study of genetically related facies within a framework of chronostratigraphically significant surfaces" (Van Wagoner *et al.*, 1990), where the key correlation surface is the sequence boundary.

Galloway method of sequence stratigraphical analysis

The Galloway (1989) approach to sequence stratigraphical analysis uses the genetic stratigraphical sequence, defined as, "a package of sediments recording a significant episode of basin margin outbuilding and basin filling, bounded by periods of widespread basin-margin flooding". The genetic

stratigraphical sequence is bounded by maximum flooding surfaces which are easily recognisable and can be correlated in both outcrop and subsurface datasets. Marine flooding surfaces define "facies sequences" which are the building blocks of genetic stratigraphical sequences and are analogous to parasequences in Exxon terminology. The genetic stratigraphical sequence is a major regressive/transgressive cycle with a duration up to 4-5 Ma (Galloway, 1989; Van Wagoner *et al.*, 1990) and forms a basic component of basin fill. Genetic stratigraphical sequences form the obvious building blocks of stratigraphy and are easy to recognise and map in a variety of datasets. Their development is controlled by the interplay of sediment supply and relative sea-level. Although an analysis of basin fill in terms of genetic stratigraphical sequences is easier than a sequence stratigraphical analysis, less information is derived on the causative controls on stratigraphical development, as no differentiation is drawn between cycles driven by relative sea-level changes (which will contain a sequence boundary) and those driven by sediment supply variations (which need contain no sequence boundary). Therefore, a genetic stratigraphical sequence may not be precisely correlatable beyond the area of local sediment supply control.

Galloway (1989) defined rock units like this in the belief that the genetic linkage was least across the major flooding surfaces, while between them the rocks were closely related by common provenance and process. However, the facies assemblages may be significantly different between the progradational and backstepping portions of the genetic stratigraphical unit. Galloway (1989) emphasised the three-dimensional nature of genetic stratigraphical sequences and highlighted the variations due to eustasy and subsidence, with particular reference to along strike variations in sediment supply. Early Exxon models were criticised as being two-dimensional until Jervey (1988) took into account both sediment flux variations and accommodation variations in three-dimensions. Tucker (1991b) concluded that a genetic stratigraphical approach to correlation would contain significant time gaps and hence be of no use in the subdivision and interpretation of carbonate-evaporite successions, similar to some of those found in the Domeyko basin.

Sequence stratigraphical methodology adopted in this thesis

The principle of accommodation space is central to sequence stratigraphy, whatever the driving mechanism for sequence development. Relative sea-level change controls the creation or reduction of accommodation space, with the rate of change through time being a key factor in the resulting stratigraphical architecture. In active extensional domains the expressions of eustatic sea-level are still present in the stratigraphical record, however these expressions are modified by complex basin margin topography and by significant, along strike variations in subsidence and accommodation creation (Gawthorpe *et al.*, 1994; Howell & Flint *in press*).

The sequence stratigraphical approach used in this thesis is similar to that of Surlyk (1990) which was based on the concepts of Posamentier *et al.* (1988); Van Wagoner *et al.* (1990); Loucks & Sarg (1993) and Posamentier & Allen (1993) combined with field sedimentological evidence for shallowing-upward trends, progradation, hiatus, condensation, and changes in water-depth. We utilise these

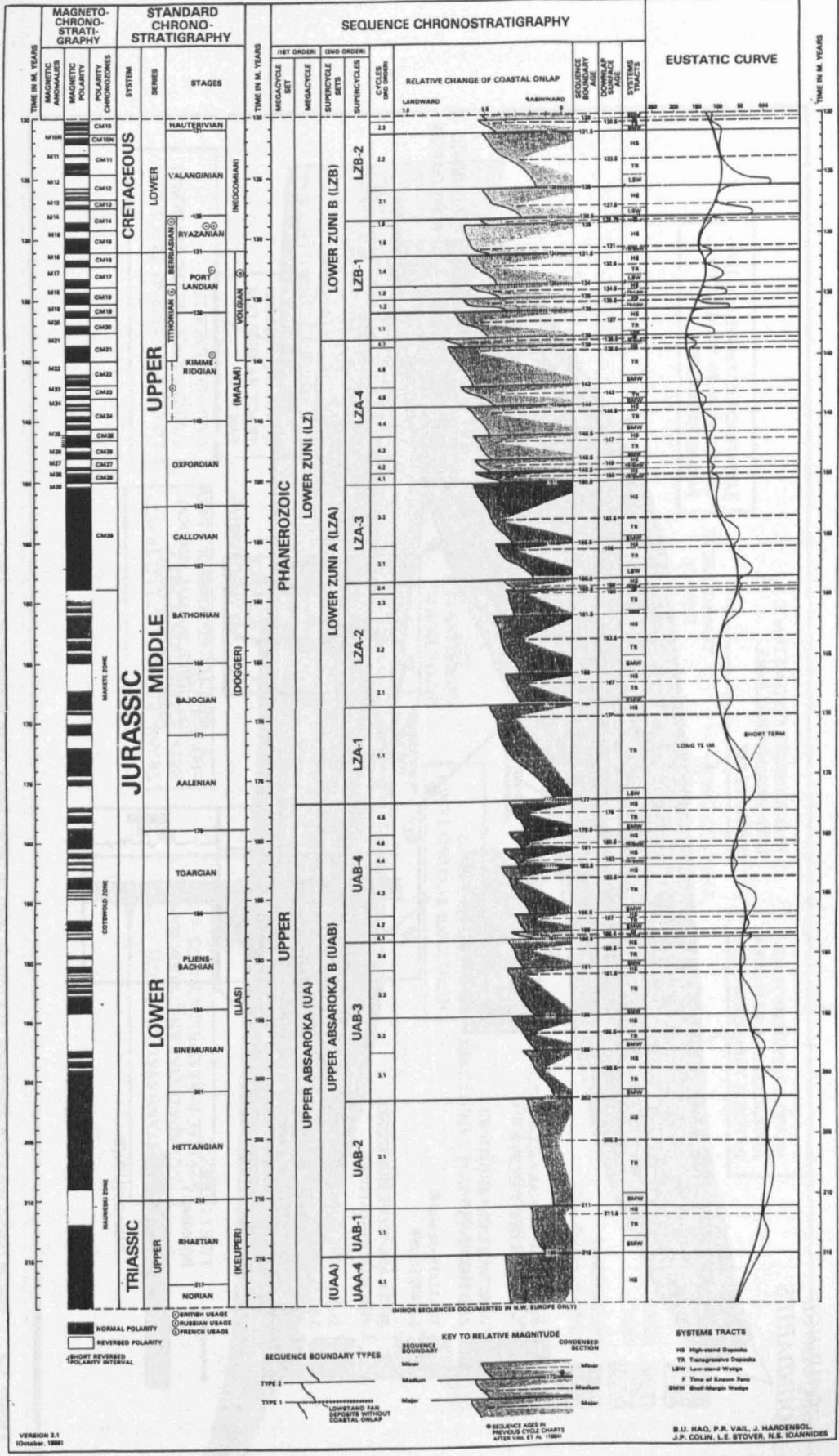


Figure 5.3 The Late Triassic-Early Cretaceous portion of the global cycle chart (Haq et al., 1988).

An Exxon Type 1 Sequence

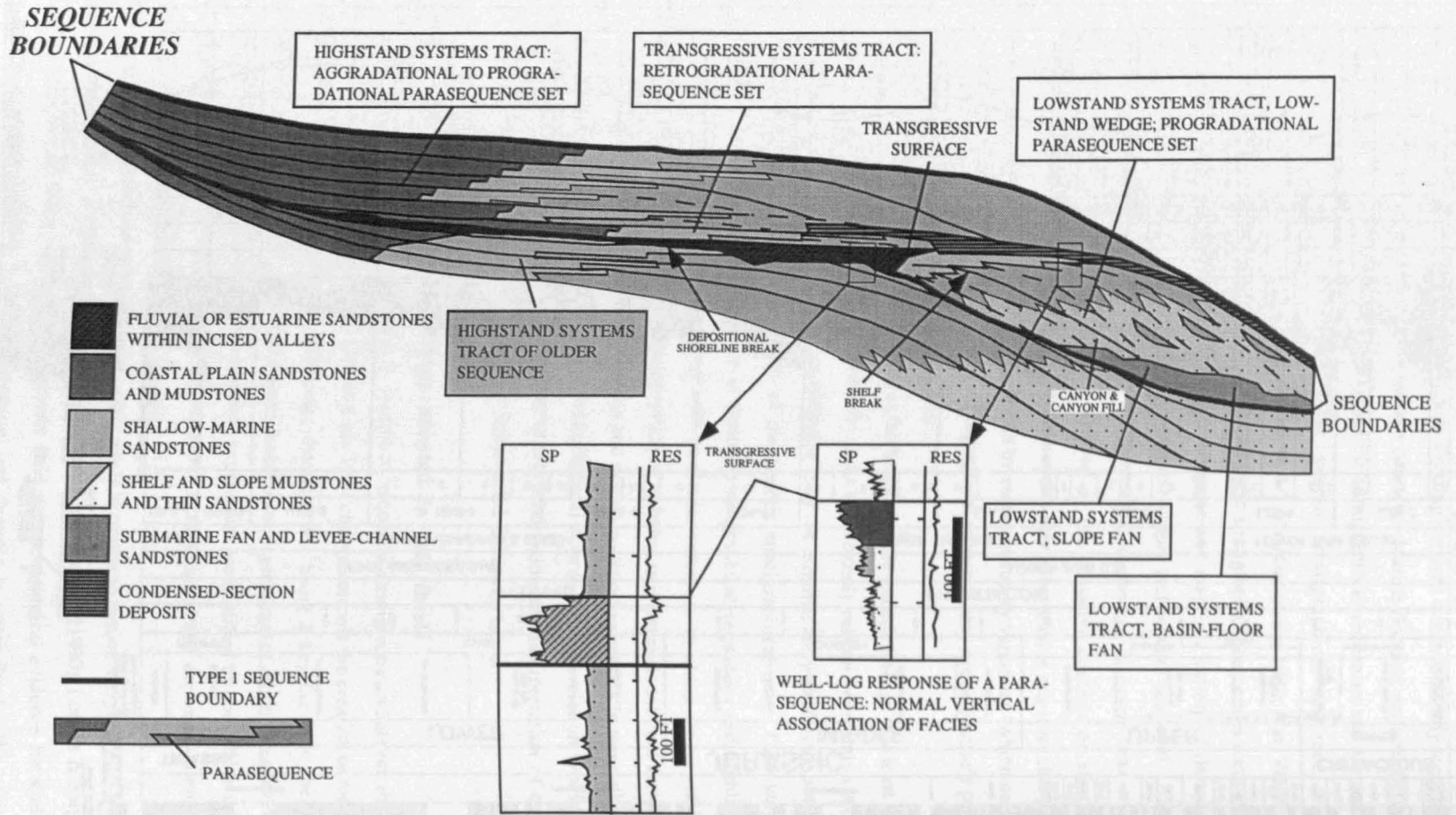


Figure 5.4 Exxon type-1 sequence developed on a margin with an offlap break (Van Wagoner *et al.*, 1990).

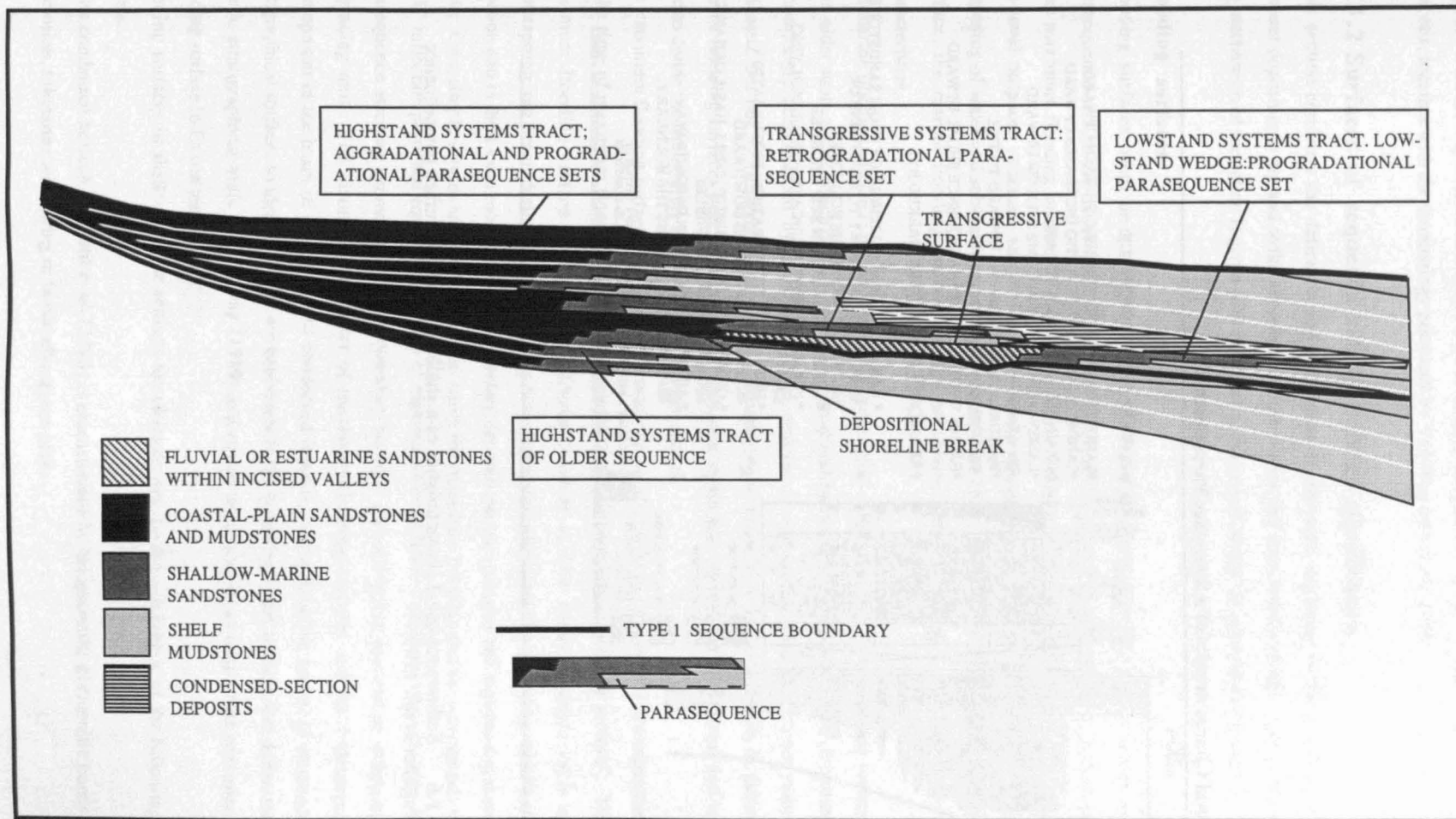


Figure 5.5 - An Exxon Type-1 sequence developed on a ramp-margin with no offlap break. From Van Wagoner *et al.* (1990).

A. Stratal Characteristics of a Shoreface Parasequence

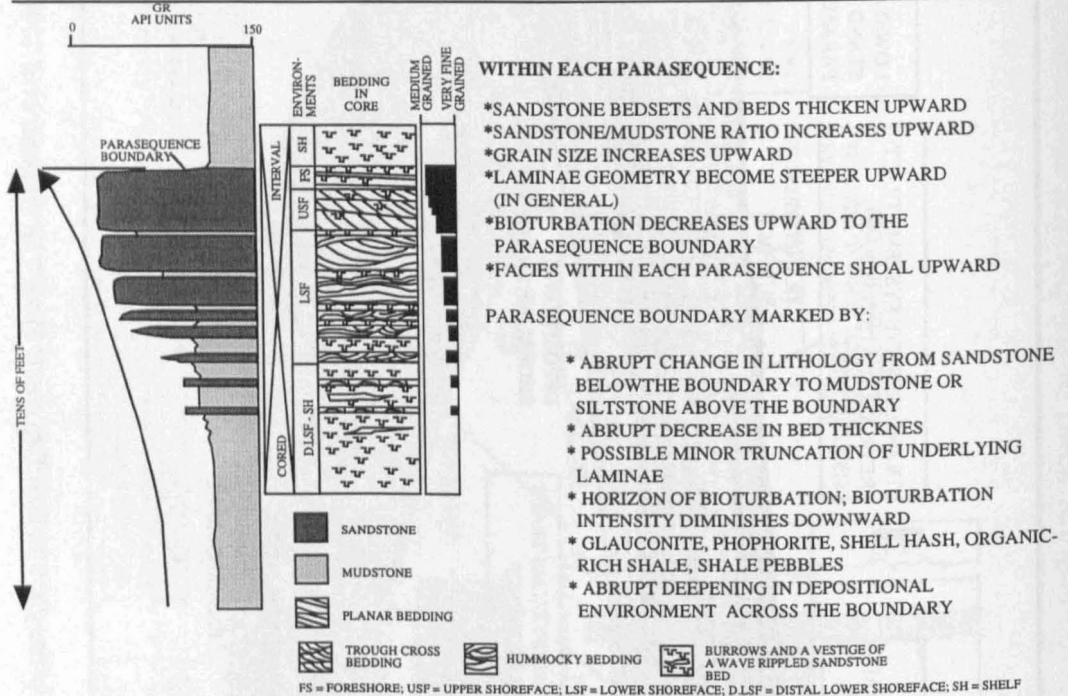


Figure 5.6 Sedimentological characteristics of a shallow-marine shoreface parasequence (Van Wagoner *et al.*, 1990).

approaches, carefully constrained by the biostratigraphy and process sedimentology in the following analysis, together with the terminology presented by Van Wagoner *et al.* (1988).

5.3.2 Surfaces of sequence stratigraphical significance

This section considers the definition and expression of particular bounding surfaces, taking into account depositional dip and strike variations in both marine and continental settings. Discussion on the mechanism of formation is given with reference to the rate of change of accommodation space.

Flooding surfaces

Flooding surfaces occur on a hierarchy of scales, from those which bound parasequences and parasequence-sets, to the major flooding surfaces which define genetic stratigraphical sequences and form maximum flooding surfaces in Exxon sequences. Flooding surfaces form when rising relative sea-level outpaces sediment supply, resulting in an abrupt increase in accommodation space, deepening of water and subsequent landward shift in facies belts. There are several types of flooding surface, the marine flooding surface and the maximum flooding surface have the following characteristics.

The marine flooding surface is defined by Van Wagoner *et al.* (1990) as, "a surface separating younger from older strata across which there is evidence of an abrupt increase in water-depth". This deepening is commonly accompanied by minor submarine erosion or non-deposition with a minor hiatus indicated, but not by subaerial erosion due to stream rejuvenation or a basinward shift in facies. Marine flooding surfaces punctuate deposition in coastal-plain and shallow-marine systems and are used to divide the stratigraphy into component parasequences.

The maximum flooding surface is defined by Posamentier *et al.* (1988) as, "the surface corresponding to the time of maximum flooding, called the downlap surface or maximum flooding surface". The maximum flooding surface is the most landward flooding surface within a single cycle of backstepping and progradation. It is commonly associated with a condensed section in a basinward direction and in the Exxon model forms the boundary between the transgressive and highstand systems tracts. On a simple sinusoidal relative sea-level curve the maximum flooding surface corresponds to the R' inflection point and equates to the time of maximum rate of relative sea-level rise. In terms of parasequence stacking geometries it is the boundary between a backstepping unit and an overlying prograding unit. The distinctive character of maximum flooding surfaces and the widespread development in the basin of the equivalent condensed interval, makes them the easiest of sequence stratigraphical surfaces to identify. They are equivalent to the bounding hiatal surfaces that define the genetic stratigraphical units of Galloway (1989) and equate to a second- or third-order maximum flooding surface in Exxon terminology.

Flooding surfaces in shallow-marine settings are characterised by the occurrence of the following criteria.

1. The condensed horizon of Loutit *et al.* (1988) is characterised by hardgrounds, glauconitic bands, bio-erosion, submarine winnowing or faunal abundance peaks.

2. Evidence for an abrupt increase in water-depth across a single surface indicated by a landward shift in facies above the flooding surface.

3. The presence of an intensely bioturbated horizon on the upper surface of the sandstone that occurs directly below the abrupt change in lithology or thin sandstones lying within the flooding zone.

Surfaces which fulfil the above criteria can be called flooding surfaces. Subsequently, an analysis of the parasequence architecture and regional extent of the surface must be carried out to determine the type and order of flooding surface. Flooding surfaces can also be recognised in non-marine settings by the cessation of clastic systems and subsequent deposition of carbonaceous shales and coals, thin algal or marine limestones. Aitken & Flint (1994) have interpreted thick, regionally extensive belts of carbonaceous shale and coal as being indicative of a prolonged period of high (and/or rising) water table caused by a rise in relative sea-level or base-level and a subsequent increase in accommodation space.

Sequence boundaries

Sequence boundaries form as a result of a fall in relative sea-level during the maximum rate of removal of accommodation space. Mitchum (1977) defined the sequence boundary as, "an unconformity and its correlative conformity". When considering a basin margin profile with a well developed offlap break, two types of sequence boundary have been described, the Type-1 and Type-2 sequence boundary (Fig. 5.4).

The Type-1 sequence boundary is characterised by subaerial exposure and concurrent subaerial erosion associated with stream rejuvenation, a basinward shift in facies, a downward shift in coastal onlap, and onlap of overlying strata (Van Wagoner *et al.*, 1988). As a result of the basinward shift in facies, non-marine or very shallow-marine rocks, such as braided stream or estuarine sandstones above a sequence boundary, may directly overlie deeper-water marine rocks, such as lower shoreface sandstones or shelfal mudstones, below a boundary with no preservation of rocks deposited in intermediate depositional environments. The intermediate facies must have been deposited but were eroded during sequence boundary formation. A Type-1 sequence boundary is interpreted to form when the rate of eustatic fall exceeds the rate of basin subsidence at the offlap break, producing a fall in relative sea-level at that position (Fig. 5.4). The Type-2 sequence boundary is marked by subaerial exposure and a downward shift in coastal onlap landward of the offlap break; however it lacks both subaerial erosion associated with stream rejuvenation and a basinward shift in facies (Van Wagoner *et al.*, 1988). Onlap of overlying strata landward of the offlap break also marks a Type-2 sequence boundary. A Type-2 sequence boundary is interpreted to form when the rate of eustatic fall is less than the rate of basin subsidence at the offlap break, so that no relative sea-level fall occurs at that position (Fig. 5.4).

Type-1 sequence boundaries are associated with incised valley formation and lowstand fan deposition, whereas if the fall is restricted to that portion of the profile landward of the offlap break, then the boundary is a Type-2 and no lowstand fans are deposited. In a basin such as a ramp margin with no clear offlap break, a Type-1 sequence boundary is based on the identification of subaerial exposure and erosion (Fig. 5.5). These criteria permit the interpretation of a candidate sequence boundary.

Subsequent, regional mapping and correlation of the surface must be carried out to ensure the event is not autocyclic, such as a distributary channel.

5.3.3 Parasequences and parasequence stacking geometries

Van Wagoner *et al.* (1988) defined the parasequence as, “a relatively conformable succession of genetically related beds or bedsets bounded by marine flooding surfaces and their correlative surfaces”. Parasequences are the products of discrete episodes of basin fill, characterised by shallowing-upward profiles with progressively younger bedsets deposited in progressively shallower water (Van Wagoner *et al.*, 1988; 1990) (Fig. 5.6). Internally, the parasequence displays an upward increase in average grain-size and bed-thickness with no abrupt decreases of water-depth (Van Wagoner *et al.*, 1990) (Fig. 5.6). Parasequence boundaries form the lowest-order practical chronostratigraphical framework for correlation and mapping. At present, parasequences are only recognised with confidence in shallow-marine settings (Fig. 5.7) and their recognition in delta and coastal-plain settings is not easily defined (Aitken & Flint, 1994). Parasequence-sets are defined as, “a succession of genetically related parasequences forming a distinctive stacking pattern”, (Van Wagoner *et al.*, 1990). Progradational, backstepping and aggradational parasequence-sets can be recognised (Fig. 5.8). In areas of high sediment input, parasequence-sets are the building blocks of systems tracts and sequences and are a class of depositional unit intermediate between parasequence and sequence. In areas of low sediment input, such as the Domeyko basin, these intermediate units may not be recognisable.

5.3.4 Systems tracts and depositional architecture

A systems tract represents the range of linked depositional systems currently active during a particular time interval, defined by Brown & Fisher (1977). Systems tracts are separated by key surfaces of sequence stratigraphical significance, defining separate parts of the relative sea-level cycle and which contain significantly different component depositional systems (Fig. 5.9-5.11). Mitchum & Van Wagoner (1990) state that, “each systems tract is interpreted to have been deposited during a specific phase or portion of one complete cycle of relative fall and rise of sea-level. The sequences and systems tracts however are defined on the basis of stratal geometry and physical relationships, using objective stratal and facies criteria that do not depend on frequency of occurrence, size or interpreted depositional mechanism”. A Type-1 sequence is composed of lowstand, transgressive and highstand systems tracts (Fig. 5.9-5.11), while a Type-2 sequence comprises, shelf-margin, transgressive and highstand systems tracts.

Lowstand systems tract

The lowstand systems tract is the lowermost systems tract in a depositional sequence bounded at its base by a Type-1 sequence boundary and at its top by a transgressive or marine-flooding surface (Van Wagoner *et al.*, 1988) (Fig. 5.9). Lowstand systems tracts are deposited during intervals characterised by relative sea-level fall, still-stand and subsequent slow relative sea-level rise (Fig. 5.9). The lowstand systems tract, if deposited in a basin with a shelf break, generally can be subdivided into

three separate units, from oldest to youngest, a basin-floor fan, a slope-fan and a lowstand-wedge (Van Wagoner *et al.*, 1988) (Fig. 5.9). Siliciclastic sediment bypasses the shelf and slope through incised valleys to feed the basin-floor fan, interpreted to occur during a fall in relative sea-level. The slope-fan is characterised by turbidite and debris-flow deposition on the middle or base of the slope. The lowstand-wedge is characterised on the shelf by proximal fluvial facies, constituting the lower portion of the incised valley fill, which commonly onlaps onto the sequence boundary. Then, on the slope by progradational fill with wedge geometry, overlying and commonly downlapping onto the basin-floor fan or the slope-fan. If deposited in a basin with a ramp-margin, the lowstand systems tract consists of a relatively thin lowstand wedge characterised by stream incision and sediment bypass followed by the infilling of incised valleys and continued shoreline progradation. The resulting lowstand wedge is composed of incised valley fill deposits up-dip and one or more progradational parasequence-sets down-dip. The incised valleys which are characteristic of the lowstand systems tract are usually filled either by proximal fluvial facies deposited as part of the aggradational late-lowstand prograding wedge (Fig. 5.9), or estuarine to marine facies deposited as part of the transgressive systems tract (Fig. 5.10). On the interfluvies to the incised valleys, the interfluvial sequence boundary is characterised by long periods of subaerial exposure with little or no lowstand deposit preserved (Fig. 5.9).

Shelf-margin systems tract

The shelf-margin systems tract is the lowermost systems tract in a depositional sequence bounded at its base by a Type-2 sequence boundary and at its top by a transgressive or marine flooding surface (Van Wagoner *et al.*, 1988). The systems tract is characterised by one or more weakly progradational to aggradational parasequence-sets which onlap onto the sequence boundary in a landward direction and downlap onto the sequence boundary in a basinward direction. The shelf-margin systems tract may be difficult to recognise in outcrop and is only differentiated from the underlying highstand systems tract by a subtle Type-2 sequence boundary and possibly a change in the parasequence stacking pattern.

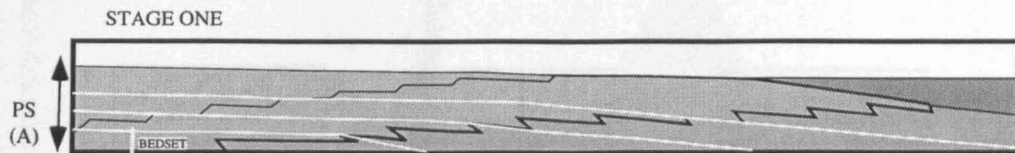
Transgressive systems tract

The transgressive systems tract occurs above the lowstand systems tract and below the maximum flooding surface, being characterised by one or more backstepping parasequences (Van Wagoner *et al.*, 1988) (Fig. 5.10). The systems tract progressively deepens upward as successively younger parasequences step farther landward. The facies of the transgressive systems tract are often more coal-rich and more strongly influenced by tidal processes than those of the highstand and lowstand systems tracts.

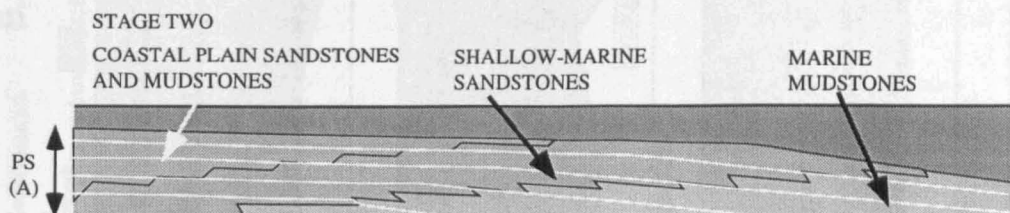
Highstand systems tract

The highstand systems tract is bounded below by a maximum flooding surface and above by a sequence boundary and may be characterised by one or more aggradational parasequence-sets that are succeeded by one or more progradational parasequence-sets with prograding clinoform geometries (Van

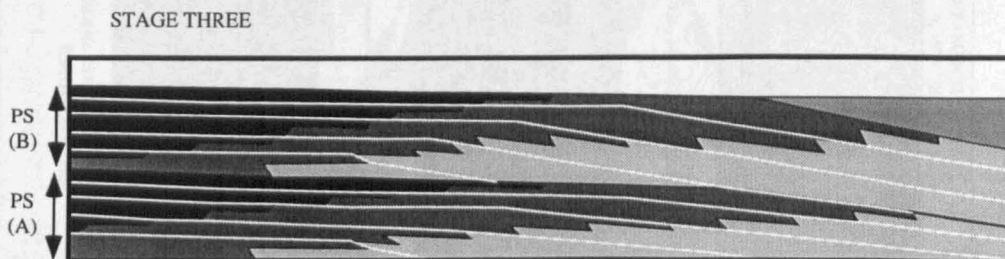
Parasequence Development



PROGRADATION OF PARASEQUENCE (A) DURING A TIME WHEN THE RATE OF DEPOSITION EXCEEDS THE RATE OF WATER DEPTH INCREASE. BEDSETS COMPOSE THE PARASEQUENCE. THE YOUNGEST BEDSET IS NON-DEPOSITIONAL.



RAPID WATER DEPTH INCREASE FLOODS THE TOP OF PARASEQUENCE (A) CREATING A SURFACE OF NON-DEPOSITION WITH RESPECT TO SILICICLASTIC SEDIMENT. THIN CARBONATES, GLAUCONITES, ORGANIC-RICH MARLS, OR VOLCANIC ASHES MAY BE DEPOSITED ON THE SURFACE.



PROGRADATION OF PARASEQUENCE (B) DURING A TIME WHEN THE RATE OF DEPOSITION EXCEEDS THE RATE OF WATER DEPTH INCREASE. BEDSETS IN PARASEQUENCE (B) DOWNLAP ONTO THE BOUNDARY OF PARASEQUENCE (A). THERE IS AN ABRUPT DEEPENING OF FACIES ACROSS THE BOUNDARY OF PARASEQUENCE (A).

Figure 5.7 Progressive development of a parasequence boundary (Van Wagoner *et al.*, 1990).

Parasequence Stacking Patterns

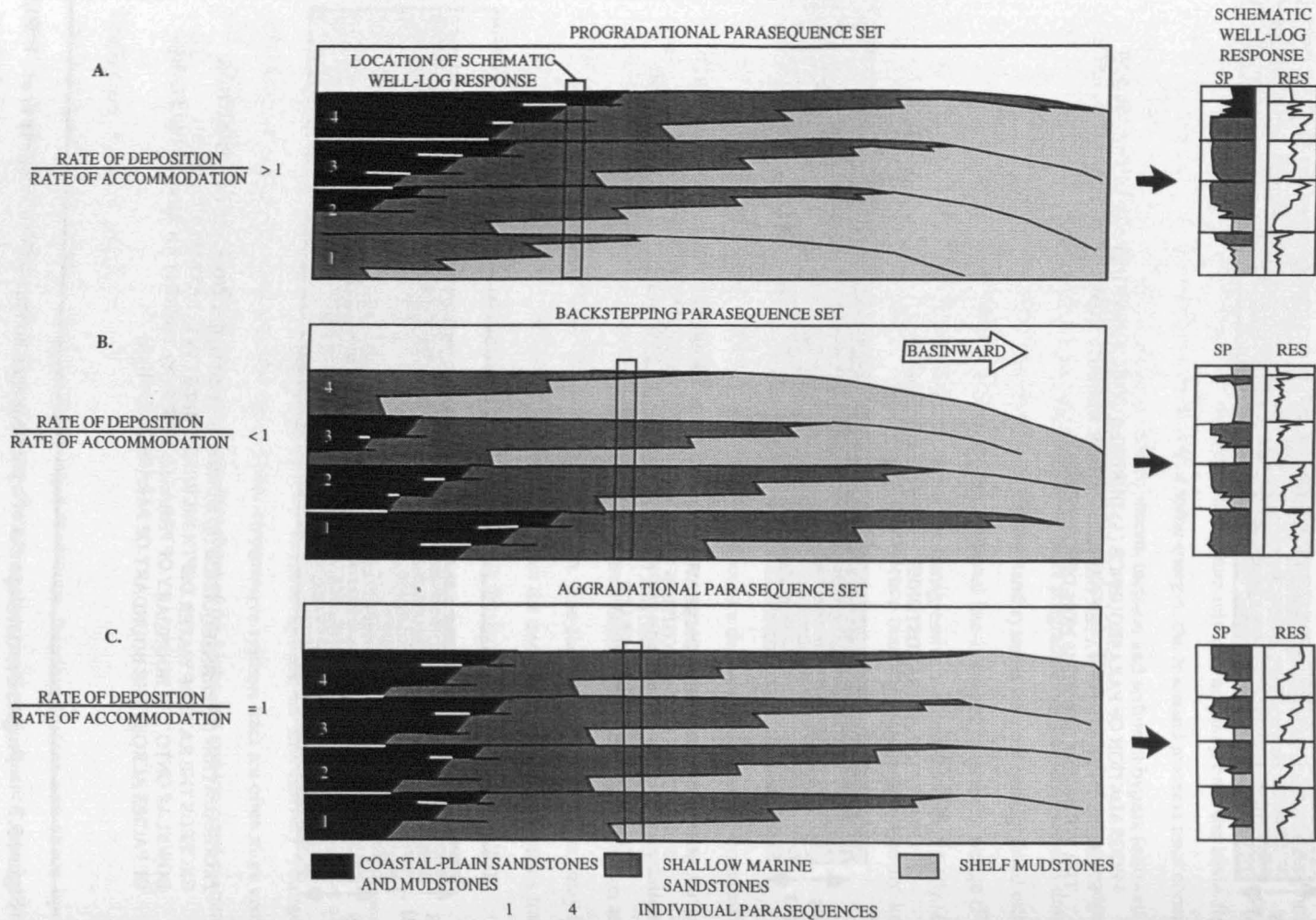


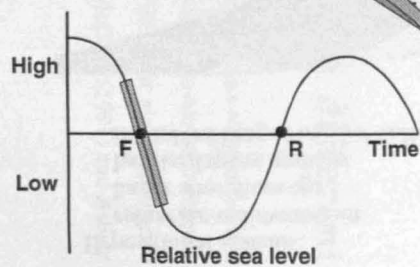
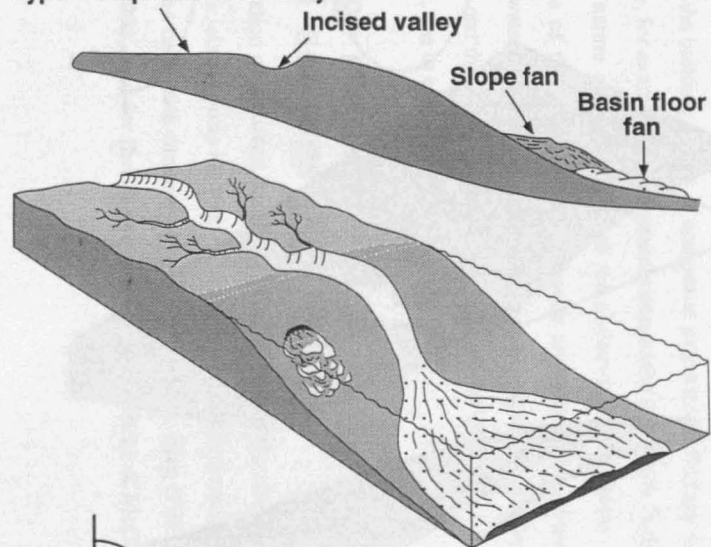
Figure 5.8 Parasequence stacking patterns (Van Wagoner *et al.*, 1990).

LOWSTAND SYSTEMS TRACT (LST) WITH SHELF BREAK

A. Early LST

Depositional systems
various mass flow processes
palaeosols on shelf
valley incision

Type 1 sequence boundary



B. Late LST

Depositional systems:
shelf edge deltas
early incised valley filling and
fluvial (and estuarine) deposits

Prograding wedge

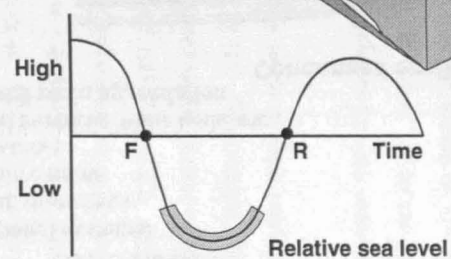
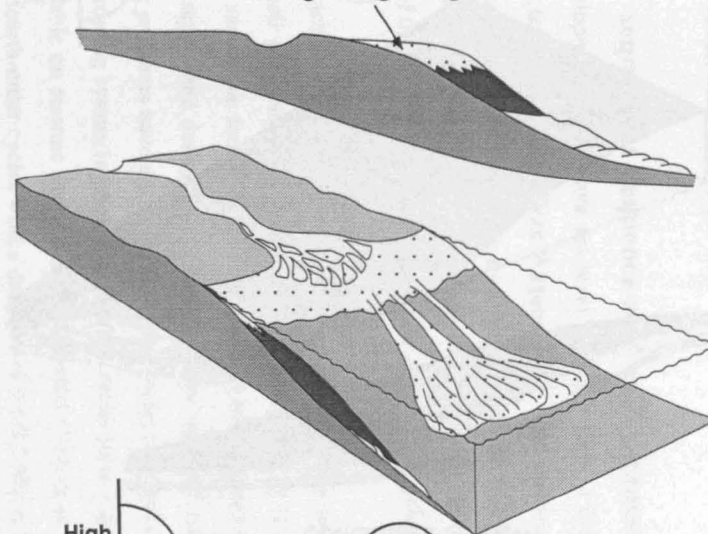
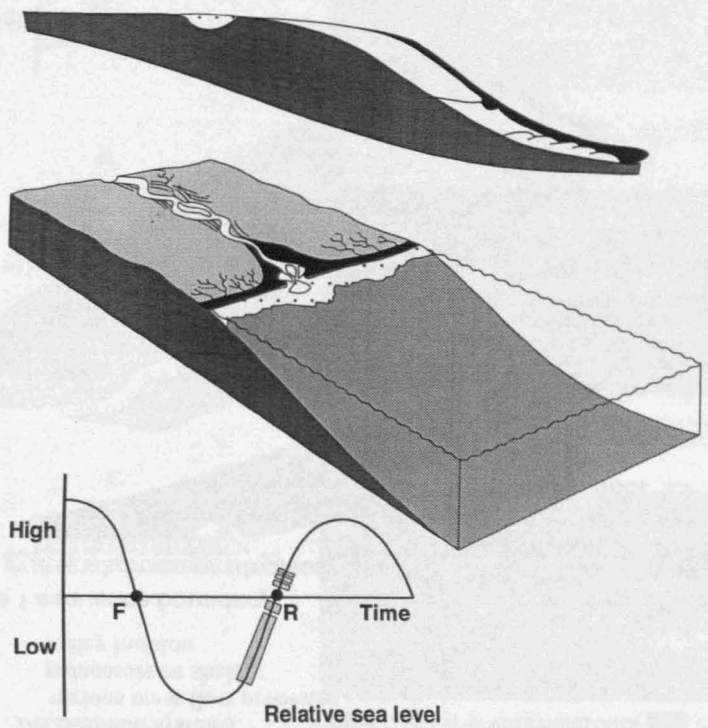


Figure 5.9 Sequence evolution represented by sequence boundary formation and lowstand systems tract, fan and wedge deposition (Van Wagoner *et al.*, 1990).

TRANSGRESSIVE SYSTEMS TRACT

A. Early TST

Depositional systems:
estuarine sedimentation
linear shorelines eg:
barrier/lagoon systems
fluvial infilling of incised valleys



B. Late TST/CONDENSED SECTION

Depositional systems:
linear shorelines
offshore muds
limestones
hiatal surfaces 'bone beds' etc.
alluvial plain aggradation

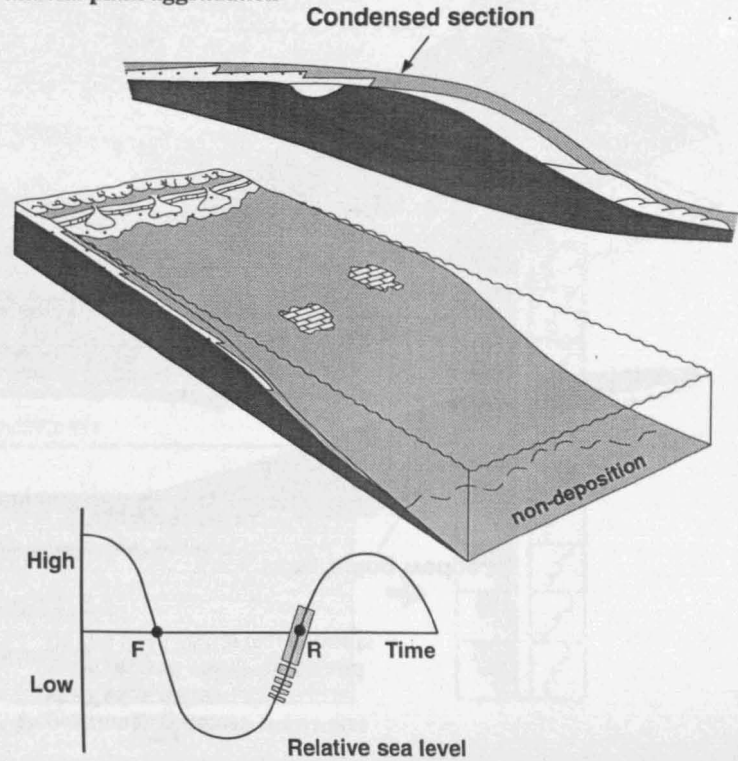


Figure 5.10 Sequence evolution represented by transgressive systems tract deposition (Van Wagoner *et al.*, 1990).

Wagoner *et al.*, 1988) (Fig. 5.11). The systems tract progressively shallows-upward as successively younger parasequences step farther basinward (Fig. 5.11).

5.3.5 Hierarchy of sequences: sequence-sets and composite sequences

Analysis of sequence development and relative sea-level generally show a hierarchy of cyclicity, demonstrated in both siliciclastic (Mitchum & Van Wagoner, 1991) and carbonate (Hunt & Tucker, 1993) environments. Higher-frequency, shorter-duration cycles form the building blocks of lower-frequency, longer-duration cycles (Fig. 5.12). Vail *et al.* (1991) assigned "orders" of hierarchy depending on the duration of the cycle and interpreted probable signatures and causes for each order of cyclicity (Fig. 5.13).

The component systems tracts of high-order sequences will be modified in terms of their relative importance according to their position in the lower-order sequences (Fig. 5.12). For example, the lowstand systems tracts of successive fourth-order sequences will be enhanced during a third-order relative sea-level fall and suppressed during a third-order relative sea-level rise (Fig. 5.12). It is unlikely that the controlling processes have a set periodicity and cycles of relative sea-level may have less organisation than an ordering system implies. Third-order cycles have a duration ranging from 0.5-5 Ma and are recognisable on seismic datasets and in outcrop (Vail *et al.*, 1977b; Haq *et al.*, 1988). Higher frequency, fourth-order cycles with a duration of 0.1-0.2 Ma are commonly beyond seismic resolution, exceptions being shallow seismic datasets or areas of high subsidence and are most readily recognised in outcrop and well-log datasets (Mitchum & Van Wagoner, 1991). A sequence-set is composed of higher-order sequences arranged in a distinctive progradational, aggradational or backstepping stacking pattern (Mitchum & Van Wagoner, 1990) (Fig. 5.8). Higher-order sequences and sequence-sets form the building blocks of composite sequences (Mitchum & Van Wagoner, 1990). Second-order sequences, for example, are commonly composite sequences formed from stacked third-order sequences. The nature and expression of the higher-order sequences will vary between the different systems tracts of the lower-order composite sequence. For example, the higher-order sequences within the lowstand systems tract of the composite sequence are affected by the background fall in relative sea-level and the transgressive systems tract of the higher-order sequences are subdued and may even be absent, due to erosional removal.

5.4 Sequence stratigraphical surfaces in different depositional settings

Criteria for the identification of sequence boundaries and maximum flooding surfaces are summarised for a shallow-marine siliciclastic ramp by Van Wagoner *et al.* (1990), for a shallow-marine carbonate ramp and shallow-marine carbonate rimmed-margin by Loucks & Sarg (1993), for marginal-marine fan-deltas by Postma (1995), and for fluvial environments by Shanley & McCabe (1991) and Aitken & Flint (1994).

5.4.1 Shallow-marine siliciclastic ramp setting

The sequence boundary displays a basinward shift in facies (Type-1), a vertical change in parasequence stacking patterns (Type-1 or Type-2) and regional distribution throughout the basin (Van Wagoner *et al.*, 1990). Within a basin, the Type-1 sequence boundary has different physical expressions depending both on where it is observed (Van Wagoner *et al.*, 1990) and on along strike variations in subsidence rates and sediment supply (Howell & Flint *in press*). Sharp-based shoreface sandstone facies are interpreted as lowstand deposits, directly overlying offshore siltstone facies interpreted to represent the previous highstand. In siliciclastic ramp settings, the production of lowstand shoreline deposits is interpreted to represent the reduction in accommodation space associated with forced regression (Posamentier *et al.*, 1992). The facies-tract dislocation is interpreted to form as a result of the high rate of accommodation space removal and is distinct from the much slower rates of accommodation space removal associated with lowstand or highstand progradation. In a basinward direction, heterolithic storm-derived sandstone facies are interpreted as lowstand deposits, directly overlying offshore siltstone facies of the previous highstand. The storm-derived sandstone facies are interpreted as resulting from lowering of storm wave base and lowstand sediment by-pass of the upper ramp during storm events into the otherwise sand-starved deep basin. In areas of complete sand-starvation the sequence boundary is recorded as a correlative surface. The reduction in accommodation space associated with sequence boundary formation is interpreted to be driven by a fall in relative sea-level.

The maximum flooding surface is defined by a change from backstepping to progradational parasequence geometries and commonly associated with a condensed section, forming at the time of maximum rate of relative sea-level rise. The condensed section is characterised by hardgrounds, authigenic minerals (glauconite, phosphorite and siderite), bio-erosion, submarine winnowing or faunal abundance peaks (Loutit *et al.*, 1988), and is interpreted to represent the time of maximum accommodation space creation and clastic sediment starvation. The maximum flooding surface is clearly developed within the area of the shoreface and offshore transition but is more subtle in the basinal sections due to low rates of sedimentation. The increase in accommodation space associated with maximum flooding surface formation is interpreted to be driven by a rise in relative sea-level.

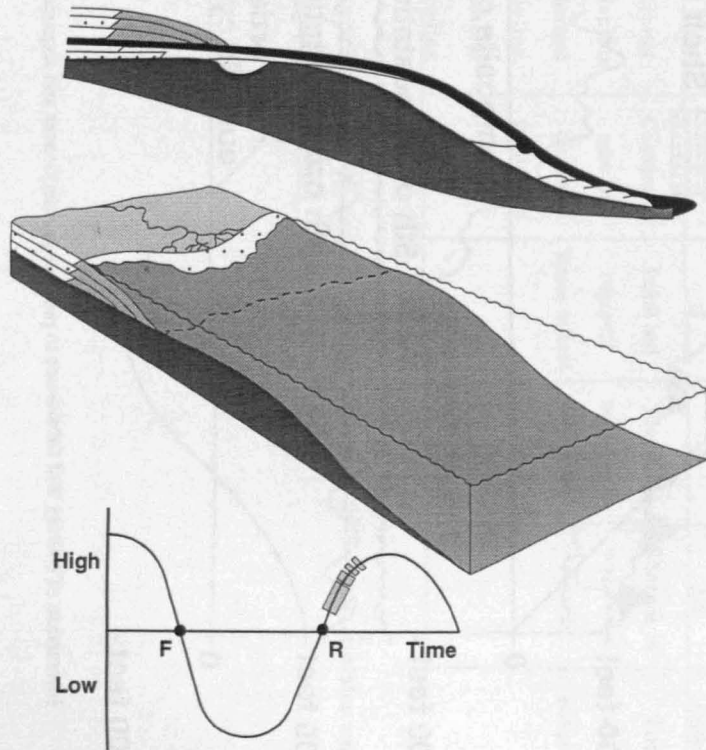
5.4.2 Shallow-marine carbonate ramp setting

The sequence boundary in a carbonate ramp setting produces a similar response to that of the siliciclastic setting, with a basinward shift in facies (Type-1), a vertical change in parasequence stacking patterns (Type-1 or Type-2) and regional distribution throughout the basin (Van Wagoner *et al.*, 1990). Sharp-based, amalgamated limestone and sandstone facies are interpreted as lowstand deposits, directly overlying offshore mudstone facies interpreted as the previous highstand. In carbonate ramp settings, the production of lowstand shoreline deposits is also interpreted to represent the reduction in accommodation space associated with forced regression (Hunt & Tucker, 1992). In a basinward direction, heterolithic storm-derived grainstone and packstone facies are interpreted as lowstand deposits, directly overlying offshore mudstone facies interpreted to represent the previous

HIGHSTAND SYSTEMS TRACT

A. EARLY HST

Depositional systems:
aggradational shelf deltas
interdeltaic shoreline systems



B. LATE HST

Depositional systems:
increasingly progradational shelf deltas

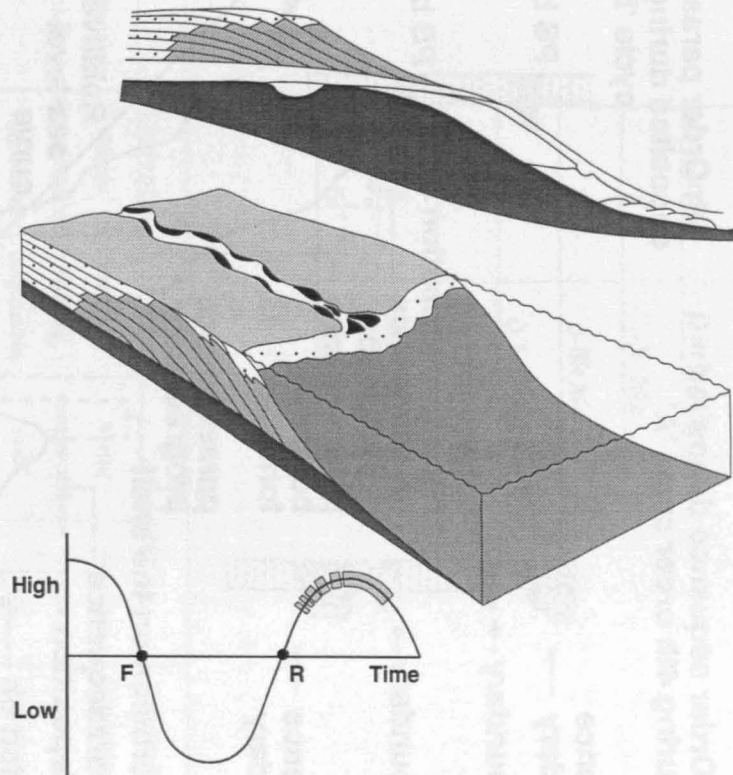


Figure 5.11 Sequence evolution represented by highstand systems tract deposition (Van Wagoner *et al.*, 1990).

RELATIVE SEA LEVEL HIERARCHY

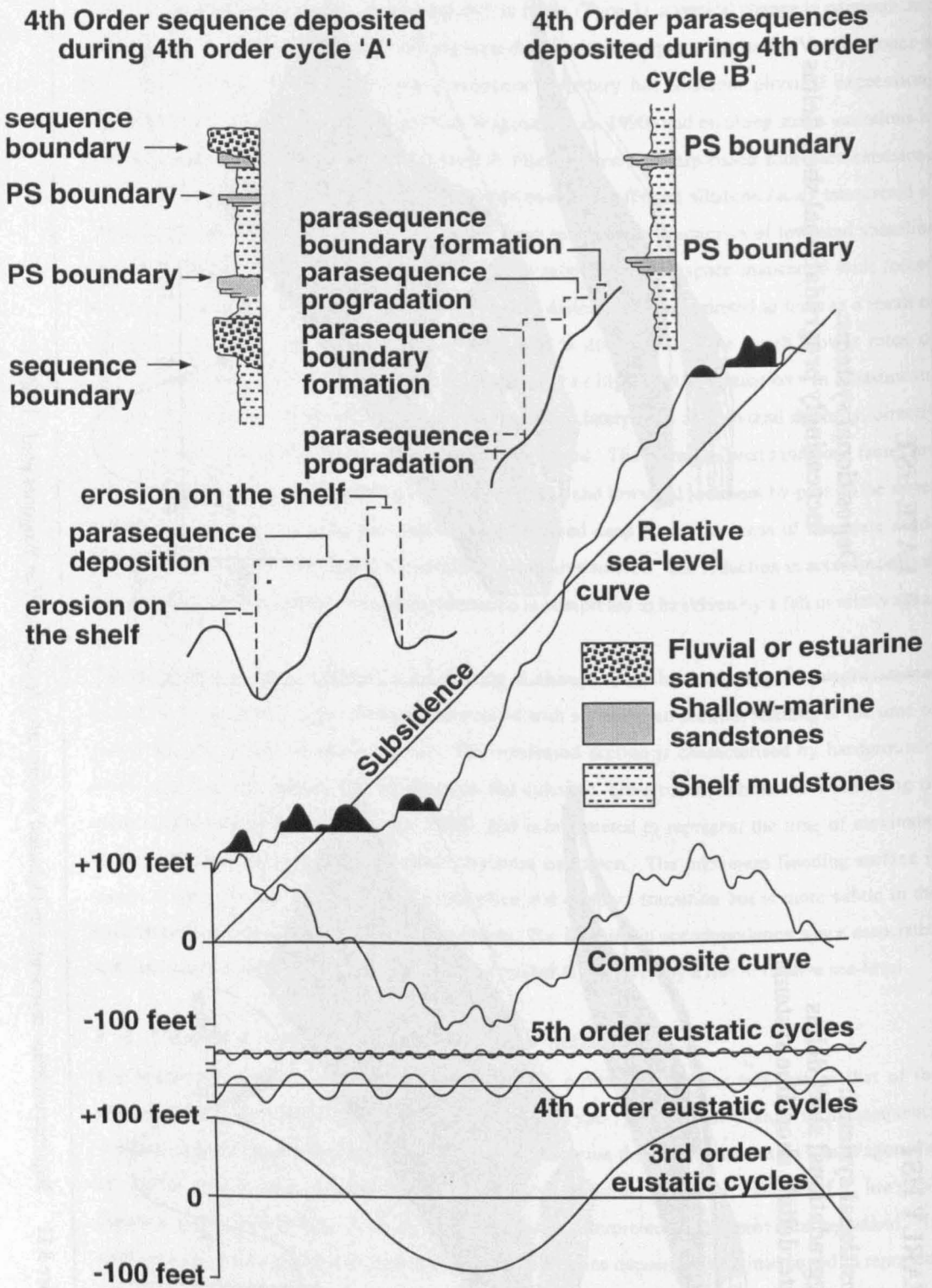


Figure 5.12 Interaction of eustasy and subsidence to produce parasequences and sequences (Van Wagoner *et al.*, 1990).

Order	Duration
1	>50 Ma
2	5-50 Ma
3	0.5-5 Ma
4	0.1-0.5 Ma
5	0.01-0.1 Ma
6	<0.01 Ma

	Tectonics			Eustasy		Sedimentation
Signature	Sedimentary basin	Major transgressive-regressive facies cycle	Flooding, faulting, magmatism, diapirism	Major continental-scale flooding cycle	Sequence, systems tract, parasequence parasequence set	Depositional systems, lithofacies marker beds, bedsets, beds
Distribution	Regional	Regional	Local	Global	Global	Local
Order	1	2	3	1	2-5	Episodic
Cause	Crustal extension, thermal cooling, flexural loading	Changes in rates of tectonic subsidence	Local and regional stress release	Change in ocean basin volume	Changes in water / ice volume	Local sedimentary processes

Figure 5.13 Orders of cyclicity and stratigraphic signatures of tectonic, eustatic and sedimentary cyclicity (Vail et al. 1991).

highstand. The storm-derived grainstone and packstone facies are interpreted as resulting from lowering of storm wave-base and similar lowstand sediment by-pass of the upper ramp during storm events into the otherwise mud-dominated deep basin. Characteristic sedimentological features of the sequence boundary include; a change from calcareous mudstones/limestones (siliciclastic-free) to sandy limestones, an abrupt increase in shell debris, the reworking of fossils and a reduction in ammonite fauna, all of which are interpreted to indicate a decrease in water-depth.

The maximum flooding surface is represented by a change from backstepping to progradational parasequence geometries and commonly associated with a condensed section. In addition to the features seen in siliciclastic settings, an abrupt increase in the abundance of calcareous concretions is interpreted to reflect the reduced rates of sedimentation associated with the condensed section.

5.4.3 Shallow-marine carbonate reef-margin setting

The sequence boundary produces a distinctly different response in a carbonate reef-margin setting, with the reduction in accommodation space resulting in exposure and a shutting-down of the carbonate "factory". Exposure of the shelf rarely results in mechanical reworking of the shelf and more commonly in chemical reworking, characterised by dolomitization in arid conditions (Tucker, 1992). Megabreccias deposited in a toe of slope apron are interpreted to result from collapse of the platform margin during negative accommodation space (Hunt & Tucker, 1992). An abrupt shift from offshore marine mudstones to thick evaporite facies is interpreted to represent a reduction in accommodation space, causing the basin to become silled with the loss of permanent marine connection.

The maximum flooding surface is commonly associated with an abrupt drowning event and landward shift in facies (Erlich *et al.*, 1993; Zempolich, 1993). Shallow-marine platform or reefal limestone facies overlain by ammonite-bearing, offshore mudstone facies are interpreted to represent an abrupt deepening of facies and increase in accommodation space. The top surface of the underlying limestone reef often shows infilling of cavities or Neptunian dykes and the blanketing of life-position framework corals by offshore mudstones, supporting an abrupt increase in accommodation space and drowning of the limestone reef.

5.4.4 Marginal-marine fan-delta setting

Erosionally-based, multi-storey conglomerate facies directly overlying shallow-marine limestone or fine-grained sandstone facies is interpreted to represent a reduction in accommodation space. This abrupt basinward shift of facies within a fan-delta succession is characterised by lateral and vertical lithofacies features and interpreted to represent the progradation of the alluvial fan during a drop in relative sea-level (Postma, 1995). Sequence boundaries can be readily distinguished from autocyclic lobe shifts on the basis of their regional extent and recognition in the marine basin.

Shallow-marine coral limestone or fine-grained sandstone facies directly overlying pebble conglomerate or coarse-grained sandstone facies is interpreted to represent the shutting-down of siliciclastic sediment supply associated with an abrupt increase in accommodation space (Postma, 1995). The maximum flooding surface is characterised by the most landward of these marine facies,

separating the backstepping transgressive and progradational highstand systems tracts. The maximum flooding surface also commonly results in complete drowning of the alluvial fan system.

5.4.5 Fluvial setting

The sequence boundary expression in a fluvial setting is modified by along strike variations in the degree of incision. Erosionally-based, multi-storey fluvial channels incising into fine-grained floodplain siltstones is characteristic of the main channel area, termed the incised-valley where the overlying fluvial/estuarine sandstones represent the lowstand-early transgressive incised-valley fill (Flint *et al.*, 1995). On the interfluvial areas the degree of incision is much less or none with well-drained paleosols recording the temporally-equivalent fall in base level (Aitken & Flint, 1994). Recent advances in the understanding of estuarine settings have permitted more sophisticated treatment of the fluvial-marine transition (Dalrymple *et al.*, 1994) and subdivision of the incised-valley fill (Zaitlin *et al.*, 1994). A loss of accommodation space and the resulting formation of incised-valleys may occur in response to factors unrelated to changes in relative sea-level, however, the majority of published examples are believed to be associated with a drop of relative sea-level (Dalrymple *et al.*, 1994).

The expression of the maximum flooding surface varies markedly within the incised-valley fill, characterised within marine shales (Loutit *et al.*, 1988) at the seaward end of the incised-valley, within thin marine limestones/estuarine sandstones in marginal-marine areas and may be associated with the fluvial sediments that have the most distal character and are the finest-grained in the non-marine domain (Zaitlin *et al.*, 1994).

5.4.6 Summary

Although the expression of the sequence boundary and maximum flooding surface may vary depending on the depositional environment, the systematic facies-shift and depositional architecture is the same for each surface, recording a temporally-equivalent relative sea-level change.

5.5 Second-order sequence stratigraphy

Sequence stratigraphical analysis of the Domeyko basin has identified five second-order Exxon-type unconformity bounded sequences (Figs 5.14-5.20). Each second-order sequence is composed of several third-order sequences which themselves comprise systems tracts, identified on the basis of parasequence stacking patterns and facies-tract shifts. In this section we restrict our discussion to the five second-order sequences, which have durations ranging from 11-17 Ma (relative durations of stages from Gradstein *et al.*, 1994).

5.5.1 Sequence 1 (Late Triassic-Sinemurian)

Transgressive systems tract

The sequence boundary and lowstand systems tract of our first defined sequence are not distinguished from the overall Triassic continental/volcanic succession. Eleven backstepping parasequences

deposited in a fan-delta setting (Quebrada Vaquillas and Punta del Viento) record an increasingly important influence of transgression in the form of thin intercalated marine limestone and wave-rippled sandstone facies, capped by a 10-40 m thick reefal limestone (Chong, 1977; Prinz, 1991) (Fig. 5.14). Down-dip (north-west), time-equivalent deposition took place in a shallow-marine carbonate-ramp (Sierra Argomedo). Here, clearly marked backstepping parasequences record a gradual deepening from lower shoreface limestone/sandstone to offshore lime mudstone facies (Fig. 5.14). The increasing marine influence and backstepping stacking pattern are interpreted to represent a progressive increase in accommodation space associated with the transgressive systems tract.

Maximum flooding surface

An abrupt landward shift in facies from shallow-marine reefal limestone facies (<10 m water-depth) to offshore siltstone facies (>50 m estimated water-depth), drowning of all coral reefs (Prinz, 1991), reduction of shallow-water bivalves, gastropods, brachiopods (Groschke *et al.*, 1988) and the first occurrence and domination of Lower Hettangian ammonites (Chong, 1977; Groschke *et al.*, 1988) are interpreted to represent a maximum rate of increase in accommodation space associated with the formation of a maximum flooding surface in the earliest Hettangian (Fig. 5.14). Figure 5.14 demonstrates the regional extent and importance of this surface as an excellent correlation horizon and approximate time line, hence its use as a reference datum.

Highstand systems tract

Deposits overlying the maximum flooding surface comprise progradational ammonite bearing offshore marine facies, displaying a gradual transition from carbonate-dominated to siliciclastic-dominated facies (Groschke *et al.*, 1988) (Fig. 5.14). This stacking pattern is interpreted to represent a progressive reduction of accommodation space associated with the highstand systems tract. The succession at Sierra de Varas records Aalenian-age marine heterolithic sandstones and siltstones directly overlying Upper Triassic marine siltstones with non-deposition and erosion resulting in a depositional hiatus spanning from Late Triassic to the Aalenian (Chong & Hillebrandt, 1985) (Fig. 5.14). This local feature is interpreted to be tectonic in origin, resulting from footwall uplift of the basement along the West Fissure Fault System. To the north between 22°-23°S, progradational Sinemurian-age floodplain siltstone, shallow-marine limestone facies (Cerro San Lorenzo) and lower shoreface limestone facies (Cerritos Bayos) are interpreted to represent the highstand systems tract (Fig. 5.15).

5.5.2 Sequence 2 (Pliensbachian-Toarcian)

Sequence boundary and lowstand systems tract

At Cerritos Bayos near the basin margin, Pliensbachian-age upper shoreface sandstone facies erosionally overlie Sinemurian-age lower shoreface limestone facies. The former are interpreted to represent forced regression lowstand deposits associated with a rapid reduction in accommodation space and the formation of a sequence boundary (Fig. 5.15). Up-dip to the north (Cerro San Lorenzo), an erosionally-based multistorey fluvial sandstone unit of 10.5 m thickness, directly overlies floodplain siltstone and shallow-marine limestone facies, also representing an abrupt basinward shift in facies

(Fig. 5.15). The erosion surface records several metres of incision over a lateral distance of 500 m, with the basal fluvial sandstone facies overlain by 130 m thick aggradational to progradational sandy limestone facies. The abrupt basinward shift from marginal-marine to non-marine facies, several metres of incision, > 500 m lateral extent of the erosion surface and incoming of non-marine to shallow-marine facies are interpreted to represent an incised valley-fill deposit (cf. Dalrymple *et al.*, 1994). Biostratigraphical evidence from the underlying floodplain siltstone/shallow-marine limestone facies and overlying sandy limestone facies suggests an Early Pliensbachian age, temporally equivalent to the forced regression in the shallow-marine ramp setting. Further south (25°S), distal carbonate-ramp deposits (East Portezuelo de la Sal) include lower shoreface-offshore transition packstone and mudstone facies directly overlying offshore mudstone facies with a sharp, non-erosional contact, interpreted to represent the same sequence boundary (Fig. 5.14). This sequence boundary represents the most significant Early Jurassic basinward shift in facies seen in the Domeyko basin.

Transgressive systems tract and maximum flooding surface

A landward shift in facies from the Pliensbachian lowstand systems tract shoreface sandstone and sandy limestone facies to anoxic basinal lime mudstone facies indicates the first well defined flooding surface in Sequence 2, which is interpreted as the transgressive surface separating the Pliensbachian lowstand and Toarcian transgressive systems tracts (Fig. 5.15). Aggradational to backstepping bedsets of offshore lime mudstone and packstone facies (65-75 m total thickness) recording siliciclastic sediment starvation and progressive deepening are interpreted as the transgressive systems tract (Fig. 5.15). Ammonite bearing black packstone facies (Cerro San Lorenzo) are strongly anoxic and characterise the most basinal facies within the Toarcian, interpreted to represent the maximum flooding surface or condensed section (Fig. 5.15). Further south (Cerritos Bayos), a single horizon of large (>0.5 m in diameter) calcareous concretions within fine-grained yellow mudstones is interpreted to represent the slowest rates of deposition associated with the condensed section of this maximum flooding surface (Fig. 5.15). These sections demonstrate the variable character of a maximum flooding surface in the anoxic and oxygenated zones of a carbonate ramp environment.

Highstand systems tract

Anoxic black mudstone (Cerro San Lorenzo) and progradational yellow mudstone facies (Cerritos Bayos) with increasingly abundant bioclastic packstone and sandstone beds upwards, record a progressive shallowing in an area of slow rates of deposition and decreasing accommodation space, interpreted to represent the highstand systems tract (Fig. 5.15).

5.5.3 Sequence 3 (Aalenian-Bajocian)

Sequence boundary and lowstand systems tract

Erosionally-based, shoreface sandstone facies at Cerritos Bayos and sharp-based, lower shoreface limestone facies at Cerro San Lorenzo which directly overlie Toarcian basinal mudstone facies are interpreted to represent a basal Aalenian sequence boundary (Fig. 5.15). Four progradational parasequences recording a marked increase in the limestone:mudstone ratio and the appearance of a distinctive mono-specific benthic bivalve assemblage of *Nuculana cf. ovum*, are interpreted to

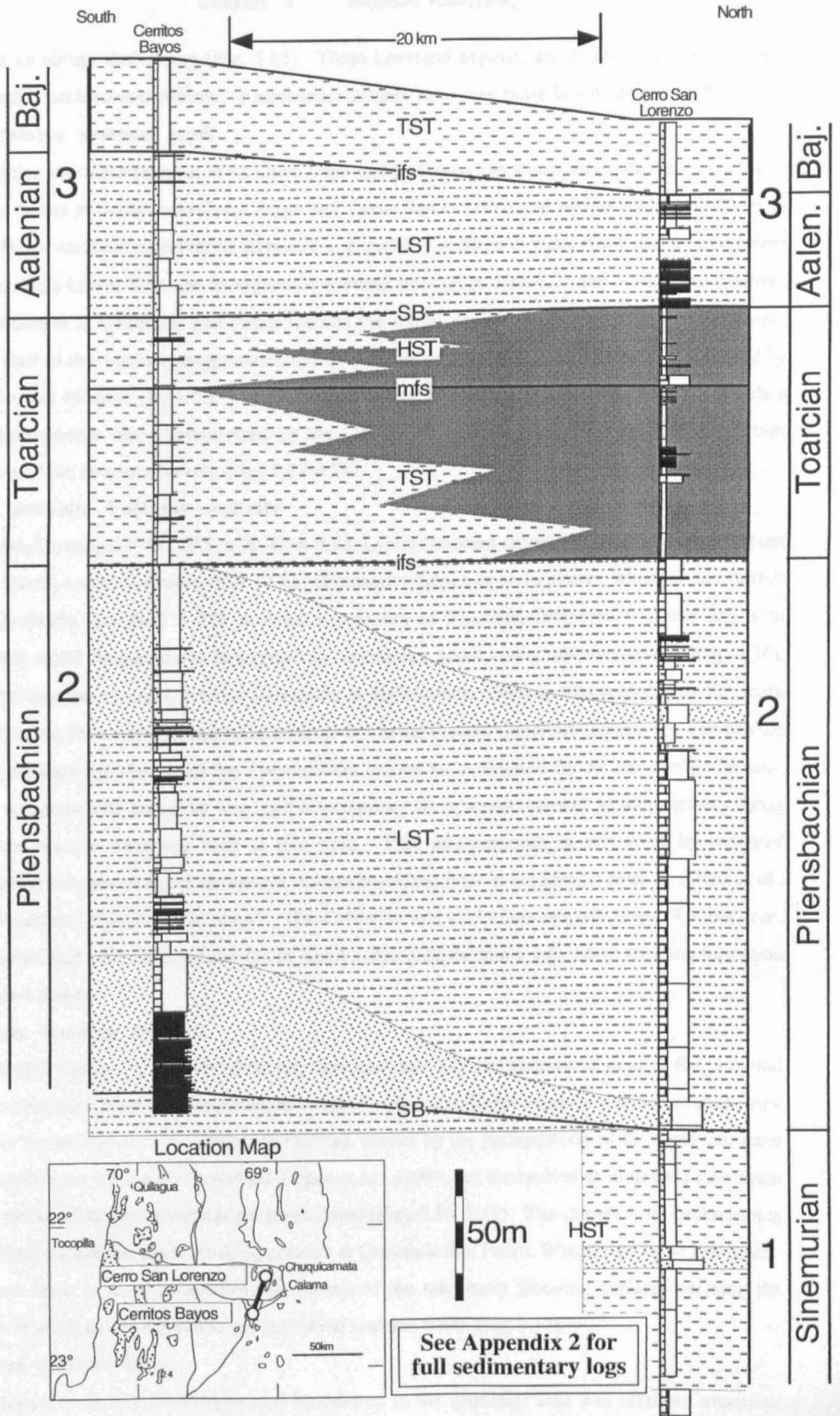


Figure 5.15 Sinemurian (Early Jurassic)-Aalenian (Middle Jurassic) correlation panel for the area between 22°-23°S.

represent an abrupt shallowing (Fig. 5.15). These lowstand deposits are distinctly coarser-grained with a higher packstone:mudstone, or sandstone:siltstone ratio than those below (Figs 5.15-5.16).

Transgressive systems tract

Backstepping shoreface facies at West Cerro Jaspe and Quebrada San Pedro, storm-dominated offshore transition facies at South-west Cerro Jaspe and Cerro San Lorenzo and offshore siltstone facies at Cerritos Bayos and Quebrada Profeta all record a progressive increase in water-depth and are interpreted to represent the Lower Bajocian transgressive systems tract (Figs 4.23-4.25 and 5.16). The shallow-marine example at Quebrada San Pedro records the initial marine transgression and transgressive systems tract as two backstepping parasequences with the upper parasequence being characterised by the *Lupherites* biozone (Figs 5.17, 5.18). The offshore succession at Quebrada Profeta records a single parasequence also characterised by the *Lupherites* biozone, thus allowing high resolution correlation of the two successions (Figs 5.17-5.19).

Middle Jurassic Volcanic Activity

In the north, between 21°40'-22°S, a 30-40 m thick Lower Bajocian submarine lava can be walked out laterally (north-south) for more than 12 km (Fernandez-Lopez *et al. in press*), while 15 km further south (Quebrada Corralas) a 225 m thick succession of Bajocian-Callovian volcanic ash with intercalated reefal limestones is interpreted to represent a small active volcanic island (Fig. 5.16). Bajocian-Callovian volcanic activity (Groschke & Hillebrandt, 1994) is also recorded in the south (25°30'S) of the Precordillera (Sierra Candeleros) and in the Coastal Cordillera (Rencoret). The Middle Jurassic volcanic activity along the Precordillera cannot be accounted for by the distant Jurassic volcanic arc, some 100 km to the west, and is interpreted to represent renewed tectonic activity along the eastern margin bounding fault at this time. This interpretation is supported by renewed transtensional movement along the eastern margin bounding fault in the Middle Jurassic (Prinz *et al.*, 1994; Fernandez-Lopez *et al. in press*). The Callovian and Oxfordian isopach maps of Prinz *et al.* (1994) record high sediment thicknesses in small isolated depocentres, consistent with the formation of pull-apart basins.

Maximum flooding surface

A deepening of facies, siliciclastic sediment starvation and a faunal abundance peak in the proximal area (Quebrada San Pedro and Cerro Jaspe) coupled with a significant depositional hiatus (condensed section) in the basinal section (Quebrada Profeta), shown by the juxtaposition of the *Lupherites* and *Stephanosphinctes* biozones (Fernandez-Lopez *et al.*, 1994), are interpreted to indicate a maximum flooding surface (Megasphaeroceras magnum Zone) (Figs 5.16, 5.17). The change from backstepping to progradational parasequence stacking patterns at Quebrada San Pedro, West Cerro Jaspe and South-west Cerro Jaspe is also a characteristic feature of the maximum flooding surface, defining the boundary between the transgressive and highstand systems tracts (Fig. 5.17).

Highstand systems tract

Progradational shoreface sandstones and limestones in the proximal area and offshore transition siltstones in Quebrada Profeta, Cerritos Bayos and Cerro San Lorenzo are interpreted to represent the progressive reduction in accommodation space within the highstand systems tract (Figs 5.16, 5.17).

The shallow-marine example at Quebrada San Pedro records the highstand systems tract as four progradational parasequences characterised by the *Stephanosphinctes* and *Strenoceras* biozones (Fig. 5.17). The offshore succession at Quebrada Profeta records five parasequences also characterised by the *Stephanosphinctes* and *Strenoceras* biozones, thus allowing high resolution correlation of the two successions (Figs 5.17-5.19).

5.5.4 Sequence 4 (Bathonian-Oxfordian)

Sequence boundary and shelf-margin systems tract

Erosionally-based, lower shoreface sandstone facies directly overlying offshore siltstone facies clearly seen in the proximal shallow-marine storm-dominated ramp sections are interpreted to represent a reduction in accommodation space and the formation of a sequence boundary (Figs 5.16, 5.17). Further evidence for a shallowing of water-depth is indicated by a change in faunal abundances from ammonite-dominant to bivalve-dominant biofacies and an increase in the degree of sediment and fossil reworking (Fernandez-Lopez *et al.*, 1994; Groschke & Hillebrandt, 1994). Non-deposition and submarine erosion in the shallow-marine proximal section at Quebrada San Pedro resulted in a depositional hiatus corresponding to the Garantiana, Parkinsoni and Zigzag ammonite Zones, spanning approximately 4.5 Ma (Fernandez-Lopez *et al.*, 1994) (Fig. 5.18). This hiatus marks the boundary between the two stages of ammonite colonisation, as discussed by Fernandez-Lopez *et al.* (1994). The time break allows us to interpret a Type-2 sequence boundary (Fig. 5.17). In the basal section (Quebrada Profeta), the influx of several closely spaced 0.3 m thick sandstones into an otherwise uninterrupted offshore mudstone succession and preservation of a complete ammonite chronology (Groschke & Hillebrandt, 1994) indicates a correlative conformity (Figs 5.17, 5.19). Aggradational lower shoreface storm-dominated facies in the proximal shallow-marine sections and thin heterolithic sandstones in the basal sections (Cerro San Lorenzo, Cerritos Bayos and Quebrada Profeta) are interpreted to represent a Bathonian shelf-margin systems tract (Fig. 5.17).

Transgressive systems tract

A landward shift in facies from the heterolithic storm-dominated sandstones of the shelf-margin systems tract to offshore siltstone facies indicates the first well defined flooding surface (Steinmanni Zone) in Sequence 4 and is interpreted as the transgressive surface separating the Bathonian shelf-margin and transgressive systems tracts (Fig. 5.17). Backstepping offshore transition and offshore siltstone facies are interpreted to represent the transgressive systems tract of Sequence 4 (Fig. 5.16, 5.17). In the north at West Cerro Jaspe (21°40'S), the transgressive systems tract is unusually thick (> 300 m). This is attributed to transtensional faulting along the eastern basin margin which results in isolated Callovian-Oxfordian depocentres (pull-apart basins) of particularly high subsidence rate, where thicknesses can reach 480 m (Prinz *et al.*, 1994).

Maximum flooding surface

Much of the Domeyko basin records Lower-Middle Oxfordian ammonite bearing black mudstone facies, representing strongly anoxic depositional conditions. These facies directly overlie yellow calcareous siltstones with a sharp, non-erosive contact, interpreted as a maximum flooding surface

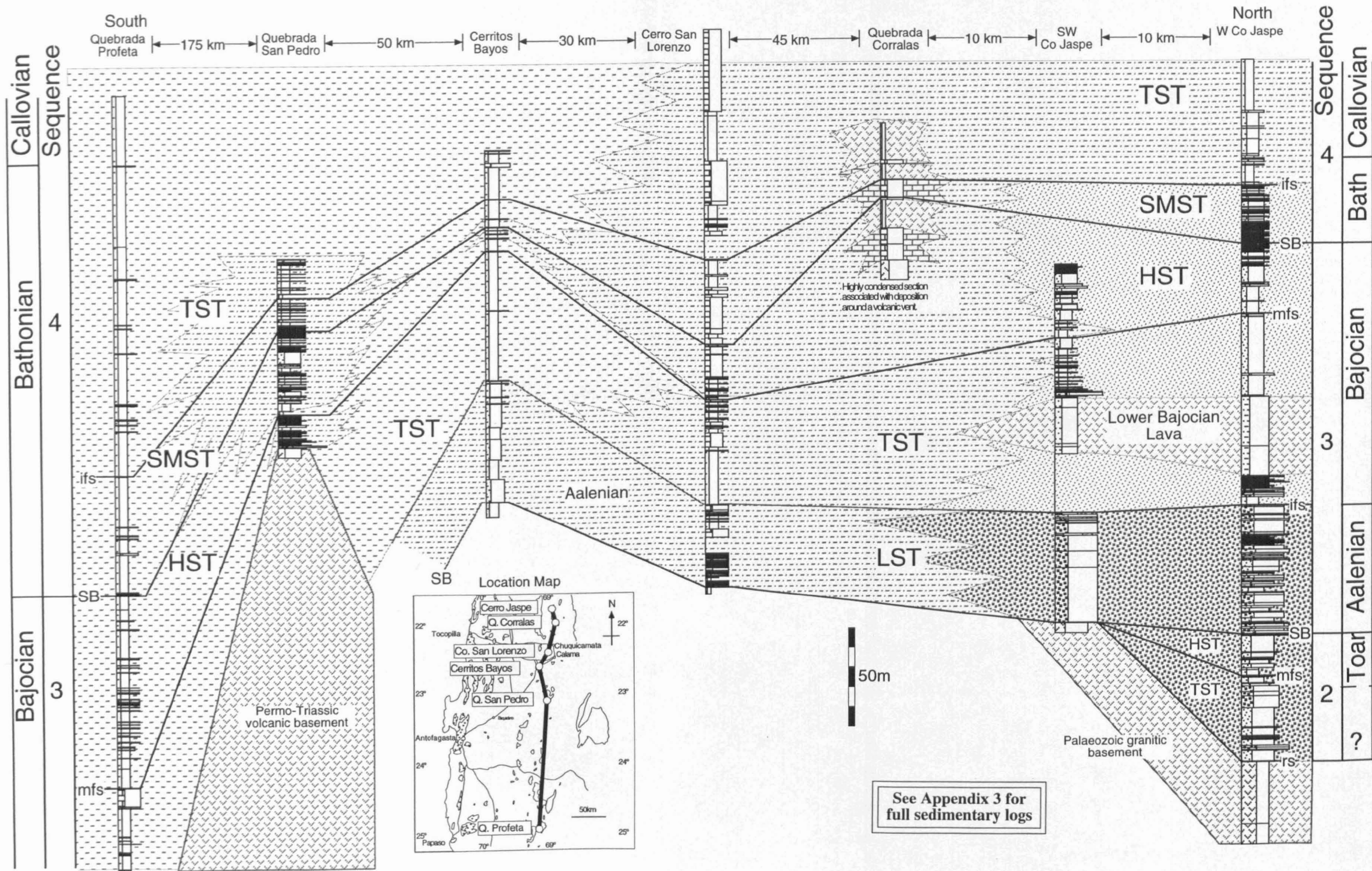


Figure 5.16 Bajocian-Bathonian (Middle Jurassic) correlation panel for the area between 21.5°-25°S.

Bajocian/Bathonian Boundary Correlation

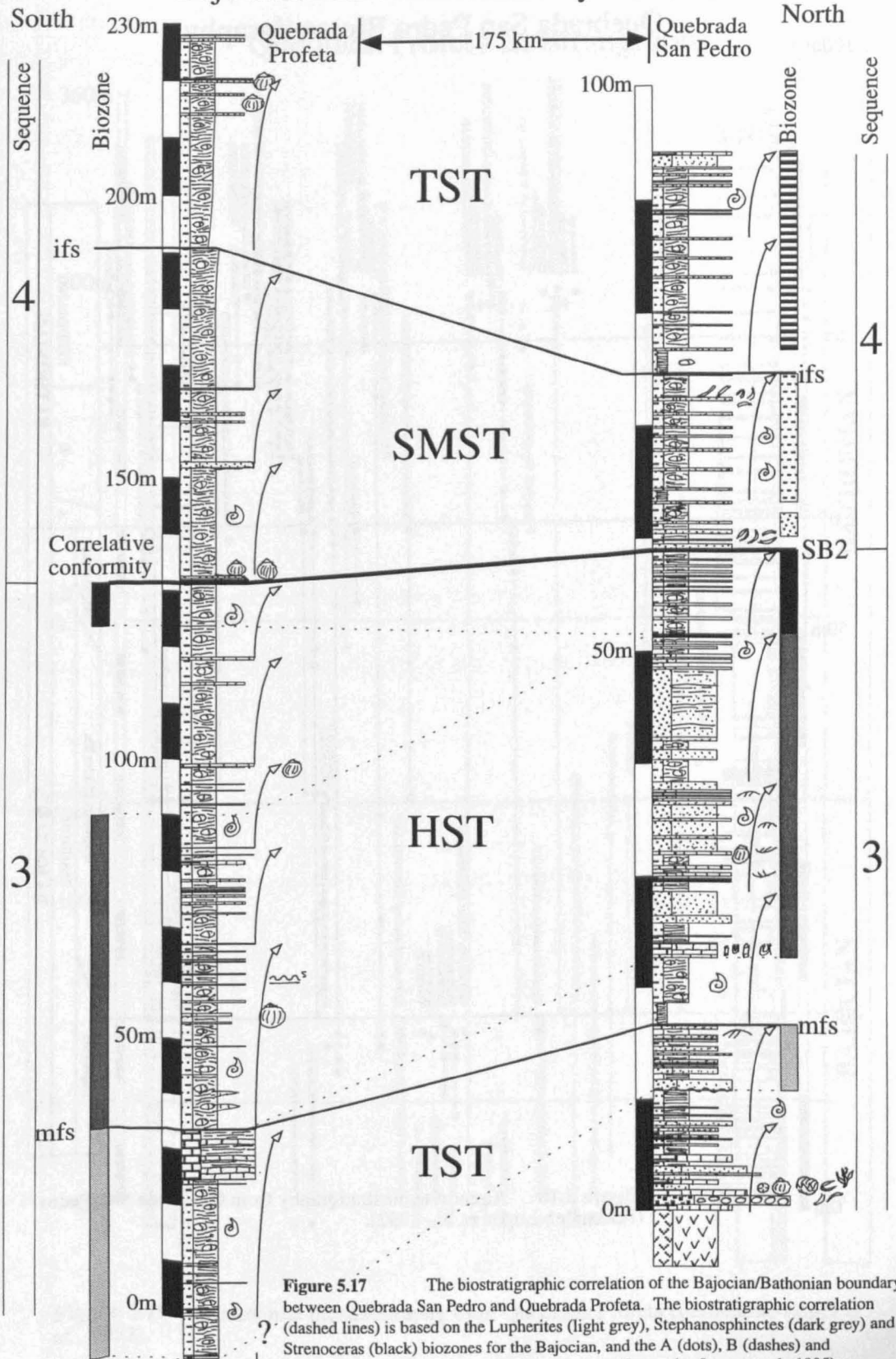


Figure 5.17 The biostratigraphic correlation of the Bajocian/Bathonian boundary between Quebrada San Pedro and Quebrada Profeta. The biostratigraphic correlation (dashed lines) is based on the *Luperites* (light grey), *Stephanosphinctes* (dark grey) and *Strenoceras* (black) biozones for the Bajocian, and the A (dots), B (dashes) and Steinmanni (stripes) biozones for the Bathonian (Fernandez-Lopez et al., 1995).

Quebrada San Pedro Biostratigraphy

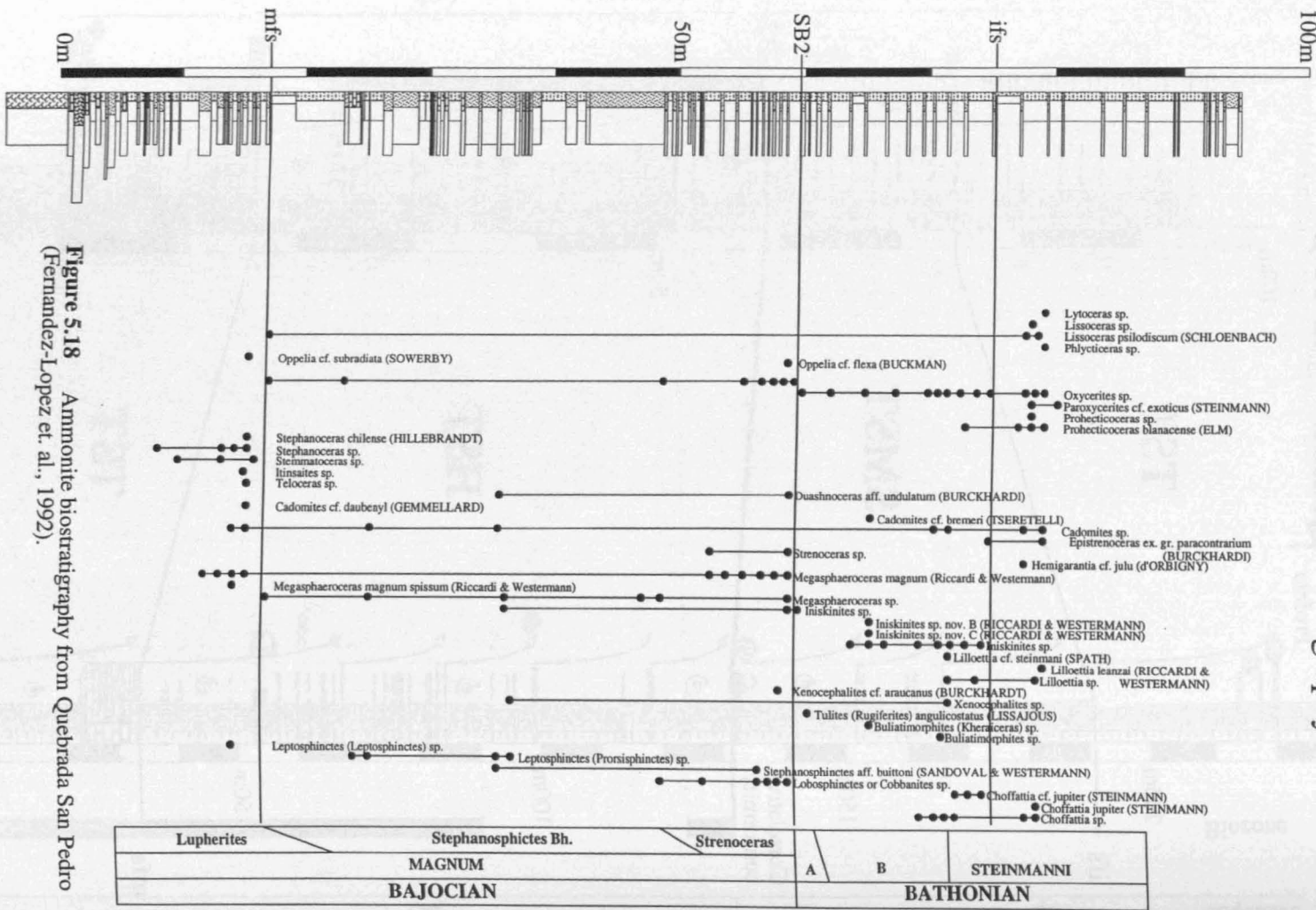


Figure 5.18 Ammonite biostratigraphy from Quebrada San Pedro (Fernandez-Lopez et. al., 1992).

Quebrada Profeta Biostratigraphy

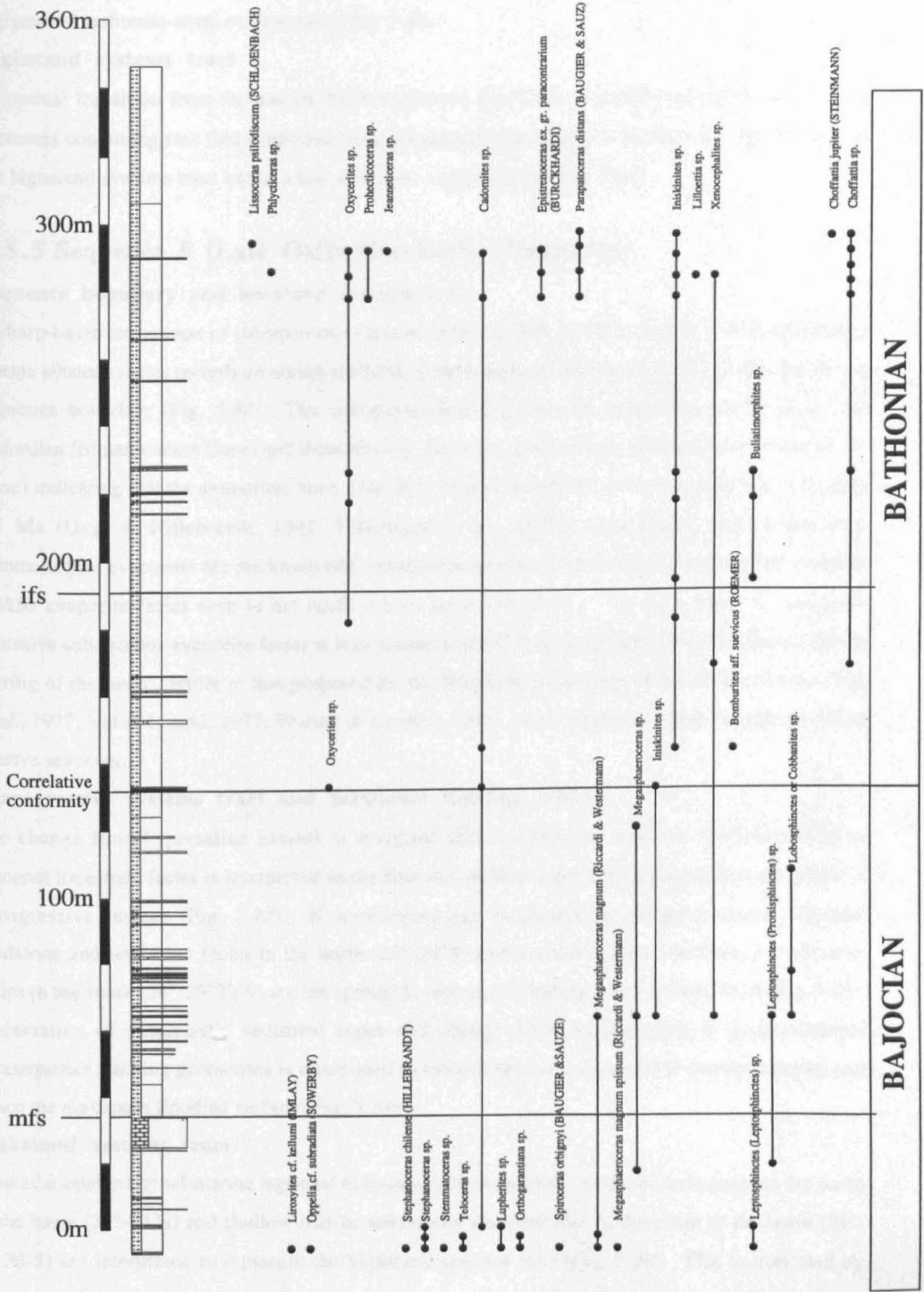


Figure 5.19 Ammonite biostratigraphy from Quebrada Profeta (Fernandez-Lopez et al., 1992).

(Fig. 5.20). In the north (West Cerro Jaspe), fine-grained yellow mudstone facies with a horizon of abundant large calcareous concretions (0.5-2 m in diameter) record the deepest marine facies and siliciclastic sediment starvation, interpreted to represent the maximum flooding surface in an oxygenated carbonate-ramp environment (Fig. 5.20).

Highstand systems tract

A gradual transition from the anoxic black mudstone facies to progradational yellow siliciclastic siltstones containing rare thin sandstone beds is interpreted to represent shallowing, characteristic of the highstand systems tract but in a low sediment supply setting (Fig. 5.20).

5.5.5 Sequence 5 (Late Oxfordian-Early Cretaceous)

Sequence boundary and lowstand systems tract

A sharp-based succession of subaqueous evaporite facies 10-200 m thick, directly overlying offshore marine siltstone facies records an abrupt shallowing and basinward shift in facies and is interpreted as a sequence boundary (Fig. 5.20). The sediments directly below the evaporites are dated as Late Oxfordian (Bimammatum Zone) and those directly above are dated as Late Kimmeridgian (Acanthicum Zone) indicating that the evaporites have a duration of five ammonite zones, spanning approximately 7.5 Ma (Gygi & Hillebrandt, 1991; Hillebrandt *et al.*, 1992). The Upper Oxfordian-Lower Kimmeridgian evaporites are predominately subaqueous basinal evaporite facies with limited marginal sabkha evaporite facies seen in the north (Cerro Jaspe, Fig. 5.20). The occurrence of regionally extensive subaqueous evaporite facies is interpreted to result from restricted marine connection due to barring of the basin, similar to that proposed for the Messinian evaporites of the Mediterranean (Hsü *et al.*, 1977; Vai & Lucchi, 1977; Warren & Kendall, 1985), hence implying a high-magnitude fall of relative sea level.

Transgressive systems tract and maximum flooding surface

The change from hypersaline basinal or marginal sabkha evaporite facies to shallow-marine or lagoonal limestone facies is interpreted as the first well defined marine flooding surface and hence, a transgressive surface (Fig. 5.20). Kimmeridgian-age, backstepping marginal-marine lagoonal sandstone and limestone facies in the north (21°-24°S) and shallow-marine sandstone and siltstone facies in the south (24°-26°30'S) are interpreted to represent a transgressive systems tract (Fig. 5.20). A cessation of siliciclastic sediment input and change from backstepping to progradational parasequence stacking geometries is interpreted to indicate the maximum rate of marine flooding and hence the maximum flooding surface (Fig. 5.20).

Highstand systems tract

Progradational marginal-marine lagoonal to hypersaline limestones (without sandstones) in the north of the basin (21°-24°S) and shallow-marine sandstones and siltstones in the south of the basin (24°-26°30'S) are interpreted to represent the highstand systems tract (Fig. 5.20). This is truncated by continental facies associated with the Early Cretaceous sequence boundary (Chong, 1977; Bogdanic, 1990). The unconformity is underlain by Upper Kimmeridgian marginal-marine facies in the north of

the basin (21°-24°S) and by Lower Cretaceous marine facies (Quebrada La Carreta) in the south of the basin (24°-26°30'S).

5.5.6 Palaeogeographical evolution and relative sea-level changes

The sequence stratigraphical analysis provides a stratigraphical framework for the understanding of palaeogeographical and chronostratigraphical development of the Domeyko basin (Figs 5.21, 5.22). The palaeogeographical development can be summarised by four maps showing the limited Late Triassic marine transgression between 23°30'-26°30'S, the continued Hettangian-Sinemurian marine transgression to the north and east, the Bajocian transgression of the Cerro Jaspe area (Early Bajocian) and Quebrada San Pedro peninsula (Late Bajocian) and the Kimmeridgian-Early Cretaceous marine to continental transition (Fig. 5.21). This progressive marine flooding to the north and east can be seen from the chronostratigraphy, highlighting the time-transgressive nature of shoreface sandstone facies and the synchronous nature of the Oxfordian-Kimmeridgian evaporite facies (Fig. 5.22).

The sequence stratigraphical analysis of the Domeyko basin succession allows the development of a Jurassic relative sea-level curve for northern Chile (Fig. 5.23). The relative sea-level curve is based on the identification of sequence boundaries and maximum flooding surfaces which define the R' and F' inflection points, respectively. The absolute magnitude of sea-level changes is difficult to measure due to a lack of abundant palaeobathymetric indicators. However, the relative magnitude of sea-level changes can be estimated on the basis of the facies juxtaposition across each particular sequence boundary and flooding surface. For example, a flooding surface which places offshore siltstones over lower-shoreface storm-dominated sandstones is interpreted to be of lower magnitude than a flooding surface which places similar offshore siltstones over marginal-marine fan-delta conglomerates. Additional biostratigraphical data which allows the identification and measurement of duration of a depositional hiatus is also interpreted to be an indicator of the relative magnitude of sea-level changes when the comparison is made between similar depositional environments. The longer duration hiatus are assigned greater relative magnitudes of sea-level change. On the basis of this approach a long-term relative sea-level curve for the five second-order sequences is presented (Fig. 5.23).

5.5 Characterisation of high-frequency third-order sequences

5.5.1 Introduction

Sequence stratigraphical evidence of second- and third-order cyclicity was presented on curves of coastal onlap and eustatic cycles (Vail *et al.*, 1977a; Haq *et al.*, 1987; 1988) (Fig. 5.3). The fundamental third-order cycle has an average duration of 1-2 Ma but may range from 0.5-5 Ma (Vail *et al.*, 1991) (Fig. 5.3). These third-order cycles are the building blocks of larger-scale cycles (second-order cycles) that have a duration of 9-10 Ma (Mitchum & Van Wagoner, 1991) (Fig. 5.3). Similarly, fourth-order cycles of duration 0.1-0.2 Ma form the building blocks of third-order cycles (Mitchum & Van Wagoner, 1991). Mitchum & Van Wagoner (1991) discussed the principle of scale-independence and gave examples of third-order composite sequences composed of fourth-order sequences, preserved in

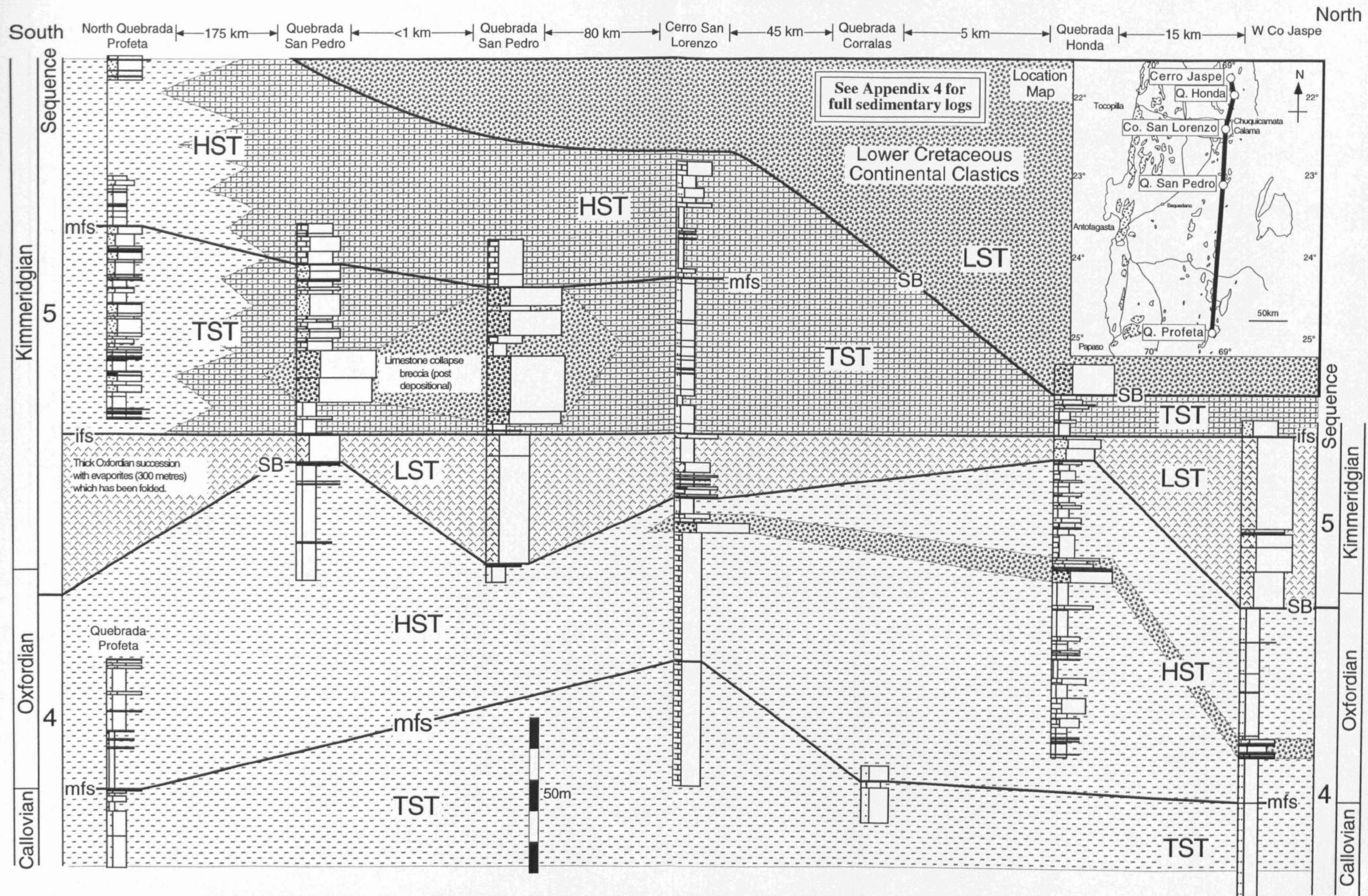


Figure 5.20 Oxfordian-Kimmeridgian (Late Jurassic) correlation panel for the area between 21.5°-25°S.

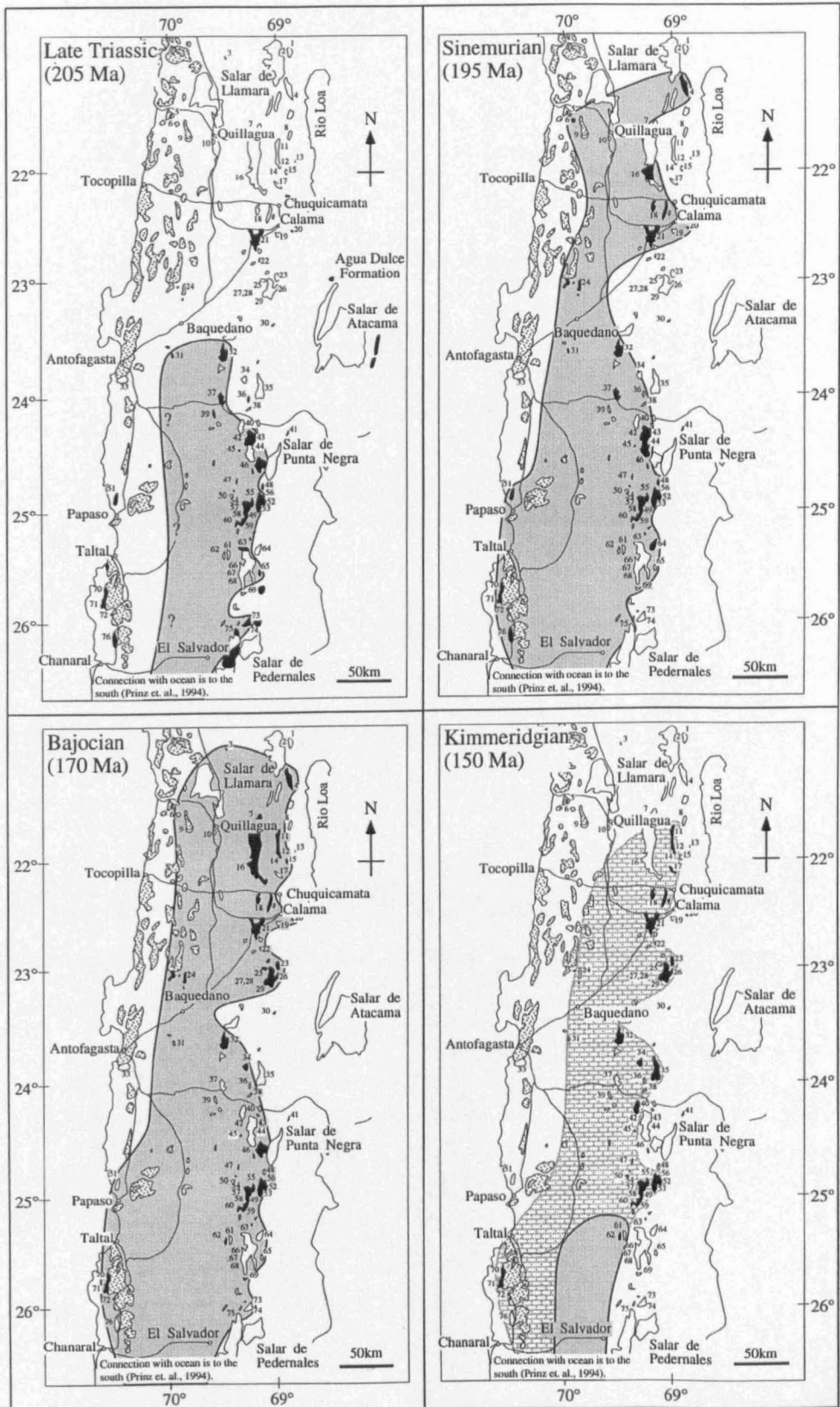


Figure 5.21 Palaeogeographic reconstructions for the: 1. Late Triassic; 2. Sinemurian; 3. Bajocian; and 5. Kimmeridgian of northern Chile. Absolute ages of stage boundaries and durations of stages are taken from Gradstein et al., (1994).

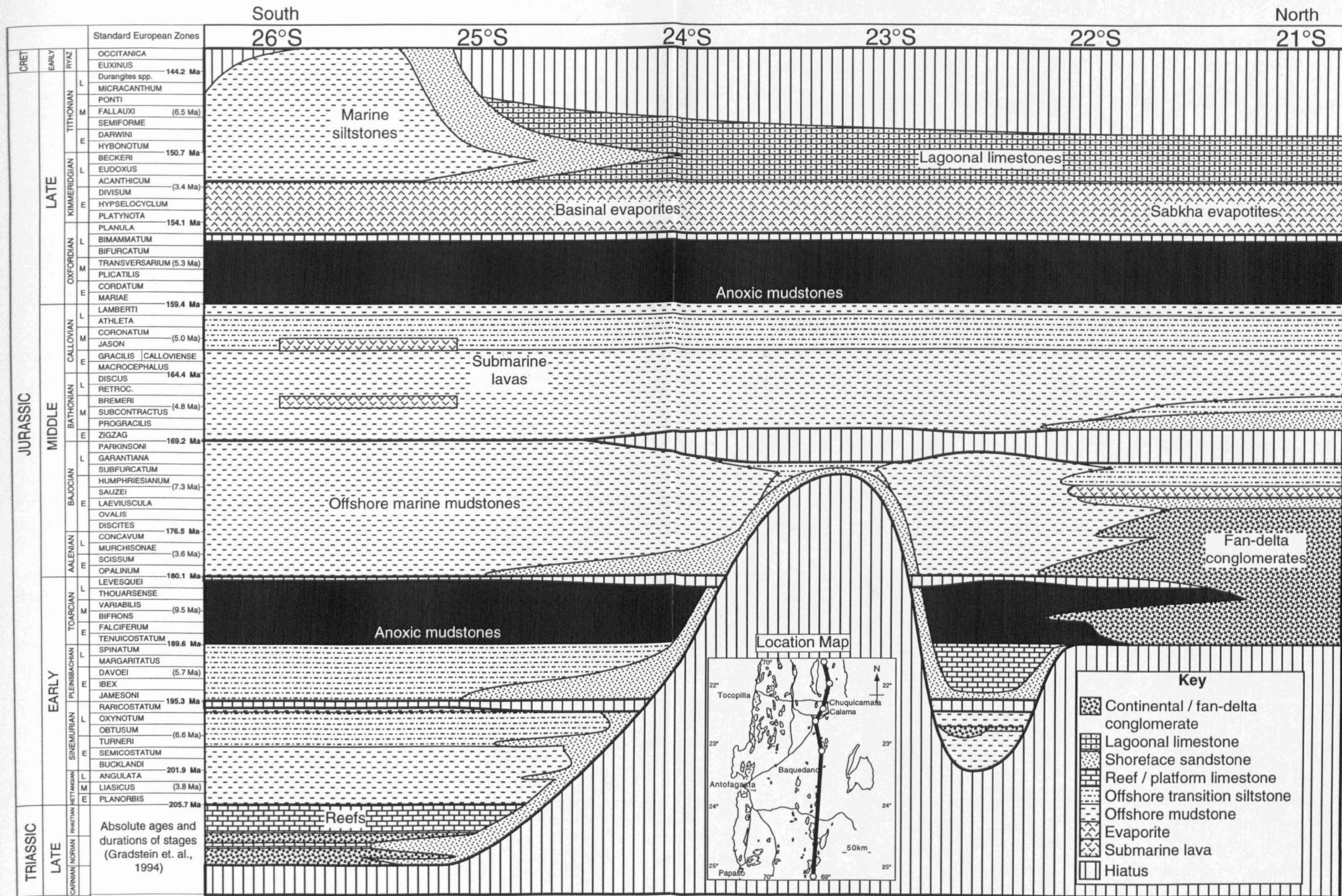


Figure 5.22 Chronostratigraphy of the Domeyko basin from Late Triassic-Early Cretaceous. Absolute ages of stage boundaries and durations of stages are taken from Gradstein et al., (1994).

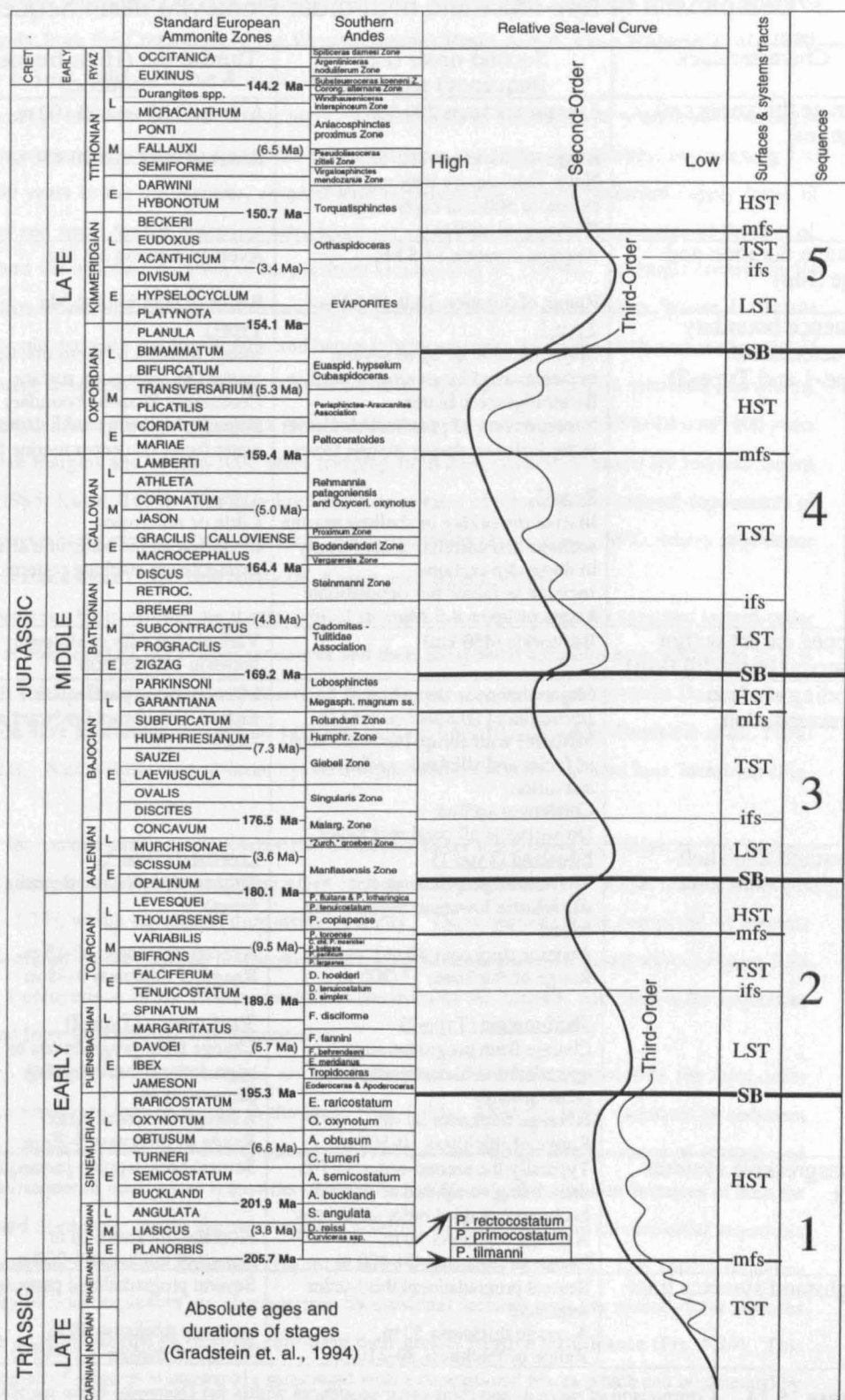


Figure 5.23 Jurassic relative sea-level changes in northern Chile. Absolute ages of stage boundaries and durations of stages are taken from Gradstein et al., (1994).

Comparison of low-order and high-order Domeyko basin Sequences

Characteristics	Second-order (Low-frequency) sequence	Third-order (High-frequency) sequence
Average thickness and range (m)	Average thickness 200-300 m Range of thickness 112-520 m Note: Thicknesses may reach in excess of 500m in depocentres (Prinz et. al. 1994)	Average thickness 50-100 m Range of thickness 20-150 m
Average duration and range (Ma)	Average duration 14.5 Ma Range of duration 10.9-17.1 Ma	Average duration 3.5 Ma Range of duration 2-5 Ma
Sequence boundary characterisation (Type-1 and Type-2)	Type-1 Major incision of up to several metres marked by an erosion surface Biostratigraphic hiatus Superposition of proximal/shallower water facies on deeper marine facies Type-2 Marine reworking in shallow-marine sections and correlative conformity in down-dip sections Incision is minor but depositional hiatus of up to 4.5 Ma	Type-1 Minor incision of up to one metre marked by an erosion surface Commonly Biozone boundary Superposition of proximal/shallower water facies on deeper marine facies Type-2 Little or no erosion Identified on the basis of a change in parasequence stacking patterns
Mapped extent within preserved basin-fill (km)	Basinwide (450 km)	Variable but with confidence between 100-450 km
Flooding surface characterisation	Major change in depositional environment (shallow-marine to offshore) with abrupt landward shift of facies and siliclastic sediment starvation Condensed section Drowning of all coral reef facies	Most landward parasequence flooding surface with abrupt landward shift of facies
Lowstand and shelf-margin system tract	Lowstand (Type-1) Well-developed thick sandy siliclastic lowstand deposits (eg. facies) Average thickness 50 m Range of thickness 15-200 m Shelf-margin (Type-2) Change from progradation to aggradational-backstepping parasequences Average thickness 30 m Range of thickness 10-167 m	Lowstand (Type-1) Thin sandy lowstand deposits (eg. facies) Average thickness 10-15 m Range of thickness 3-75 m Shelf-margin (Type-2) Change from progradation to aggradational-backstepping parasequences Average thickness 10 m Range of thickness 5-20 m
Transgressive systems tract	Typically the second-order TST is thick being composed of several backstepping third-order sequences Average thickness 70 m Range of thickness 50-400 m	Several backstepping parasequences Average thickness 20 m Range of thickness 5-200 m
Highstand systems tract	Several progradational third-order sequences Average thickness 50 m Range of thickness 30-210 m	Several progradational parasequences Average thickness 30 m Range of thickness 10-45 m

Figure 5.24 Comparison of second- and third-order sequences within the Domeyko basin succession.

areas of rapid subsidence and high sedimentation rates. Fourth-order sequences have been described extensively from the Cretaceous of the Western Interior Basin, U.S.A. (Van Wagoner *et al.*, 1990; Mellere & Steel, 1995; O'Byrne & Flint, 1995).

The Domeyko basin succession records highly variable rates of sediment and water loaded basement subsidence commonly ranging from 5-20 mm/1000 years out of the depocentres, but reaching 110 mm/1000 years in the depocentres, coupled with relatively low rates of sediment supply (rates of sediment and water loaded basement subsidence are calculated using the thicknesses of Prinz *et al.* (1994) and the absolute duration of stages from Gradstein *et al.* (1994)). A simple correction for compaction based on lithology and following the porosity functions presented by Sclater & Christie (1980) would decrease the thicknesses, and hence subsidence rates by 40 %. Such a correction would give average decompacted subsidence rates of 2-8 mm/1000 years, reaching 44 mm/1000 years in the depocentres. These average subsidence rates are relatively low when compared to 10 mm/1000 years for passive margins and 33 mm/1000 years (ranging from 23-43 mm/1000 years) for foreland basins (Cross, 1986; Kukul, 1990). The very high subsidence rates observed in the isolated depocentres of the Domeyko basin are thought to represent pull-apart basins (Prinz *et al.*, 1994), where subsidence rates can exceed those of foreland basins (N. Kusnir pers. comm., 1996).

In the Domeyko basin setting, the stratigraphical succession could be expected to record second-order sequences composed of third-order sequences and their component parasequences (Mitchum & Van Wagoner, 1991). The five previously described second-order sequences composing the Domeyko basin succession have an average duration of 14.5 Ma, ranging from 10.9-17.1 Ma (Gradstein *et al.*, 1994) (Fig. 5.23). Within these second-order cycles a higher-order cyclicity has also been identified (Fig. 5.23).

Each of the second-order sequences in the Domeyko basin is composed of three to five higher-frequency sequences. Simple averaging gives each an average duration of 3.5 Ma, ranging from 2-5 Ma (Fig. 5.23), which equates to third-order cyclicity. These sequences are composed of systems tracts, identified on the basis of parasequence stacking patterns and facies-tract shifts. Figure 5.24 presents a comparison of the fundamental characteristics of the second- and third-order sequences interpreted from the Domeyko basin succession.

Typically, the second-order sequences are hundreds of metres thick as opposed to the third-order sequences which are tens of metres in thickness (Fig. 5.24). Although large variations in sediment thickness are seen within the basin (Prinz *et al.*, 1994), at any one section the range of second- and third-order sequence thicknesses is an order of magnitude different. The absolute durations of both the second- and third-order cycles are quite regular, resulting in the longer-term second-order sequences being composed of between three and five third-order sequences (Fig. 5.24). The Type-1 sequence boundaries of both sequences are characterised by erosional incision with the second-order surfaces recording a greater degree of incision, reflecting their greater relative significance (Fig. 5.24). This greater degree of incision is commonly associated with a depositional hiatus which can be detected by missing ammonite zones. Sequence 4 is the only second-order Type-2 sequence interpreted within the Domeyko basin succession, characterised by a change in parasequence stacking patterns from

progradational to aggradational with a depositional hiatus spanning three ammonite zones (4.5 Ma) (Fernandez-Lopez *et al.*, 1994). The third-order Type-2 sequences are identified solely on the basis of a change in parasequence stacking patterns and any depositional hiatus is beyond local biostratigraphical resolution (Fig. 5.24). All the second-order surfaces can be mapped throughout the basin (over a distance of 450 km) with confidence, while the third-order surfaces are readily observed in the shallow-marine environments but are sometimes difficult to detect in the deeper marine environments. This problem results from the lower-magnitude third-order relative sea-level changes being recorded as the correlative conformity with no physical expression in the offshore environment. The character of the flooding surfaces in both second- and third-order sequences is similar but the magnitude of second-order rises is much greater, resulting in siliciclastic sediment starvation, abrupt landward shift in facies and juxtaposition of different depositional environments (ie. offshore marine facies overlying fan-delta facies) (Fig. 5.24).

In the following two examples we consider stacked third-order sequences and their internal characteristics on the basis of their position within the longer-term second-order sequence (Fig. 5.24). In particular, by studying the high resolution anatomy of second-order Sequences 1 and 4 it has been possible to characterise the component third-order sequences (Fig. 5.24). The examples demonstrate the nature of the two scales of cyclicity and their interaction which results in a second-order composite sequence, but does not produce the "typical" sequence-sets (*sensu* Mitchum & Van Wagoner, 1991) normally associated with composite sequences. A full analysis of all seventeen identified high-frequency sequences and their parasequences is beyond the scope of this thesis.

5.5.2 High resolution anatomy of Sequence 1

The Upper Triassic transgressive systems tract of Sequence 1 is composed of three backstepping third-order sequences (transgressive sequence-set) overlain by the earliest Hettangian second-order maximum flooding surface and Hettangian-Sinemurian second-order highstand systems tract, composed of two third-order sequences which show a gross progradational trend, interpreted as a highstand sequence-set (*sensu* Mitchum & Van Wagoner, 1991).

Sequence 1: Transgressive sequence-set

The transgressive sequence-set contains three backstepping third-order sequences, herein named 1.1, 1.2 and 1.3, deposited in basin margin fan-delta settings (Quebrada Vaquillas & Punta del Viento) and down-dip (north-west), in a shallow-marine carbonate-ramp setting (Sierra Argomedo) (Fig. 5.25).

Sequence 1.1

Sequence 1.1 is unusually thick, composed of 100-130 m of aggradational to backstepping coarse-grained conglomerate facies which is overlain by 20-50 m of similar backstepping conglomerates with intercalated medium- to coarse-grained wave-rippled sandstone and in-situ coral limestone facies (Fig. 5.25). The substantial sediment thickness is interpreted to result from high rates of deposition characteristic of fan-delta systems in an active tectonic setting, coupled with increasing accommodation space during a long-term rise in relative sea-level. These deposits are interpreted to

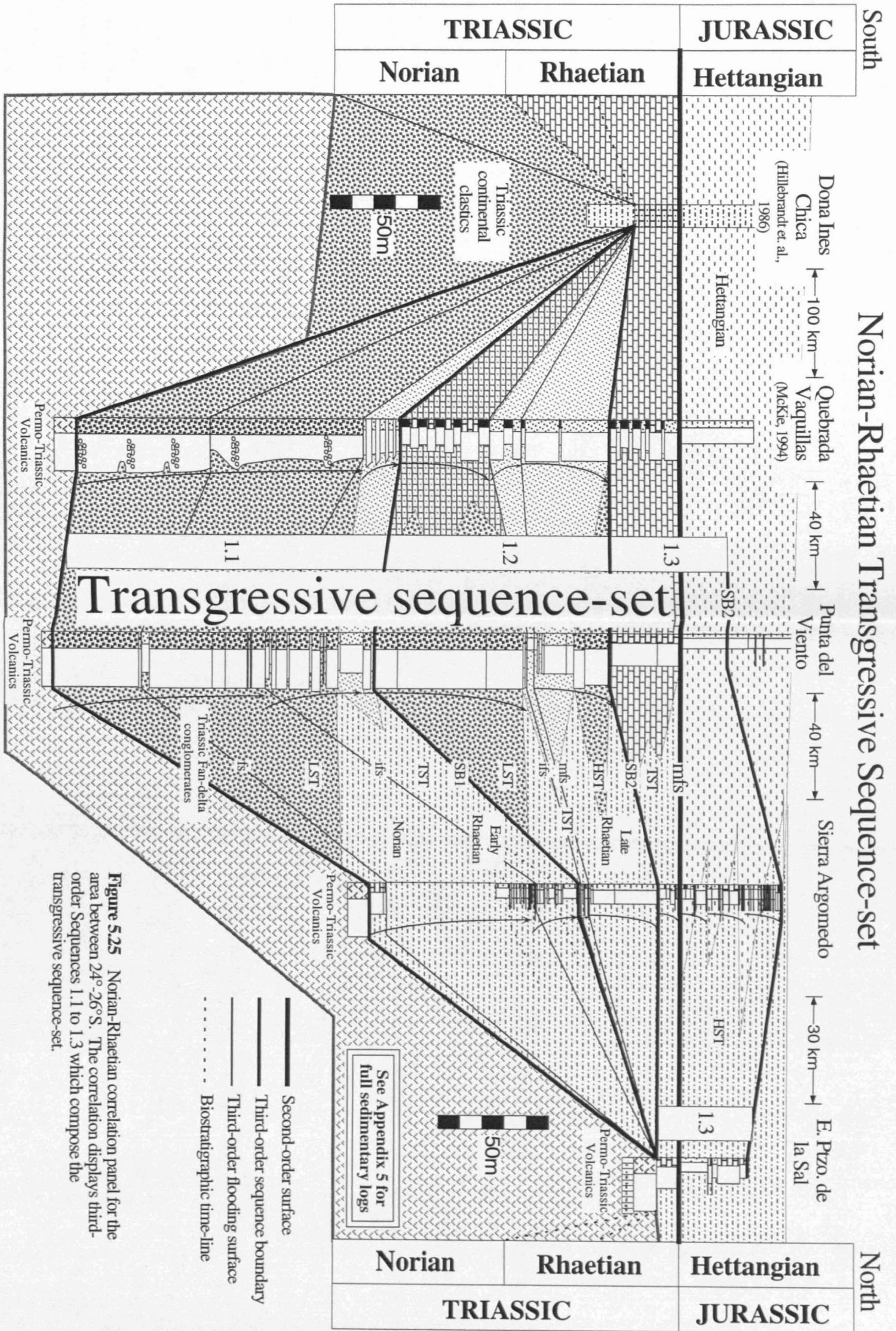


Figure 5.25 Norian-Rhaetian correlation panel for the area between 24°-26°S. The correlation displays third-order Sequences 1.1 to 1.3 which compose the transgressive sequence-set.

represent the late-lowstand and transgressive systems tracts of Sequence 1.1. At Sierra Argomedo, time-equivalent backstepping heterolithic limestone parasequences record the initial marine transgression and a progressive deepening in the Norian (Fig. 5.25). There appears to be no preservation of highstand deposits.

Sequence 1.2

A 70 m thick unit of erosionally-based conglomerates (Punta del Viento) and 40 m thick unit of progradational lagoonal limestone facies (Quebrada Vaquillas) record an abrupt basinward shift in facies marking the sequence boundary and lowstand systems tract of third-order Sequence 1.2 (Fig. 5.25). These lowstand deposits are overlain by a 40-50 m thickness of medium- to coarse-grained wave-rippled sandstone and coral limestone facies recording a thin transgressive systems tract, maximum flooding surface and thick highstand systems tract. Down-dip, a 1 m thick bed of coarse-grained gravelly sandstone with trough cross-bedding is interpreted to record the formation of a sequence boundary, with overlying siltstones and heterolithic limestones recording the transgressive and highstand systems tracts, respectively (Fig. 5.25).

Shelf-margin and transgressive systems tracts of Sequence 1.3

A 30 m thick unit of coral reef (*Thecosmilia*) and thin wave-rippled siliciclastic sandstone facies indicates renewed marine transgression and shallow-marine conditions (Fig. 5.25). This unit is interpreted as the shelf-margin and transgressive systems tracts of Type-2 Sequence 1.3 and is overlain by offshore marine mudstones indicating an abrupt landward shift in facies, the maximum flooding surface. This surface records the drowning of all coral reefs and the most landward facies shift seen in the Norian-Sinemurian, and hence is assigned second-order significance (Figs 5.23, 5.25).

In the fan-delta environment, the backstepping Sequences, 1.1-1.3, record an increasingly important influence of transgression in the form of thin intercalated shallow-marine limestone and wave-rippled sandstone facies, interpreted to represent the transgressive sequence-set of second-order Sequence 1 (Fig. 5.25). The fan-delta succession records an overall rise in relative sea-level with superimposed fall (Sequence 1.2) and overlying stillstand without significant fall (Sequence 1.3), supporting the R_s and R_f architectural models of Postma (1995), respectively.

Sequence 1: Highstand sequence-set

Overlying the second-order maximum flooding surface is the Hettangian-Sinemurian highstand sequence-set, composing of the highstand systems tract of Sequence 1. This 75-95 m thick succession includes three third-order Sequences, 1.3, 1.4 and 1.5 (Fig. 5.26).

Highstand systems tract of Sequence 1.3

At Sierra Argomedo, ammonite bearing offshore siltstones and storm-dominated sandstones of 50 m thickness compose three progradational parasequences and are interpreted to form the Hettangian-age highstand systems tract of Sequence 1.3 (Fig. 5.26).

Sequence 1.4

The storm-dominated sandstones of the highstand are overlain by backstepping offshore transition siltstones (Sierra Argomedo) which indicate renewed transgression and are interpreted to represent the

shelf-margin and transgressive systems tracts of Type-2 Sequence 1.4 (Fig. 5.26). This 20 m thick unit of offshore siltstones contains the Hettangian-Sinemurian Stage-boundary. The presence of a condensed horizon overlain by a 10 m thick unit of fine-grained marine mudstones records an abrupt landward shift in facies and is interpreted as the maximum flooding surface and overlying early highstand of Sequence 1.4 (Fig. 5.26).

Sequence 1.5

A 3-13 m thick unit of erosionally-based storm-dominated sandstones and sandy limestones directly overlying the mudstones indicates an abrupt lowering of mean storm wave-base and is interpreted to represent the sequence boundary and lowstand systems tract of Sequence 1.5 (Fig. 5.26). Overlying these sandstones is a 10 m thick unit of heterolithic sandy limestones with an abrupt transition into 10 m of fine-grained mudstones, interpreted to represent the transgressive systems tract and maximum flooding zone, respectively. The subsequent deposition of progradational storm-dominated sandy limestones is interpreted to represent a progressive lowering of accommodation space, indicative of the highstand systems tract (Fig. 5.26).

5.5.2 High resolution anatomy of Sequence 4

The Bathonian-Oxfordian second-order Sequence 4 is bounded at the base by the basal Bathonian sequence boundary and at the top by the Late Oxfordian sequence boundary, with a Middle Bathonian shelf-margin sequence-set, Upper Bathonian-Callovian transgressive sequence-set and Lower-Middle Oxfordian highstand sequence-set (Figs 5.27, 5.28). The second-order Sequence 4 is composed of four third-order Sequences, 4.1-4.4.

Sequence 4: Shelf-margin sequence-set

Shelf-margin and transgressive systems tract of Sequence 4.1

Erosionally-based aggradational to backstepping lower shoreface storm-dominated sandstones in the shallow-marine sections (West Cerro Jaspe & Quebrada San Pedro) and thin heterolithic sandstones in the basinal sections are interpreted to represent the shelf-margin and transgressive systems tracts of third-order Type-2 Sequence 4.1. These sandy deposits are overlain by offshore marine siltstones of Late Bathonian age interpreted to represent the maximum flooding surface (Steinmanni Zone) and subsequent muddy highstand systems tract of third-order Sequence 4.1.

On a second-order time-scale, this maximum flooding surface (Steinmanni Zone) marks the first well-defined flooding surface associated with a general change from sandy storm-dominated deposits to muddy offshore deposits, and hence is interpreted to represent the marine flooding surface of second-order Sequence 4.

Hettangian-Sinemurian Highstand Sequence-set

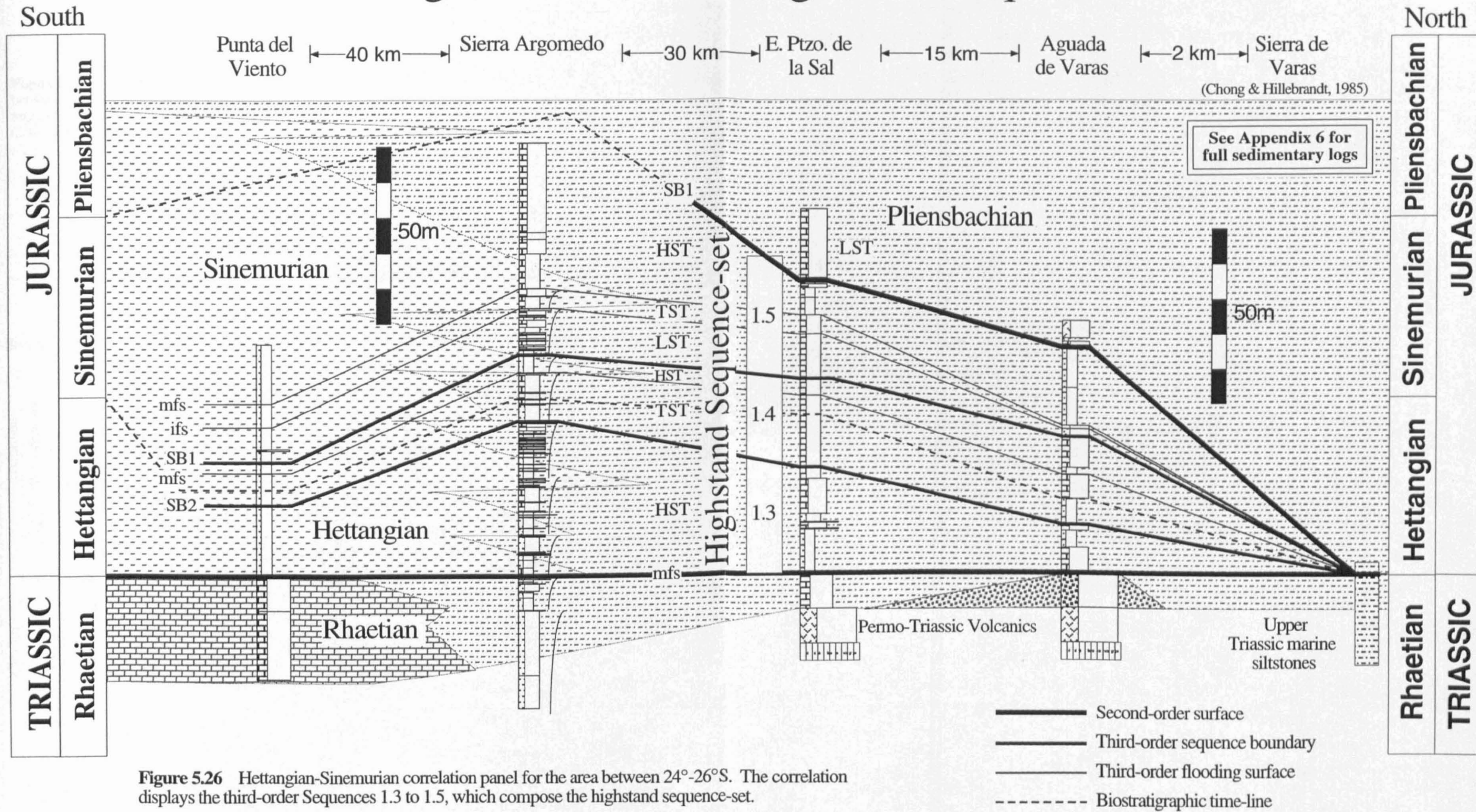


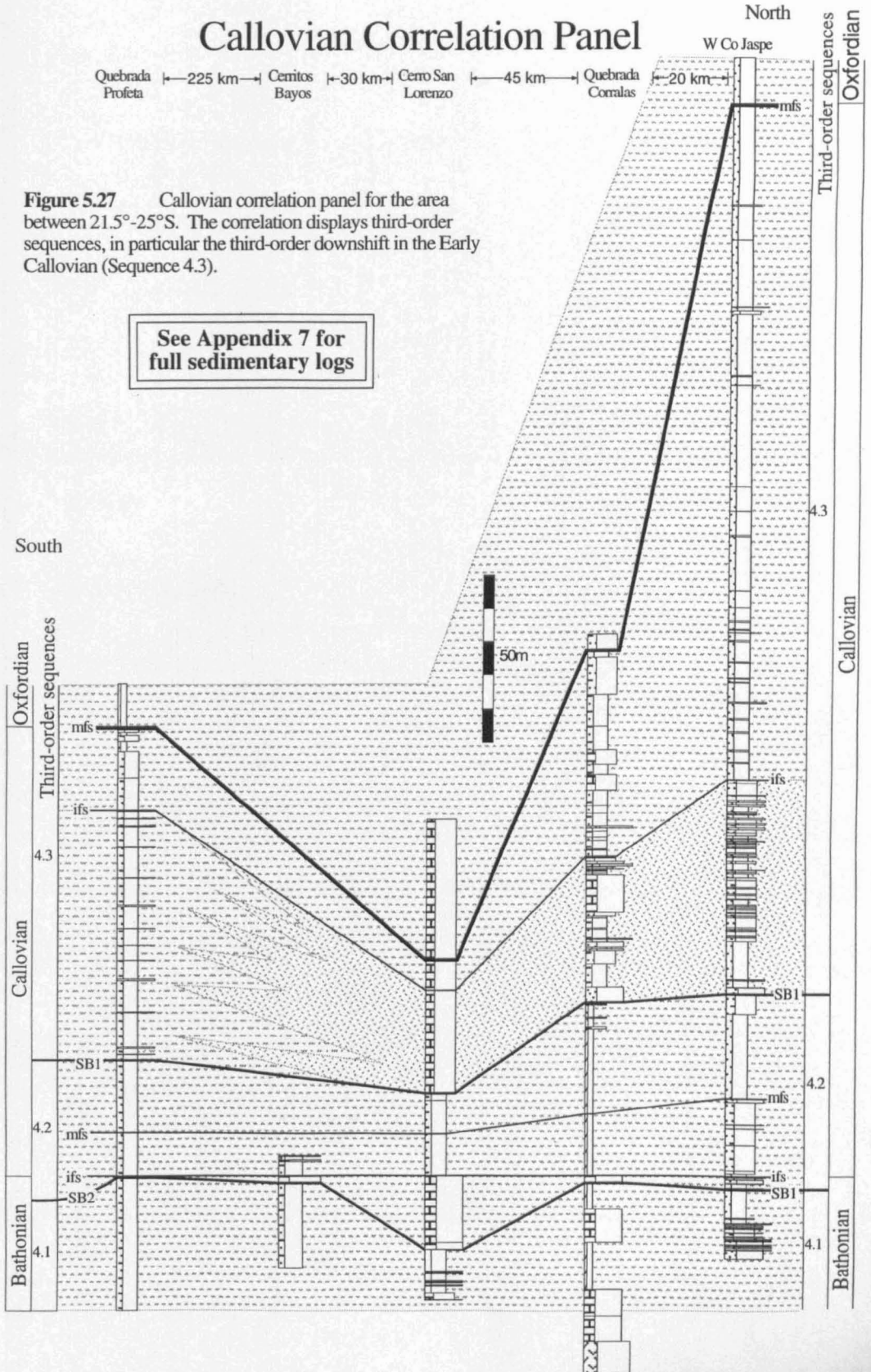
Figure 5.26 Hettangian-Sinemurian correlation panel for the area between 24°-26°S. The correlation displays the third-order Sequences 1.3 to 1.5, which compose the highstand sequence-set.

Callovian Correlation Panel

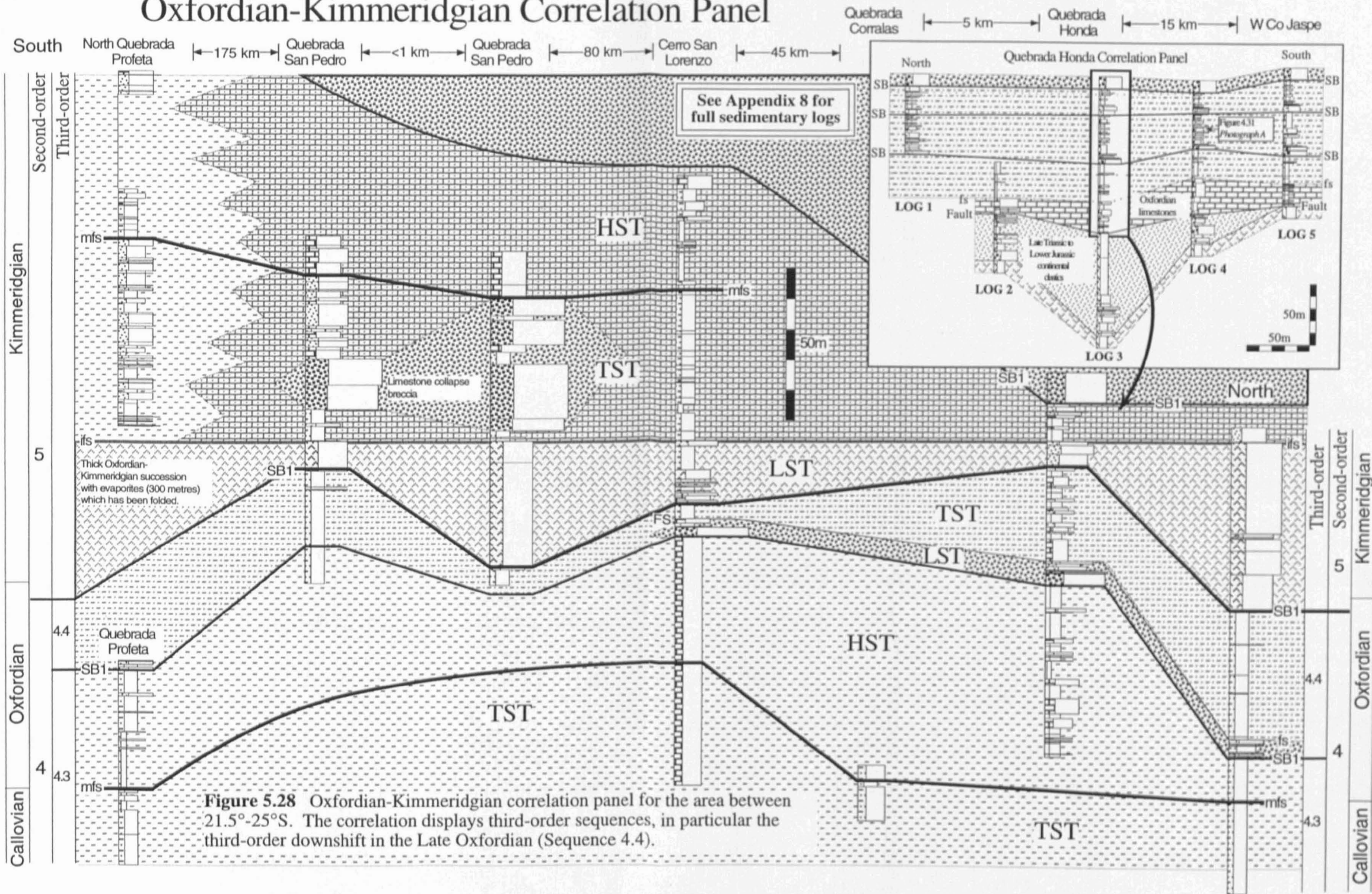
Quebrada Profeta ← 225 km → Cemitos Bayos ← 30 km → Cerro San Lorenzo ← 45 km → Quebrada Corralas ← 20 km → North
W Co Jaspe

Figure 5.27 Callovian correlation panel for the area between 21.5°-25°S. The correlation displays third-order sequences, in particular the third-order downshift in the Early Callovian (Sequence 4.3).

See Appendix 7 for full sedimentary logs



Oxfordian-Kimmeridgian Correlation Panel



Sequence 4: Transgressive sequence-set**Highstand systems tract of Sequence 4.1.**

Overlying the Steinmanni Zone maximum flooding surface are Upper Bathonian muddy marine siltstones ranging from 15-50 m in thickness, interpreted to characterise the highstand systems tract of Sequence 4.1.

Sequence 4.2

Up to 20 m of erosionally-based sandstones and sandy limestones overlying offshore calcareous mudstones at West Cerro Jaspe and Cerro San Lorenzo are interpreted to record the formation of a sequence boundary and overlying Upper Bathonian lowstand systems tract of Sequence 4.2. Overlying Lower Callovian sandy siltstones of 12-25 m in thickness are interpreted to represent an initial marine flooding surface and overlying transgressive systems tracts. The Bathonian-Callovian Stage boundary is coincident with this marine flooding surface. The sandy siltstones of the transgressive systems tract are abruptly overlain by up to 30 m of offshore mudstones which are thought to record the maximum flooding surface and overlying highstand systems tract of Sequence 4.2.

Lowstand and transgressive systems tract of Sequence 4.3

Erosionally-based heterolithic sandstones and sandy limestones of 50-60 m thickness overlying offshore calcareous mudstone facies are interpreted to represent an abrupt basinward shift in facies and record the lowstand systems tract of Sequence 4.3 (Fig. 5.27). To the south at Quebrada Profeta, a 70 m thick unit of storm-derived heterolithic sandstones and sandy limestones is interpreted to record the sequence boundary as a correlative conformity in the deep basin (Fig. 5.27). This third-order sequence boundary can be correlated with confidence for 450 km within the basin, but is not associated with any measurable biostratigraphical hiatus (Fig. 5.27). The progradational lowstand sandstones are overlain by backstepping offshore heterolithic siltstones indicating the first well defined marine flooding and have been interpreted to record the marine flooding surface and overlying transgressive systems tract of Sequence 4.3 (Fig. 5.27). The Callovian transgressive deposits of Sequence 4.3 record up to 200 m of fine-grained marine siltstones in the depocentres, with no apparent basinward shifts in facies (Prinz *et al.*, 1994). The marine siltstones are overlain by anoxic black shales of Early Oxfordian age, interpreted to indicate the maximum flooding surface of Sequence 4.3 and second-order maximum flooding surface of Sequence 4 (Fig. 5.27).

Sequence 4: Highstand sequence-set**Highstand systems tract of Sequence 4.3**

The Lower Oxfordian anoxic black shale facies display a gradual transition to more sandy progradational yellow siltstone facies with rare thin sandstones (Cerritos Bayos, Caracoles & Quebrada Profeta), interpreted to indicate a progressive shallowing characteristic of the highstand systems tract (Fig. 5.28).

Sequence 4.4

A distinctive 10 m thick unit of erosionally-based coarse-grained siliciclastic sandstone and conglomerate facies can be correlated with confidence for 85 km between 21.5°-22.5°S and possibly up

to 450 km (Quebrada Profeta), interpreted to represent sequence boundary 4.4 (Fig. 5.28). The conglomerates are overlain by aggradational to backstepping heterolithic sandstones and siltstones indicating renewed marine flooding during the transgressive systems tract (Fig. 5.28). It is not possible to confidently identify a maximum flooding surface and a highstand systems tract may have been erosionally removed by the overlying second-order sequence boundary. I interpret the lowstand conglomerates of Sequence 4.4 to record the initial stages of second-order relative sea-level fall; however, the maximum rate of relative sea-level fall and hence second-order sequence boundary formation does not occur until the Late Oxfordian sequence boundary and subsequent lowstand evaporites of Sequence 5 (Fig. 5.23). Sequence 4.4 could therefore be regarded as a second-order falling stage systems tract (Hunt & Tucker, 1992).

5.5.4 Third-order sequences and relative sea-level change

In the above examples, third-order sequences can be seen to stack in a characteristic pattern controlled by the longer-duration, second-order sequence. The relative significance of each high-frequency third-order surface can be identified, with the most significant high-frequency surfaces indicating the longer-term second-order surfaces (Fig. 5.29). Figure 5.29 shows an example of the transgressive and highstand sequence-sets from second-order Sequence 1. The relative sea-level curve displays the progressive changes in accommodation space associated with third-order sequence development during the longer-term second-order cycle (Fig. 5.29). The changing character of the third-order sequences is summarised in Fig. 5.30. The detailed analysis of second-order Sequences 1 and 4 within the Domeyko basin succession has permitted the development of a higher-order relative sea-level curve for these time-intervals, the Norian to Sinemurian and Bathonian to Late Oxfordian.

5.6 Summary

- (1) Sequence stratigraphical analysis of the Domeyko basin succession has permitted the identification and characterisation of both sequence boundaries and flooding surfaces, defining five second-order sequences. The correlation of these chronostratigraphical surfaces, constrained within the ammonite biostratigraphy, has allowed an analysis of both the stratigraphical evolution of the Domeyko basin succession and subsequently second-order changes in relative sea-level.
- (2) The Domeyko basin mixed carbonate and siliciclastic ramp environment is characterised by the deposition of siliciclastic-dominated successions at times of low accommodation space (lowstand and late highstand systems tracts) and carbonate-dominated successions during periods of high accommodation space (transgressive and early highstand systems tracts).
- (3) Second-order relative sea-level falls in the earliest Pliensbachian, earliest Aalenian, earliest Bathonian, Late Oxfordian, earliest Valanginian, and rises in the earliest Hettangian, earliest and Late Toarcian, Early and Late Bajocian, Late Bathonian, earliest Oxfordian and Late Kimmeridgian have been identified within the Domeyko basin succession. Within these second-order cycles a higher-frequency cyclicity has also been identified.

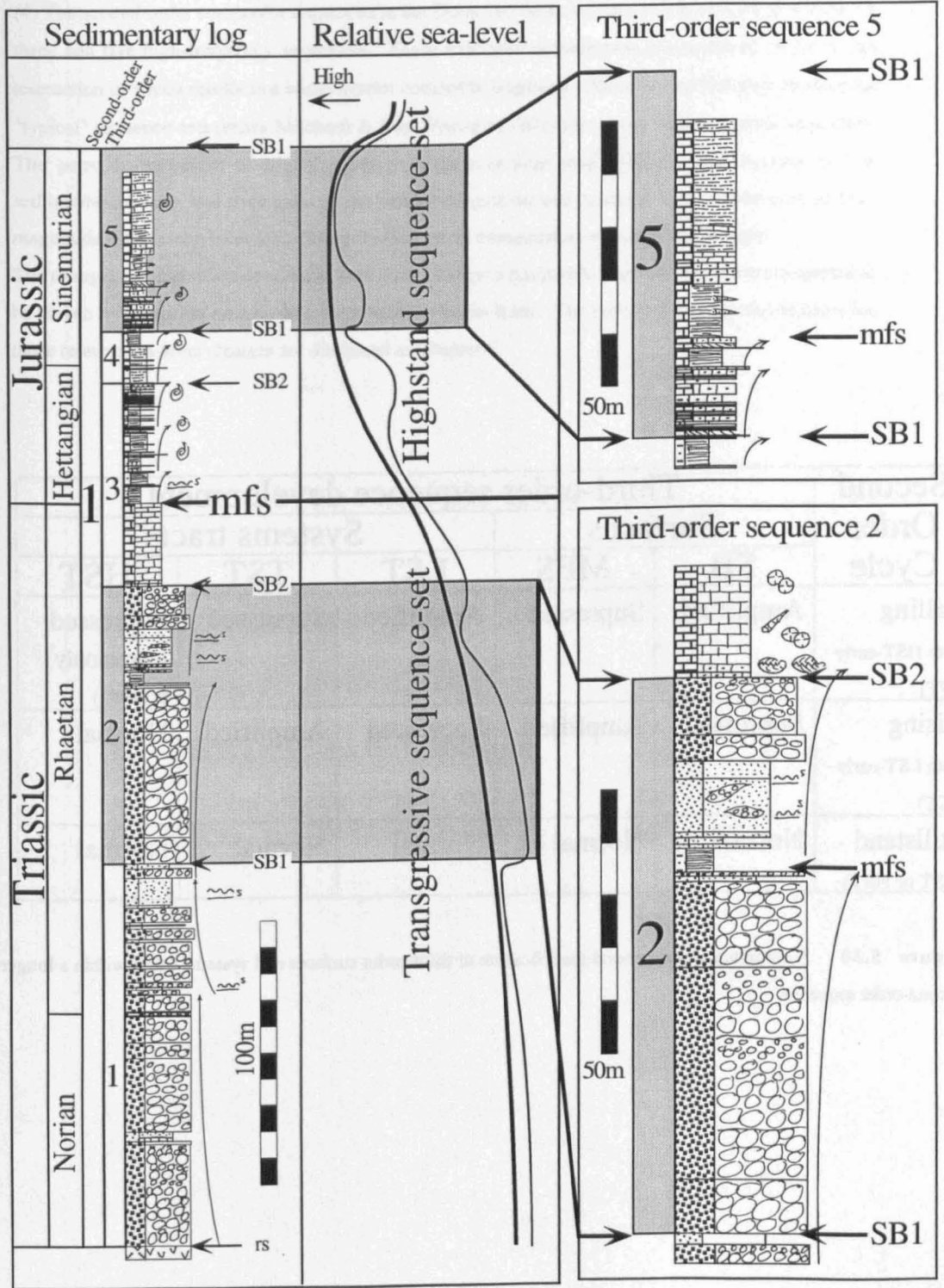


Figure 5.29 Sedimentary log of the Norian-Sinemurian based on sections at Punta del Viento (Norian-Rhaetian) and Sierra Argomedo (Hettangian-Sinemurian), correlated on the base Hettangian maximum flooding surface. The relative sea-level curve displays the five third-order sequences which compose the transgressive and highstand sequence-sets of second-order Sequence 1.

Second Order Cycle	Third-order sequence development				
	Surfaces		Systems tracts		
	SB	MFS	LST	TST	HST
Falling (late HST-early LST)	Amplified	Supressed	Amplified	Supressed	Supressed (commonly eroded)
Rising (late LST-early HST)	Supressed	Amplified	Supressed	Amplified	Normal
Stillstand (LST or HST)	Normal	Normal	Normal	Normal	Normal

Figure 5.30 A summary of the general modification of third-order surfaces and systems tracts within a longer-term second-order sequence.

(4) The second-order composite sequences in the Domeyko basin succession are composed of between three and five high-frequency sequences. These examples demonstrate two scales of cyclicity, the interaction of which results in a second-order composite sequence. This does not however produce the "typical" sequence-sets (sensu Mitchum & Van Wagoner, 1991) associated with composite sequences. The poor development of high-frequency sequences may result from a combination of low sedimentation rates and time gaps in the preserved rock-record, coupled with suppression of low-magnitude relative sea-level falls during the long-term transgressive nature of the Jurassic. The changes in relative sea-level have been correlated on a basinwide-scale and hence are interpreted to be driven by a process on a scale greater than the basin itself. The potential driving mechanisms for these relative sea-level changes are discussed in Chapter 6.

Chapter 6

Comparison of the Domeyko basin sequences with other northern and southern hemisphere basins and the controls on sequence development

6.1 Objectives of chapter

The principal objective of this chapter is to investigate potential driving mechanisms for the relative sea-level changes interpreted from the Domeyko basin succession (Chapter 5). Comparison of these relative sea-level fluctuations with those documented from other similar age South American marginal basins and northern hemisphere basins allows the distinction of regional from global events. The potential driving mechanisms for global sea-level fluctuations are discussed. Finally, the tectonically-driven sequence boundaries are characterised and a potential plate tectonic model to account for their formation is presented.

6.2 Comparison of the sequences with other northern and southern hemisphere basins

A relative sea-level analysis for the Jurassic Andean basins based on regional palaeontological data (Hallam, 1991) revealed several fluctuations, most notably, long-term relative sea-level falls in the earliest Bathonian and Late Oxfordian (Fig. 6.1). Hallam (1991) concluded that eustasy was the driving mechanism of Jurassic relative sea-level change. The relative sea-level analysis for the Domeyko basin based on sequence stratigraphy in this study (Chapter 5) allows a higher resolution analysis of changes in accommodation space through time, and hence determination of relative sea-level change (Figs 5.23 and 6.1).

Comparison of these relative sea-level fluctuations with those documented from other South American marginal basins (Antarctic Peninsula (Riccardi *et al.*, 1992), the Argentinean/Chilean Rocas Verdes (Dalziel *et al.*, 1974), Magallanes (Ramos, 1989), Rio Transito (Hillebrandt & Schmidt-Effing, 1981) and Neuquén Basins (Legarreta, 1991; Legarreta & Uliana, 1991; Uliana & Legarreta, 1993; Vergani *et al.*, 1995), together with basins in Peru, Ecuador and Colombia (Jaillard *et al.*, 1990)) and northern hemisphere basins (Jameson Land basin, East Greenland (Suryk, 1990; 1991; Dam & Suryk, 1992; 1995); southern Subalpine Basin, S.E. France (Graciansky *et al.*, 1993); Venetian Alps, Italy (Zempolich, 1993); Lusitanian Basin, Portugal (Wilson *et al.*, 1989); North Sea and onshore U.K. (Rathey & Hayward, 1993; Underhill & Partington, 1993; Sinclair & Riley, 1995)) allows the distinction of regional from global events, and hence a preliminary interpretation of the controls on sequence development (Fig. 6.1). The choice of these basins permits an objective analysis of relative sea-level change using basins of different tectonic setting, on different continental plates. The problems associated with Bajocian-Bathonian ammonite provincialism and biostratigraphical correlation between South America and Europe are inherent if these continental plates are to be compared.

It is important to note that the exact positions of the R' and F' inflection points (maximum flooding surfaces and sequence boundaries respectively) on each curve do not always fall on single time-lines (Fig. 6.1). This degree of exactness is beyond the 1.5 Ma resolution of the sea-level curves themselves, and where possible the biostratigraphically dated position of the sequence boundaries and maximum flooding surfaces have been taken from the original source reference.

6.2.1 Correlation of key surfaces within the Domeyko basin

(1) Earliest Hettangian maximum flooding surface and overlying highstand systems tract (Sequence 1)

The earliest Hettangian (Planorbis Zone) records the maximum rate of relative sea-level rise (maximum flooding surface) in the Late Triassic-lower Early Jurassic of the Domeyko basin. This flooding event is seen in other Andean basins (Hallam, 1991), while the base of the Jurassic in Europe is a marked transgressive surface (Haq *et al.*, 1987; Hallam, 1988) (Fig. 6.1). The problems of accurate dating and correlation within Europe do not permit confident identification of an earliest Hettangian flooding surface, however an earliest Jurassic rise in global sea-level is interpreted (Fig. 6.1).

The highstand systems tract of Sequence 1 records a long-term decreasing rate of relative sea-level rise punctuated by a flooding event in the Early Sinemurian (Bucklandi Zone), a late Early Sinemurian sequence boundary (Turneri Zone) and an early Late Sinemurian flooding event (Obtusum Zone) (Fig. 6.1). Synchronous third-order relative sea-level fluctuations have been documented in other Andean basins (Hallam, 1991), including Peru (Loughman & Hallam, 1982; Jaillard *et al.*, 1990), Ecuador and Colombia (Geyer, 1980; Jaillard *et al.*, 1990) and the Neuquén Basin, Argentina (Gulisano & Gutierrez-Pleimling, 1994), as well as in the Jameson Land basin, Greenland (Dam & Surlyk, 1993; 1995) and feature in the global cycle chart (Haq *et al.*, 1987). They are therefore interpreted to be driven by global glacio-eustatic sea-level fluctuations (Fig. 6.1). Dam & Surlyk (1993; 1995) noted the close similarity between lacustrine base-level change in the Rhaetian-Sinemurian Kap Stewart Formation, Jameson Land, Greenland and the global studies (Haq *et al.*, 1987; Hallam, 1988), suggesting a link between eustasy and long-term lake-level fluctuations (Fig. 6.1).

(2) Base Pliensbachian sequence boundary (Sequence 2)

The base Pliensbachian was marked by an abrupt fall in relative sea-level resulting in formation of a regional unconformity (Chong, 1973; Chong, 1977) and lowstand deposition (Fig. 6.1). A similar base Pliensbachian relative sea-level fall is seen in the Neuquén Basin, Argentina, defining the base of the Los Molles Formation turbidites (Gulisano & Gutierrez-Pleimling, 1994) (Fig. 6.1). The sediments in the Jameson Land basin, East Greenland record a basin-wide unconformity with Early Pliensbachian-age tidally-influenced marine facies (Neill Klintor Formation) directly overlying Hettangian lacustrine facies (Kap Stewart Formation). This juxtaposition is interpreted as a poorly dated sequence boundary containing the Sinemurian Stage (Surlyk, 1990) (Fig. 6.1). More recently, Dam & Surlyk (1993) have dated the correlative conformity to the north as being of base Pliensbachian age, indicating a base Pliensbachian fall in relative sea-level. Haq *et al.* (1987) and Hallam (1988) have documented a base Pliensbachian global sea-level fall from data collected in northern hemisphere basins which is supported by the South American examples, thus implying a global control which I interpret as global glacio-eustasy (Fig. 6.1).

Eustatic and relative sea-level curves

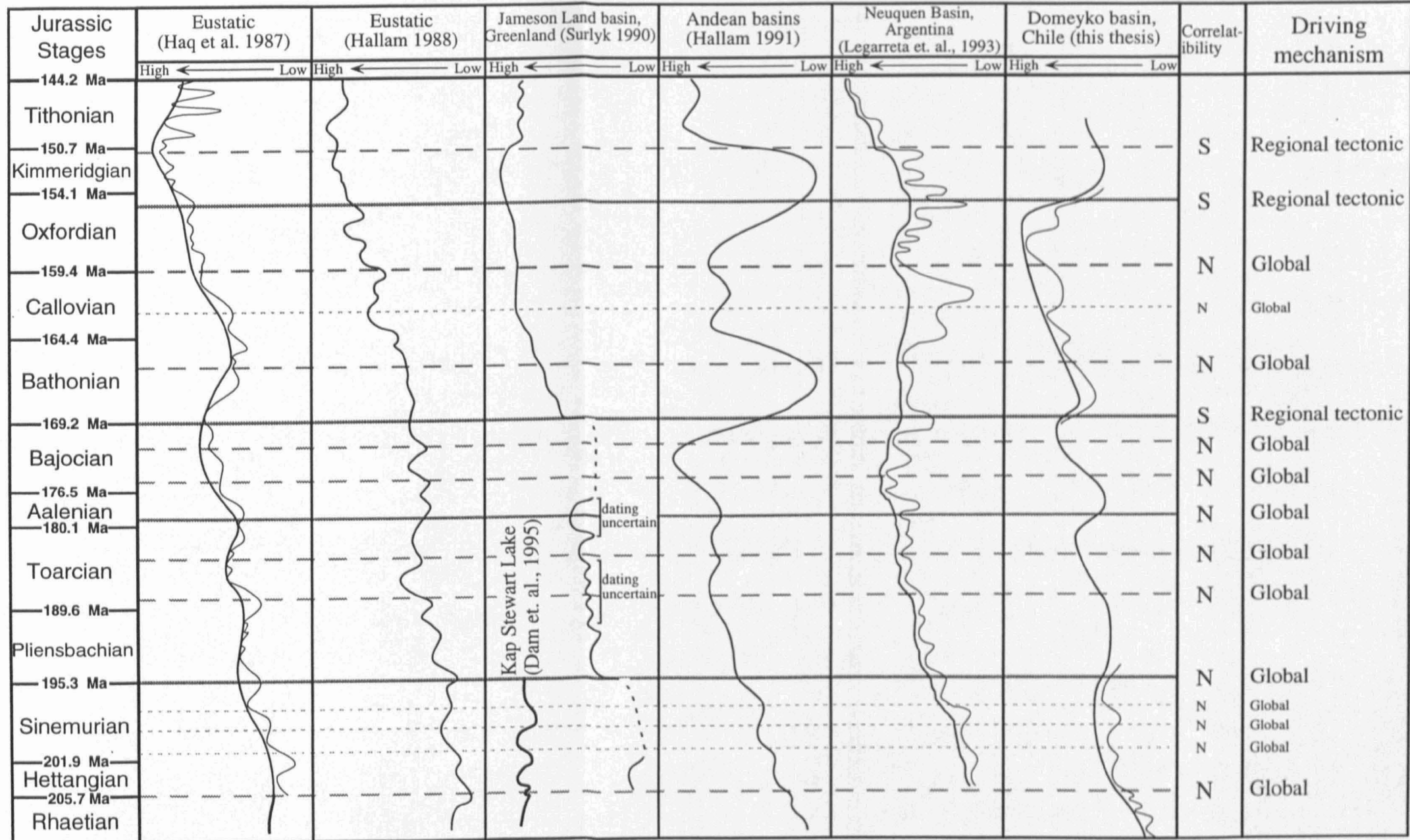


Figure 6.1 Comparison of Jurassic relative sea-level changes in northern Chile with global (Haq et al. 1987; Hallam 1988) and relative sea-level changes in the Jameson Land basin, Greenland (Surlyk 1990), Andean basins (Hallam 1991) and Neuquen Basin (Legarreta et al., 1993). Absolute ages of stage boundaries are taken from Gradstein et al., (1994). The F' and R' inflection points mark sequence boundaries (Solid lines) and flooding surfaces (Dashed lines) respectively with prominent third-order surfaces (Dotted lines) indicated. Correlatability of events is based on whether the event is seen throughout the South American basins (S) or if it can be traced into the northern hemisphere basins (N). The subsequent interpretation of principle driving mechanism is explained in the text and indicated as either regional tectonic or global.

(3) Toarcian flooding surfaces (Sequence 2)

The Early Toarcian succession records the onset of relative sea-level rise (initial flooding surface) with the maximum rate of relative sea-level rise (maximum flooding surface) being interpreted in the Late Toarcian (Hillebrandt, 1971; 1973; Hallam, 1991) (Fig. 6.1). These two Toarcian flooding events, which are marked by anoxic facies, are characteristic of the South American marginal basins of Rio Transito, central Chile (Hillebrandt & Schmidt-Effing, 1981); Neuquén Basin, Argentina (Legarreta & Uliana, 1991; Riccardi & Gulisano, 1992; Gulisano & Gutierrez-Pleimling, 1994) and the northern hemisphere basins of Jameson Land, East Greenland (Late Toarcian only; Surlyk, 1990; Dam & Surlyk, 1995), southern Subalpine, S.E. France (Graciansky *et al.*, 1993), Venetian Alps, Italy (Zempolich, 1993) and U.K./North Sea (Jenkyns, 1988) (Fig. 6.1). Again, the extent and synchronicity of the two Toarcian flooding events and associated anoxic facies imply a global eustatic control on relative sea-level, as recently proposed by Little & Benton (1995) (Fig. 6.1).

(4) Earliest Aalenian sequence boundary (Sequence 3)

The earliest Aalenian is marked throughout the Domeyko basin by a fall in relative sea-level resulting in the formation of a regional unconformity (Hillebrandt & Schmidt-Effing, 1981) (Fig. 6.1). This event is also recorded in the Neuquén Basin, Argentina (Legarreta & Uliana, 1991; Riccardi & Gulisano, 1992; Gulisano & Gutierrez-Pleimling, 1994) and in northern hemisphere basins (Hallam, 1988; Haq *et al.*, 1988) (Fig. 6.1). These data imply that the formation of the sequence boundary is controlled by a global mechanism, again considered to be a glacio-eustatic fall. In northwestern Europe the well-developed "mid-Cimmerian unconformity" is of earliest Aalenian age at its correlative conformity in the sections at Skye and Raasay, Scotland (Underhill & Partington, 1993). In the area of the North Sea rift basin this unconformity was amplified by regional thermal uplift in the Toarcian-Aalenian (Ziegler *et al.*, 1983; Underhill & Partington, 1993).

(5) Bajocian flooding surfaces (Sequence 3)

The Early Bajocian of the Domeyko basin records a flooding event (Gliebeli Zone marine flooding surface) and continued rise in relative sea-level resulting in regional transgression (Groschke & Wilke, 1986; Fernandez-Lopez *et al.*, 1994; 1995; Groschke & Hillebrandt, 1994) (Fig. 6.1). The maximum rate of relative sea-level rise occurred in the Late Bajocian (Megasphaeroceras magnum Zone maximum flooding surface), after which the rate of rise decreased and subsequently relative sea-level began to fall. An identical trend is documented from the Neuquén Basin, Argentina (Legarreta & Uliana, 1991; Riccardi & Gulisano, 1992; Gulisano & Gutierrez-Pleimling, 1994) and within the global studies of Haq *et al.* (1988) and Hallam (1988), thus implying a global sea-level rise during the Bajocian. The position of the R' inflection points on the global sea-level curves do not occur at exactly the same time in the Bajocian, however both curves record well defined flooding surfaces in the Early and Late Bajocian superimposed on a rising sea-level (Hallam, 1988; Haq *et al.*, 1988). The relative sea-level record for the Jameson Land basin, East Greenland is incomplete for the Bajocian Stage due to a regional unconformity (Surlyk, 1990). However, more recently Surlyk (1991)

identified marine flooding and transgression of Late Boreal-Bajocian age in East Greenland. The Andean relative sea-level analysis of Hallam (1991) implies a falling relative sea-level in the Late Bajocian, while in the Domeyko basin the Late Bajocian (Rotundum Zone) is characterised by continued flooding and marine transgression (Fernandez-Lopez *et al.*, 1994), implying an error at this section of Hallam's curve (Fig. 6.1).

(6) Earliest Bathonian sequence boundary (Sequence 4)

The earliest Bathonian relative sea-level fall is interpreted as a Type-2 sequence boundary, implying that the fall was of low magnitude notably less than the Andean relative sea-level fall proposed by Hallam (1991) (Fig. 6.1). Earliest Bathonian relative sea-level fall is seen in the Neuquén Basin, Argentina (Gulisano & Gutierrez-Pleimling, 1994) and throughout the Jurassic of Chile and Argentina (Riccardi, 1983) (Fig. 6.1).

Correlation between the Tethyan and Boreal ammonite Realms is not possible in the Late Bajocian-Bathonian due to a lack of north-south faunal transfer, resulting in high provincialism. Therefore, the Boreal-Bathonian of the Jameson Land basin, East Greenland (Surlyk, 1990; 1991) and global studies of Haq *et al.* (1988) and Hallam (1988) do not permit accurate correlation with South America. In the North Sea, the basinward shift in facies associated with the Great Estuarine Group is dated as earliest Boreal-Bathonian, occurring between the Parkinsoni and Progracilis Zones (Underhill & Partington, 1993), this could be tentatively interpolated as being time-equivalent to the sequence boundary in the South American basins. The earliest Bathonian event is assigned a continental-scale tectonic control throughout western South America with tentative correlation to the North Sea Basin (Fig. 6.1). No earliest Boreal-Bathonian relative sea-level fall is recorded on the global cycle chart (Haq *et al.*, 1987).

(7) Late Bathonian marine and earliest Oxfordian maximum flooding surfaces

The Late Bathonian marine flooding surface (Steinmanni Zone) in the Domeyko basin records an abrupt landward shift in facies and can be correlated with a Late Bathonian flooding event in the Neuquén Basin, Argentina (Gulisano & Gutierrez-Pleimling, 1994) and possibly a Late Boreal-Bathonian flooding event seen in the Jameson Land basin, East Greenland (Surlyk, 1990; 1991) and in both northern hemisphere studies (Haq *et al.*, 1987; Hallam, 1988), thus implying a global control. The Callovian records an increasing rate of relative sea-level rise and transgression in the Domeyko basin (Fig. 6.1). Long-term rising sea-level in the Callovian was typical for the Neuquén Basin, Argentina (Gulisano & Gutierrez-Pleimling, 1994), Jameson Land basin, East Greenland (Surlyk, 1990; Surlyk, 1991) and the northern hemisphere basins, which tends to suggest a global rise in sea-level (Haq *et al.*, 1988; Rattey & Hayward, 1993) (Fig. 6.1). The Callovian deepening in the Domeyko basin is punctuated by a third-order fall in the Middle Callovian (Riccardi, 1983; Riccardi *et al.*, 1989) (Fig. 6.1). The Neuquén Basin, Argentina (Gulisano & Gutierrez-Pleimling, 1994) records a minor regressive event in the Middle Callovian, marked by gypsum horizons (Tabanos Formation) in the Rio Atuel and Chacay Melehue sections (Riccardi, 1983; Riccardi *et al.*, 1989). A Middle

Callovian relative sea-level fall is seen on both global studies and therefore a global control is interpreted (Haq *et al.*, 1987; Hallam, 1988).

The earliest Oxfordian records the maximum rate of relative sea-level rise (maximum flooding surface) in the Late Jurassic of the Domeyko basin. This flooding event is seen in other Andean basins (Hallam, 1991) including the Neuquén Basin, Argentina (Legarreta *et al.*, 1993), the Jameson Land Basin, Greenland (Surluk, 1990) and other northern hemisphere basins (Haq *et al.*, 1987; Hallam, 1988), therefore suggesting a global rise in sea-level (Fig. 6.1). In the North Sea Basin this flooding event was tectonically-enhanced by a major phase of rifting (Ratley & Hayward, 1993).

(8) Late Oxfordian sequence boundary (Sequence 5)

The maximum rate of relative sea-level fall in the Late Jurassic of the Domeyko basin occurs within the Bimammatum Zone (latest Oxfordian) resulting in formation of an unconformity and low sea-level stand during the remaining latest Oxfordian-Late Kimmeridgian (Bimammatum-Acanthicum Zones, Gygi & Hillebrandt, 1991). Latest Oxfordian relative sea-level fall and evaporite deposition is clearly seen in the Neuquén Basin, Argentina (Gulisano & Gutierrez-Pleimling, 1994) and throughout Chile and Argentina (Riccardi, 1983) (Fig. 6.1). In marked contrast, the northern hemisphere basins of Europe and Greenland typically record rising sea-levels during the Oxfordian-Kimmeridgian and deposition of the Kimmeridge Clay source rock, thus implying a long-term global sea-level rise (Haq *et al.*, 1987; Hallam, 1988).

The large spatial distribution of lowstand evaporites traceable for over 2000 km along the marginal basins of Chile and Argentina (Riccardi, 1983), with a marked Late Oxfordian unconformity in southern Peru (Jaillard *et al.*, 1990) and poorly dated Oxfordian-Kimmeridgian evaporites at Galeana, Mexico (Gotte, 1988) are interpreted to represent a continental-scale tectonic event affecting all the marginal basins of western Gondwana, which completely overprints the global eustatic rise. It has been suggested that a progressive shallowing during the Callovian-Oxfordian as a result of uplift in the Coastal Cordillera (volcanic arc) culminated in the Late Oxfordian-Late Kimmeridgian lowstand of relative sea-level (Riccardi, 1992). However, such a shallowing is not seen in the Domeyko basin, with widespread Callovian deepening and anoxic conditions in the Early Oxfordian. An alternative driving mechanism is discussed below.

(9) Late Kimmeridgian-Early Cretaceous flooding

In the Domeyko basin the Late Kimmeridgian is characterised by rising relative sea-level and renewed marine transgression, leading to a maximum rate of relative sea-level rise (maximum flooding surface) in the Late Kimmeridgian-Early Tithonian (Fig. 6.1). A time-equivalent flooding event is seen in the Neuquén Basin, Argentina (Riccardi, 1983; Gulisano & Gutierrez-Pleimling, 1994) and throughout southern and central Chile (Hallam, 1991), however this event is of a larger magnitude than that seen in the Domeyko basin (Fig. 6.1). An abrupt Late Kimmeridgian relative sea-level fall is seen in the Jameson Land basin, East Greenland (Surluk, 1990; 1991) with sea-level still-stand and fall recorded

in the studies of Haq *et al.* (1987) and Hallam (1988), respectively. A regional tectonic control is proposed owing to the opposite trend to the global eustatic signal (Fig. 6.1).

(10) Early Cretaceous sequence boundary

The Early Cretaceous sequence boundary resulted in closure of the marine connection to the Domeyko basin and continental clastic deposition. An Early Valanginian sequence boundary is seen in the Neuquén Basin, Argentina (Gulisano & Gutierrez-Pleimling, 1994), Peru and Ecuador (Jaillard *et al.*, 1990; Jaillard, 1994) and throughout Chile and Argentina (Riccardi, 1983). In the Neuquén Basin structural inversion (Vergani *et al.*, 1995) is dated as Early Valanginian and has been correlated throughout much of western South America (Macellari, 1988). An earliest Valanginian sequence boundary is noted in the Lusitanian Basin, Portugal (Wilson *et al.*, 1989) and northern hemisphere basins (Haq *et al.*, 1987) where it has been interpreted as a breakup megasequence boundary (Hubbard, 1988; Sinclair, 1988; Couzens, 1992; Sinclair & Riley, 1995). This Early Valanginian sequence boundary is interpreted to record a fall in global sea-level which was tectonically-enhanced by regional uplift in the Andean marginal basins.

6.2.2 Global and regional tectonic controls on sedimentation

Global eustatic sea-level fluctuations appear to have been the primary control on sequence development in the Domeyko basin during the Early-Middle Jurassic. The Middle to Late Jurassic records the interplay between eustasy and initiation of the supercontinental fragmentation of Pangea at this time. The potential driving mechanisms for global sea-level fluctuations are discussed below for first- to fifth-order cycles followed by presentation of a model to account for the non-globally correlative sequence boundaries.

First-order cycles (Continental encroachment cycles).

First-order rising global sea-level during the Jurassic is widely interpreted to be related to the accretion and subsequent splitting apart of supercontinents (Vail *et al.*, 1977b; Worsley *et al.*, 1984). When continents are amalgamated together (as in the Permian Pangea), the volume of spreading ocean ridges is minimised and ocean basin volume is maximised due to thermal subsidence (Plint *et al.*, 1994). This results in a global lowering of eustatic sea-level. These conditions are reversed at times of supercontinent break-up, when new spreading ridges form and displace water onto continental margins (as in the Jurassic). The youngest continental encroachment cycle is represented by the smoothed long-term sea-level curve on the Haq *et al.* (1987) chart (Fig. 5.3).

Second-order cycles (Major transgressive-regressive facies cycles).

Second-order cycles have been interpreted to reflect changes in the volume of ocean ridges, related to changes in spreading rate (Hallam, 1963; Pitman, 1978) and due to glacio-eustatic cycles (Vail *et al.*, 1977b). The second-order cycles are shown as variations on the long-term sea-level curve of Haq *et al.* (1987) (Fig. 5.3).

Third-order cycles (Sequences).

Third-order cycles have durations of 1-10 Ma, but are typically around 3 Ma in duration. They are ubiquitous in the Phanerozoic record (Haq *et al.*, 1988; Miall, 1990) but their control is problematic and controversial (Plint *et al.*, 1992). Vail *et al.* (1977b) and Haq *et al.* (1988) implied that third-order sequences are controlled by the waxing and waning of continental ice masses but this model has been recently reassessed due to the rate of growth and decay of ice sheets which is thought to take place over much shorter periods of time (0.1-1 Ma) (Plint *et al.*, 1992).

Several other potential driving mechanisms have been proposed including explanations relating to spreading and subduction (Harrison, 1990), changes in the horizontal stress field within plates (Cloetingh, 1988), stress-induced changes in lithospheric density (Cathles & Hallam, 1991), geoidal eustasy (Mörner, 1981), and variations in polar wander (Sabadini *et al.*, 1990). However, the processes of tectono-eustasy, tectonic movement of the basin floor, or any of the potential mechanisms listed previously cannot convincingly explain the high-frequency (0.5-5 Ma) changes in relative sea-level of the magnitude (50-100 m) suggested by the Jurassic rock-record. Third-order sequence cycles are shown as the short-term sea-level curve on the Haq *et al.* (1987) chart (Fig. 5.3).

Fourth- and fifth-order cycles (Sequences and parasequences).

Fourth- (0.2-0.5 Ma) and fifth-order (0.01-0.2 Ma) cycles are most easily explained by changes in climate driven by cyclic perturbations known as Milankovich Cycles (Milankovich, 1941). There are three principle orbital rhythms related to (1) changes in eccentricity of the Earth's orbit around the sun (400,000 and 100,000 years), (2) changes in the tilt of the Earth's axis with respect to the plane in which it orbits the sun (41,000 years), and (3) a wobble (precession) due to the tilt axis sweeping out a cone (21,000 years) (Milankovich, 1941). Milankovich (1941) also suggested the link between orbital changes and ice-sheet volumes, which are now known to result in slow ice-sheet growth and rapid decay (Imbrie & Imbrie, 1980; Ruddiman & McIntyre, 1981; Berger, 1988). Shackleton & Opdyke (1973) demonstrated how changes in global ice-volumes affect sea-water composition during the Pleistocene, and in particular oxygen-isotope values. These oxygen isotope variations can be very closely matched with calculated insolation changes resulting from Milankovich cyclicity (Hays *et al.*, 1976). The standard record of oxygen isotope stages has now been extended back to 2.5 Ma before present (Imbrie *et al.*, 1984; Raymo *et al.*, 1989; Ruddiman *et al.*, 1989; Shackleton *et al.*, 1990).

Examples of ancient sedimentary cyclicity attributed to orbital-forcing have now been described from the Precambrian and every period in the Phanerozoic (Einsele, 1982; Arthur *et al.*, 1984; Fischer *et al.*, 1985; 1990; Fischer, 1986; Berger, 1989). These examples cover a wide range of facies including evaporitic (Anderson, 1982; 1984), lacustrine (Olsen, 1986), clastic shoreline (Clifton, 1981), deltaic (Van Tassell, 1987), platform carbonate (Schwarzacher & Haas, 1986), shelf carbonate (Schwarzacher, 1989), siliciclastic shelf (Van Echelpoel & Weedon, 1990), hemipelagic (Weedon, 1985), pelagic (Herbert & Fischer, 1986), and turbiditic (Foucault *et al.*, 1987) facies. Therefore, Pleistocene orbital-climate models characterising the regularity and periods of the sedimentary cyclicity and studies of the likely environmental changes involved present a strong case for there being many examples of orbital-climate control of sedimentary cyclicity in a wide range of facies since the Proterozoic.

Fourth- and fifth-order Milankovich cycles exert an orbital-control on global climate which are interpreted to result in changes in the global ice-volumes, termed glacio-eustasy. The suggestion by Mitchum & Van Wagoner (1991) and Plint (1991) that third-order sequences are in fact built of fourth-order sequences permits the interpretation that glacio-eustasy can provide a potential driving mechanism to explain third-order sequence development. A glacio-eustatic control with Milankovich periodicities may be the only currently-available driving mechanism to support the sea-level changes recorded in the Jurassic rock-record. However, a Jurassic glacio-eustatic control is difficult to prove due to a lack of direct evidence for continental glaciation (ie. tillite or boulder-clay), with an apparent gap in the Earth's glacial record from the Triassic to the early Tertiary. Spicer (1987) and Frakes & Francis (1988) provided good evidence of seasonal pack-ice formation at sea-level during the Cretaceous. The oxygen-isotope record for the past 40 Ma indicates the presence of a significant ice budget, while the record between 50 to 65 Ma (early Tertiary) appears intermittently ice-free (Prentice & Matthews, 1988). Recent climate modelling work predicts significant Antarctic ice accumulation during the Mesozoic, and hence the potential for Jurassic glacio-eustatic cyclicity (Oglesby, 1989; B. W. Sellwood pers. comm., 1996). Although it is not currently possible to prove glacio-eustatic cyclicity in the Jurassic there is increasing evidence to suggest the presence of continental ice accumulation during the Mesozoic.

6.3 Fragmentation of Pangea and its sequence stratigraphical record in the Andean back-arc basins

Introduction

Recent sequence stratigraphical studies in the western back-arc basins of Gondwana have examined the effects of regional tectonic events versus global eustatic cyclicity on the resultant stratigraphy (Legarreta & Uliana, 1996). This section characterises a series of tectonically-driven sequence boundary unconformities in well-dated successions and presents a model to account for their formation. It draws on published data from the Cretaceous continental succession at the top of the Domeyko succession which although not described in detail within this thesis does allow testing of the synchronicity of regional tectonic signals during the final fill and initial inversion of the basin.

Within the Jurassic succession of the Domeyko basin as discussed above (Fig. 6.1), the majority of relative sea-level changes were found to correspond temporally with published global eustatic events (Haq *et al.*, 1988), but two long-term relative sea-level falls (sequence boundaries) in the earliest Bathonian and Late Oxfordian (Fig. 6.1) do not accord with eustatic sea-level changes defined in the northern hemisphere. In the Late Oxfordian of the Domeyko basin, a sequence boundary occurs at a time when global eustatic sea-level continued to rise (Haq *et al.*, 1988; Rattey & Hayward, 1993), implying a tectonic control.

Some 1800 km to the south, the well-dated successions of the Neuquén back-arc Basin of Argentina (34°-41°S) also record the same two tectonically-driven sequence boundaries indicating that the tectonic driving mechanism was not due to local fault movement, but of sub-continental scale (Fig. 6.2). In

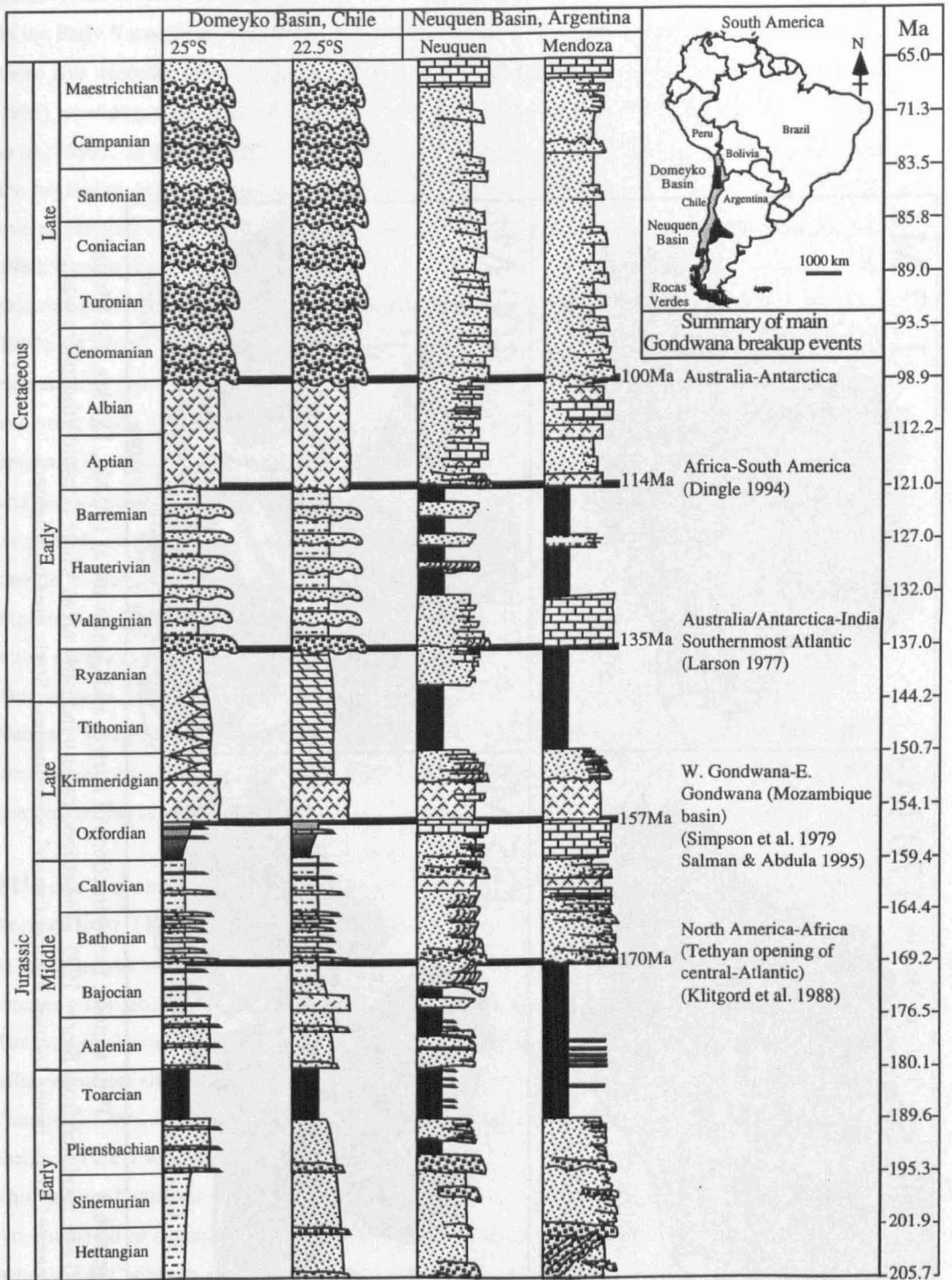


Figure 6.2 Generalised stratigraphic logs from the Domeyko and Neuquén Basins (Gulisano & Gutierrez-Pleimling 1994) with location map. Major tectonically-driven sequence boundaries are marked and related to significant Pangean fragmentation episodes.

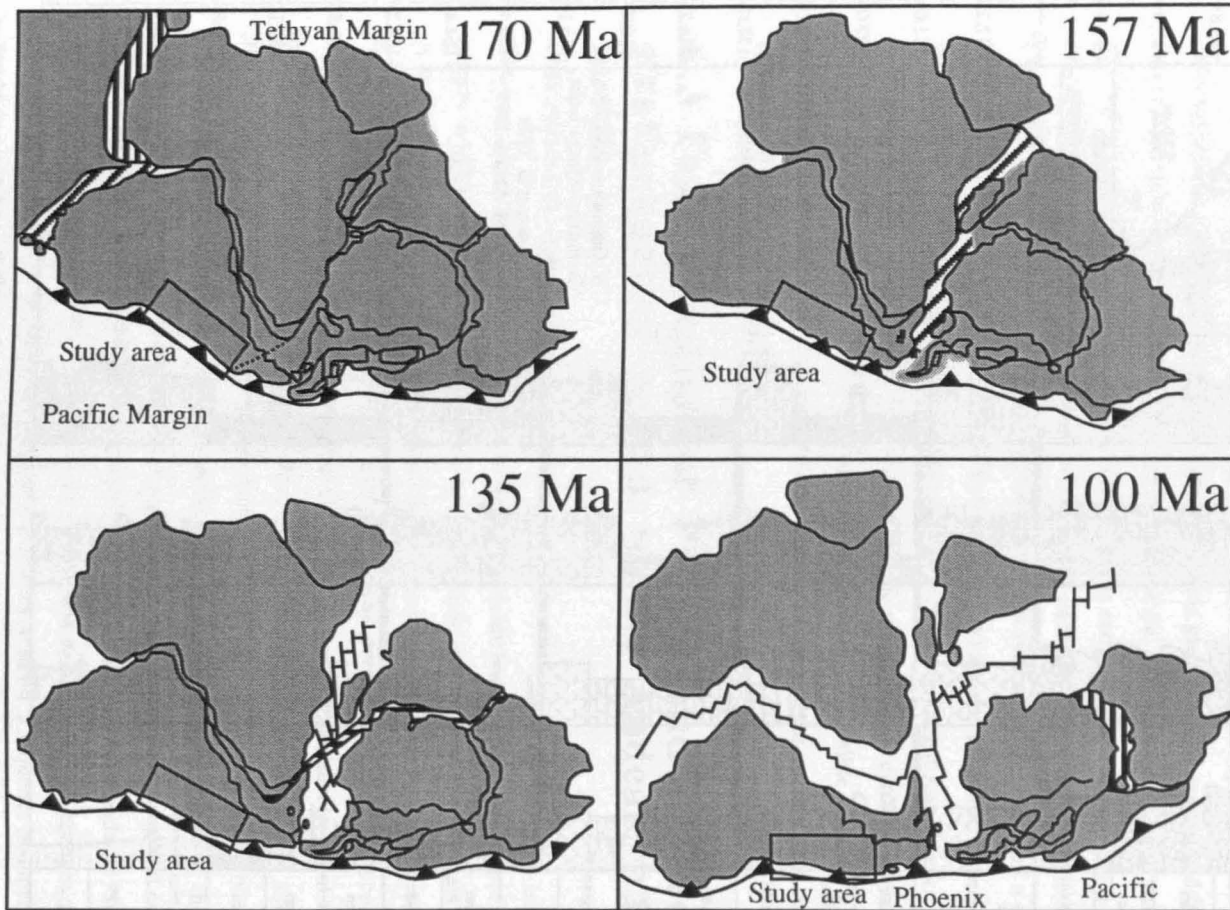


Figure 6.3 Plate tectonic reconstructions of Pangea and Gondwana at 170 Ma, 157 Ma, 135 Ma and 100 Ma, modified from Storey 1995. The striped pattern indicates areas where oceanic lithosphere was generated in the newly formed intercontinental ocean basins. Study area highlighted.

addition, the Cretaceous successions in the two basins record three further synchronous tectonic events in the Early Valanginian, Aptian and Cenomanian (Macellari, 1988). In the Neuquén Basin three of these five unconformities are associated with major phases of structural inversion (Vergani *et al.*, 1995), providing more direct evidence of a tectonic control and principal driving mechanism (Tankard *et al.*, 1995). In the Domeyko basin the Early Aptian and Early Cenomanian tectonic events define the beginning and end of arc volcanism within the basin (Fig. 6.2) as an incremental stage in the overall eastward migration of the Andean volcanic arc during the Mesozoic and Cenozoic (Coira *et al.*, 1982; Reutter *et al.*, 1988).

Outwith specific episodes of contraction, the Andean margin was dominantly extensional (Flint *et al.*, 1993). A recent study has shown a temporal coincidence between back-arc basin extension and extension in intracontinental rift networks within Gondwana, particularly the earliest stage in the evolution of the southernmost Atlantic (Legarreta & Uliana, 1991). This accords with a recent re-emphasis on the significance of thermal mechanisms *within* Gondwana in driving extensional rifting and the subsequent fragmentation of Pangea (Storey, 1995). Previously the emphasis has been exclusively on variations in sea-floor spreading rates in the Pacific area to control western Andean margin evolution (Jordan *et al.*, 1983; Pardo-Casas & Mölnar, 1987). In this section we further explore the fragmentation episodes within Pangea by assessing their effects on the South American active margin as recorded in the evolution of the western back-arc basins.

The positions of the five synchronous tectonically-driven sequence boundaries in the Domeyko and Neuquén Basins are displayed in Fig. 6.2. The characteristics of each boundary and its temporal correlation with well constrained fragmentation events with Pangea are dealt with in chronostratigraphical order below.

Middle Jurassic subduction coupling and Laurasia/Gondwana separation (170 Ma)

In the Domeyko basin, the Type-2 sequence boundary unconformity defining the base of Sequence 4 is interpreted to record a tectonically-driven regional fall in relative sea-level, as previously discussed. The time-equivalent siliciclastic succession of the Neuquén basin shows a more dramatic change from offshore marine siltstone to erosively-based tidal and fluvial sandstone facies (Gulisano & Gutierrez-Pleitling, 1994), interpreted as incised valley fills (Zavala, 1993) indicating subaerial exposure of the shelf and Type-1 sequence boundary formation.

This earliest Bathonian sequence boundary developed at a crucial time during Pangean evolution. After a period of supercontinent stability, Tethyan spreading propagated westward into the Central Atlantic and Caribbean regions. North America initially separated from Africa between 175-170 Ma (Klitgord *et al.*, 1988) and in the Caribbean between 175-165 Ma (Pindell & Dewey, 1982; Anderson & Schmidt, 1983). Jaillard *et al.* (1990) related this spreading episode to southward propagation of extensional stresses into basins of Colombia and Peru that are synchronous with the Domeyko and Neuquén Basins. Additional information pertaining to this separation between Gondwana and Laurasia comes from ammonite provinciality and biogeography (Westermann, 1993). Between Pliensbachian-

Late Bajocian (~180-175 Ma) there was limited faunal transfer from Tethys to the East Pacific prior to oceanic spreading along a seaway between Laurasia and Gondwana. This is coincident with pre-break-up subsidence caused by stretching and mechanical rifting. At about 173 Ma faunal transfer ceased and the endemic East Pacific sub-realm was established along the eastern Pacific margin, isolated by segmentation of the newly spreading oceanic area by transform faults and a fall in relative sea-level (Westermann, 1993).

Figure 6.3 illustrates the degree of oceanic spreading between Gondwana and Laurasia at 170 Ma. Pangean fragmentation would have initiated a major plate re-organisation impacting on the circum-Gondwana subduction zone. I interpret increased subduction coupling and uplift of back-arc basins to have resulted in relative sea-level fall and sequence boundary formation.

Late Jurassic salinity crisis and West/East Gondwana separation (157 Ma)

In the Domeyko basin, the Type-1 sequence boundary (Sequence 5) defining the base of the Upper Oxfordian-Upper Kimmeridgian evaporites is interpreted to record a tectonically-driven regional fall in relative sea-level, as previously discussed. The Neuquén Basin records similar aged Upper Oxfordian-Upper Kimmeridgian evaporite facies directly overlying marine carbonates interpreted to have resulted from restricted marine connection associated with barring of the basin (Legarreta & Uliana, 1991). The large spatial distribution of lowstand evaporites traceable for over 2000 km along the back-arc basins of Chile and Argentina, with a marked Late Oxfordian unconformity in southern Peru (Jaillard *et al.*, 1990) are interpreted to record a continental-scale tectonic event affecting all the back-arc basins of western Gondwana. In the Neuquén basin there is abundant evidence for structural inversion in the Late Oxfordian (Vergani *et al.*, 1995). Uplift of the basin floor and volcanic arc caused the barring and relative sea-level fall within the basins (Legarreta & Uliana, 1996), despite a pronounced Late Jurassic global eustatic sea-level rise (Haq *et al.*, 1988).

The first episode of oceanic spreading within Gondwana took place with its bisection along the Somali, Mozambique and Weddell Sea Basins. Upper Jurassic sea-floor has been recognised along the length of this ocean strait (Bergh, 1977; Simpson *et al.*, 1979). Oceanic onset is well constrained particularly midway along the strait in the Mozambique Basin, where the Jurassic Magnetic Quiet Zone has been detected adjacent to the continental margin (Simpson *et al.*, 1979) and the onset unconformity on the Mozambique shelf is dated at 157 Ma (Salman & Abdula, 1995). Pre-spreading lithospheric extension was associated with the emplacement of the Drakensberg (Africa) and the Queen Maud Land (Antarctica) flood basalts (Fig. 6.4) during the late Middle Jurassic (Tankard *et al.*, 1982; White & McKenzie, 1989).

The effect of Gondwana bisection on the Southern Andes was to introduce northward transgression from the newly formed ocean in the south. Previously all marine transgressions entered the basins from the north, through Peru (Jaillard *et al.*, 1990) and northern Chile.

I suggest that it was this intra-Gondwana spreading event that caused regional contraction, resulting in barring of the Andean back-arc basins and triggering regional evaporite precipitation. The scale of the

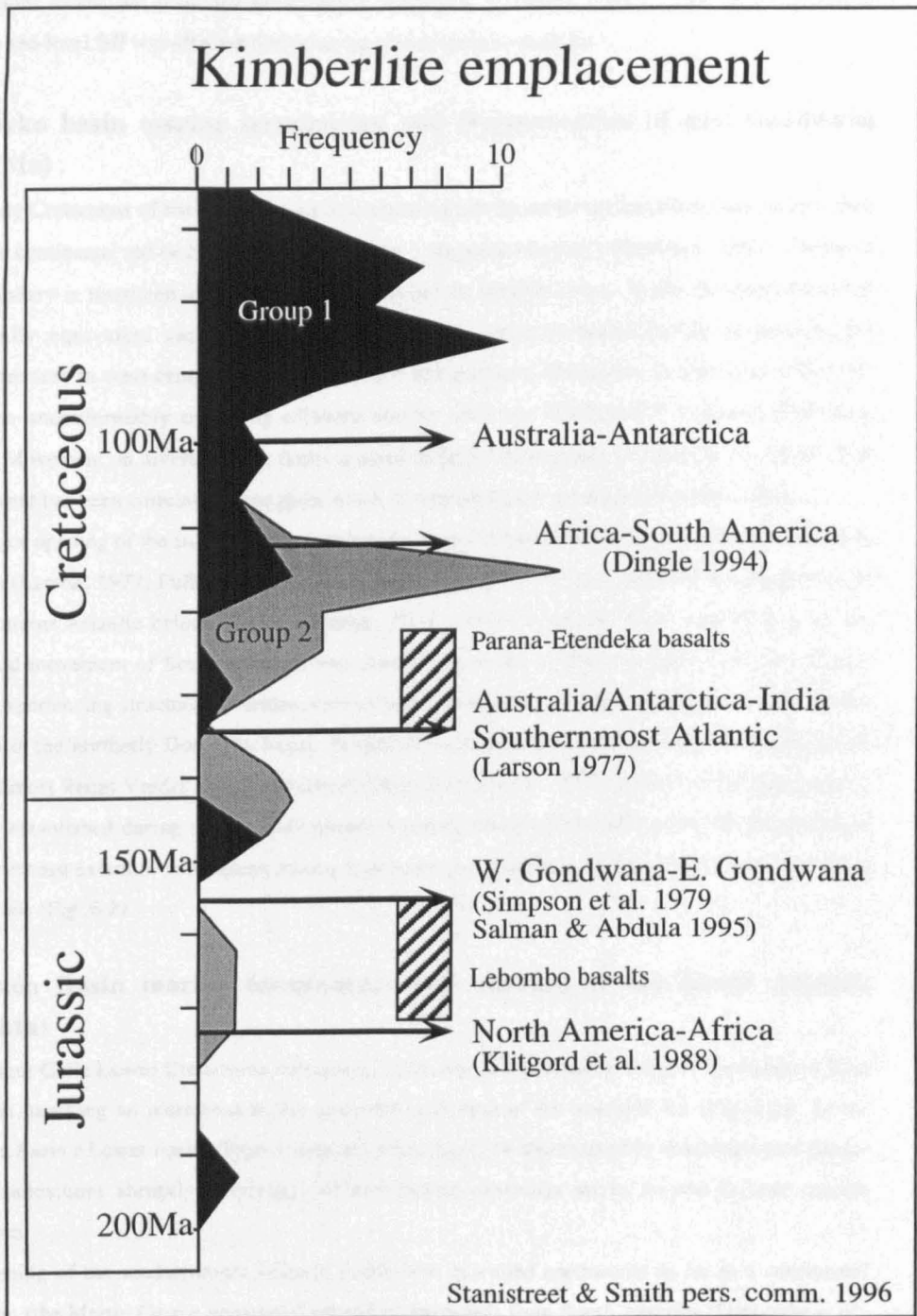


Figure 6.4 Kimberlite emplacement frequency (Smith et al. 1994; Stanistreet & Smith pers. comm. 1996) and southern African flood basalt events compared to the timing of the Pangean fragmentation episodes discussed in the text. Note that where data density is sufficient, fragmentation is preceded by a kimberlite emplacement pulse.

evaporite deposits is similar to that of the Messinian evaporites of the Mediterranean and such an ocean-spill model has provided an analogue (Legarreta & Uliana, 1996). This continental-scale relative sea-level fall was effected during rising global eustatic sea-level.

Domeyko basin marine termination and fragmentation of east Gondwana (135 Ma)

The Early Cretaceous of the Domeyko basin is characterised by an abrupt transition from marine shelf facies to continental red-beds interpreted as a Type-1 sequence boundary (Bogdanic, 1990). Dating of the boundary is restricted to Early Cretaceous, based on bivalve fauna. In the Neuquén Basin the temporally equivalent sequence boundary comprises erosively-based fluvial sandstones and conglomerates in west-central Neuquén Province and platform limestones in south-west Mendoza Province unconformably overlying offshore marine siltstones (Gulisano & Gutierrez-Pleimling, 1994). Movement on inverted basin faults is dated as Early Valanginian (Vergani *et al.*, 1995). This uplift event has been correlated throughout much of western South America (Macellari, 1988).

The major opening of the Indian Ocean between India and Australasia/Antarctica initiated as early as 135 Ma (Larson, 1977; Fullerton *et al.*, 1989; Veevers *et al.*, 1991) and extended westward into the southernmost Atlantic before 133 Ma (Martin, 1984; 1987). I suggest that a consequence of this westward movement of South America was contraction at the subduction zone, with the marginal basins experiencing structural inversion, erosion and a switch from marine to continental depositional systems in the northerly Domeyko basin. In contrast oceanic lithosphere initiated at this time in the southernmost Rocas Verdes marginal basin of Chile (Dalziel *et al.*, 1974) reinforced the transgressive polarity established during the previous oceanic opening event which had formed the Weddell Sea. The northward extent of subsequent marine transgressions decreased incrementally during the Early Cretaceous (Fig. 6.2).

Neuquén Basin marine termination and opening of the South Atlantic (114 Ma)

In northern Chile Lower Cretaceous continental rocks are unconformably overlain by Aptian-Albian arc lavas, marking an increment in the eastward migration of the volcanic arc (Fig. 6.2). In the Neuquén Basin a Lower Aptian Type-1 sequence boundary (114 Ma) marked by erosively-based fluvio-deltaic sandstones abruptly overlying offshore marine siltstones marks an end to open marine conditions.

The opening of the southernmost Atlantic ocean now extended northwards as far as a continental transform (the Martín García lineament) extending eastwards from South America (Unternehner *et al.*, 1988; Tankard *et al.*, 1995). Oceanic opening symmetrically affected both South America and southern Africa (Dingle, 1994, Fig. 6) and extension in Africa would have been accommodated by a continental transform zone along the southern margin of the Congo craton that includes the Waterberg Thrust and is associated with sub-volcanic centres (Milner *et al.*, 1995). The operation of these continental transforms resolves the mismatch between South America and Africa recorded in the plate

reconstruction at 118.7 Ma by Scotese *et al.* (1988), and thus the major part of the South Atlantic did not open until after this date (Dingle, 1994). The opening has been estimated by Dingle (1994) at 114 Ma just following the emplacement of the Etendeka and Parana flood basalts (White & McKenzie, 1989; Milner *et al.*, 1995). The fragmentation of West Gondwana and westward movement of the South American plate have been linked to unconformity development in the Central Andes (Flint *et al.*, 1993; Jaillard, 1994).

The Peruvian tectonic event and major basin inversion (100 Ma)

The Mid-Cretaceous of the Domeyko basin is recorded by an angular unconformity and transition from arc volcanics to Upper Cretaceous alluvial conglomerates (Bogdanic, 1990). The onset of folding and uplift is dated as 100 Ma (Andriessen & Reutter, 1994), with the main inversion phase continuing into the Santonian (Megard, 1987).

In the Neuquén Basin, erosively-based fluvial sandstones directly overlying restricted marginal marine limestones and evaporites (Type-1 sequence boundary), mark the switch to fully continental conditions. It is recognised both in outcrop and on seismic, by moderate reflection truncation (Vergani *et al.*, 1995). The sequence boundary is dated as Early Cenomanian (Mid-Cretaceous) and has been recognised elsewhere in western South America (Macellari, 1988).

The Peruvian tectonic event is one of the most significant episodes to affect deposition in the Andean back-arc basins, marking a long-term change from extensional to contractional tectonic style. At 100 Ma Australia separated from Antarctica (Fig. 6.3). This continental separation took place a long distance away from the South American margin but is associated with enhanced oceanic spreading within Gondwana (Scotese *et al.*, 1988). Indeed, measured oceanic spreading rates in the intra-Gondwanan oceans did increase significantly at this time following the final opening of the South Atlantic (Larson, 1991) and I believe this would have impacted on the circum-supercontinental subduction zone.

6.4 Pangean plate re-organisations and their thermal signature

I have explained the temporal links between tectonically-driven sequence boundaries of the western South American active plate margin and supercontinental fragmentation episodes. Plate motions are a direct response to thermal driving mechanisms whereby heat is brought from the planetary interior to the underside of the lithosphere to be cooled close to the Earth's surface. The Gondwana-wide fragmentation episodes and associated plate reorganisations that I have proposed as a major control on continent-ocean coupling imply a thermal driving mechanism, widespread beneath the supercontinent. White & McKenzie (1989) and Storey (1995) have suggested the importance of mantle plumes in the fragmentation process. However, the effects of mantle plumes tend to be localised and may be a symptom of more widespread thermal activity on a supercontinental scale (Anderson, 1994), particularly prevalent beneath Gondwana (Veevers, 1995). Such widespread thermal activity would affect the underside of continental lithosphere as well as driving continental break-up.

Kimberlites result when wholesale melting of deep continental lithospheric mantle takes place and the kimberlite emplacement frequency thus provides a potential thermal record (Stanistreet & Smith pers. comm., 1996). Lying at the centre of Gondwana, southern Africa exhibits the most complete and well documented kimberlite record (Smith *et al.*, 1994; Stanistreet & Smith pers. comm., 1996) during the fragmentation history that I have considered. Figure 6.4 compares the kimberlite frequency record to the fragmentation episodes I have identified. It is significant that each of the episodes that I document is preceded by a kimberlite frequency maximum, interpreted to result from a pulse of lithospheric mantle melting (Stanistreet & Smith pers. comm., 1996). The lack of more evolved Group 2 kimberlites in the Late Cretaceous has been explained as resulting from the isolation of Africa from other Gondwanan continental elements (Stanistreet & Smith pers. comm., 1996). Subsequently a lack of lithospheric extension in the African continental lithosphere can explain an abrupt cessation of decompressional melting to provide Group 2 kimberlites.

Gurnis (1993) encountered an inconsistency in his modelling, whereby Late Permian and Early Cretaceous heating beneath Pangea predicted an associated subsidence at the subducting margins that was not evident. However, by the process envisaged here heating results in supercontinental expansion involving extension, fragmentation and collision with the oceanic plate, thus explaining the lack of marginal subsidence.

6.5 Importance of supercontinental fragmentation episodes

Previously the origin of contractional tectonic events affecting the South American margin have been difficult to explain (Jaillard, 1994; Vergani *et al.*, 1995). Almost exclusively changes in subduction activity associated with oceanic spreading and ocean plate splitting in the Pacific area have been proposed as their principal cause (Vaughan, 1995). This is despite the fact that there are no particular signatures in terms of the variation in spreading rates (Larson, 1991) that stand out to explain each of the compressional episodes that I document. I believe that thermally induced Gondwanan fragmentation episodes provide a more immediately viable explanation, in that they provide a mechanism for plate re-organisations driving changes along the circum-supercontinental subduction zone. Increased subduction coupling is considered to result in uplift recorded in the marginal basins as tectonically-driven sequence boundaries. Specific basin responses include: (a) Type-1 and -2 sequence boundaries in fully marine successions; (b) basin barring and regionally extensive evaporite formation by spill replenishment; (c) incremental and overall changeover from marine to continental deposition systems; and (d) stepwise eastward migration of the volcanic arc.

Chapter 7

Conclusions

7.1 Conclusions

The following conclusions have been drawn from the work presented in this thesis.

(1) The Upper Triassic to Lower Cretaceous Domeyko basin-fill comprises a highly diverse sedimentary succession including continental clastic, mixed carbonate and siliciclastic marine and evaporite deposits. The majority of the mixed carbonate and siliciclastic marine basin-fill is interpreted to have been deposited in a ramp-type setting. Stratal architecture appears to be predominantly controlled by siliciclastic sediment input, basin-margin morphology and rate of relative sea-level change. The distal offshore facies of the mixed carbonate and siliciclastic ramp are dominated by carbonate mudstones, while further up-dip siliciclastic sediment input resulted in sandy shoreface facies. Reef-building coral facies are both temporally and spatially restricted in the Domeyko basin as a result of cool water conditions and a lack of suitable substrate. The marine deposits record an almost complete ammonite biochronology indicating open marine connection, with only a minor input of volcanic material from the Jurassic volcanic arc to the west.

(2) Sequence stratigraphical analysis of the Domeyko basin succession has permitted the identification and characterisation of both sequence boundaries and flooding surfaces, defining five second-order sequences. The correlation of these chronostratigraphical surfaces, constrained within the ammonite biostratigraphy, has allowed an analysis of both the stratigraphical evolution of the Domeyko basin succession and subsequently second-order changes in relative sea-level.

(3) The Domeyko basin mixed carbonate and siliciclastic ramp environment is characterised by the deposition of siliciclastic-dominated successions at times of low accommodation space (lowstand and late highstand systems tracts) and carbonate-dominated successions during periods of high accommodation space (transgressive and early highstand systems tracts).

(4) Second-order relative sea-level falls in the earliest Pliensbachian, earliest Aalenian, earliest Bathonian, Late Oxfordian, earliest Valanginian, and rises in the earliest Hettangian, earliest and Late Toarcian, Early and Late Bajocian, Late Bathonian, earliest Oxfordian and Late Kimmeridgian have been identified within the Domeyko basin succession. Within these second-order cycles a higher-frequency cyclicity has also been identified.

(5) The second-order composite sequences in the Domeyko basin succession are composed of between 3 and 5 high-frequency sequences. These examples demonstrate two scales of cyclicity, the interaction of which results in a second-order composite sequence. This does not however produce the "typical" sequence-sets (*sensu* Mitchum & Van Wagoner, 1991) associated with composite sequences. The poor development of high-frequency sequences may result from a combination of low sedimentation

rates and time gaps in the preserved rock-record, coupled with suppression of low-magnitude relative sea-level falls during the long-term transgressive nature of the Jurassic.

(6) Examples of high-frequency relative sea-level fall in the Late Rhaetian (two stages), late Early Sinemurian, Middle Callovian, and rises in the Late Rhaetian (two stages), Early Sinemurian, early Late Sinemurian and Middle-Late Callovian have been identified within the Domeyko basin succession.

(7) Comparison of the relative sea-level fluctuations interpreted from the Domeyko basin succession with those documented from other similar aged South American marginal basins and northern hemisphere basins allows the distinction of regional from global events, and a methodology for potentially differentiating between eustatic and tectonic driving mechanisms. The choice of these basins permits an objective analysis of relative sea-level change using basins of different tectonic setting, on different continental plates. The problems associated with Bajocian-Bathonian ammonite provincialism and biostratigraphical correlation between South America and Europe are inherent if these continental plates are to be compared, however a general comparison can still be made.

(8) Relative sea-level fall in the late Early Sinemurian, earliest Pliensbachian, earliest Aalenian, Early Callovian, earliest Valanginian, and rises in the earliest Hettangian, earliest and Late Toarcian, Early and Late Bajocian, Late Bathonian and earliest Oxfordian of the Domeyko basin appear time-equivalent to similar events in other southern and northern hemisphere basins and thus are interpreted to be products of eustatically driven, global sea-level cycles.

(9) Relative sea-level falls in the earliest Bathonian, Late Oxfordian, earliest Valanginian and rises in the Late Kimmeridgian are interpreted to be tectonically-driven, continental-scale changes in accommodation space. Although the earliest Valanginian relative sea-level fall has been documented in northern hemisphere basins, the sequence boundary is interpreted to be tectonically-enhanced through regional uplift in Chile and Argentina.

(10) The Domeyko basin succession thus appears to be dominantly controlled by global sea-level fluctuations during the Early-Middle Jurassic and by continental-scale (but not global) fluctuations during the Middle Jurassic to mid-Cretaceous. The global sea-level fluctuations are interpreted to have been driven by glacio-eustasy, while the continental-scale tectonic events are interpreted to have been driven by the break-up of Pangea and subsequent fragmentation of Gondwana.

(11) The following five long-term relative sea-level falls in the Domeyko and Neuquén basins have no time correlative expressions in northern hemisphere basins and display a close temporal association with five major Gondwanan fragmentation phases. (A) the earliest Bathonian (170 Ma) fall was driven by the separation of Laurasia and Gondwana; (B) the Late Oxfordian (157 Ma) salinity crisis

was driven by the separation of west from east Gondwana; (C) the termination of the marine Domeyko basin was driven by the fragmentation of east Gondwana; (D) the termination of the marine Neuquén Basin (114 Ma) was driven by the opening of the South Atlantic; and (E) the major basin inversion associated with the Peruvian tectonic event (100 Ma) was driven by the final fragmentation phase within east Gondwana.

(12) Previously the origin of episodic contractional tectonic events affecting the normally extensional Andean margin have been attributed to changes in subduction zone dynamics associated with oceanic spreading and ocean plate splitting in the Pacific area. This is despite the fact that there are no particular signatures in terms of the variation in spreading rates that stand out to explain each of the contractional episodes documented herein. I believe that thermally induced Gondwanan fragmentation episodes provide a more immediately viable explanation, in that they provide a mechanism for plate re-organisations driving changes along the circum-supercontinental subduction zone. Increased subduction coupling owing to westward movement of the continental plate is considered to result in uplift, recorded in the marginal basins as tectonically-driven sequence boundaries. Specific basin responses include: (a) Type-1 and -2 sequence boundaries in fully marine successions; (b) basin barring and regionally extensive evaporite formation by spill replenishment; (c) incremental and overall changeover from marine to continental deposition systems; and (d) stepwise eastward migration of the volcanic arc. Thus, careful sequence stratigraphical analysis of active margin sedimentary basins provides a high resolution record, presently under-utilised in detecting, identifying and analysing global tectonic events in time.

7.2 Future Research

Although this thesis provides a potential stratigraphical framework to further understand the sedimentary evolution of the Domeyko basin succession there is considerable potential for future work. The stratigraphical framework presented in this thesis is intended to provide an analysis of the complete Jurassic succession in this little known basin, and hence concentrates on long-term changes in sedimentary basin-fill characteristics.

Therefore, by describing and characterising each of the high-frequency sequences the correlation could be further enhanced, with the possible identification of a higher, fourth-order cyclicity. The correlation of high-frequency sequences will be made easier as increasing biostratigraphical subdivision of the Southern Andes ammonite zonation becomes available, coupled with an increased ability to identify subtle depositional hiati.

A significant contribution to the understanding of the Jurassic Domeyko basin succession would be gained from the acquisition and analysis of subsurface data (ie. seismic and well-log data). Such a dataset is currently lacking and will probably remain absent unless a potential for hydrocarbon exploration and exploitation is discovered.

References

References

- Aberhan, M. 1993a. Benthic macroinvertebrate associations on a carbonate/clastic ramp in segments of the early Jurassic back-arc basin of northern Chile (26°-29°S). *Revista Geologica de Chile*, **20**, 105-136.
- 1993b. Faunal replacement in the Early Jurassic of Northern Chile: implications for the evolution in Mesozoic benthic shelf ecosystems. *Palaeogeography, Palaeoclimatology, Palaeoecology*, **103**, 155-177.
- Acenolaza, F., Benedetto, J. & Salfity, J. 1972. El Neopaleozoico de la Puna Argentina: su fauna y relacion con areas vecinas. *An. Acad. Brasil. Cienc.*, **44**, 5-20.
- Acenolaza, G.F. & Durand, F.R. 1984. The trace fossil *Oldhamia*. Its interpretation and occurrence in the lower Cambrian of Argentina. *N. Jahrb. Geol. Palaeont. Munster*, **12**, 728-740.
- 1986. Upper Precambrian-Lower Cambrian biota from the northwest of Argentina. *Geological Magazine*, **123**, 367-375.
- Aitken, J.F. & Flint, S.S. 1994. High-Frequency sequences and the nature of incised-valley fills in fluvial systems of the Breathitt Group (Pennsylvanian), Appalachian Foreland Basin, Eastern Kentucky. *Society of Economic Paleontologists and Mineralogists, Special Publication 51*, 353-368.
- Allmendinger, R.W., Gubbels, T., Isaacks, B. & Cladouhos. 1993. Lateral variations in late Cenozoic deformation, Central Andes, 20°-28°S. *Second International Symposium on Andean Geodynamics*, Oxford, England, 155-158.
- Allmendinger, R.W., Ramos, V.A., Jordan, T.E., Palma, M. & Isaacks, B.L. 1983. Paleogeography and Andean structural geometry, north-west Argentina. *Tectonics*, **2**, 1-16.
- Anderson, D.L. 1994. Superplumes or supercontinents? *Geology*, **22**, 39-42.
- Anderson, R.Y. 1982. A long geoclimatic record from the Permian. *Journal of Geophysical Research*, **87C**, 7285-7294.
- 1984. Orbital forcing of evaporitic sedimentation. In: Berger, A., Imbrie, J., Hays, J., Kukla, G. & Slatzman, B. (eds.), *Milankovich and climate*. Reidel, Dordrecht, 147-162.
- Anderson, T.H. & Schmidt, V.A. 1983. The evolution of middle America and the Gulf of Mexico Caribbean Sea region during Mesozoic time. *Geological Society of America Bulletin*, **94**, 941-966.
- Andriessen, P.A.M. & Reutter, K.J. 1994. K-Ar and fission track mineral age determination of igneous rocks related to multiple magmatic arc systems along the 23°S latitude of Chile and NW Argentina. In: Reutter, K.J., Scheuber, E. & Wigger, P.J. (eds.), *Tectonics of the southern Central Andes*. Springer-Verlag, Berlin, 141-153.
- Archangelsky, S. 1987. *El Sistema Carbonifero en el Republica Argentina*. Acad. Nac. Cienc., Cordoba, 383 pp.
- Arthur, M.A., Dean, W.E., Bottjer, D. & Scholle, P.A. 1984. Rhythmic in Mesozoic-Cenozoic pelagic carbonate sequences: the primary and diagenetic origin of Milankovich-like cycles. In: Berger, A., Imbrie, J., Hays, J., Kukla, G. & Slatzman, B. (eds.), *Milankovich and climate*. Reidel, Dordrecht, 191-222.
- Atherton, M.P., Pitcher, W.S. & Warden, V. 1983. The Mesozoic marginal basin of central Peru. *Nature*, **305**, 303-306.
- Baeza, L. 1976. *Geologia de Cerritos Bayos y areas adyacentes entre los 22°30'-22°45'S y los 68°55'-69°25'W, II Region, Antofagasta, Chile*. Universidad del Norte, Antofagasta.
- Bahlburg, H. 1985. Sedimentological aspects of the El Toco Formation (Palaeozoic; Coastal Cordillera) NW of Quillagua, northern Chile. *IV Congreso Geol. Chileno, Antofagasta*, **1**, 17-29.

References

- 1987. Sedimentology, petrology and geotectonic significance of the Paleozoic flysch in the Coastal Cordillera of Northern Chile. *N. Jb. Geol. Palaont. Mh.*, **9**, 527-599.
- 1990. The Ordovician basin in the Puna of N.W. Argentina and N. Chile: geodynamic evolution from back-arc to foreland basin. *Geotektonische Forschungen*, **75**, 107 pp.
- 1991. The Ordovician back-arc to foreland successor basin in the Argentinian-Chilean Puna: tectono-sedimentary trends and sea-level changes. In: (eds.), *International Association of Sedimentologists. Special Publication 12*, 465-484.
- 1993. Hypothetical southeast Pacific continent revisited: New evidence from the middle Palaeozoic basins of northern Chile. *Geology*, **21**, 909-912.
- Bahlburg, H. & Breitzkreuz, C. 1991. Palaeozoic evolution of active margin basins in the southern Central Andes (northwestern Argentina and northern Chile). *Journal of South American earth sciences*, **4**, 171-188.
- 1993. Differential response of a Devonian-Carboniferous platform-deeper basin system to sea-level change and tectonics, N. Chilean Andes. *Basin Research*, **5**, 21-40.
- Bahlburg, H., Breitzkreuz, C., Maletz, J., Moya, C. & Salfity, J.A. 1990. The Ordovician sedimentary rocks in the northern Puna of Argentina and Chile: New stratigraphical data based on graptolites. *Newsletter Stratigraphy*, **23**, 69-89.
- Bahlburg, H., Breitzkreuz, C. & Zeil, W. 1986. Palaeozoische Sedimente Nord-Chiles. *Berliner Geowissenschaftliche Abhandlungen*, **66**, 147-168.
- Bahlburg, H., Moya, M. & Zeil, W. 1994. Geodynamic evolution of the Early Palaeozoic Continental Margin of Gondwana in the Southern Central Andes of Northwestern Argentina and Northern Chile. In: Reutter, K.J., Scheuber, E. & Wigger, P.J. (eds.), *Tectonics of the Southern Central Andes*. Springer-Verlag, Berlin, 293-302.
- Bartok, P., Renz, Q. & Westermann, G.E.G. 1985. The Siquisique ophiolites, northern Lara State, Venezuela: a discussion of their middle Jurassic ammonites and tectonic implications. *Geological Society of America Bulletin*, **96**, 105-155.
- Bell, C.M. 1991. The relationships between sedimentary structures, transport directions and dune types in Mesozoic aeolian sandstones, Atacama Region, Chile. *Sedimentology*, **38**, 289-300.
- Bell, C.M. & Suarez, M. 1993. The depositional environments and tectonic development of a Mesozoic intra-arc basin, Atacama Region, Chile. *Geological Magazine*, **130**, 417-430.
- Berger, A. 1988. Milankovich theory and climate. *Rev. Geophysics*, **26**, 624-657.
- 1989. The spectral characteristics of pre-Quaternary climatic records, an example of the relationship between Astronomical Theory and Geosciences. In: Berger, A., Schneider, S. & Duplessy, J.C. (eds.), *Climate and geosciences*. Kluwer Academic Publishers, The Netherlands, 47-76.
- Bergh, H.W. 1977. Mesozoic sea-floor off Dronning Maud Land, Antarctica. *Nature*, **269**, 686-687.
- Bertram, G.T. & Milton, N.J. 1990. Reconstructing basin evolution from sedimentary thickness: the importance of palaeobathymetric control, with reference to the North Sea. *Basin Research*, **1**, 247-257.
- Besley, B.M. & Turner, P. 1983. *Origin of red-beds in a moist tropical climate (Etruria Formation, Upper Carboniferous, U.K.)*. Geol. Soc. Lond., London, 131-147.
- Biese, W.A. 1961. *El Jurassico de Cerritos Bayos*. Ph.D., Universidad de Chile, Santiago, Chile.
- Bogdanic, T. 1990. *Kontinentale Sedimentation der Kreide und des Alttertiars in Umfeld des subduktionsbedingten Magmatismus in der chilenischen Prakordillere (21°-23°S)*. Freie Universität, Berlin, 120 pp.

References

- Bogdanic, T. & Espinoza, S. 1994. Tectono-sedimentary evolution of the Cretaceous-early Tertiary and metallogenic scheme of northern Chile, between 20° and 26°S. In: Salfity, J.A. (eds.), *Cretaceous tectonics of the Andes*. Earth Evolution Sciences, Vieweg, Berlin, 213-265.
- Bogdanic, T., Hillebrandt, A.v. & Quinzio, L.A. 1985. El Aaleniano de Sierra de Varas, Cordillera de Domeyko, Antofagasta, Chile. *IV Congreso Geológico Chileno*, **1**, 58-75.
- Bond, G.C., Nickeson, P.A. & Kominz, M.A. 1984. Breakup of a supercontinent between 625 Ma and 555 Ma: new evidence and implications for continental histories. *Earth and Planetary Science Letters*, **70**, 325-345.
- Brandt, K. 1986. Glacieustatic cycles in the early Jurassic. *N. Jb. Geol. Palaontol. Mh.*, **5**, 257-274.
- Breitkreuz, C. 1985. Presentation of a marine volcano-sedimentary sequence of presumably pre-Devonian age in the Sierra de Argomedo (24°45'S-69°22'W), northern Chile. *IV Congreso Geológico Chileno*, Antofagasta, **1**, 1-76.
- 1986a. Das Palozoikum in den Kordilleren Nordchiles (21°-25°S). *Geotektonische Forschungen*, **70**, 88.
- 1986b. Plutonism in the central Andes. *Zbl. Geol. Palaont.*, **9/10**, 1283-1293.
- 1991. Fluvio-lacustrine sedimentation and volcanism in the Late Carboniferous tensional intra-arc basin, Northern Chile. *Sedimentary Geology*, **74**, 173-187.
- Breitkreuz, C., Helmdach, F.-F., Kohring, R. & Mosbrugger, V. 1992. Late Carboniferous intra-arc sediments in the North Chilean Andes: Stratigraphy, Paleogeography and Paleoclimate. *Facies*, **26**, 67-80.
- Breitkreuz, C. & Zeil, W. 1984. Geodynamic and magmatic stages on a traverse through the Andes between 20° and 24°S (N. Chile, S. Bolivia, N. W. Argentina). *Journal of the Geological Society of London*, **141**, 861-868.
- 1994. The late Carboniferous to Triassic volcanic belt in northern Chile. In: Reutter, K.J., Scheuber, E. & Wigger, P. (eds.), *Tectonics of the Southern Central Andes*. Springer-Verlag, Berlin, 277-292.
- Brown, L.F. & Fisher. 1977. *Seismic stratigraphic interpretation of depositional systems: examples from Brazil rift and pull-apart basins*. American Association of Petroleum Geologists, 213-248.
- Brown, M., Dallmeyer, R.D., Diaz, F. & Grocott, J. 1991. The role of the Atacama Fault System in the post Late Palaeozoic evolution of Northern Chile: Is it a terrane boundary. *Comunicaciones*, **42**, 30-35.
- Buchelt, M. & Tellez, C. 1988. The Jurassic La Negra Formation in the area of Antofagasta, northern Chile (Lithology, Petrography, Geochemistry). In: Bahlburg, H., Breitkreuz, C. & Giese, P. (eds.), *The Southern Central Andes*. Lecture Notes in Earth Sciences, **17**, Springer-Verlag, Berlin Heidelberg, 171-182.
- Butler, R.W.H., Lickorish, W.H., Grasso, M., Pedley, H.M. & Ramberti, L. 1995. Tectonics and sequence stratigraphy in Messinian basins, Sicily: Constraints on the initiation and termination of the Mediterranean salinity crisis. *Geological Society of America Bulletin*, **107**, 425-439.
- Callomon, J.H. 1984. A review of the biostratigraphy of the post lower Bajocian ammonites of western and northern North America. In: Westermann, G.E.G. (eds.), *Jurassic-Cretaceous biochronology and palaeogeography of North America*. **Special Paper 27**, Geological Association of Canada, 143-174.
- 1985. Biostratigraphy, chronostratigraphy and all that-again! *International symposium on Jurassic stratigraphy, Erlangen 1984*, Geological survey of Denmark, Copenhagen, 612-624.

References

- 1995. Time from fossils: S. S. Buckman and Jurassic high-resolution geochronology. *In*: Bas, M.J.L. (eds.), *Milestones in Geology*. **Memoir 16**, Geological Society of London, London, 127-150.
- Cariou, E. 1984. Structure, origin et paleobiogeographie de la famille des Reineckeidae, Ammonitina du Jurassique moyen. *C. R. Academy of Science (Paris)*, **298**, 245-248.
- Cathles, L.M. & Hallam, A. 1991. Stress-induced changes in plate density, Vail sequences, epirogeny and short-lived global sea-level fluctuations. *Tectonics*, **10**, 659-671.
- Charrier, R. 1979. El Triasico en Chile y regiones adyacentes de Argentina-Una reconstruccion paleogeografica y paleoclimatica. *Comunicaciones (Santiago)*, **26**, 1-47.
- Charrier, R. & Munoz, N. 1994. Jurassic Cretaceous Palaeogeographic evolution of the Chilean Andes at 23°-24°S latitude and 34°-35°S latitude: A comparative analysis. *In*: Reutter, K.J., Scheuber, E. & Wigger, P.J. (eds.), *Tectonics of the southern Central Andes*. Springer-Verlag, Berlin, 233-248.
- Chong, G.D. 1973. *Reconocimiento Geologico del area Catalina-Sierra de Varas y Estratigrafia del Jurassico del Profeta*. Ph.D. thesis, Universidad de Chile, Santiago, Chile.
- 1977. Contributions to the knowledge of the Domeyko Range, Northern Chile. *Geologisches Rundschau*, **66**, 374-404.
- Chong, G.D. & Gasparini, Z.B. 1975. Los Vertebrados Mesozoicos de Chile y su aporte Geo-Paleontologico. *Sexto Congreso Geologico Argentino*, Buenos Aires.
- Chong, G.D. & Hillebrandt, A. 1985. El Triasico preandino de Chile entre los 23° 30' y 26° 00' de lat. sur. *4th Congreso Geologico Chileno*, Antofagasta, **1**, 162-209.
- Clifton, H.E. 1981. Progradational sequences in Miocene shoreline deposits, southeastern Caliente Range, California. *Journal of Sedimentary Petrology*, **51**, 165-184.
- Cloetingh, S. 1988. Intraplate stresses: a tectonic cause for third-order cycles in apparent sea-level? *In*: Wilgus, C.K., Hastings, B.S., Kendall, C.G.S.C., Posamentier, H.W., Ross, C.A. & Van Wagoner, J.C. (eds.), *Sea-level changes: an integrated approach*. **Special Publication 42**, Society of Economic Paleontologists and Mineralogists, Tulsa, 19-29.
- Coira, B., Davidson, J., Mpodozis, C. & Ramos, V. 1982. Tectonic and magmatic evolution of the Andes of N.Argentina and Chile. *Earth Science Reviews*, **18**, 303-332.
- Couzens, T.J. 1992. *The rift to drift transition and sequence stratigraphy at passive continental margins*. Ph.D. thesis, University of Liverpool, Liverpool, U.K.
- Cross, T.A. 1986. Controls of foreland basin subsidence. *In*: Allen, P.A. & Homewood, P. (eds.), *Foreland basins*. **Special publication 8**, International association of sedimentologists, Oxford, 15-40.
- Dalmayrac, B., Lancelot, J.R. & Leyreloup, A. 1977. Two-billion-year granulites in the Late Precambrian metamorphic basement along the southern Peruvian coast. *Science*, **198**, 49-51.
- Dalmayrac, B., Laubacher, G., Marocco, R., Martinez, C. & Tomasi, P. 1980. La chaine Hercynienne d'Amerique du Sud. Structure y evolution d'un orogene intracratonique. *Geologisches Rundschau*, **69**, 1-21.
- Dalrymple, R.W., Boyd, R. & Zaitlin, B.A. 1994. History of research, types and internal organisation of incised-valley systems: Introduction to the volume. *In*: Dalrymple, R.W., Boyd, R. & Zaitlin, B.A. (eds.), *Incised-valley systems: Origin and sedimentary sequences*. **Special Publication 51**, Society of Economic Paleontologists and Mineralogists, Tulsa, 3-10.
- Dalziel, I.W.D. 1986. Collision and Cordilleran orogenesis: an Andean perspective. *In*: Coward, M.P. & Ries, A.C. (eds.), *Collision Tectonics*. **Special Publication 19**, Geological Society of London, London, 389-404.

References

- 1991. Pacific margins of Laurentia and East Antarctica-Australia as a conjugate rift pair: Evidence and implications for an Eocambrian supercontinent. *Geology*, **19**, 598-601.
- Dalziel, I.W.D., Salda, L.H.D. & Gahagan, L.M. 1994. Palaeozoic Laurentia-Gondwana interaction and the origin of the Appalachian-Andean mountain system. *Geological Society of America Bulletin*, **106**, 243-252.
- Dalziel, I.W.D., Storey, B.C., Garrett, S.W., Grunow, A.M., Herrod, L.D.B. & Pankhurst, R.J. 1987. *Extensional tectonics and the fragmentation of Gondwanaland*. Geol. Soc. Lond., London, 433-441.
- Dalziel, I.W.D., Wit, M.J.D. & Palmer, K.F. 1974. A fossil marginal basin in the southern Andes. *Nature*, **250**, 291-294.
- Dam, G. & Surlyk, F. 1992. Forced regressions in a large wave-dominated and storm-dominated anoxic lake, Rhaetian-Sinemurian Kap Stewart Formation, East Greenland. *Geology*, **20**, 749-752.
- 1993. Cyclic sedimentation in a large wave and storm-dominated anoxic lake; Kap Stewart Formation (Rhaetian-Sinemurian), Jameson Land, East Greenland. In: Posamentier, H.W., Summerhayes, C.P., Haq, B.U. & Allen, G.P. (eds.), *Sequence stratigraphy and facies associations. Special Publication 18*, International Association of Sedimentologists, 419-438.
- 1995. Sequence stratigraphic correlation of lower Jurassic shallow-marine and paralic successions across the Greenland-Norway seaway. In: Steel, R.J., Felt, V.L., Johannessen, E.P. & Mathieu, C. (eds.), *Sequence stratigraphy on the northwest European margin. Special Publication 5*, Norwegian Petroleum Society (NPF), Amsterdam, 483-510.
- Damm, K.W. & Pichowiak, S. 1981. Geodynamik und Magmengenese in der Kustenordillere Nordchiles zwischen Taltat und Chanaral. *Geotekton. Forsch. Stuttgart*, **61**.
- Damm, K.W., Pichowiak, S. & Todt, W. 1986. Geochemie, Petrologie und Geochronologie der Plutonite und des metamorphen Grundgebirges in Nordchile. *Berliner Geowissenschaftliche Abhandlungen*, **66**, 73-146.
- Damm, K.W., Pichowiak, S. & Zeil, W. 1981. The plutonism in the North Chilean coastal-range and its geodynamic significance. *Geologisches Rundschau*, **70**, 1054-1076.
- Davidson, J., Mpodozis, C. & Rivano, S. 1981a. El Paleozoico de Sierra de Almeida, al Oeste de Monturaqui, Alta Cordillera de Antofagasta, Chile. *Revista Geologica de Chile*, **12**, 3-23.
- 1981b. Evidencias de tectogenesis de Devonico Superior-Carbonifero Inferior al Oeste de Augusta Victoria Antofagasta, Chile. *Revista Geologica de Chile*, **12**, 79-86.
- Dickinson, W.R. & Coney, P.J. 1980. *Plate tectonic constraints on the origin of the Gulf of Mexico*. Baton Rouge: Louisiana State University, Louisiana, 27-36.
- Dingle, R.V. 1994. Structural and sedimentary development of the continental margin off southwestern Africa. *Communications of the Geological Survey of Namibia*, **8**, 35-43.
- Dingman, R.J. 1963. *Cuadrangulo Tulo*, Provincia de Antofagasta, Carta Geologica de Chile 14 edn. Instituto de Investigaciones Geologicas.
- Dommergue, J.L., Cariou, E., Contini, D., Hantzpergue, P., Marchand, D., Meister, C. & Thierry, J. 1989. Homeomorphies et canalisations evolutive; le role de l'ontogenese. Quelques exemples pris chez les ammonites du Jurassique. *Geobios*, **22**, 5-48.
- Einsele, G. 1982. Limestone-marl cycles (periodites): diagnosis, significance, causes-a review. In: Einsele, G. & Seilacher, A. (eds.), *Cyclic and event stratification*. Springer, Berlin, 8-53.
- Erlich, R.N., Longo, A.P. & Hyare, S. 1993. Response of carbonate platform margins to drowning: evidence of environmental collapse. In: Loucks, R.G. & Sarg, J.F. (eds.), *Carbonate sequence stratigraphy-Recent developments and applications. Memoir 57*, American Association of Petroleum Geologists, Tulsa, 241-266.

References

- Fernandez-Lopez, S., Chong, G. & Hans, G.W. *in press*. Sedimentacion y volcanismo durante el Jurassico medio en el area de Cerro Jaspe (Precordillera Chilena).
- Fernandez-Lopez, S., Chong, G., Quinzio, L.A. & Wilke, H.G. 1994. The upper Bajocian and Bathonian in the Cordillera de Domeyko, North-Chilean Precordillera: Sedimentological and Biostratigraphical Results. *Geobios*, **M. S. 17**, 187-201.
- Ferraris, B. & Di-Biase, F. 1978. *Hoja Antofagasta, Region de Antofagasta, Chile*, 33 edn. Instituto de Investigaciones Geologicas.
- Fischer, A.G. 1986. Climatic rhythms recorded in strata. *Annual Review Earth Planet Science*, **14**, 351-376.
- Fischer, A.G., De Boer, P.L. & Premoli Silva, I. 1990. Cyclostratigraphy. *In: Ginsburg, R.N. & Beaudoin, B. (eds.), Cretaceous resources, events and rhythms*. Kluwer Academic Publishers, The Netherlands, 139-172.
- Fischer, A.G., Herbert, T.D. & Premoli Silva, I. 1985. Carbonate bedding cycles in Cretaceous pelagic and hemipelagic sequences. *In: Pratt, L. & Kauffman, E. (eds.), Fine-grained deposits and biofacies of the Western Interior Seaway: Evidence of cyclic sedimentary processes*. **Guidebook 4**, Society of Economic Palaeontologists and Mineralogists, 1-10.
- Fischer, R. 1984. Some problems of Toarcian biostratigraphy. *In: Michelson, O. & Zeiss, A. (eds.), International symposium on Jurassic stratigraphy*. **1**, International Subcommittee on Jurassic Stratigraphy, Copenhagen, 30-44.
- Flint, S., Aitken, J. & Hampson, G. 1995. Application of sequence stratigraphy to coal-bearing coastal plain successions: implications for the UK Coal Measures. *In: Whateley, M.K.G. & Spears, D.A. (eds.), European Coal Geology*. **Special Publication 82**, Geological Society of London, London, 1-16.
- Flint, S. & Turner, P. 1988. *Alluvial fan and fan-delta sedimentation in a forearc extensional setting: the Cretaceous Coloso Basin of northern Chile*. Blackie, Glasgow.
- Flint, S., Turner, P., Jolley, E.J. & Hartley, A.J. 1993. Extensional tectonics in convergent margin basins: An example from the Salar de Atacama, Chilean Andes. *Geological Society of America Bulletin*, **105**, 603-617.
- Folk, R., Andrews, P. & Lewis, D. 1970. Detrital sedimentary rock classification and nomenclature for use in New Zealand. *New Zealand J. Geol. Geophys*, **13**, 937-968.
- Forster, R. & Hillebrandt, A.v. 1984. Das Kimmeridge des Profeta-Jura in Nordchile mit einer Mecochirus-Favreina-Vergesellschaftung (Decapoda, Crustacea-Ichnogenus). *Mitt. Bayer Staatsammlung Palaont. Hist. Geol.*, **24**, 67-84.
- Foucault, A., Powichrowski, L. & Prud'Homme, A. 1987. Le Controle astronomique de la sedimentation turbiditique: exemple du Flysch a Helminthoides des Alpes Ligures (Italie). *Comptes Rendus Academie Scientifique Paris, Series II*, **305**, 1007-1011.
- Frakes, L.A. & Francis, J.E. 1988. A guide to Phanerozoic cold polar climates from high-latitude ice-rafting in the Cretaceous. *Nature*, **333**, 547-549.
- Fullerton, L.G., Sager, W.L. & Handschumacher, D.W. 1989. Late Jurassic-early Cretaceous evolution of the eastern Indian Ocean adjacent to north-west Australia. *Journal of Geophysical Research*, **94**, 2937-2953.
- Galloway, W.E. 1989. Genetic stratigraphic sequences in basin analysis I: Architecture and genesis of flooding-surface bounded depositional systems. *Bulletin of the American Association of Petroleum Geologists*, **73**.
- Garcia, F.A., Perez, E. & Zeballos, E. 1962. El Ordoviciano de Aguada de La Perdiz, Puna de Atacama, Provincia de Antofagasta. *Revista Minera*, **77**, 52-61.

References

- Garcia, F.A. 1967. Geología del Norte Grande de Chile. *Symposium Sobre el Geosinclinal Andino*, Santiago, Chile, Sociedad Geologica de Chile, 3, 138.
- Gawthorpe, R., Frazer, A. & Collier, R. 1994. Tectonic controls on accommodation and sediment flux in rift basins: implications for sequence development in fault controlled basins. *High Resolution Sequence Stratigraphy: Innovations and Applications*, 28th-30th March, University of Liverpool, Liverpool, U.K., 24-25.
- Gebelein, C.D. 1976. *Open marine subtidal and intertidal stromatolites (Florida, the Bahamas and Bermuda)*. Elsevier, 381-388.
- Geyer, O.F. 1980. Die mesozoische Magnafazies-Abfolge in den nordlichen Anden (Peru, Ekuador, Kolumbien). *Geologisches Rundschau*, 69, 875-891.
- Golubic, S. & Fischer, A.G. 1975. Ecology of calcareous nodules forming in Little Conestoga Creek near Lancaster, Pennsylvania. *Verh. Intern. Verein. Limnol.*, 19, 2315-2323.
- Gotte, M. 1988. Estudio geologico-Estructural de Galeana/N. L. (Mexico) y sus alrededores. *Actas Fac. Ciencias Tierra UANL Linares, Linares, Mexico*, 3, 61-87.
- Graciansky, P.C., Dardeau, G., Dumont, T., Jacquin, T., Marchand, D., Mouterde, R. & Vail, P.R. 1993. Depositional sequence cycles, transgressive-regressive facies cycles and extensional tectonics: example from the southern Subalpine Jurassic basin, France. *Bulletin of the Geological Society of France*, 164, 709-718.
- Gradstein, F.M., Agterberg, F.P., Ogg, J.G., Hardenbol, S., Vanveen, P., Thierry, J. & Huang, Z.H. 1994. A Mesozoic time-scale. *Journal of Geophysical Research-Solid Earth*, 99, 24051-24074.
- Grier, M.E., Salfity, J.A. & Allmendinger, R.W. 1991. Andean reactivation of the Cretaceous Salta rift, north-west Argentina. *Journal of South American Earth Sciences*, 4, 351-372.
- Grocott, J., Taylor, G.K., Treloar, P.J. & Wilson, J. 1995. Magmatic arc fault systems in the Mesozoic of northern Chile. *Andean Geosciences Workshop (IGCP 345)*, Kingston University, London.
- Groschke, M. & Hillebrandt, A. 1994. The Bathonian in northern Chile. *Geobios*, M. S. 17, 255-264.
- Groschke, M., Hillebrandt, A.v., Prinz, P., Quinzio, L.A. & Wilke, H.G. 1988. Marine Mesozoic Palaeogeography in northern Chile between 21°-26°S. In: Bahlburg, H., Bretkreuz, C. & Giese, P. (eds.), *The Southern Central Andes*. Lecture Notes in Earth Sciences, 17, Springer-Verlag, Berlin Heidelberg, 105-117.
- Groschke, M. & Wilke, H.G. 1986. Lithology and stratigraphy of Jurassic sediments in the north Chilean Pre-cordillera between 21°30' and 22°S. *Zbl. Geol. Palaont. Teil I*, 9/10, 1317-1324.
- Gulisano, C.A. & Gutierrez-Pleimling, A.R. 1994. Neuquén Basin, Neuquén Province, Argentina Field-guide A. *4th International Congress on Jurassic Stratigraphy and Geology*, Mendoza, Argentina, 120 pp.
- Gurnis, M. 1993. Phanerozoic marine inundation of continents driven by dynamic topography above subducting slabs. *Nature*, 364, 589-593.
- Gygi, R.A. & Hillebrandt, A.v. 1991. Ammonites (mainly Gregoryceras) of the Oxfordian (late Jurassic) in northern Chile and time-correlation with Europe. *Memoires Suisses de Paleontologie*, 113, 136-167.
- Hallam, A. 1967a. The depth significance of shales with bituminous laminae. *Marine geology*, 5, 481-493.
- 1967b. An environmental study of the upper Domerian and lower Toarcian in Great Britain. *Royal society of London philosophical transactions, Series B*, 252, 393-445.

References

- 1978. Eustatic cycles in the Jurassic. *Palaeogeography, Palaeoclimatology & Palaeoecology*, **23**, 1-32.
- 1983. Early- and mid-Jurassic molluscan biogeography and the establishment of the central Atlantic seaway. *Palaeogeography, Palaeoclimatology & Palaeoecology*, **43**, 181-193.
- 1988. A reevaluation of Jurassic eustasy in the light of new data and the revised Exxon curve. In: Wilgus, C.K., Hastings, B.S., Kendall, C.G.S.C., Posamentier, H.W., Ross, C.A. & Van Wagoner, J.C. (eds.), *Sea-level changes: an integrated approach*. **Special Publication 42**, Society of Economic Paleontologists and Mineralogists, Tulsa, 261-273.
- 1991. Relative importance of regional tectonics and eustasy for the Mesozoic of the Andes. In: Macdonald, D. (eds.), *Sedimentation, tectonics and eustasy: Sea-level changes at active margins*. **Special Publication 12**, International Association of Sedimentologists, 189-200.
- Hallam, A. & Bradshaw, M.J. 1979. Bituminous shales and oolitic ironstones as indicators of transgressions and regressions. *Journal of the Geological Society of London*, **136**, 157-164.
- Halpern, M. 1978. Geological significance of Rb-Sr isotopic data of northern Chile crystalline rocks of the Andean orogen between 23° and 27°S. *Geological Society of America Bulletin*, **89**, 522-532.
- Halpern, M. & Latorre, C.O. 1973. Estudio geocronologico inicial de rocas del noroeste Argentino. *Asociacion Geologica de Argentina Revista*, **28**, 195-205.
- Haq, B.U., Hardenbol, J. & Vail, P.R. 1987. Chronology of fluctuating sea levels since the Triassic. *Science*, **235**, 1156-1167.
- 1988. Mesozoic and Cenozoic chronostratigraphy and eustatic cycles. In: Wilgus, C.K., Hastings, B.S., Kendall, C.G.S.C., Posamentier, H.W., Ross, C.A. & Van Wagoner, J.C. (eds.), *Sea-level changes: an integrated approach*. **Special Publication 42**, Society of Economic Paleontologists and Mineralogists, Tulsa, 71-108.
- Hardy, L.A. & Ginsburg, R.M. 1977. *Layering: The origin and environmental significance of lamination and thin bedding*. In: *Sedimentation on the modern carbonate tidal flats of northwest Andros Island, Bahamas*. Johns Hopkins University Press, Baltimore, 50-123.
- Harland, W.B., Armstrong, R.L., Cox, A.V., Craig, L.E., Smith, A.G. & Smith, D.G. 1990. *A geological time scale 1989*. Cambridge University Press.
- Harrington, H. 1961. Geology of parts of Antofagasta and Atacama provinces of northern Chile. *American Association of Petroleum Geologists Bulletin*, **45**, 169-197.
- 1967. Devonian of South America. *International Symposium on the Devonian System*, Calgary, **2**, 551-671.
- Harrison, C.G.A. 1990. Long-term eustasy and epirogeny in continents. In: Revelle, R. (eds.), *Sea-level change*. National research council, studies in geophysics, National Academy Press, Washington D.C., 141-158.
- Hays, J.D., Imbrie, J. & Shackleton, N.J. 1976. Variations in the Earth's orbit: pacemaker of the ice-ages. *Science*, **194**, 1121-1132.
- Herbert, T.D. & Fischer, A.G. 1986. Milankovich climatic origin of mid-Cretaceous black shale rhythms in central Italy. *Nature*, **321**, 739-743.
- Herve, F., Davidson, J., Godoy, E., Mpodozsis, C. & Covacevich, V. 1981. The late Palaeozoic in Chile: stratigraphy, structure and possible tectonic framework. *An. Acad. Brasil. Ciencias*, **53**, 361-373.
- Hillebrandt, A.v. 1971. Der Jura in der chileno-argentinischen Hochkordillere (25° bis 32°30'S). *Munstersche Forsch. Geol. Palaont.*, **20/21**, 63-87.

References

- 1973. Neue Ergebnisse über den Jura von Chile und Argentinien. *Munstersche Forsch. Geol. Palaont.*, **31/32**, 167-199.
- 1987. *Liassic ammonite zones of South America and correlations with other provinces-description of new genera and species of ammonites*. Commission for Southamerican Jurassic/Cretaceous, Mendoza, 111-157.
- 1988. Ammonite biostratigraphy of the South American Hettangian-description of two new species of *Psiloceras*. *2nd International Symposium on Proceedings of the Jurassic Stratigraphy*, Lisbon: Centro Geocien. Univ. Coimbra, 13-27.
- 1990. The Triassic/Jurassic boundary in northern Chile. *Meeting on the Triassic/Jurassic boundary*, Lyon: Inst. Cathol., Cahiers Ser. Sci., 27-53.
- 1994. The Triassic/Jurassic boundary and Hettangian biostratigraphy in the area of the Utcubamba Valley (northern Peru). *Geobios*, M. S. **17**, 297-307.
- Hillebrandt, A.v. & Schmidt-Effing, R. 1981. Ammoniten aus dem Toarcium (Jura) von Chile (Sudamerica). *Zitteliana*, **6**, 3-74.
- Hillebrandt, A.v., Smith, P., Westermann, G.E.G. & Callomon, J.H. 1992. Ammonite zones of the circum-Pacific region. In: Westermann, G.E.G. (eds.), *The Jurassic of the Circum-Pacific*. Cambridge University Press, New York, 247-272.
- Hillebrandt, A.v. & Westermann, G.E.G. 1985. Aalenian (Jurassic) ammonite faunas and zones of the Southern Andes. *Zitteliana*, **12**, 3-55.
- Hillebrandt, A.v., Westermann, G.E.G., Callomon, J.H. & Determan, R.L. 1992. Ammonites of the circum-Pacific region. In: Westermann, G.E.G. (eds.), *The Jurassic of the Circum-Pacific*. Cambridge University Press, New York, 342-359.
- Hollingworth, S.E. & Rutland, R.W.R. 1968. Studies of Andean uplift. Part 1-Post Cretaceous evolution of the San Bartolo area, N. Chile. *Geology*, **6**, 49-62.
- Holmes, A. 1965. *Principles of Physical Geology*. Thomas Nelson, London, 1288 pp.
- Holmes, A.E. & Christie-Blick, N. 1993. Origin of sedimentary cycles in mixed carbonate/siliciclastic systems: An example from the Canning basin, western Australia. In: Loucks, R.G. & Sarg, J.F. (eds.), *Carbonate sequence stratigraphy-recent developments & applications*. American Association of Petroleum Geologists, Tulsa, 181-212.
- Howell, J.A. & Flint, S.S. *in press*. A model for high resolution sequence stratigraphy within extensional basins.
- Hsü, K.J., Montadert, L., Bernoulli, D., Cita, M.B., Erickson, A., Garrison, R.E., Kidd, R.B., Melieres, F., Muller, C. & Wright, R. 1977. History of the Mediterranean salinity crisis. *Nature*, **267**, 399-403.
- Hubbard, R.J. 1988. Age and significance of sequence boundaries on Jurassic and early Cretaceous rifted continental margins. *American Association of Petroleum Geologists Bulletin*, **72**, 49-72.
- Huete, C., Maksiav, V., Moscoso, R., Ulriksen, C. & Vergara, C. 1977. Antecedentes geocronologicas de rocas intrusivas y volcanicas en la Cordillera de los Andes comprendida entre la Sierra Moreno y el Rio Loa y los 21 y 22° latitud Sur. II Region. *Revista Geologica de Chile*, **4**, 35-41.
- Hughes, D.A. & Lewin, J. 1982. A small-scale flood plain. *Sedimentology*, **29**, 891-895.
- Hunt, D. & Tucker, M.E. 1992. Stranded parasequences and the forced regressive wedge systems tract: deposition during base-level fall. *Sedimentary Geology*, **81**, 1-9.

References

- 1993. Sequence stratigraphy of carbonate shelves with an example from the mid-Cretaceous (Urgonian) of southeast France. *International Association of Sedimentologists, Special Publication 18*, 307-341.
- Imbrie, J., Hays, J.D., Martinson, D.G., McIntyre, A., Mix, A.C., Morley, J.J., Pisias, N.G., Prell, W.L. & Shackleton, N.J. 1984. The orbital theory of Pleistocene climate: support from a revised chronology of the marine $\delta^{18}\text{O}$ record. In: Berger, A., Imbrie, J., Hays, J., Kukla, G. & Slatzman, B. (eds.), *Milankovich and climate. Part 1*, Reidel, Dordrecht, 269-305.
- Imbrie, J. & Imbrie, J.Z. 1980. Modelling the climatic response to orbital variations. *Science*, **207**, 943-953.
- Isaacs, B.L. 1988. Uplift of the central Andean plateau and bending of the Bolivian orocline. *Journal of Geophysical Research*, **93**, 3211-3231.
- Isaacson, P.E. 1975. Evidence for a western extracontinental land source during the Devonian period in the Central Andes. *Geological Society of America Bulletin*, **86**, 39-46.
- Isaacson, P.E. & Sablock, P.E. 1989. Devonian system in Bolivia, Peru and northern Chile. In: McMillan, N.J., Embry, A.F. & Glass, D.J. (eds.), *Devonian of the world. Memoir 14*, Canadian Society of Petroleum Geology, 719-728.
- Jaillard, E. 1994. Kimmeridgian to Paleocene tectonic and geodynamic evolution of the Peruvian (and Ecuadorian) margin. In: Salfity, J.A. (eds.), *Cretaceous tectonics of the Andes*. Springer, 101-167.
- Jaillard, E., Soler, P., Carlier, G. & Mourier, T. 1990. Geodynamic evolution of the northern and central Andes during early to middle Mesozoic times: a Tethyan model. *Journal of the Geological Society of London*, **147**, 1009-1022.
- James, D.E. 1971. Plate tectonic model for the evolution of the Central Andes. *Geological Society of America Bulletin*, **82**, 3325-3346.
- Jansa, L.F. 1986. Palaeoceanography and evolution of the North Atlantic basin during the Jurassic. In: Vogt, P.R. & Tucholke, B.E. (eds.), *The Geology of North America. Vol. M: The western North Atlantic region*. Geological Society of America, 603-616.
- Jenkyns, H.C. 1988. The early Toarcian (Jurassic) anoxic event: Stratigraphic, sedimentary and geochemical evidence. *American Journal of Science*, **288**, 101-151.
- Jervey, M.T. 1988. Quantitative geological modelling of siliciclastic rock sequences and their seismic expression. In: Wilgus, C.K., Hastings, B.S., Kendall, C.G.S.C., Posamentier, H.W., Ross, C.A. & Van Wagoner, J.C. (eds.), *Sea-level changes: an integrated approach. Special Publication 42*, Society of Economic Paleontologists and Mineralogists, Tulsa, 47-70.
- Jones, B. & Goodbody, Q.H. 1985. Oncolites from a shallow lagoon, Grand Cayman Island. *Bull. Can. petrol. Geol.*, **32**, 254-260.
- Jordan, T.E. & Alonso, R.N. 1987. Cenozoic stratigraphy and basin tectonics of the Andes Mountains, 20-28°S latitude. *American Association of Petroleum Geologists Bulletin*, **71**, 49-64.
- Jordan, T.E., Isaacs, B.L., Allmendinger, R.W., Brewer, J.A., Ramos, V.A. & Ando, C.J. 1983. Andean tectonics related to the geometry of subducted Nazca Plate. *Bulletin of the Geological Society of America*, **94**, 341-361.
- Kay, S.M., Ramos, V.A., Mpodozis, C. & Sruoga, P. 1989. Late Palaeozoic to Jurassic silicic magmatism at the Gondwana margin: Analogy to the middle Proterozoic in North America? *Geology*, **17**, 324-328.
- Kendall, A.C. 1992. Evaporites. In: Walker, R.G. & James, N.P. (eds.), *Facies Models (Response to Sea Level Change)*. Geological Society of Canada.
- Klimek, K. 1974. The structure and mode of sedimentation of the flood-plain deposits in the Wisloka Valley (South Poland). *Stud. Geomorph. Carpatho-Balcanica*, **8**, 135-151.

References

- Klitgord, K.D., Hutchinson, D.R. & Schouten, H. 1988. U.S. continental margin: structural and tectonic framework. In: Sheridan, R.E. & Grow, J.A. (eds.), *The geology of north America-The Atlantic continental margin U.S. I-2*, Geological Society of America, Boulder, Colorado, 19-55.
- Kokogian, D.A. & Mancilla, O. 1989. *Analisis estratigrafico secuencial de la Cuenca Cuyana*. Instituto Superior de Correlacion Geologica, Universidad Nacional de Tucuman, Argentina, 169-202.
- Kukal, Z. 1990. *The rate of geological processes*. Elsevier, Amsterdam.
- Larson, R.L. 1977. Early Cretaceous breakup of Gondwanaland off western Australia. *Geology*, **5**, 57-60.
- 1991. Latest pulse of Earth-Evidence for a mid-Cretaceous superplume. *Geology*, **19**, 547-550.
- Legarreta, L. 1991. Evolution of a Callovian-Oxfordian carbonate margin in the Neuquén basin of west-central Argentina-facies, architecture, depositional sequence and global sea-level changes. *Sedimentary geology*, **70**, 209-240.
- Legarreta, L., Gulisano, C.A. & Uliana, M.A. 1993. Las secuencias sedimentarias jurasico-cretacicas. *Geologia y recursos naturales, Relatorio XII° Congreso Geologico Argentino/II° Congreso Exploracion de Hidrocarburos*, Buenos Aires, 87-114.
- Legarreta, L. & Uliana, M.A. 1991. Jurassic-Cretaceous marine oscillations and geometry of back-arc basin-fill, central Argentine Andes. In: McDonald, D.c.M. (eds.), *Sedimentation, tectonics and eustasy. Special Publication 12*, International Association of Sedimentologists, 429-450.
- *in press*. The Jurassic succession in west-central Argentina: stratal patterns, sequences and palaeogeographic evolution. *Palaeogeography, palaeoclimatology and palaeoecology*.
- Little, C.T.S. & Benton, M.J. 1995. Early Jurassic mass extinction: A global long-term event. *Geology*, **23**, 495-498.
- Loucks, R.G. & Sarg, J.F. 1993. *Carbonate sequence stratigraphy-Recent developments and applications*. American Association of Petroleum Geologists, Tulsa, 545 pp.
- Loughman, D.L. & Hallam, A. 1982. A facies analysis of the Pucara Group (Norian to Toarcian carbonate, organic-rich shale and phosphate) of central and northern Peru. *Sedimentary Geology*, **32**, 161-194.
- Loutit, T.S., Hardenbol, J., Vail, P.R. & Baum, G.R. 1988. *Condensed sections: the key to age determination and correlation of continental margin sequences*. Society of Economic Paleontologists and Mineralogists, 183-213.
- Macellari, C. 1988. Cretaceous palaeogeography and depositional cycles of western South America. *Journal of South American Earth Sciences*, **1**, 373-418.
- Mack, G.H., James, W.C. & Monger, H.C. 1993. Classification of paleosols. *Bulletin of the Geological Society of America*, **105**, 129-136.
- Maksaev, V. 1990. *Metallogeny, geological evolution, and thermochronology of the Chilean Andes between latitudes 21° and 26° south, and the origin of major porphyry copper deposits*. Ph.D., Dalhousie University, Halifax, Nova Scotia, Canada.
- Maksaev, V. & Marinovic, N. 1980. *Cuadrangulos Cerro de la Mica, Quillagua, Cerro Posada y Oficina Prosperidad, Region de Antofagasta*. Institute Investigation Geologica Chile, Santiago.
- Marinovic, N. & Lahsen, A. 1984. *Hoyo Calama, Region de Antofagasta, Chile*. Servicio Nacional de Geologia y Minería, Santiago.
- Martin, A.K. 1984. Propagating rifts-Crustal extension during continental rifting. *Tectonics*, **3**, 611-617.

References

- 1987. Plate re-organisations around southern-Africa, hot-spots and extinctions. *Tectonophysics*, **142**, 309-316.
- McKie, F.J.L. 1994. The interplay of Triassic marine and continental facies of the former extensional marginal basin of the north Chilean Cordillera de Domeyko. *7th Congreso Geologico Chileno*, Concepcion, **1**, 484-487.
- Megard, F. 1987. Cordilleran Andes and marginal Andes: a review of Andean geology north of the Arica Elbow (18°S). In: Monger, J.W. & Francheteau, J. (eds.), *Circum-Pacific orogenic belts and evolution of the Pacific Ocean Basin*. **18**, American Geophysical Union Geodynamic Series, 71-95.
- Mellere, D. & Steel, R.J. 1995. Facies architecture and sequentiality of nearshore and shelf sandbodies-Haystack Mountains Formation, Wyoming, U.S.A. *Sedimentology*, **42**, 551-574.
- Miall, A.D. 1990. *Principles of sedimentary basin analysis*. Springer, New York, 668 pp.
- Milankovich, M. 1941. *Canon of Insolation and the Ice-age problem (English translation by Isreal Program for Scientific Translation, Jerusalem 1969)*. Royal Serbian Academy, Belgrade, 633 pp.
- Milner, S.C., P., L.R.A. & O'Connor, J.M. 1995. Age of Mesozoic igneous rocks in northwestern Namibia and their relationship to continental breakup. *Journal of the Geological Society of London*, **152**, 97-104.
- Mingramm, A., Russo, A., Pozzo, A. & Cazau, L. 1979. Sierras Subandinas. *Symp. Geol. Region Argent.*, **1**, 95-138.
- Mitchum, R.M. 1977. *Seismic stratigraphy and global changes of sea-level, Part 1: Glossary of terms used in seismic stratigraphy*. American Association of Petroleum Geologists, 205-212.
- Mitchum, R.M. & Van Wagoner, J.C. 1990. High-frequency sequences and eustatic cycles in the Gulf of Mexico basin. *GCSSEPM 11th Research Conference*, Society of Economic Paleontologists and Mineralogists, 257-267.
- 1991. High-frequency sequences and their stacking patterns: sequence stratigraphic evidence of high-frequency eustatic cycles. *Sedimentary Geology*, **70**, 131-160.
- Mon, R. & Hongn, F. 1991. The structure of the Precambrian and lower Palaeozoic basement of the Central Andes between 22° and 32°S latitude. *Geologische Rundschau*, **80**, 745-758.
- Montano, J.M. 1976. Estudio geologico de la zona de Caracoles y areas vecinas, con enfasis en el Sistema Jurasic, Provincia de Antofagasta, II Region, Chile. *Universidad de Chile, Santiago*.
- Moraga, B., Chong, G., Fortt, M.A. & Henrique, H. 1974. Estudio geologico de Salar de Atacama, Provincia de Antofagasta, Chile. *Instituto del Investigaciones Geologica Chile*, **29**, 56.
- Morel, P. & Irving, E.C. 1978. Tentative paleocontinental maps for the early Phanerozoic and Proterozoic. *Journal of Geology*, **86**, 535-561.
- Mörner, N.A. 1981. Revolution in Cretaceous sea-level analysis. *Geology*, **9**, 344-346.
- Mpodozis, C. & Kay, S.M. 1990. Provincias magmaticas acidas y evolucion tectonica de Gondwana: Andes Chilenos (28°-31°S). *Revista Geologica de Chile*, **17**, 153-180.
- 1992. Late Palaeozoic to Triassic evolution of the Gondwana margin-Evidence from Chilean frontal Cordilleran batholiths (28°S to 31°S). *Geological Society of America Bulletin*, **104**, 999-1014.
- Nance, R.D., Worsley, T.R. & Moody, J.B. 1988. *The Supercontinent Cycle*. 177-187.
- Naranjo, J.A. & Puig, A. 1984. *Hojos Taltal y Chanaral, Regiones de Antofagasta y Atacama, Chile*. Servicio Nacional de Geologia y Minería, Santiago.

References

- Nemec, W. & Steel, R.J. 1988a. *Fan-deltas: Sedimentology and tectonic setting*. Blackie, Glasgow, 444 pp.
- 1988b. What is a fan-delta and how do we recognise it? *In: Nemec, W. & Steel, R.J. (eds.), Fan-deltas: Sedimentology and tectonic setting*. Blackie, Glasgow, 3-13.
- Noble, D.C., Miles, L.S., Megard, F. & Bowman, H. 1978. Comendite (peralkaline rhyolite) and basalt in the Mitu Group, Peru: evidence for Permian-Triassic lithospheric extension in the Central Andes. *Journal of Research U.S. Geological Survey*, **6**, 453-457.
- O'Byrne, C.J. & Flint, S.S. 1995. Sequence, parasequence and intraparasequence architecture of the Grassy Member, Blackhawk Formation, Book Cliffs, Utah, U.S.A. *In: C., V.W.J. & T., B.G. (eds.), Sequence stratigraphy of foreland basin deposits-outcrop and subsurface examples from the Cretaceous of North America. Memoir 64*, American Association of Petroleum Geologists, Tulsa, 225-256.
- Odin, G.S. 1992. Numerical time scale in 1988. *In: Westermann, G.E.G. (eds.), The Jurassic of the Circum-Pacific*. Cambridge University Press, New York, 3-11.
- Ogg, J.G. 1992. Jurassic magnetic polarity time scale. *In: Westermann, G.E.G. (eds.), The Jurassic of the Circum-Pacific*. Cambridge University Press, New York, 12-13.
- Ogg, J.G. 1994. Oxfordian magnetic polarity time scale. *IV International Congress on Jurassic Stratigraphy and Geology*, Mendoza, Argentina, **1**, 34.
- Oglesby, R.J. 1989. A CGM study of Antarctic glaciation. *Climate dynamics*, **3**, 135-156.
- Olsen, P. 1986. A 40 million year lake record of early Mesozoic orbital climatic forcing. *Science*, **234**, 842-848.
- Omarini, R., Cordani, U.G., Viramonte, J.A., Salfity, J.A. & Kawashita, K. 1979. Estudio isotopico Rb/Sr de la Faja Eruptiva de la Puna a los 22°35' lat. Sur, Argentina. *II Congreso Geologica Chileno*, Santiago, **3**, 257-269.
- Omarini, R., Reutter, K. & Bogdanic, T. 1991. Geological development and structures. *In: (eds.), Central Andean Transect*.
- Orchard, M.J. 1983. Epigondolella populations and their phylogeny & zonation in the Norian (upper Triassic). *Fossils & Strata*, **15**, 177-192.
- Padula, E., Rolleri, E.O., Mingramm, A.R.G., Criado-Roque, P., Flores, M.A. & Baldis, B.A. 1967. Devonian of Argentina. *In: Oswald, D.H. (eds.), International Symposium on the Devonian System*. **2**, Alberta Society of Petroleum Geology, 165-199.
- Paijmans, K., Blake, D.H., Bleeker, P. & McAlpine, J.R. 1971. Land resources of the Marchead-Kiunga area, Territory of Papua and New Guinea. *CSIRP Australia Land Res. Ser.*, **29**, 124.
- Pardo-Casas, F. & Molnar, P. 1987. Relative motions of the Nazca (Farallon) and South American plates since Late Cretaceous time. *Tectonics*, **6**, 233-248.
- Parrish, J.M., Parrish, J.T. & Ziegler, A.M. 1986. *Permian-Triassic palaeogeography and palaeoclimatology and implications for therapsid distributions*. Smithsonian Press, Washington D. C., 109-132.
- Parrish, J.T. 1992. *Jurassic climate and oceanography of the Pacific region*. Cambridge University Press, Cambridge, 365-380.
- Parrish, J.T. & Curtis, R.L. 1982. Atmospheric circulation, upwelling and organic-rich rocks in the Mesozoic and Cenozoic Eras. *Palaeogeography, Palaeoclimatology & Palaeoecology*, **40**, 31-66.
- Parrish, J.T. & Doyle, J.A. 1984. Predicted evolution of global climate in late Jurassic-Cretaceous time. *International Organic Palaeobotany Conference*, London.

References

- Parrish, J.T., Hansen, K.S. & Ziegler, A.M. 1979. Atmospheric circulation and upwelling in the Palaeozoic, with reference to petroleum source beds. *American Association of Petroleum Geologists Bulletin*, **63**, 507-508.
- Parrish, J.T. & Peterson, F. 1988. Wind directions predicted from global circulation models and wind directions determined from aeolian sandstones of the western United States—a comparison. *Sedimentary Geology*, **56**, 261-282.
- Parrish, J.T., Ziegler, A.M. & Scotese, C.R. 1982. Rainfall patterns and the distribution of coals and evaporites in the Mesozoic and Cenozoic. *Palaeogeography, Palaeoclimatology & Palaeoecology*, **40**, 67-101.
- Payton, C.E. 1977. *Seismic stratigraphy- applications to hydrocarbon exploration*. American Association of Petroleum Geologists, Tulsa.
- Perez, d.E. & Levi, B. 1961. Relacion estratigrafica entre la Formation Moctezuma y el granito subyacente, Calama, provincia de Antofagasta, Chile. *Minerales*, **74**, 39-48.
- Pettijohn, F.J. 1975. *Sedimentary Rocks*. Harper & Row, New York, 526 pp.
- Philander, S.G.H. & Pacanowski, R.C. 1980. The oceanic response to cross-equatorial winds (with application to coastal upwelling in low latitudes). *Tellus*, **33**, 201-210.
- Pichowiak, S. 1994. Early Jurassic to early Cretaceous magmatism in the Coastal Cordillera and the Central Depression of North Chile. In: Reutter, K.J., Scheuber, E. & Wigger, P.J. (eds.), *Tectonics of the southern Central Andes*. Springer-Verlag, Berlin, 203-217.
- Pindell, J. & Dewey, J.F. 1982. Permo-Triassic reconstruction of western Pangea and the evolution of the Gulf of Mexico Caribbean Region. *Tectonics*, **1**, 179-211.
- Piper, J.D.A. 1976. Palaeomagnetic evidence for a Late Proterozoic Supercontinent. *Philosophical Transactions of the Royal Society of London*, **280**, 469-290.
- 1983. Proterozoic palaeomagmatism and single continent plate tectonics. *Geophysics Journal of Research Astronomical Society*, **74**, 163-197.
- Pitcher, W.S. 1984. *Phanerozoic plutonism in the Peruvian Andes*. Shiva, London, 152-167.
- Plint, A.G. 1991. High-frequency relative sea-level fluctuations in Upper Cretaceous shelf clastics of the Alberta Foreland Basin: possible evidence for a glacio-eustatic control? In: MacDonald, D.c.M. (eds.), *Sedimentation, tectonics and eustasy*. **Special publication 12**, International Association of Sedimentologists, 409-428.
- Plint, A.G., Eyles, N., Eyles, C.H. & Walker, R.G. 1992. Controls of sea-level change. In: Walker, R.G. & James, N.P. (eds.), *Facies models-Response to sea-level change*. Geological Society of Canada, 15-25.
- Posamentier, H.W. & Allen, G.P. 1993. Variability of the sequence stratigraphic model: effects of local basin factors. *Sedimentary Geology*, **86**, 91-109.
- Posamentier, H.W., Allen, G.P., James, D.P. & Tesson, M. 1992. Forced regressions in a sequence stratigraphic framework: concepts, examples, and exploration significance. *American Association of Petroleum Geologists Bulletin*, **76**, 1687-1709.
- Posamentier, H.W., Jervey, M.T. & Vail, P.R. 1988. Eustatic controls on clastic deposition I- conceptual framework. In: Wilgus, C.K., Hastings, B.S., Kendall, C.G.S.C., Posamentier, H.W., Ross, C.A. & VanWagoner, J.C. (eds.), *Sea-level Change: An Intergrated Approach*. **Special Publication 42**, Society of Economic Paleontologists and Mineralogists, 109-124.
- Posamentier, H.W. & Vail, P.R. 1988. Eustatic controls on clastic deposition II-sequence and systems tract models. In: Wilgus, C.K., Hastings, B.S., Kendall, C.G.S.C., Posamentier, H.W., Ross, C.A. & VanWagoner, J.C. (eds.), *Sea-level Changes: An Intergrated Approach*. **Special Publication 42**, Society of Economic Paleontologists and Mineralogists, 125-154.

References

- Postma, G. 1995. Sea-level related architectural trends in coarse-grained delta complexes. *Sedimentary Geology*, **98**, 3-12.
- Prentice, M.L. & Matthews, R.K. 1988. Cenozoic ice-volume history: Development of a composite oxygen isotope record. *Geology*, **16**, 963-966.
- Prinz, P. 1991. *Mesozoische Korallen Aus Nordchile*. Stuttgart 1, 147-209.
- Prinz, P., Wilke, H. & Hillebrandt, A. 1994. Sediment accumulation and subsidence history in the Mesozoic marginal basin of northern Chile. In: Reutter, K.J., Scheuber, E. & Wigger, P.J. (eds.), *Tectonics of the southern Central Andes*. Springer-Verlag, Berlin, 219-232.
- Quinzio, L.A. 1987. *Stratigraphische Untersuchungen im Unterjura des Sudteils der Provinz Antofagasta in Nord-Chile*. Berlin, 100 pp.
- Rachocki, A.H. 1981. *Alluvial Fans*. John Wiley, Chichester, 161 pp.
- Raiswell, R. 1987. Non-steady state microbiological diagenesis and the origin of concretions and nodular limestones. In: Marshall, J.D. (eds.), *Diagenesis of sedimentary sequences*. **Special Publication 36**, Geological Society of London, London, 41-54.
- Ramirez, C.F. & Gardeweg, M.P. 1982. *Hoja Toconao, Region de Antofagasta, Chile*, Carta Geologica de Chile 1:250000 edn. Servicio Nacional de Geologia y Minería, Santiago.
- Ramos, V. 1994. Terranes of Southern Gondwanaland and their control in the Andean Structure (30'-33'S Latitude). In: Reutter, K.J., Scheuber, E. & Wigger, P.J. (eds.), *Tectonics of the Southern Central Andes-Structure and Evolution of an active continental margin*. Springer-Verlag, Berlin, 249-262.
- Ramos, V. & Kay, S.M. 1991. Triassic rifting and associated basalts in the Cuyo Basin, central Argentina. In: Harmon, R.S. & Rapela, C.W. (eds.), *Andean magmatism and its tectonic setting*. **Special Publication 265**, Geological Society of America, 79-91.
- Ramos, V.A. 1988. Late Proterozoic-Early Paleozoic of South America-A Collisional History. *Episodes*, **11**.
- Ramos, V.A. 1989. Andean foothills structures in northern Magallanes Basin, Argentina. *American Association of Petroleum Geologists Bulletin*, **73**, 887-903.
- Rapalini, A.E. 1989. *Estudio paleomagnetico del volcanismo Permo-Triasico de la region andina de la Republica Argentina. Consecuencias tectonicas y geodinamicas*. Ph.D. thesis, University of Buenos Aires, Buenos Aires, Argentina.
- Rapela, C.W., Heaman, L.M. & McNutt, R.H. 1982. Rb/Sr geochronology of granitoid rocks from the Pampean Ranges, Argentina. *Geology*, **90**, 574-582.
- Rathey, R.P. & Hayward, A.B. 1993. Sequence stratigraphy of a failed rift system: the Middle Jurassic to Early Cretaceous basin evolution of the Central and Northern North Sea. *Proceedings of the 4th conference, Petroleum geology of northwest Europe*, London, Geological Society of London, 215-249.
- Raymo, M.E., Ruddiman, W.F., Backman, J., Clement, B.M. & Martinson, D.G. 1989. Late Pliocene variations in northern hemisphere ice-sheets and Northern Atlantic deep-water circulation. *Palaeoceanography*, **4**, 413-446.
- Reading, H.G. 1986. *Sedimentary Environments and Facies*. Blackwell Scientific Publishers, Oxford, 615 pp.
- Retallack, G.J. 1988. *Field recognition of paleosols*. Geological Society of America.

References

- Reutter, K.J., Giese, P., Gotze, H.J., Scheuber, E., Schwab, K., Schwarz, G. & Wigger, P. 1988. Structures and crustal development of the central Andes between 21° and 25°S. In: (eds.), *Lecture notes in Earth Sciences*, **17**, Springer, Berlin, 231-261.
- Reutter, K.J., Scheuber, E. & Helmcke, D. 1991. Structural evidence of orogen-parallel strike-slip displacements in the Precordillera of Northern Chile. *Geologische Rundschau*, **80**, 135-153.
- Riccardi, A.C. 1983. The Jurassic of Argentina and Chile. In: Moullade, M. & Nairn, A.E.M. (eds.), *The Phanerozoic Geology of the World II: the Mesozoic*. Elsevier, Amsterdam, 201-264.
- 1992. Palaeogeography of Argentina and Chile: Regional review. In: Westermann, G.E.G. (eds.), *The Jurassic of the circum-Pacific*. Springer, New York, 147-150.
- Riccardi, A.C., Damborenea, S.E., Mancenido, M.O. & Ballent, S.C. 1988. Hettangiano y Sinemuriano marinos en Argentina. *V Congr. Geol. Chileno*, Santiago, **2**, 359-373.
- Riccardi, A.C. & Gulisano, C.A. 1992. Unidades limitadas por discontinuidades. Su aplicacion al Jurásico andino. *Asociacion Geologica Argentina, Revista, Buenos Aires*, **XLV**, 346-364.
- Riccardi, A.C., Gulisano, C.A., Mojica, J., Palacios, O., Schubert, C. & Thomson, M.R.A. 1992. Western South America and Antarctica. In: Westermann, G.E.G. (eds.), *The Jurassic of the Circum-Pacific*. Cambridge University Press, New York, 122-161.
- Riccardi, A.C. & Westermann, G.E.G. 1991. The middle Jurassic ammonoid fauna and biochronology of the Argentine-Chilean Andes III: Eurycephalitinae, Stephanocerataceae IV: Bathonian-Callovian Reineckeidae. *Palaeontographica*, **A216**, 1-110.
- Riccardi, A.C., Westermann, G.E.G. & Elmi, S. 1989. Les zones d'ammonites du Bathonien-Callovien (Jurassique moyen) des Andes argentine-chiliennes. *Geobios*, **22**, 553-597.
- Rocha-Campos, A.C. 1971. *Upper Palaeozoic and lower Mesozoic palaeogeography and palaeoclimatology and tectonic events in south America*. Canadian Society of Petroleum Geology, 398-424.
- Rogers, L. 1985. *A geochemical traverse across the north Chilean Andes*. Ph.D. thesis, Open University, Milton Keynes, England.
- Rowley, D.B. 1992. *Reconstructions of the circum-Pacific region*. Cambridge University Press, Cambridge.
- Ruddiman, W.F. & McIntyre, A. 1981. Oceanic mechanisms for amplification of the 23 000-year ice-volume cycle. *Science*, **212**, 617-627.
- Ruddiman, W.F., Raymo, M.E., Martinson, D.G., Clement, B.M. & Backman, J. 1989. Pleistocene evolution: northern hemisphere ice-sheets and North Atlantic Ocean. *Palaeoceanography*, **4**, 353-412.
- Rutland, R.W.R. 1971. Andean orogeny and sea-floor spreading. *Nature*, **233**, 252-255.
- Sabadini, R., Doglioni, C. & Yuen, D.A. 1990. Eustatic sea-level fluctuations induced by polar wander. *Nature*, **345**, 708-710.
- Salfity, J.A. 1985. Lineamentos transversales al rumbo andino en el noroeste argentino. *IV Congreso Geología Chileno*, **2**, 119-137.
- Salfity, J.A. & Gorustovich, S. 1983. Paleogeografía de la cuenca del Grupo Paganzo (Paleozoico Superior). *Revista of Geologists Association of Argentina*, **38**, 437-453.
- Salfity, J.A. & Marquillas. 1994. Tectonic and sedimentary evolution of the Cretaceous-Eocene Salta Group basin, Argentina. In: Salfity, J.A. (eds.), *Cretaceous tectonics of the Andes*. Earth Evolution Sciences, Vieweg, Berlin, 266-315.
- Salman, G. & Abdula, I. 1995. Development of the Mozambique and Ruvuma sedimentary basins, offshore Mozambique. *Sedimentary Geology*, **96**, 7-41.

References

- Sangree, J.B. & Widmier, J.M. 1977. *Seismic interpretations of clastic depositional facies*. American Association of Petroleum Geologists, 165-184.
- Sarg, J.F. 1988. Carbonate sequence stratigraphy. *In: Wilgus, C.K., Hastings, B.S., Kendall, C.G.S.C., Posamentier, H.W., Ross, C.A. & Van Wagoner, J.C. (eds.), Sea-level changes: an integrated approach. Special Publication 42, Society of Economic Paleontologists and Mineralogists, Tulsa, 155-182.*
- Scheuber, E., Bogdanic, T., Jensen, A. & Reutter, K.J. 1994. Tectonic development of the North Chilean Andes in relation to Plate Convergence and Magmatism since the Jurassic. *In: Reutter, K.J., Scheuber, E. & Wigger, P.J. (eds.), Tectonics of the Southern Central Andes*. Springer-Verlag, Berlin, 121-140.
- Schlatter, R. 1982. Zur Grenze Pliensbachian-Toarcian im Klettgau (Kanton Schaffhausen, Schweiz). *Ecolgae Geologica Helvetica*, **75**, 759-771.
- Schumm, S.A. 1977. *The Fluvial System*. J. Wiley, New York, 338 pp.
- Schwab, K. 1973. Die Stratigraphie in der Umgebung des Salar de Cauchari (NW Argentina). *Geotekt. Forsch.*, **43**, 1-168.
- Schwarzacher, W. 1989. Milankovich-type cycles in the Lower Carboniferous of NW Ireland. *Terra Nova*, **1**, 468-473.
- Schwarzacher, W. & Haas, J. 1986. Comparative statistical analysis of some Hungarian and Austrian Upper Triassic peritidal carbonate sequences. *Acta Geol. Hung.*, **29**, 179-196.
- Sclater, J.G. & Christie, P.A.F. 1980. Continental stretching: an explanation of the post-mid-Cretaceous subsidence of the central North Sea basin. *Journal of geophysical research*, **85**, 1711-1739.
- Scotese, C.R., Gahagan, L.M. & Larson, R.L. 1988. Plate tectonic reconstructions of the Cretaceous and Cenozoic ocean basins. *Tectonophysics*, **155**, 27-48.
- Scotese, C.R. & McKerrow, W.S. 1990. *Revised world maps and introduction*. Geological Society of London, London, 1-21.
- Sengör, A.M.C., Altiner, D., Cin, A., Ustaomer, T. & Hsu, K.T. 1988. Origin and assembly of the Tethyside orogenic collage at the expense of Gondwana Land. *In: Audley-Charles, M.G. & Hallam, A. (eds.), Gondwana and Tethys. Special Publication 37, Geological Society of London, 119-181.*
- Shackleton, N.J., Berger, A.L. & Peltier, W.R. 1990. An alternative astronomical calibration of the Lower Pleistocene timescales based on ODP Site 677. *Transactions of the Royal Society of Edinburgh*, **81**, 251-261.
- Shackleton, N.J. & Opdyke, N.D. 1973. Oxygen isotope and palaeomagnetic stratigraphy of equatorial Pacific core V28-238: oxygen isotope temperatures and ice-volumes on a 10^5 and 10^6 year scale. *Quaternary Research*, **3**, 39-55.
- Shackleton, R.M., Ries, A.C., Coward, M.P. & Cobbold, P.R. 1979. Structure, metamorphism and geochronology of the Arequipa Massif of coastal Peru. *Journal of the Geological Society of London*, **136**, 195-214.
- Shanley, K.W. & McCabe, P.J. 1991. Predicting facies architecture through sequence stratigraphy- An example from the Kaiparowits Plateau, Utah. *Geology*, **19**, 742-745.
- Simpson, E.S.W., Sclater, J.G., Parsons, B., Norton, I. & Meinke, L. 1979. Mesozoic magnetic lineations in the Mozambique basin. *Earth and Planetary Science Letters*, **43**, 260-264.

References

- Sinclair, I.K. 1988. Evolution of Mesozoic-Cenozoic sedimentary basins in the Grand Banks area of Newfoundland and comparison with Falvey's (1974) rift model. *Canadian Petroleum Society Bulletin*, **36**, 255-273.
- Sinclair, I.K. & Riley, L.A. 1995. Separation of late Cimmerian rift and post-rift megasequences: comparison of the Jeanne d'Arc Basin, Grand Banks and the Outer Moray Firth, North Sea. In: Steel, R.J., Felt, V.L., Johannessen, E.P. & Mathieu, C. (eds.), *Sequence stratigraphy on the northwest European margin*. **Special Publication 5**, Norwegian Petroleum Society (NPF), Amsterdam, 347-364.
- Singh, I.B. 1972. On the bedding in the natural-levee and point bar deposits of the Gomti River, Uttar Pradesh, India. *Sedimentary Geology*, **7**, 309-317.
- Sloss, L.L. 1950. Palaeozoic stratigraphy in the Montana area. *American Association of Petroleum Geologists Bulletin*, **34**, 423-451.
- 1963. Sequences in the cratonic interior of North America. *Geol. Soc. Am. Bull.*, **74**, 93-113.
- Sloss, L.L., Krumbein, W.C. & Dapples, E.C. 1949. *Integrated facies analysis*. Geological Society of America, 91-124.
- Smith, C.B., Clark, T.C., Barton, E.S. & Bristow, J.W. 1994. Emplacement ages of kimberlite occurrences in the Prieska region, south-west border of the Kaapvaal Craton, South Africa. *Chemical Geology*, **113**, 149-169.
- Smith, P.L. 1983. The Pliensbachian ammonite *Dayiceras dayiceroides* and early Jurassic palaeogeography. *Canadian Journal of Earth Sciences*, **20**, 86-91.
- Smith, P.L., Tipper, H.W., Taylor, D.G. & Guex, J. 1988. An ammonite zonation for the Lower Jurassic of Canada and the United States: the Pliensbachian. *Canadian Journal of Earth Sciences*, **25**, 1503-1523.
- Southgate, P.N., Kennard, J.M., Jackson, M.J., O'Brien, P.E. & Sexton, M.J. 1993. Reciprocal lowstand clastic and highstand carbonate sedimentation, subsurface Devonian reef complex, Canning basin, western Australia. In: Loucks, R.G. & Sarg, J.F. (eds.), *Carbonate sequence stratigraphy-recent developments & applications*. American Association of Petroleum Geologists, Tulsa, 157-180.
- Spicer, R.A. 1987. The significance of the Cretaceous flora of northern Alaska for the reconstruction of the climate of the Cretaceous. *Geologisches Jahrbuch, Reihe A*, **96**, 265-291.
- Stevens, G.R. 1980. South-west Pacific faunal palaeobiogeography in Mesozoic and Cenozoic times: a review. *Palaeogeography, Palaeoclimatology & Palaeoecology*, **31**, 153-196.
- Stipanovic, P. 1983. *The Triassic of Argentina and Chile*. Elsevier, Amsterdam, The Netherlands, 181-200.
- Storey, B.C. 1995. The role of mantle plumes in continental breakup: case histories from Gondwanaland. *Nature*, **377**, 301-308.
- Suarez, M. & Bell, C.M. 1991a. Depositos triasicos continentales y jurasicos marinos en la Cordillera de la Costa, Region de Atacama, Chile. *VI Congreso Geologico Chileno*, Vina del Mar, 664-667.
- 1991b. Sedimentos lacustres de probable edad triasica, en el area de La Coipa, Region Atacama, Chile. *VI Congreso Geologico Chileno*, Vina del Mar, 660-663.
- 1992. Triassic rift-related sedimentary basins in northern Chile (24°-29°S). *Journal of South American Earth Sciences*, **6**, 109-121.
- Suarez, M., Naranjo, J.A. & Puig, A. 1985. Estratigrafia de la Cordillera de la Costa, al sur de Taltal: Etapas iniciales de la evolucion andina. *Revista Geologica de Chile*, **24**, 19-28.

References

- Surlyk, F. 1990. A Jurassic sea-level curve for East Greenland. *Palaeogeography, Palaeoclimatology, Palaeoecology*, **78**, 71-85.
- 1991. Sequence stratigraphy of the Jurassic-Lowermost Cretaceous of East Greenland. *American Association of Petroleum Geologists Bulletin*, **75**, 1468-1488.
- Tankard, A.J., Jackson, M.P.A., Eriksson, K.A., Hobday, D.K., Hunter, D.R. & Minter, W.E.L. 1982. *Crustal evolution of southern Africa*. Springer-Verlag, New York, 523 pp.
- Tankard, A.J., Uliana, M.A., Welsink, H.J., Ramos, V.A., Turic, M., Franca, A.B., Milani, E.J., Brito-Neves, B.B., Eyles, N., Skarmeta, J., Santa-Ana, H., Wiens, F., Cirbian, M., Lopez, O., Germs, G.J.B., De-Wit, M.J., Machacha, T. & Miller, R.M. 1995. Structural and tectonic controls of basin evolution in southwestern Gondwana during the Phanerozoic. In: Tankard, A.J., Saurez-Soruco, R. & Welsink, H.J. (eds.), *Petroleum basins of South America*. **Memoir 62**, American Association of Petroleum Geologists, 5-52.
- Taylor, D.G., Callomon, J.H., Hall, R., Smith, P.L., Tipper, H.W. & Westermann, G.E.G. 1984. *Jurassic ammonite biogeography of western North America: the tectonic implications*. IGCP Project 171: Geological Society of Canada, 121-141.
- Toth, J. 1995. *Geodynamic evolution of the Central Andes*. Ph.D. thesis, University of Liverpool, England.
- Tucker, M.E. 1991a. *Sedimentary petrology-an introduction to the origin of sedimentary rocks*. Blackwell scientific publications, Oxford.
- 1991b. Sequence stratigraphy of carbonate-evaporite basins: models and application to the Upper Permian (Zechstein) of northeast England and adjoining North Sea. *Journal of the Geological Society of London*, **148**, 1019-1036.
- 1992. Carbonate diagenesis and sequence stratigraphy. In: Wright, V.P. (eds.), *Sedimentology Review*. **1**, Blackwell, London, 51-72.
- Turner, J.C. 1970. The Andes of northwestern Argentina. *Geologisches Rundschau*, **59**, 1028-1063.
- Turner, J.C. & Mon, R. 1979. *Cordillera Oriental*. Academia Nacional de Ciencias, Cordoba, 57-94 pp.
- Turner, P. 1980. *Continental Red-beds*. Elsevier, Amsterdam, 562 pp.
- Uliana, M.A. & Biddle, R.T. 1988. Mesozoic-Cenozoic paleogeographic and geodynamic evolution of southern South America. *Revista Brasileira de Geociencias*, **18**, 172-190.
- Uliana, M.A. & Legarreta, L. 1993. Hydrocarbons habitat in a Triassic-to-Cretaceous sub-Andean setting: Neuquén basin, Argentina. *Journal of Petroleum Geology*, **16**, 397-420.
- Underhill, J.R. & Partington, M.A. 1993. Jurassic thermal doming and deflation in the North Sea: implications of the sequence stratigraphic evidence. *Petroleum geology of northwest Europe*, London, Geological Society of London, **1**, 337-345.
- Unternehr, P., Curie, D., Olivet, J.L., Goslin, J. & Beuzart, P. 1988. South Atlantic fits and intraplate boundaries in Africa and South America. *Tectonophysics*, **155**, 169-179.
- Vai, G.B. & Lucchi, F.R. 1977. Algal crusts, autochthonous and clastic gypsum in a cannibalistic evaporite basin: a case history from the Messinian of northern Apennines. *Sedimentology*, **24**, 211-244.
- Vail, P.R., Audemard, F., Bowman, S.A., Eisner, P.N. & Perez-Cruz, G. 1991. The stratigraphic signatures of tectonics, eustasy and sedimentation: an overview. In: Seilacher, A. & Eisner, G. (eds.), *Cycles and events in stratigraphy*. Springer, Tubingen.

References

- Vail, P.R., Mitchum, R.M. & Thompson, S. 1977a. Seismic stratigraphy and global changes of sea level, Part III: Relative changes of sea level from coastal onlap. In: Payton, C.E. (eds.), *Seismic Stratigraphy-Applications to Hydrocarbon Exploration*. **Memoir 26**, American Association of Petroleum Geologists, Tulsa, 63-82.
- Vail, P.R., Mitchum, R.M., Jr., Todd, R.G., Widmier, J.M., Thompson, S., III, Sangree, J.B., Bubb, J.N. & Hatlelid, W.G. 1977b. Seismic stratigraphy and global changes of sea level. In: Payton, C.E. (eds.), *Seismic stratigraphy-applications to hydrocarbon exploration*. **Memoir 26**, American Association of Petroleum Geologists, Tulsa, 49-212.
- Valencio, D.A., Vilas, J.F. & Pacca, I.G. 1983. The significance of the magmatism of Jurassic-Cretaceous rocks from South America: Predrift movements, hairpins and magnetostratigraphy. *Royal Astronomical Society, Geophysical Journal*, **73**, 135-151.
- Van Echelpoel, E. & Weedon, G.P. 1990. Milankovich cyclicity and the Boom Clay Formation: an Oligocene siliciclastic shelf sequence in Belgium. *Geological Magazine*, **127**, 599-604.
- Van Houten, F.B. 1982. *Red-beds*. McGraw-Hill, 441-442.
- Van Tassell, J. 1987. Upper Devonian Catskill delta margin cyclic sedimentation: Brallier, Scherr and Foreknobs Formations of Virginia and West Virginia. *Geological Society of America Bulletin*, **99**, 414-426.
- Van Wagoner, J.C., Mitchum, R.M., Campion, K.M. & Rahmanian, V.D. 1990. *Siliciclastic sequence stratigraphy in well logs, cores and outcrops*. American Association of Petroleum Geologists, Tulsa, 55 pp.
- Van Wagoner, J.C., Nummedal, D., Jones, C.R., Taylor, D.R., Jennette, D.C. & Riley, G.W. 1991. Sequence stratigraphy applications to shelf sandstone reservoirs: outcrop to subsurface examples. *American Association of Petroleum Geologists Field Conference September 21-28, 1991*, American Association of Petroleum Geologists.
- Van Wagoner, J.C., Posamentier, H.W., Mitchum, R.M., Vail, P.R., Sarg, J.F., Loutit, T.S. & Hardenbol, J. 1988. An overview of the fundamentals of sequence stratigraphy and key definitions. In: Wilgus, C.K., Hastings, B.S., Kendall, C.G.S.C., Posamentier, H.W., Ross, C.A. & Van Wagoner, J.C. (eds.), *Sea-level changes: an integrated approach*. **Special publication 42**, Society of Economic Paleontologists and Mineralogists, Tulsa, 39-46.
- Vaughan, A.P.M. 1995. Circum-Pacific mid-Cretaceous deformation and uplift: A superplume-related event? *Geology*, **23**, 491-494.
- Veevers, J.J. 1995. Emergent, long-lived Gondwanaland vs. submergent, short-lived Laurasia: Supercontinental and Pan-African heat imparts long-term buoyancy by mafic underplating. *Geology*, **23**, 1131-1134.
- Veevers, J.J., Powell, C.M. & Rotts, S.R. 1991. Review of sea-floor spreading around Australia 1. Synthesis of the patterns of spreading. *Australian Journal of Earth Sciences*, **39**, 373-389.
- Vergani, G.D., Tankard, A.J., Belotti, H.J. & Welsink, H.J. 1995. Tectonic evolution and palaeogeography of the Neuquén basin, Argentina. In: Tankard, A.J., Saurez-Soruco, R. & Welsink, H.J. (eds.), *Petroleum basins of South America*. **Memoir 62**, American Association of Petroleum Geologists, 383-402.
- Volkheimer, W. 1967. La palaeoclimatología y los climas del Mesozoico argentino. *Revista Mineralogical Society of Argentina*, **28**, 41-48.
- Warren, J.K. & Kendall, C.G.S.C. 1985. Comparison of sequences formed in marine sabkha (subaerial) and salina (subaqueous) settings-Modern and ancient. *American Association of Petroleum Geologists Bulletin*, **69**, 1013-1023.
- Weedon, G.P. 1985. Hemipelagic shelf sedimentation and climatic cycles: the basal Jurassic (Blue Lias) of South Britain. *Earth and Planetary Science Letters*, **76**, 321-335.

References

- Westermann, G.E.G. 1981. *Ammonite biochronology and biogeography of the circum-Pacific middle Jurassic*. Academic Press, London, 459-498.
- 1984a. Middle Jurassic ammonite evolution in the Andean Province. *IGCP Project 171: Circum-Pacific Jurassic, Report 2*, 69-71.
- 1984b. *Summary of symposium papers on the Jurassic-Cretaceous biochronology and palaeogeography of North America*. Geological Society of Canada, 307-315.
- 1992. *The Jurassic of the Circum-Pacific*. Cambridge University Press, New York, 670 pp.
- 1993. Global bio-events in mid-Jurassic ammonites controlled by seaways. *In: House, M.R. (eds.), The Ammonoidea: environment, ecology and environmental change*. London.
- Westermann, G.E.G. & Riccardi, A.C. 1972. Middle Jurassic ammonoid fauna and biochronology of the Argentine-Chilean Andes I Hildocerataceae. *Palaeontographica*, **A140**, 1-116.
- 1979. Middle Jurassic ammonoid fauna and biochronology of the Argentine-Chilean Andes II Bajocian Stephanocerataceae. *Palaeontographica*, **A164**, 85-188.
- 1982. Ammonoid fauna from the early Middle Jurassic of Mendoza province, Argentina. *Journal of Palaeontology*, **56**, 11-41.
- 1985. Middle Jurassic ammonite evolution in the Andean Province and emigration to Tethys. *Lecture notes in Earth Sciences*, **1**, 6-32.
- White, R.S. & McKenzie, D.J. 1989. Magmatism at rift zones: the generation of volcanic continental margins and flood basalts. *Journal of Geophysical Research*, **94**, 7685-7729.
- Whittaker, A., Cope, J.C.W., Cowie, J.W., Gibbons, W., Hailwood, E.A., House, M.R., Jenkins, D.G., Rawson, P.F., Rushton, A.W.A., Smith, D.G., Thomas, A.T. & Wimbledon, W.A. 1991. A guide to stratigraphical procedure. *Journal of the Geological Society of London*, **148**, 813-824.
- Wignall, P.B. 1991. Model for transgressive black shales? *Geology*, **19**, 167-170.
- Wignall, P.B. & Maynard, J.B. 1993. The sequence stratigraphy of transgressive black shales. *In: Katz, B.J. & Pratt, L.M. (eds.), Source rocks in a sequence stratigraphic framework. AAPG Studies in geology 37*, American Association of Petroleum Geologists, Tulsa, 35-47.
- Willner, A.P., Lottner, U.S. & Miller, H. 1987. Early Palaeozoic structural development in the N. W. Argentine basement of the Andes and its implications for geodynamic reconstructions. *In: McKenzie, G.D. (eds.), Gondwana Six: Structure, Tectonics and Geophysics*. American Geophysical Union.
- Wilson, J.L. 1974. Characteristics of carbonate platform margins. *American Association of Petroleum Geologists Bulletin*, **58**, 810-824.
- Wilson, R.C.L., Hiscott, R.N., Willis, M.G. & Gradstein, F.M. 1989. The Lusitanian basin of west-central Portugal Mesozoic and Cenozoic tectonic, stratigraphic and subsidence history. *In: Tankard, A.J. & Balkwill, H.R. (eds.), Extensional tectonics and stratigraphy of the north Atlantic margins. Memoir 46*, American Association of Petroleum Geologists, 341-361.
- Worsley, T.W., Nance, D. & Moody, J.B. 1984. Global tectonics and eustasy for the past 2 billion years. *Marine Geology*, **58**, 373-400.
- Zaitlin, B.A., Dalrymple, R.W. & Boyd, R. 1994. The stratigraphic organisation of incised-valley systems associated with relative sea-level change. *In: Dalrymple, R.W., Boyd, R. & Zaitlin, B.A. (eds.), Incised-valley systems: Origin and sedimentary sequences. Special Publication 51*, Society of Economic Paleontologists and Mineralogists, Tulsa, 45-60.
- Zavala, C.A. 1993. *Estratigrafia y analisis de facies de la Formacion Lajas (Jurásico medio) en el sector suroccidental de la Cuenca Neuquina, Provincia del Neuquen, Republica Argentina*. Ph.D. thesis, Universidad Nacional del Sur, Bahia, Argentina.

References

- Zeil, W. 1981. Vulkanismus und Geodynamik an der Wende Palaozoikum/Mesozoikum in den zentralen und sudlichen Anden (Chile und Argentinien). *Zbl. Geol. Palaont.*, **1**, 298-318.
- Zempolich, W.G. 1993. The drowning succession in Jurassic carbonates of the Venetian Alps, Italy: A record of supercontinent breakup, gradual eustatic rise and eutrophication of shallow-water environments. In: Loucks, R.G. & Sarg, J.F. (eds.), *Carbonate sequence stratigraphy-Recent developments and applications*. **Memoir 57**, American Association of Petroleum Geologists, Tulsa, 63-107.
- Ziegler, A.M., Parrish, J.T. & Scotese, C.R. 1981. Cambrian World Palaeogeography. *U. S. Geological Survey*, **81-743**, 252.
- Ziegler, A.M., Scotese, C.R. & Barrett, S.F. 1983. *Mesozoic and Cenozoic palaeogeographic maps*. Springer-Verlag, Berlin, 240-252.

Appendices

References

List of appendices

Appendix 1-Norian (Late Triassic)-Pliensbachian (Early Jurassic) correlation panel between 24° and 26°S.

Appendix 2-Sinemurian (Early Jurassic)-Aalenian (Middle Jurassic) correlation panel between 22° and 23°S.

Appendix 3-Bajocian-Bathonian (Middle Jurassic) correlation panel between 21.5° and 25°S.

Appendix 4-Oxfordian-Kimmeridgian (Late Jurassic) correlation panel between 21.5° and 25°S.

Appendix 5-Norian-Rhaetian (Late Triassic) correlation panel for the area between 24° and 26°S. The correlation displays third-order Sequences 1.1 to 1.3 which compose the transgressive sequence-set.











Appendix 6-Hettangian-Sinemurian (Early Jurassic) correlation panel for the area between 24° and 26°S. The correlation displays third-order Sequences 1.3 to 1.5 which compose the highstand sequence-set.

Appendix 7-Callovian (Middle Jurassic) correlation panel for the area between 24° and 26°S. The correlation displays third-order sequences, in particular the third-order downshift in the Early Callovian (Sequence 4.3).









Appendix 8-Oxfordian (Late Jurassic) correlation panel for the area between 24° and 26°S. The correlation displays third-order sequences, in particular the third-order downshift in the Late Oxfordian (Sequence 4.4).

Quick Reference Card

Lithology

<u>Siliciclastic sediments</u>	<u>Carbonate sediments</u>	<u>Others</u>
 Conglomerate	 Limestone	 Gypsum / anhydrite
 Sandstone	 Sandy-limestone	 Intrusive igneous
 Siltstone		 Extrusive volcanics
 Shale / mudstone		
 Bituminous shale		

Facies



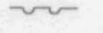
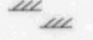


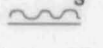

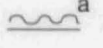

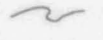
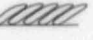
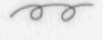
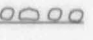




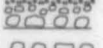

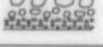

<u>Siliciclastic facies</u>	<u>Carbonate and evaporite facies</u>
 Continental / fan-delta conglomerate	 Lagoonal limestone
 Shoreface sandstone	 Shallow-marine limestone
 Offshore transition siltstone	 Evaporite
 Offshore shale	Note
 Anoxic offshore shale	Figures 5.14, 5.15, 5.16, 5.20, 5.22, 5.25, 5.26, 5.27, 5.28

Sequence stratigraphic surfaces and systems tracts















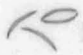




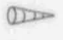




<u>Bounding Surfaces</u>	<u>Systems Tracts</u>
— SB — Sequence boundary	HST Highstand systems tract
— mfs — Maximum flooding surface	TST Transgressive systems tract
— ifs — Initial flooding surface	SMST Shelf margin systems tract
— rs — Ravinement surface	LST Lowstand systems tract
— ts — Transgressive surface	
----- Biostratigraphic time-line	

Quick Reference Card

Sedimentary Structures

	Flute cast		Parallel lamination
	Load cast		Cross lamination
	Dessication crack		Wave-ripple lamination
	Symmetrical ripples		Swaley-cross-stratification
	Asymmetrical ripples		Hummocky-cross-stratification
	Slump structure		Imbrication
	Convolute bedding		Pebble lag
	Trough cross-bedding		Flaser bedding
	Tabular cross-bedding		Lenticular bedding
	Normal grading		Calcareous concretion
	Reverse grading		Teepee structures

Fossils

	Ammonites (Name if identified)		Coral (solitary)		Stromatolite
	Conodonts (Name if identified)		Coral (colonial) (Name if identified)		Algal mat
	Bivalves (Name if identified)		Crinoids		Fish
	Brachiopods (Name if identified)		Echinoids		Burrows (Name if identified)
	Plant fragments (Name if identified)		Gastropods		Broken shell debris
	Roots		Ooid		Oncolite / pisolite > 2mm in diameter
Bed contacts			Bedding data		Belemnites
	Erosive		Palaeocurrent data		
	Sharp				
	Gradational				

Quick Reference Card

Sedimentary Structures











	Flute cast		Parallel lamination
	Load cast		Cross lamination
	Desiccation crack		Wave-ripple lamination
	Symmetrical ripples		Swaley-cross-stratification
	Asymmetrical ripples		Hummocky-cross-stratification
	Slump structure		Imbrication
	Convolute bedding		Pebble lag
	Trough cross-bedding		Flaser bedding
	Tabular cross-bedding		Lenticular bedding
	Normal grading		Calcareous concretion
	Reverse grading		Teepee structures

Fossils









	Ammonites (Name if identified)		Coral (solitary)		Stromatolite
	Conodonts (Name if identified)		Coral (colonial) (Name if identified)		Algal mat
	Bivalves (Name if identified)		Crinoids		Fish
	Brachiopods (Name if identified)		Echinoids		Burrows (Name if identified)
	Plant fragments (Name if identified)		Gastropods		Broken shell debris
	Roots		Ooid		Oncolite / pisolite > 2mm in diameter
Bed contacts			Bedding data		Belemnites
	Erosive		Palaeocurrent data		
	Sharp				
	Gradational				

Quick Reference Card

Lithology

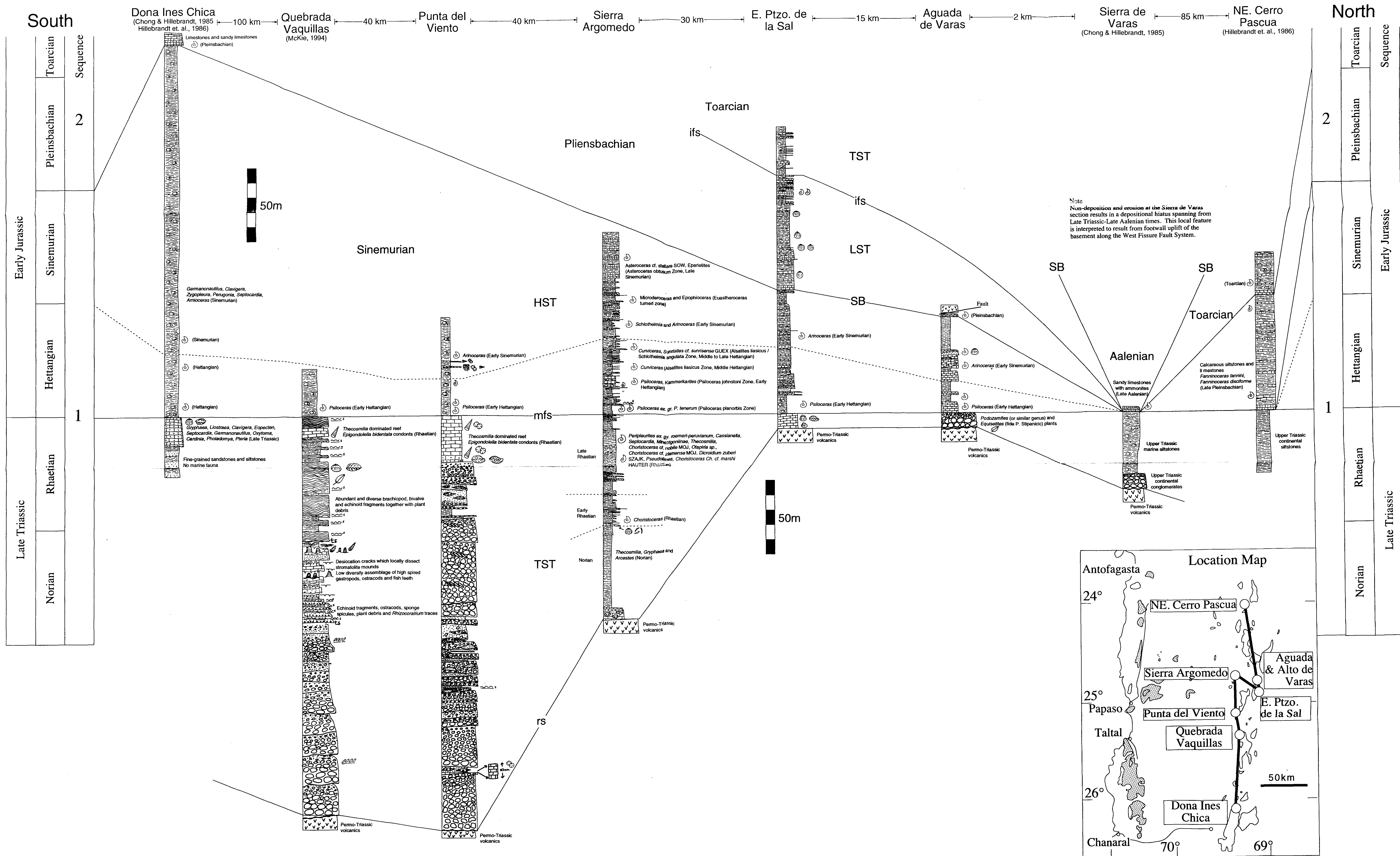
<u>Siliciclastic sediments</u>		<u>Carbonate sediments</u>	<u>Others</u>	
	Conglomerate			Gypsum / anhydrite
	Sandstone			Intrusive igneous
	Siltstone			Extrusive volcanics
	Shale / mudstone			
	Bituminous shale			

Facies

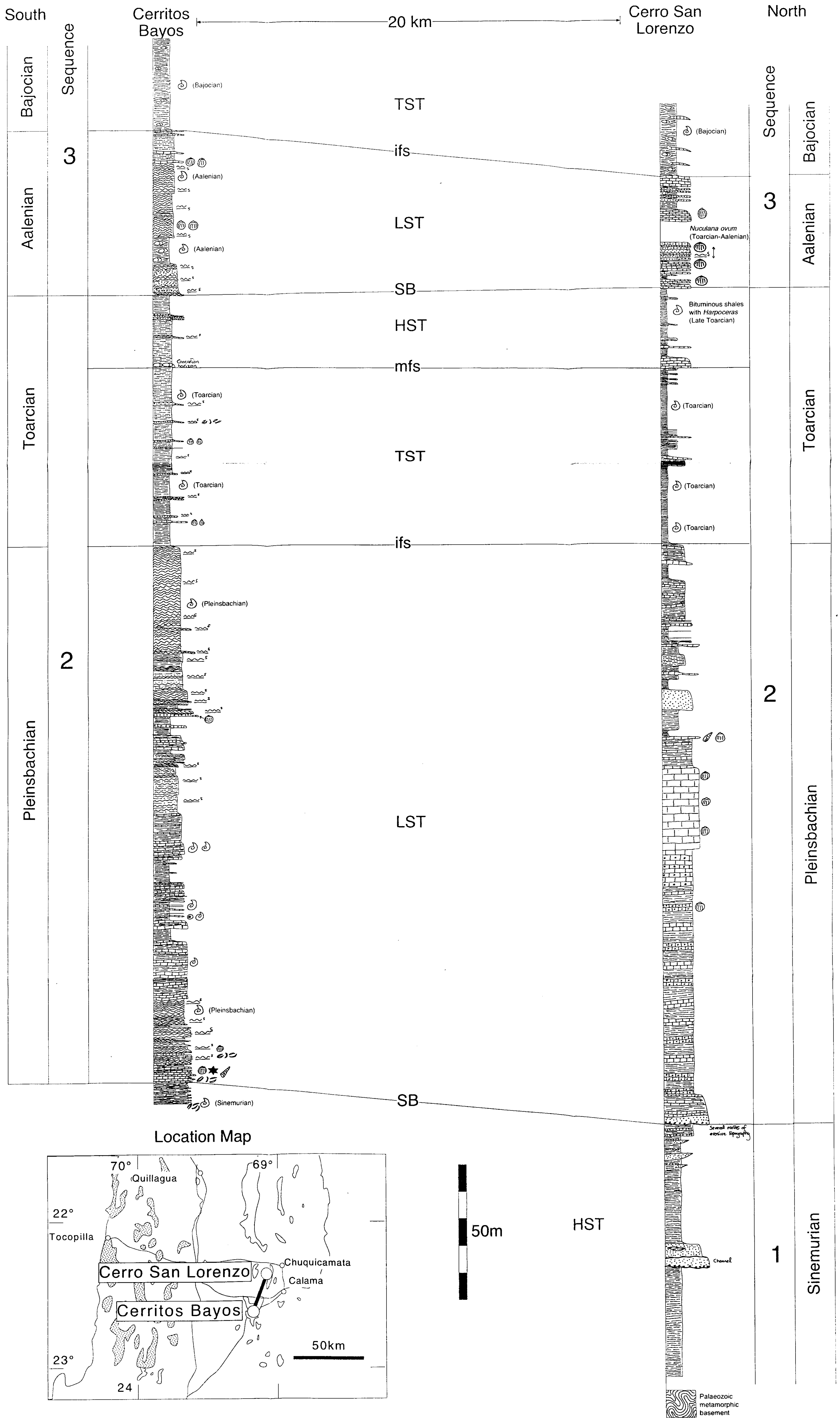
<u>Siliciclastic facies</u>	<u>Carbonate and evaporite facies</u>		
		Continental / fan-delta conglomerate	Lagoonal limestone
		Shoreface sandstone	Shallow-marine limestone
		Offshore transition siltstone	Evaporite
		Offshore shale	
		Anoxic offshore shale	
	<u>Note</u> Figures 5.14, 5.15, 5.16, 5.20, 5.22, 5.25, 5.26, 5.27, 5.28		

Sequence stratigraphic surfaces and systems tracts

<u>Bounding Surfaces</u>	<u>Systems Tracts</u>
— SB — Sequence boundary	HST Highstand systems tract
— mfs — Maximum flooding surface	TST Transgressive systems tract
— ifs — Initial flooding surface	SMST Shelf margin systems tract
— rs — Ravinement surface	LST Lowstand systems tract
— ts — Transgressive surface	
----- Biostratigraphic time-line	



Appendix 1-Norian (Late Triassic)-Pliensbachian (Early Jurassic) correlation panel between 24° and 26°S.

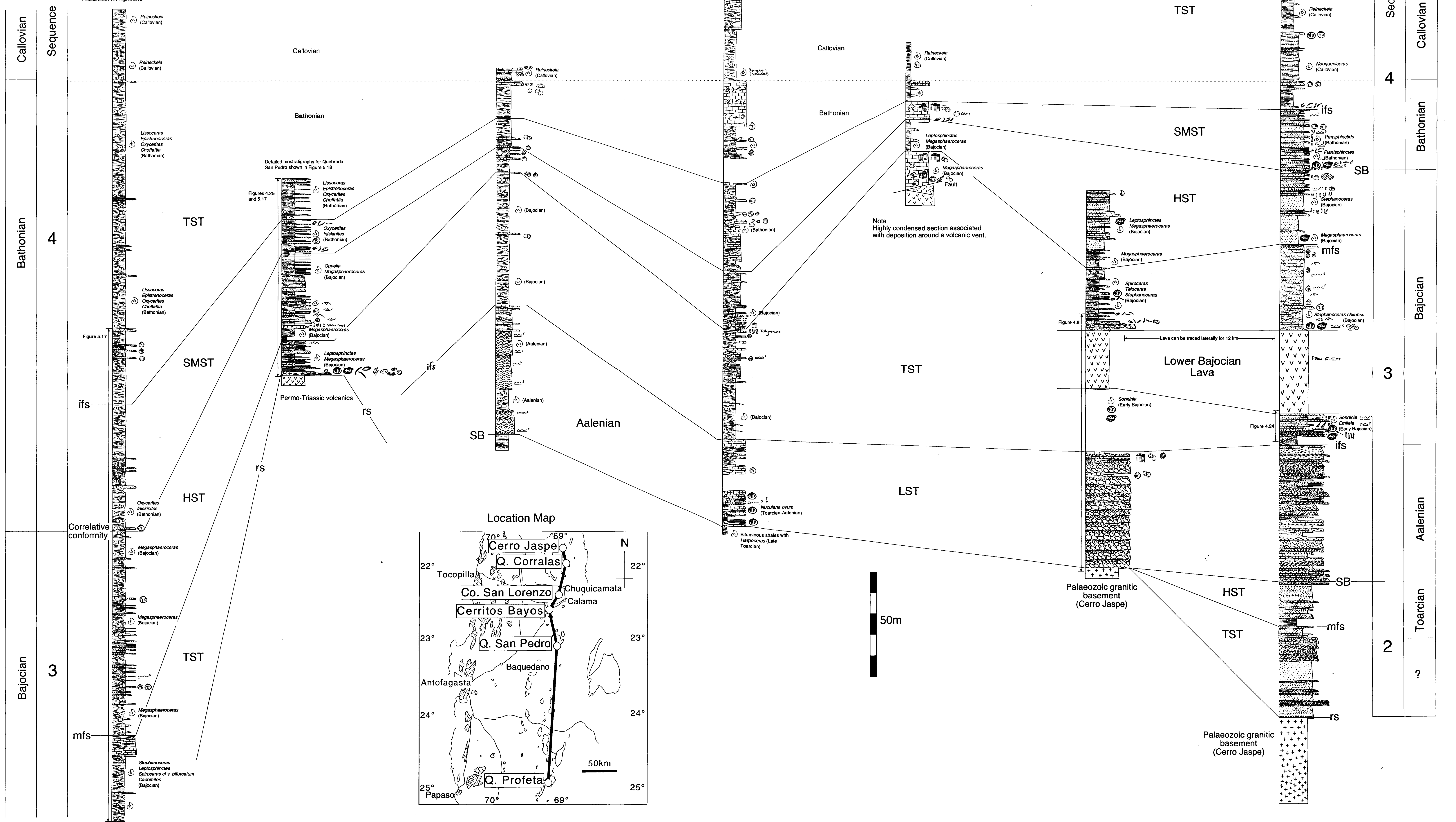


Appendix 2-Sinemurian (Early Jurassic)-Aalenian (Middle Jurassic) correlation panel between 22°-23°S.

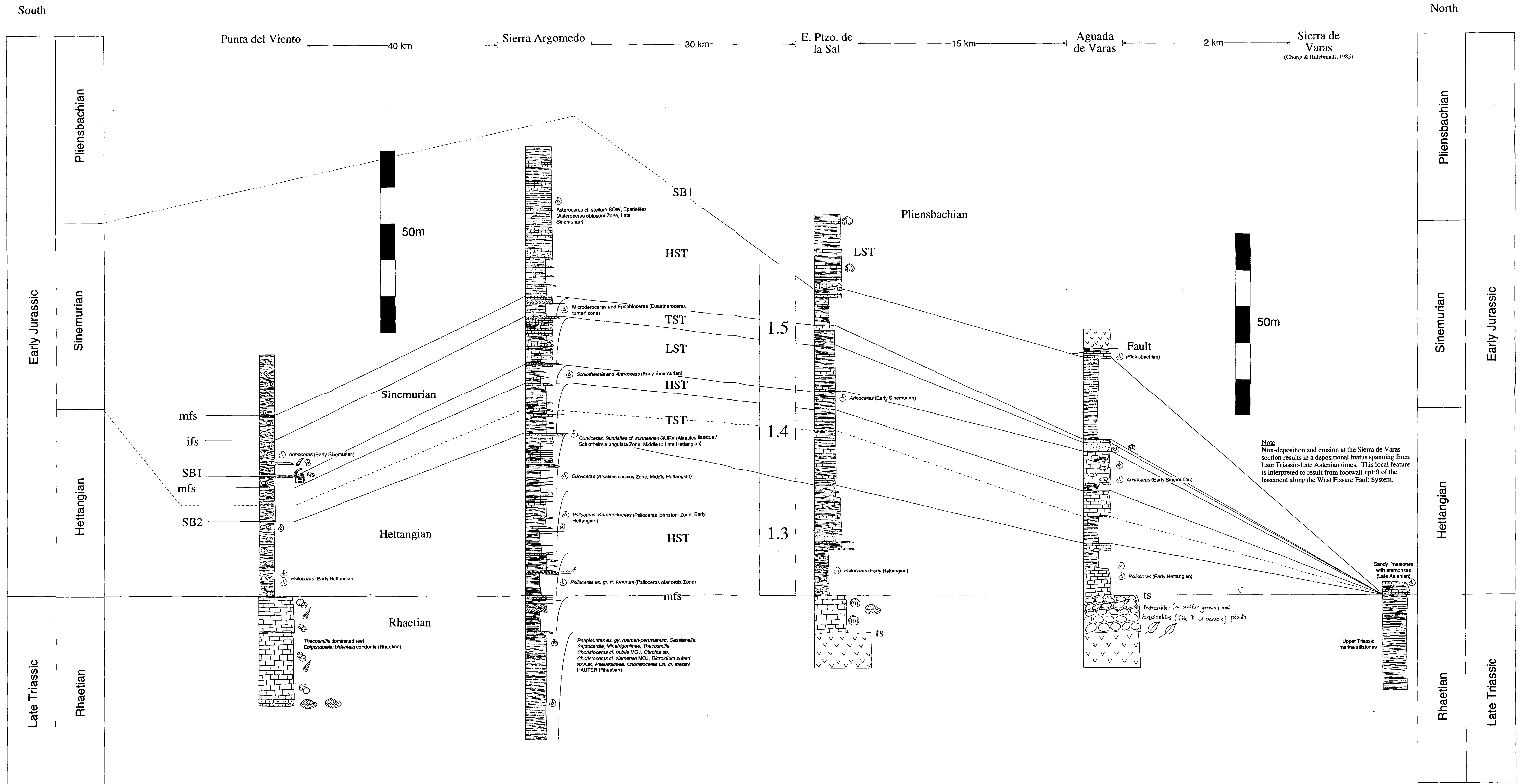
North

Quebrada Profeta 175 km Quebrada San Pedro 50 km Cerritos Bayos 30 km Cerro San Lorenzo 45 km Quebrada Corralas 10 km SW Co Jaspe 10 km W Co Jaspe

South



Appendix 3-Bajocian-Bathonian (Middle Jurassic) correlation panel between 21.5° and 25°S.



Appendix 6-Hettangian-Sinemurian (Early Jurassic) correlation panel between 24°-26°S. The correlation displays the third-order Sequences 1.3 to 1.5, which compose the highstand sequence-set.

Quebrada Profeta — 225 km — Cerritos Bayos — 30 km — Cerro San Lorenzo — 45 km — Quebrada Corralas — 20 km — W Co Jaspe

Appendix 7-Callovian correlation panel for the area between 21.5°-25°S. The correlation displays third-order sequences, in particular the third-order downshift in the Early Callovian (Sequence 4.3).

